Technical Report

VOLUMES FOUR THROUGH SIX OF

ACQUISITION, STORAGE, AND CLASSIFICATION OF ENGINEERING AND GEOLOGICAL DATA FOR SURFACE-MINE DESIGN AND RECLAMATION

UNDER GRANT NUMBERS

G1195018, G1105068

Institute for Mining and Minerals Research
University of Kentucky
Lexington, Kentuck

Form 6-1602
(Revised November 1982)
(480 EBM 7.1)

Date prepared April 23, 1984

UNITED STATES
DEPARTMENT OF THE INTERIOR
BUREAU OF MINES

APPROVAL AND DISTRIBUTION OF GRANT REPORTS

Title: Volumes IV Through VI of Acquisition, Storage, and Classification of Engineering and Geological Data for Surface-Mine Design and Reclamation.

331 pp.

Authors: Volume IV: Edward A Kryza; Volume V: Joseph G. Turner, III Volume VI: Roger L. Weinheimer

Report Date: June 1983 Type of Report (Final/Interim): FINAL

Sponsoring Organization: OSM/Bureau of Mines

Value/Impact of results: Impact of geological environment on the design of mines.

Users/Audience: Mining engineers

grantee Name: University of Kentucky

grant Number: G1195019 and G1105068 Total grant Funding: $126,688

TPO: Program Manager:

Has grantee filed a Patent Form DI 1217? ☐ Yes ☒ No If yes, attach Solicitor's approval to make public.

Press Release Recommendation: ☐ Yes ☒ No
Recommended for Open File: ☒ Yes ☐ No
Recommended for NTIS: ☐ Yes ☒ No

If no, explain: Report does not meet NTIS standards

WASHINGTON OFFICE ONLY

Date Rec'd
OFR # 104(2)-84
NTIS # NA
# of pages
Price $

Distribution: *(Check or fill in as appropriate)*

DOI Library [2] OSM Library [2] Office of Assistant Director Mining Research (1) MS 6000

10 BOM Research Centers ☐ All ☒ These only: Denver (2)

4 Field Office Centers ☐ All ☐ These only:

BOM library, Forbes Ave., Pittsburgh, PA [2] MSHA, Arlington, VA ☐ National Mine H&S Academy, Beckley, WV ☐

State Geologists in

Other: Grants Management Office (sent one copy 2/27/84)

If not recommended for distribution, state why:

CONCURRENCE

Signature

Staff Engineer or Scientist

Date APR 23 1984

Chief, Office of Mineral Institutes

Division Chief

Assistant Director

APPROVAL

Signature

Chief, Office of Technical Information

Date 4-23-84

(no press release)

ATTACHMENT CHECKLIST
☐ Summary of results
☐ Summary and evaluation of final report

VOLUMES FOUR THROUGH SIX OF

ACQUISITION, STORAGE, AND CLASSIFICATION OF ENGINEERING AND GEOLOGICAL DATA FOR SURFACE-MINE DESIGN AND RECLAMATION

UNDER GRANT NUMBER

G1195018, G1105068

This is a final report for a grant awarded by the Office of Surface Mining under the Mineral Institutes program of support for graduate education in mineral sciences and engineering. This program was transferred to the Bureau of Mines prior to the completion of the report. The views and conclusions contained are those of the authors and should not be interpreted as necessarily representing the official policies or recommendations of the Interior Department's Bureau of Mines or Office of Surface Mining, or of the U.S. Government.

VOLUME IV:

PETROLOGY, DEPOSITIONAL ENVIRONMENTS, AND SLAKE DURABILITY OF SOME MIDDLE PENNSYLVANIAN COAL MEASURES SHALES

by

Edward A. Kryza
University of Cincinnati
Cincinnati, Ohio

June 1983

Volume IV of Acquisition, Storage, and Classification of Engineering and Geological Data for Surface-Mine Design and Reclamation under Grant Number G5195018 or G1195018, September 1979.

Prepared for the University of Kentucky Institute for Mining and Minerals Research Title III Program.

ABSTRACT

Forty-seven shale samples from the coal measures of the Middle Pennsylvanian Breathitt Formation were examined petrographically to determine, which shale attributes most directly influence slake durability. The petrographic study combined thin section examination with x-ray diffraction analyses of clay mineral orientation and clay mineralogy. Slake durability indices were obtained using a 60 minute, one cycle test and oven-dried samples. Multiple linear regression indicates a high degree of correlation between slake durability indices and two measured shale characteristics, clay percent and clay mineral orientation. A discriminant function, using these two characteristics, proved successful in differentiating slakable from durable shales, correctly classifying 37 of the 47 tested samples.

All shales studied were deposited in shallow, upper delta plain, interdistributary bays, and eight distinct shale types were identified. Detailed petrographic descriptions are provided for claystones, clayshales, mudstones, mudshales, siltstones, laminated siltstones, sideritic shales, and organic shales.

ACKNOWLEDGEMENTS

Dr. Wayne A. Pryor, principal advisor, along with the other members of my thesis committee, Drs. Paul E. Potter and Warren D. Huff, offered helpful suggestions and reviewed the manuscript. Dr. Roger Steubing of the Behavioral Science Laboratory, University of Cincinnati, provided valuable assistance with the statistical analysis. Dr. James C. Cobb and other members of the Kentucky Geological Survey, helped me obtain the cores, well logs, and testing apparatus needed for this study. Sincere thanks are extended to all. Special thanks go to Mom, Dad, and the rest of my family whose constant encouragement made this work possible.

CONTENTS

TABLES

FIGURES

ABSTRACT

Forty-seven shale samples from the coal measures of the Middle Pennsylvanian Breathitt Formation were examined petrographically to determine, which shale attributes most directly influence slake durability. The petrographic study combined thin section examination with x-ray diffraction analyses of clay mineral orientation and clay mineralogy. Slake durability indices were obtained using a 60 minute, one cycle test and oven-dried samples. Multiple linear regression indicates a high degree of correlation between slake durability indices and two measured shale characteristics, clay percent and clay mineral orientation. A discriminant function, using these two characteristics, proved successful in differentiating slakable from durable shales, correctly classifying 37 of the 47 tested samples.

All shales studied were deposited in shallow, upper delta plain, interdistributary bays, and eight distinct shale types were identified. Detailed petrographic descriptions are provided for claystones, clayshales, mudstones, mudshales, siltstones, laminated siltstones, sideritic shales, and organic shales.

INTRODUCTION

When describing an outcrop, geologists often note the slope-forming nature of interbedded shale units, resulting from weathering. However, some shales seem to resist physical breakdown much better than others, leading one to wonder if some subtle difference in shale composition may be responsible for this phenomena. An investigation of shale weathering could answer several related problems. From a geologic viewpoint, for example, what sedimentologic factors controlled the compositional variation within the shale units? Fine-grained deposits are often described in rather vague terms, and a detailed petrographic analysis may provide information on shale deposition that is frequently overlooked. An engineer might ask if geologic data and interpretation could be used to predict the slake durability of a particular shale. This is an especially significant question in coal measure shales which are removed, and later used for backfill in strip mining operations.

This investigation uses shale petrology to clearly characterize the depositional environment, and to better explain slake durability test results. The slake durability test, often used by engineers to evaluate shale weatherability, measures a rock sample's resistance to weakening and disintegration during a cycle of drying and wetting (Franklin and Chandra, 1972). Slake durability predictions, based on a practical, field classification for shales are also examined.

Samples were obtained from the Middle Pennsylvanian Breathitt Formation, which contains many coal seams resulting from cyclic sedi-

mentation (Wanless, 1975, p. 40). Breathitt sediments were deposited in numerous, deltaic sequences prograding into a shallow, epeiric sea (Baganz et al., 1975, p. 190). This depositional setting provides many, fine-grained units suitable for study, but they tend to be very discontinuous laterally, making correlation very difficult even for the coals, the most continuous facies in these units (Hester, 1977, p. 39). To examine lateral variations in correlative shale units, the field area was confined to the Vest Quadrangle in Knott County, Kentucky where three, recently drilled cores, and several geophysical logs were obtained within a 12.2 $mile^2$ (31.6 km^2) area (Fig. 1).

GEOLOGIC SETTING

Over 27,000 km^2 of Pennsylvanian rocks are exposed in eastern Kentucky (Rice et al., 1979, p. F-14). This study concentrates on Middle Pennsylvanian sediments deposited in the Pocohontas Basin, situated between the Dunkard and Warrior Basins. All three major basins are located in the Appalachian Plateau. A more detailed, regional setting for the Pocohontas Basin, as discussed by Horne and Ferm (1976, p. 3-6) follows.

The basin is elongate, extending from Tennessee, through most of eastern Kentucky and southern West Virginia. The folded Appalachian Mountains bound the basin to the east, while the Cincinnati Arch and the Nashville Dome form the western boundary. East-west trending, growth faults separate the Pocohontas Basin from the Dunkard Basin, to the north, and the Warrior Basin, to the south. Sedimentary deposits

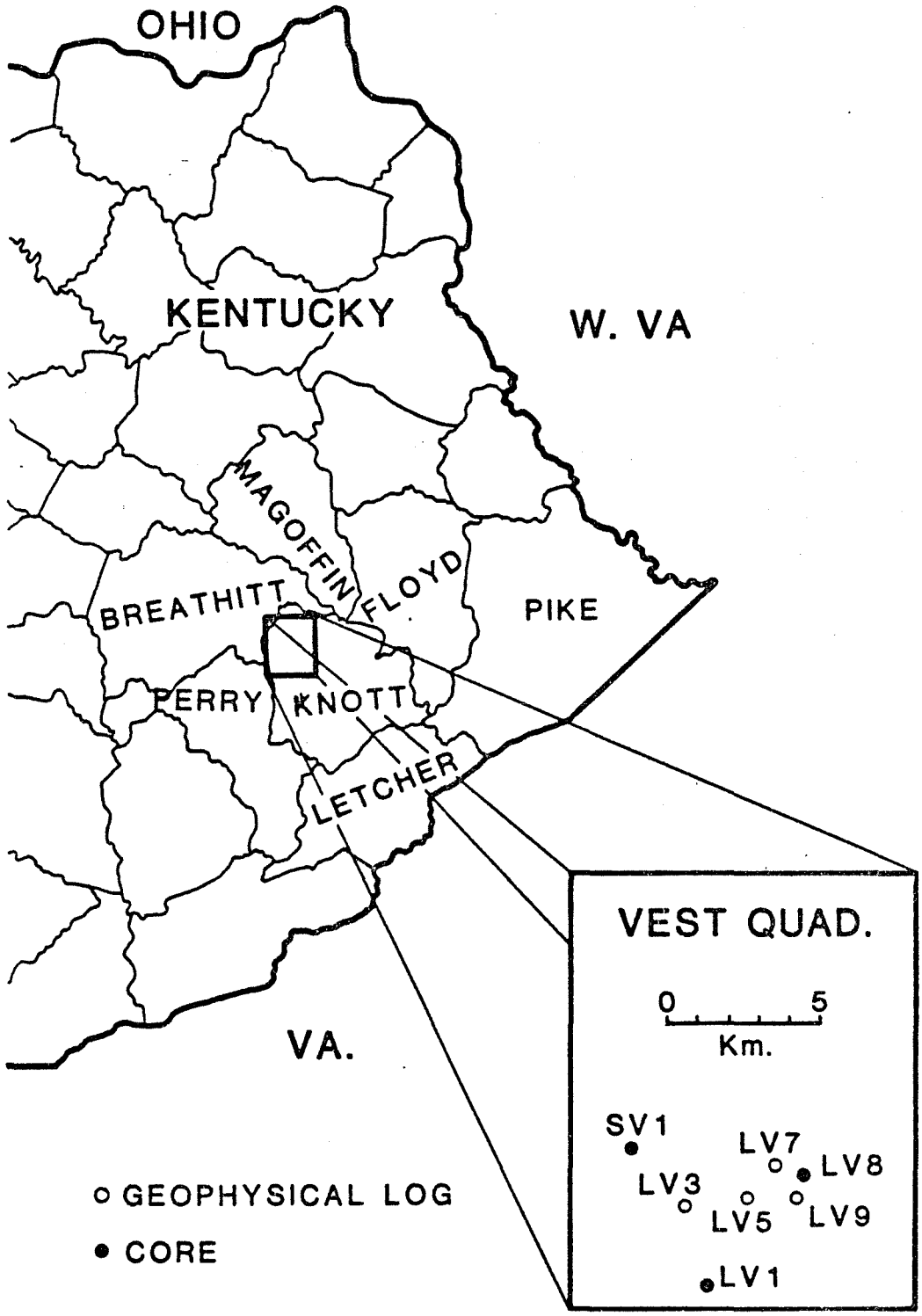

Figure 1. Location of study area, cores, and well logs.

begin a tenfold increase in thickness as they cross the Paint-Creek Fault Zone, at the basin's northern border. These faults have little or no surface expression (Smith, 1971, p. 2). Pennsylvanian sediments in the Pocohontas Basin, accumulated on the down-thrown (south) side of this fault system, where they expand to over 1,160 meters. Post-Carboniferous thrusting has altered the minor faults forming the basin's southern border, effectively concealing these structures.

No structural deformation exists in the Vest Quadrangle, Knott County, Kentucky, with Middle Pennsylvanian strata dipping gently (0.5°) to the east.

STRATIGRAPHY

Pennsylvanian stratigraphy in eastern Kentucky has been thoroughly described by Rice et al. (1979), Rice (1981), and Wanless (1975) with the following brief review compiled from all three sources. As Fig. 2 shows, the Lee, Breathitt, and Conemaugh Formations compose the entire Pennsylvanian section.

When the Mississippian Period drew to a close, predominantly marine deposition gave way to shallow water, clastic deposition in eastern Kentucky. As a result, the sparsely fossiliferous, red, green, and gray shales of the Mississippian Pennington Formation were, in places, unconformably overlain by the orthoquartzitic sands of the Pennsylvanian Lee Formation. The Lee has been divided into three members, which intertongue with the Breathitt Formation in Lower to Middle Pennsylvanian strata. Massive, pebbly orthoquartzites characterize the basal Livingston Conglomerate, Rockcastle Sandstone, and

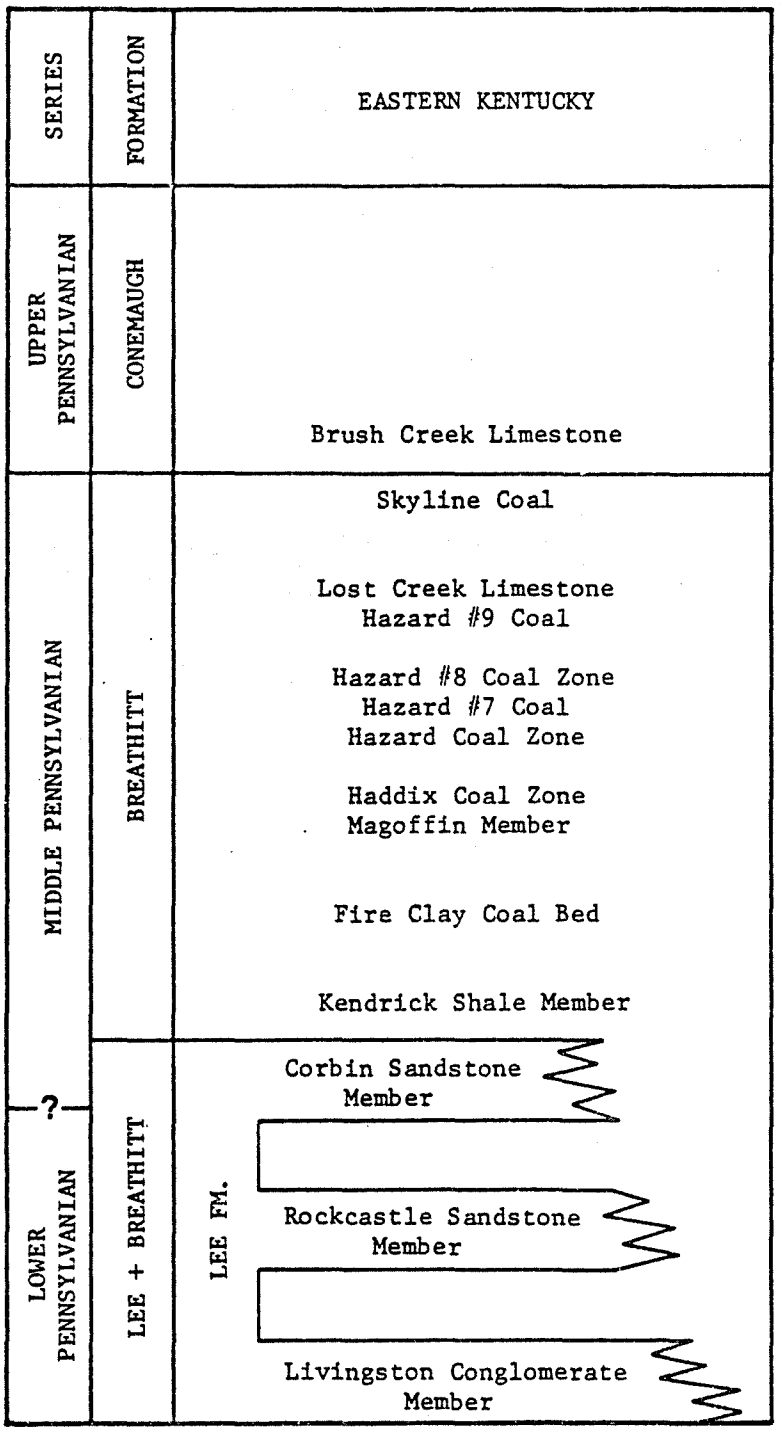

Figure 2. Generalized stratigraphy for Pennsylvanian rocks in eastern Kentucky, showing selected members and coal beds in the Breathitt Formation (modified from Rice, 1981, Fig. 1).

Corbin Sandstone Members.

Lithic graywackes, gray shales and siltstones, and coals characterize the Middle Pennsylvanian Breathitt Formation. Most economic coal beds in the Pocohontas Basin are found in this formation. This investigation deals primarily with the shales surrounding the Hazard Coals. Danilchik and Waldrop (1978) discuss the extent and thickness of the coals found in the Vest Quadrangle. The Hazard Coal Zone can be as thick as 12.0 meters, and contain as many as four coal beds, all less than 0.3 meters thick. The Hazard No. 7 Coal typically splits into numerous, thin coal beds in the southeast quarter of the quadrangle. The Hazard No. 8, or Francis Coal Zone, refers to a 6.0 meters thick, shale and coal sequence, in which combined coal thickness averages about 3.6 meters. The Hazard No. 9, or Hindman Coal, varies from 0 to 1.5 meters thick across the Vest Quadrangle, and has not been mined in the southeast quarter.

Rapid, lateral variations in lithology make it difficult to correlate these coal beds across the coal field. However, other beds can be used as stratigraphic markers within the Breathitt Formation. These include the Fire Clay Coal Bed, and the marine units, such as, the Kendrick Shale, the Magoffin Member, and the Lost Creek Limestone.

Erosion has removed the siltstones and shales of the Upper Pennsylvanian Conemaugh Formation from all but northeastern Kentucky.

CLASSIFICATION

Over the years, the term shale has developed two separate meanings.

One definition restricts shales to laminated, clay-rich rocks, while the other refers to the entire class of fine-grained rocks (Tourtelot, 1960, p. 342). Fine-grained rocks are those with over 50 percent of their components less than 62 microns in size. In this study, shale refers to the entire class of fine-grained rocks - not just the laminated variety.

Traditionally, color and fissility are used to classify shales (Pettijohn, 1975, p. 278). Classifications dependent on fissility, a shale attribute not exhibited in the subsurface (Spears, 1980), are restricted to field use, while two, recently proposed classifications (Picard, 1971; Lewan, 1978) are more applicable to the laboratory than to the field. This study requires a classification equally well suited to outcrop, subsurface, and laboratory work. Classifications based on texture (grain size), and presence or absence of laminae (Lundegard and Samuels, 1980; Potter et al., 1980, p. 16) most satisfactorily describe the coal measure shales in question, both in cores and thin sections.

The classification used (Table 1) is essentially that of Potter et al. (1980), modified by adding two new classes based on percent siderite (greater than 15 percent), and percent organic matter (greater than 20 percent). These two classes were added to accommodate shales that obviously contain abundant siderite either as nodules or thick laminae, and the black, organic-rich shales, both easily identified in core samples. Eight shale types were recognized (Plate 1): claystone, with 66-100 percent clay, and its laminated equivalent clayshale;

TABLE 1

CLASSIFICATION FOR COAL MEASURE SHALES

% CLAY SIZE CONSTITUENTS	0-32	33-65	66-100
MASSIVE	SILTSTONE	MUDSTONE	CLAYSTONE
LAMINATED	LAMINATED SILTSTONE	MUDSHALE	CLAYSHALE
> 15% SIDERITE	SIDERITIC SHALE		
> 20% ORGANICS	ORGANIC SHALE		

(modified from Potter et al., 1980, Table 1.2)

Plate 1. Typical slabbed cores of: A) claystone, B) clayshale, C & D) mudshale, E) siltstone, F) laminated siltstone, G) sideritic shale, and H) organic shale.

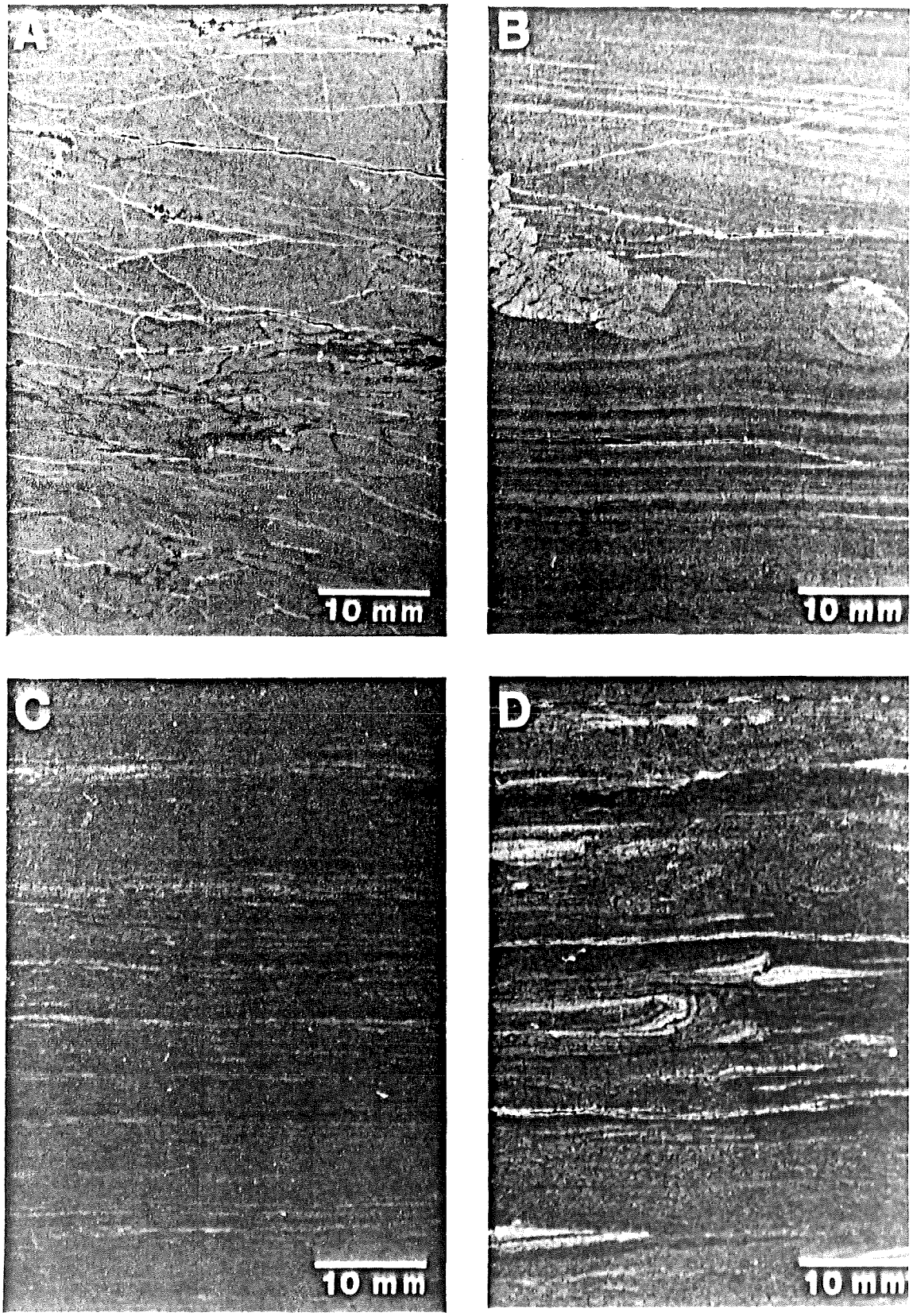
A
10 mm
B
10 mm
C
10 mm
D
10 mm

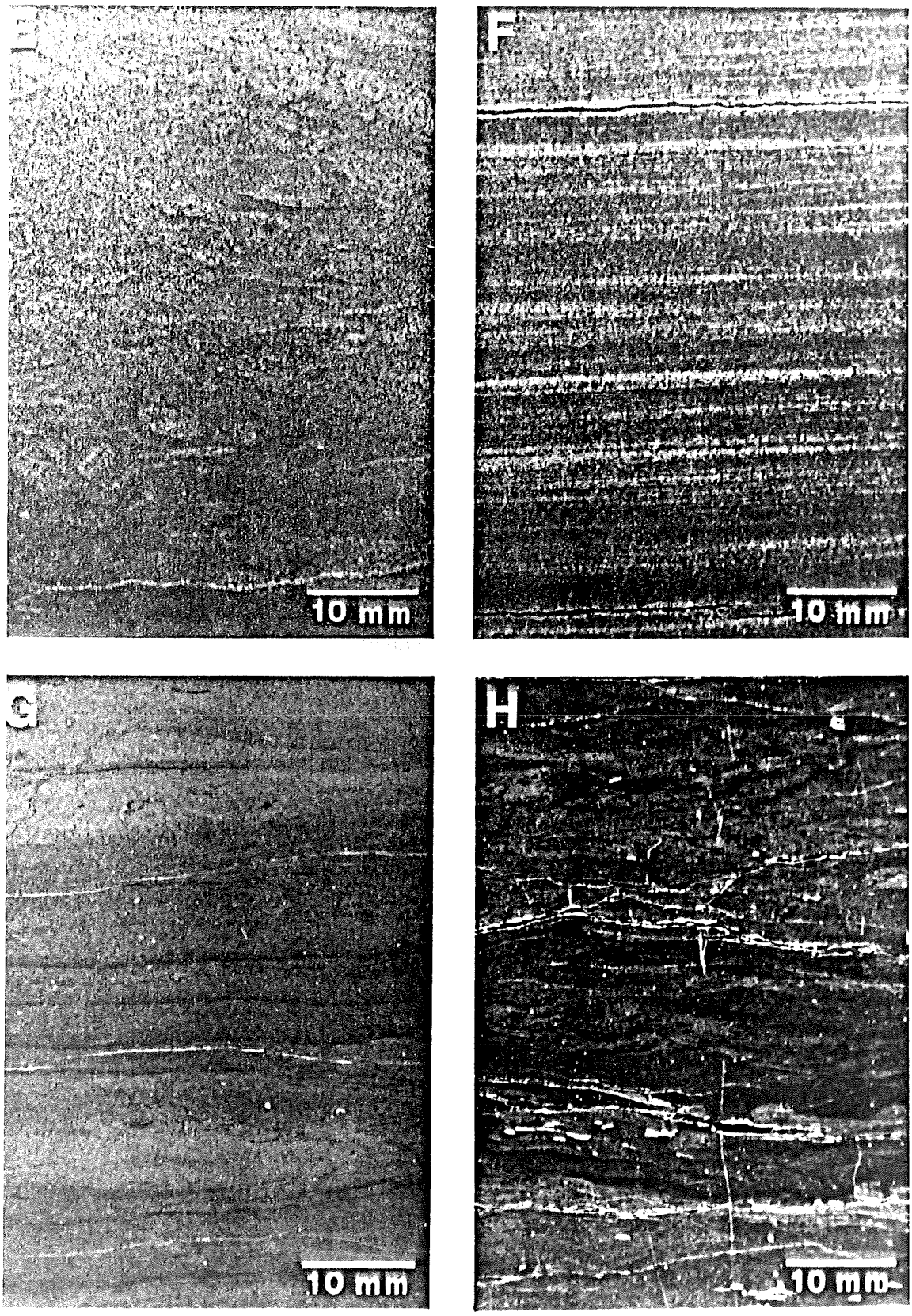
E
10 mm
F
10 mm
G
10 mm
H
10 mm

mudstone, with 33-65 percent clay, and its laminated equivalent mudshale; siltstone and laminated siltstone, with 0-32 percent clay; sideritic shale, with greater than 15 percent siderite; and organic shale, with greater than 20 percent organic material.

The term 'stone' applies to massive rocks, and the term 'shale' to rocks comprised of greater than 10 percent laminations (Lundegarde and Samuels, 1980, p. 783). Laminae are less than 10 mm. thick, and may result from changes in grain size, color, or fabric. Alternating layers of silt-sized quartz and clay minerals, commonly produce laminae in these shales. The quartz grains are rarely graded. Concentrations of either siderite or organic matter result in color laminae. Fabric laminae, resulting from the parallel arrangement of clay flakes, are only a few microns thick, very discontinuous in thin section, and nearly impossible to see in polished slabs. The terms even, wavy, discontinuous, and parallel or non-parallel (Fig. 3) describe laminae shape (Cole and Picard, 1975).

SHALE PETROLOGY

Complete description of shales involves both x-ray diffraction analyses, and thin section examination. X-ray diffraction identifies clay and carbonate minerals, and quantitatively determines clay mineral orientation. Thin section description provides information on overall composition, laminae, and biogenic structures. The procedures used are outlined below. The section entitled 'Petrographic Types' combines the results from all the analyses.

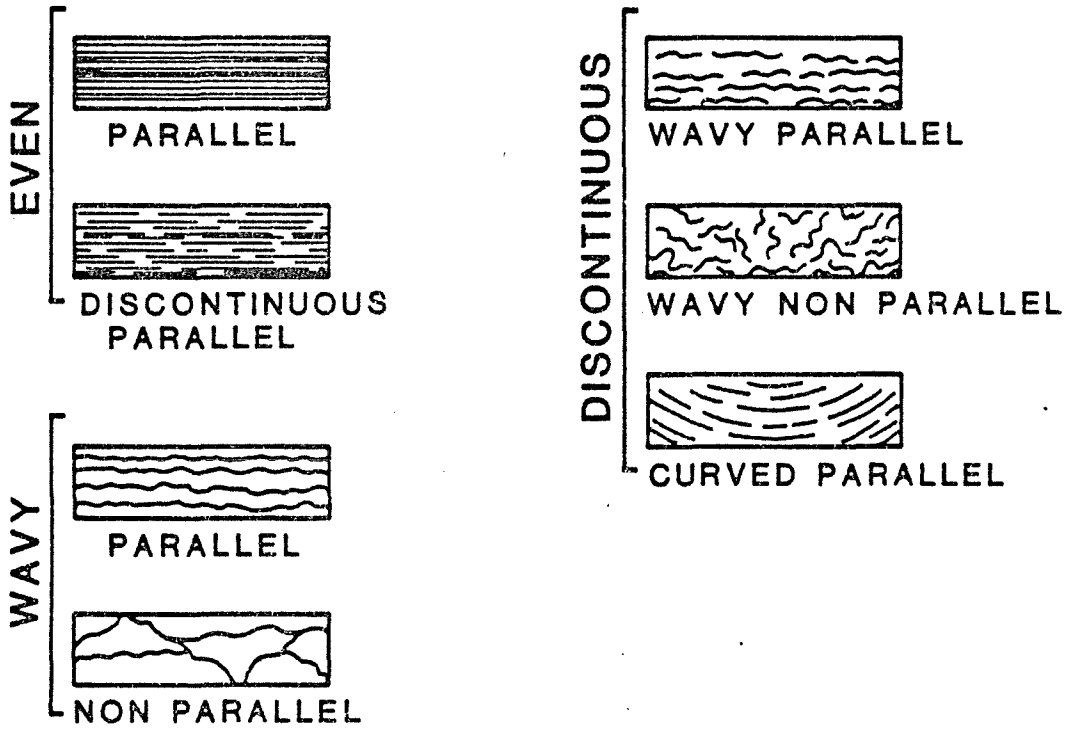

Figure 3. Shale laminae descriptions (from Cole and Picard, 1975, Fig. 2).

Methods

Representative samples were selected from each of the three, described cores, and divided so that approximately 300-400 grams could be saved and used later in the slake durability test. The remainder was then embedded in a plastic casting resin to help prevent any destruction resulting from parting or slaking during further preparations.

Two chips were cut from each embedded sample, one perpendicular to bedding, and one parallel to bedding. Both chips were then polished on progressively finer, carborundum sandpaper until all scratches were removed, and a perfectly flat surface obtained. After grinding, the chips were approximately 8 mm. thick. Three separate x-ray diffraction traces were obtained from each chip, using a General Electric XRD-5, x-ray diffraction unit.

The fabric index (FI), a measure of the clay mineral orientation, was calculated using the equation:

$$FI = V/(P+V)$$

where V= peak height from the perpendicular chip, and P= peak height from the parallel chip (Fig. 4) (Odom, 1967, p. 611). Three separate runs allowed averaging the peak heights, as recommended by Meade (1961, p. B-276). The above equation yields values ranging from 0.0 (perfect orientation) to 0.5 (random orientation). Odom (1967, p. 613) associated fabric indices to the degree of clay mineral orientation as follows:

0.0

Very Good

0.10

Good

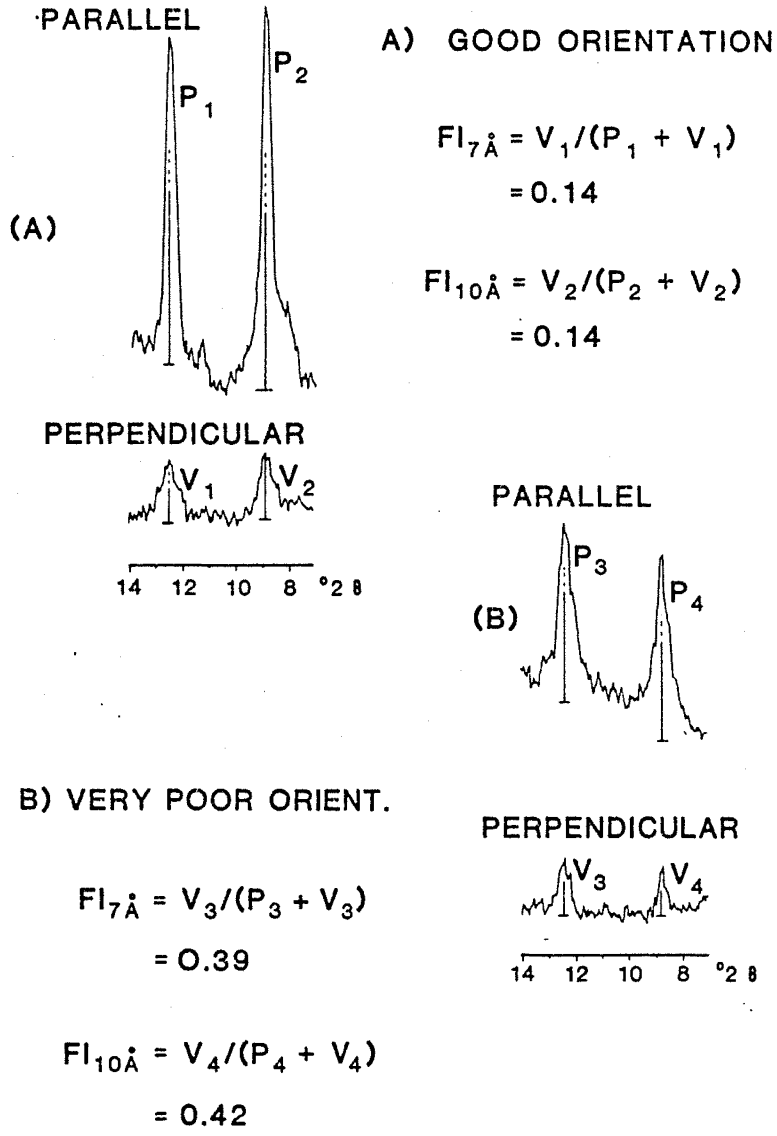

Figure 4. Technique used in determining the 10 angstrom and 7 angstrom clay mineral orientations (fabric indices).

0.20

Fair

0.30

Poor

0.40

Very Poor

0.50

The chip cut perpendicular to bedding was then used to make ultra-thin, thin sections, approximately 10 microns thick. Two hundred points were counted on a Zeiss, student microscope at a magnification of 500X, as suggested by Broadhead and Potter (1980, p. 6). Seven components were recognized (Table 2): clay, mica, quartz and feldspar, carbonate, organics, pyrite, and others. Several textural parameters were noted, including quartz grain size, largest mica, and sorting of the quartz and feldspar fraction. Fifty grains were measured to arrive at the average quartz size. The long axis of several, randomly chosen micas in each thin section were also measured. Laminae thickness, shape, and contacts with the surrounding matrix were noted.

Semi-quantitative, clay mineral analyses were performed on several samples, by first suspending the less than 2 micron size fraction in water. Using the techniques of Kinter and Diamond (1965), two, oriented clay mineral mounts were made for each tested sample. One oriented mount was air-dried, and then analyzed on the x-ray diffractometer, subsequently solvated with ethylene glycol, and analyzed again. The second oriented mount was heated to 350°C., analyzed, then heated to 550°C., and analyzed again. These procedures permitted accurate identification of the clay minerals present, and an estimation of their relative abundance.

TABLE 2

SUMMARY OF SHALE COMPONENTS

*Quartz: Monocrystalline, angular to sub-rounded, equant to elongate, straight extinction common.

*Feldspar: Fresh, twinned plagioclase, or orthoclase partially altered to clay.

Clay Minerals: Identified as illite, mixed-layer (illite-smectite), kaolinite, and chlorite. Less than 20 microns.

Micas: Commonly muscovite and chlorite, with very rare biotite. Greater than 20 microns.

Organics: Opaque, amorphous material, and translucent, amorphous, reddish-orange material. Opaque matter dominates.

Pyrite: Ubiquitous, pyritized organics, rare euhedral grains.

Carbonate: Identified as siderite. Occurs as disseminated anhedral to euhedral grains, cements, nodules, or laminae.

Others: Trace amounts of zircon, hornblende, tourmaline, and chert.

* Quartz and feldspar counted together.

Sixty-two polished slabs were assigned rock names, and approximate clay percentages based on comparisons with similar samples examined in thin section. Additionally, selected samples were studied with a scanning electron microscope to inspect clay mineral orientation effects on porosity.

Clay Mineral Orientation

Optical and scanning electron microscopy can be used to qualitatively examine clay mineral orientation. However, x-ray diffraction techniques are considered superior, providing quantitative results for several different clay minerals (Tchalenko et al., 1971, p. 69). The principles involved are straight-forward. X-ray diffraction intensity varies with the amount and orientation of the clay minerals within the analyzed area. Peak heights, the vertical distance from the peak maxima to the base line (Kazi, 1975, p. 883), serve to measure the diffraction intensity. The fabric index equation $FI = V/(P+V)$, compares the relative abundance of clay minerals with basal planes oriented in the plane of the perpendicular section to the relative abundance of the same minerals with basal planes oriented in the plane of the parallel section (Odom, 1967, p. 611). Using this ratio effectively cancels out any changes in intensity caused by variations in crystallinity or clay mineral abundance (Meade, 1961, p. B-276).

The 7Å and 10Å reflections occur consistently in all the samples tested, and fabric indices were calculated for both. In almost every case, the 7Å and 10Å indices are slightly different, resulting from

the presence of muscovite and micaceous chlorite in many samples. These micas do not exhibit the same degree of uniform extinction as the surrounding clay matrix, when examined in thin section. To alleviate this discrepancy, the 7Å and 10Å fabric indices were averaged (Table 3). This "average orientation" provides a more complete description of the overall shale fabric.

Gipson (1965), and O'Brien (1970) relate preferred clay mineral orientation to shale fissility. Assuming that a fissile shale is more susceptible to physical breakdown (slaking), the factors controlling clay mineral orientation could be significant to this investigation. However, the effect different variables have on shale fabric is controversial, as the following conclusions from Odom (1967), and Gipson (1966) indicate. Orientation improves as organic matter becomes more abundant, while preferred orientation diminishes with an increase in silt, and carbonate content. Both authors agree that overburden weight does not effect orientation, but disagree on improved orientation with increasing clay content. More recently, Spears (1976, p. 724), and Curtis et al. (1980, p. 338) concluded that fissility is dependent on shale laminae, and that although bioturbation may destroy these laminae, the shale fabric is left undisturbed.

Clay Mineralogy

The clay mineralogy seems to be relatively constant throughout the stratigraphic interval studied, judging by the similar diffraction patterns acquired from the orientation analysis. To determine exactly how

TABLE 3

CLAY MINERAL ORIENTATION RESULTS
(FIx100)

SAMPLE	10Å°	7Å°	AVERAGE ORIENTATION
SV1-1	23	25	24
SV1-3	18	28	23
SV1-8	25	32	28
SV1-10	29	36	33
SV1-13	17	26	22
SV1-14A	12	26	19
SV1-16	11	19	15
SV1-17	15	23	19
SV1-18A	15	25	20
SV1-19	15	23	19
SV1-20	15	18	16
SV1-22	14	21	18
SV1-25A	22	24	23
SV1-32	23	37	30
SV1-32A	18	33	26
SV1-33	10	16	13
SV1-36	16	28	22
SV1-39	20	21	21
SV1-40	22	22	22
LV8-3	27	27	27
LV8-6	17	18	18
LV8-9	22	26	24
LV8-10	18	20	19
LV8-12	18	27	22
LV8-13	30	25	28
LV8-14	10	14	12
LV8-17	10	16	13
LV8-19	27	33	30
LV8-21	21	26	24
LV8-22	17	26	22
LV8-25	12	15	14
LV8-38	16	31	24
LV8-42	32	32	32
LV1-1	16	24	20
LV1-6	42	39	41
LV1-7	13	17	15
LV1-11	11	17	14
LV1-12	18	30	24
LV1-13	11	17	14
LV1-14	17	17	17
LV1-16	42	39	41
LV1-30	14	14	14
LV1-31	12	13	12
LV1-33	17	27	22
Lv1-34	17	27	22
Lv1-37	26	32	29
LV1-41	32	33	32

much, if any, variation exists in the clay mineralogy, samples displaying the most widely differing macroscopic characteristics were selected for the clay mineral analysis.

After interpreting the air-dryed, glycolated, and heated (to 350° and 550° C.) diffraction traces (Fig. 5), four clay minerals, illite, expandable mixed-layer, kaolinite, and chlorite, were identified. The broad peak on the low angle side of the 10Å, air-dryed reflection is produced by the expandable component (smectite) in the mixed-layer clay. Upon heating to 350° C., this peak intensifies as the expandable layer collapses. Following treatment with ethylene glycol, the 10Å peak area represents only pure illite, the smectite layers having expanded to a higher d spacing (Hosterman and Loferski, 1978, p. 11). Kaolinite loses its crystallinity after heating to 550° C., causing the 7Å peak to almost completely disappear. The 14 Å peak intensifies, and shifts to 13.8 Å at 550° C., an indication that a Mg-chlorite is present (Chen, 1977, p. 46). Kaolinite and chlorite were differentiated using the couplet at 3.54 Å (chlorite), and 3.58 Å (kaolinite).

Percentages of the various clay components were calculated using the weighting factors of Biscaye (1965), Johns et al. (1954), and the following equations:

$$(A)(100)/(A+B) = \%\ \text{illite}$$
$$(B)(100)/(A+B) = \%\ B$$
$$(C)(\%B) = \%\ \text{kaolinite}$$
$$\%B - \%\ \text{kaolinite} = \%\ \text{chlorite}$$
$$(D)(100)/(A_1-D) = \%\ \text{mixed layer}$$

Where; A = area under the 10A glycolated peak x 4
A_1 = area under the 10A glycolated peak
B = area under the 7A air-dryed peak
$\%B$ = relative amount of kaolinite + chlorite

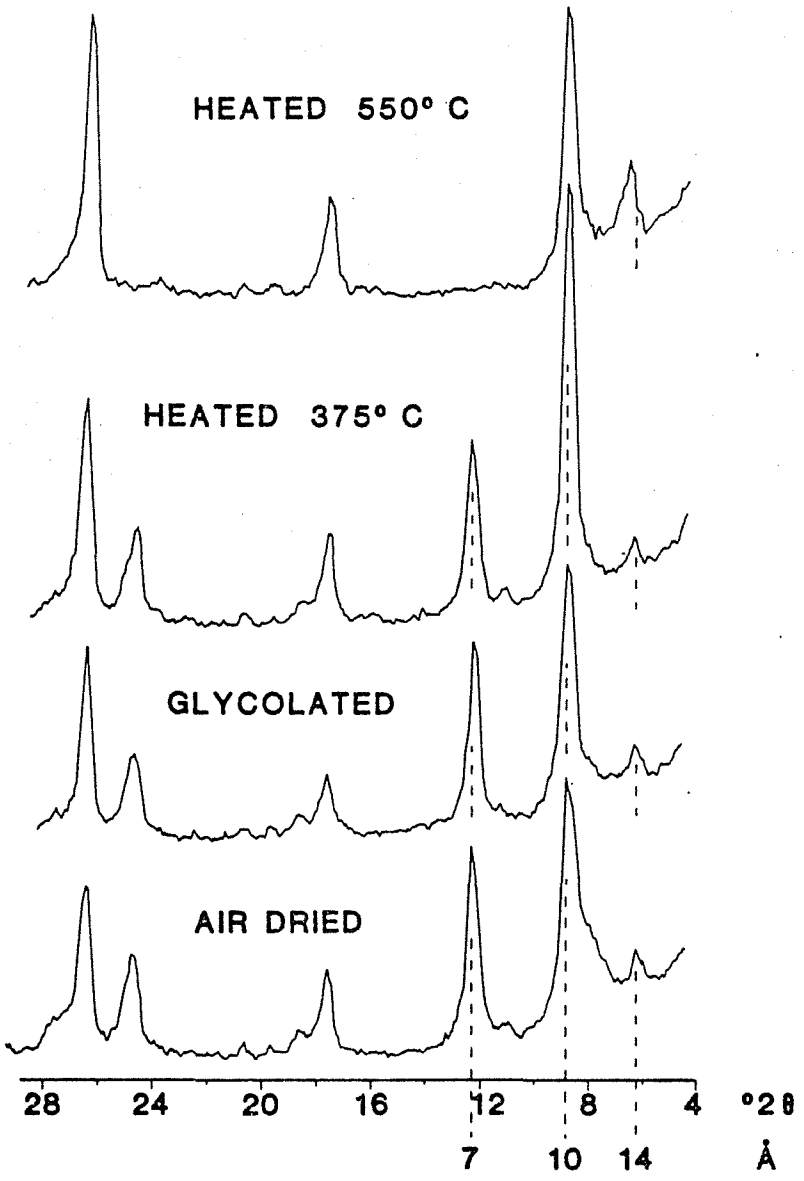

Figure 5. Typical diffraction traces, obtained from one of the sampled Breathitt Fm. shales, indicate the presence of illite, expandable mixed-layer, kaolinite, and chlorite.

TABLE 5

AVERAGE COMPOSITION FOR EACH SHALE TYPE
(Percent)

SHALE TYPE	CLAY	QUARTZ + FELDSPAR	MICA	ORGANICS	PYRITE	CARBONATE	OTHERS
Claystones	77.1	6.9	5.9	6.5	2.1	1.4	0.1
Clayshales	78.3	7.7	5.0	5.7	1.3	1.5	0.5
Mudstones	45.6	28.8	14.8	4.9	1.7	3.9	0.4
Mudshales	43.7	24.3	17.0	8.2	1.2	5.2	0.3
Siltstones	29.8	43.0	15.0	4.5	2.1	5.5	0.1
Lam. Silt-stones	28.5	41.2	13.0	6.0	2.2	9.0	-
Sideritic Shales	53.8	12.2	7.9	4.0	2.1	19.8	0.2
Organic Shales	65.0	3.0	1.2	27.5	3.2	-	-

TABLE 6

AVERAGE TEXTURAL PARAMETERS FOR EACH SHALE TYPE
(Microns)

SHALE TYPE	AVERAGE QUARTZ SIZE	LARGEST QUARTZ	LARGEST MICA	CLAY ORIENTATION
Claystones	14.8	62.8	70.6	0.26
Clayshales	9.6	29.2	70.8	0.15
Mudstones	28.0	84.4	178.6	0.22
Mudshales	29.8	80.8	176.4	0.21
Siltstones	43.6	134.4	202.5	0.25
Lam. Silt-stones	37.6	98.1	193.8	0.24
Sideritic Shales	19.9	48.8	103.1	0.17
Organic Shales	10.0	30.0	31.2	0.28

percent, averaging 6.9 percent. The quartz grains are angular to subangular, elongate to equant, and very well sorted. Average grain size varies from 2.5 to 187.5 microns, averaging 14.8 microns. Quartz is monocrystalline with straight extinction, and is found scattered throughout the clay matrix, except in rare cases, where it is concentrated in remnant silt laminae. No feldspars were observed, but x-ray diffraction indicates their presence.

Clay minerals are the dominant components, varying from 67 to 89 percent, averaging 77.1 percent. Clays are light brown and light green in thin section, and have been identified as mostly illite and mixed-layer (illite-smectite), with lesser amounts of kaolinite and chlorite. The clay minerals seldom display uniform extinction, which is in accord with fabric indices ranging from 0.17 (good) to 0.42 (very poor), and averaging 0.26 (fair). Equidimensional kaolinite booklets up to 9 microns wide were observed.

Micas consist of muscovite and chlorite in amounts ranging from 2 to 9 percent, and average 6.9 percent. The largest micas are between 27.5 and 125.0 microns long, and average 70.6 microns in length. Micas are oriented either parallel or subparallel to bedding.

Claystones contain from 3 to 12 percent organic material, averaging 6.5 percent. Opaque, amorphous, black material is much more abundant than translucent, amorphous, orange-red material. Very fine, disseminated opaque matter is ubiquitous, and spheroidal masses up to 30 microns in diameter are rare. These pellet-like structures are commonly aggregated, and arranged diagonally, cutting across bedding,

as do burrows. Translucent material regularly appears as strands up to 4 mm. long. Most claystones are rooted, with rootlets comprising much of the organic material.

Pyrite varies from trace amounts to 7 percent, averaging 2.1 percent. Finely disseminated, anhedral crystals are ubiquitous. Euhedral crystals up to 12 microns wide are also present. Most opaque, amorphous, black organic matter is pryritized.

Carbonate, identified as siderite by x-ray diffraction, is seldom present in claystones, and occurs only in trace amounts, or rarely up to 8 percent, with an average of 1.4 percent. Disseminated grains 120.0 microns wide, appear similar to radiaxial fibrous cements. Siderite is commonly associated with burrows.

Mudstones: The quartz and feldspar fraction ranges from 12 to 48 percent, averaging 28.8 percent. These grains are subangular to angular, elongate to equant, and well sorted. Grain size varies from 2.5 to 155.0 microns, and averages 28.0 microns. Quartz grains are monocrystalline and clear, with only rare inclusions. Straight extinction is more characteristic than undulose extinction. Twinned plagioclase, and feldspars partially altered to clays are present in small quantity.

Clays may be the dominant component, or be subordinate to silt in the mudstone group. Amounts vary from 33 to 65 percent, averaging 45.6 percent. This wide variation produces a notable difference between the clay-rich muds (50 to 65 percent clay), and the silt-rich muds (33 to 50 percent clay). Although this differentiation is easily made in thin section, it was judged too difficult to use in the field,

and was not pursued. The clay fraction consists mostly of illite and mixed-layer (illite-smectite), with lesser amounts of kaolinite and chlorite. Fabric indices vary from 0.10 (good) to 0.33 (poor), with an average value of 0.22 (fair).

Micas range from 6 to 20 percent, averaging 14.8 percent. Muscovite is most abundant, followed by chlorite and very rare biotite. The largest micas have lengths from 75.0 to 225.0 microns. Long axes may be oriented parallel or almost perpendicular to bedding.

Opaque, amorphous organic matter exceeds that of the translucent, reddish-orange variety in all cases. Total organics vary from trace amounts to 12 percent, and average 4.9 percent. The opaque material occurs as small disseminated grains, large irregular particles 1.5 mm. long, or spheroidal masses 15.0 microns in diameter. Strands of translucent material up to 700.0 microns long, result from rooting. Organic matter is commonly squashed, or bent around quartz grains.

Pyrite occurs in pyritized organic matter, and as very rare, small disseminated grains. Amounts range from trace values to 3 percent, averaging 1.7 percent.

Siderite varies from trace amounts to 13 percent, averaging 3.9 percent. Elongate patches up to 130.0 microns long are arranged parallel to bedding. These patches may appear opaque, resulting from concentrations of many, small (less than 2 microns) siderite rhombs and intermixed clay. Siderite also appears as nodules 4.5 x 1.2 mm., or as rare, euhedral rhombs 105.0 microns wide.

Chert, and the heavy minerals zircon and tourmaline commonly occur

in trace amounts.

Mudshales: Compositionally, mudshales are very similar to mudstones. Only the minor variations in abundance and size of the major components are discussed.

Quartz and feldspar range from 16 to 42 percent, averaging 24.3 percent. Grain size varies from 2.5 to 165.0 microns, and averages 29.8 microns.

Clays vary from 33 to 57 percent, averaging 43.7 percent. Fabric indices range from 0.14 (good) to 0.41 (poor). This unusually poor orientation for a laminated shale, most likely results from bioturbation. The average fabric index is 0.21 (good).

The amount of mica varies from 13 to 27 percent, and averages 17.0 percent, with the largest micas ranging from 20.0 to 350.0 microns long, averaging 176.4 microns in length.

Organics range from 3 to 13 percent, and average 8.2 percent. Rooting is absent in these laminated rocks. Mudshales contain up to 3 percent, pyritized organic matter. Pyrite averages 1.2 percent.

Siderite varies from trace amounts to 11 percent, averaging 5.2 percent. Irregular patches may be 112.0 microns long, and isolated, anhedral crystals up to 35.0 microns wide were noted.

Mudshales contain silt, clay, organic, and sideritic laminae. Silt, clay, and organic laminae may occur together, although alternating silt and clay are the most typical combination. Silt laminae, consisting of poorly sorted quartz grains, which float in a clay matrix, range from 0.2 to 2.2 mm. thick. Long and point grain-to-grain contacts

are common.

Organic laminae 0.1 to 0.2 mm. thick, consist of abundant, long, thin, parallel strands of organic material, interspersed with clay and silt. Sideritic laminae contain concentrations of siderite and clay, and average 2.4 mm. thick. Silt and clay laminae are even parallel, even discontinuous parallel, or discontinuous wavy parallel. Organic laminae are discontinuous. Sideritic laminae are even parallel. Contacts with the surrounding rock are commonly gradational, and rarely sharp.

Siltstones: Quartz and feldspar range from 37 to 54 percent, averaging 43.0 percent. The grains are subrounded to angular (mostly subangular), and poorly sorted, with sizes varying from 5.0 to 225.0 microns. The average grain size is 43.6 microns. Quartz is dominantly monocrystalline, but rare polycrystalline grains are present. Both straight and undulatory extinction are common. Twinned plagioclase, and orthoclase partially altered to clay are relatively abundant (approximately 5 percent).

These fairly clay-rich siltstones contain clay in amounts from 29 to 31 percent, averaging 29.8 percent. Illite and mixed-layer (illite-smectite) are the most abundant clay minerals, followed by kaolinite and chlorite. Fabric indices range from 0.22 (fair) to 0.30 (poor), with an average of 0.25 (fair).

Micas consist predominantly of muscovite and chlorite, along with rare biotite. Amounts range from 12 to 23 percent, and average 15.0 percent. Largest micas vary from 20.0 to 270.0 microns long, with the

average long axis being 202.5 microns in length. Micas are commonly oriented subparallel to bedding, and often bend around quartz grains.

Opaque, amorphous, organic matter dominates over the translucent, reddish-orange variety. Total organics vary from 1 to 8 percent, averaging 4.5 percent. Rooting accounts for most organic material, but opaque organics are scattered throughout the matrix. Some organic matter is aligned parallel to bedding.

Pyrite ranges from trace amounts to 3 percent, averaging 2.1 percent. Pyritized organics are common, while disseminated grains occur only rarely.

Siderite occurs as isolated crystals, and elongate, irregular patches from trace amounts to 15 percent, averaging 5.5 percent. Subhedral to euhedral rhombs range in size from 18.0 to 60.0 microns. Siderite replacing quartz is rare.

Trace amounts of chert, zircon, and tourmaline are present.

Laminated Siltstones: Compositionally, laminated siltstones are essentially the same as siltstones, and only the slight differences in abundance and grain size, of the major components, are discussed.

Quartz and feldspar vary from 32 to 51 percent, and average 41.2 percent. The moderately sorted grains range from 5.0 to 130.0 microns, averaging 37.6 microns.

Laminated siltstones contain clay in amounts from 21 to 32 percent, with an average of 28.5 percent. Fabric indices between 0.19 (good) and 0.32 (poor) exist, and average 0.24 (fair).

Micas are present in amounts from 9 to 18 percent, averaging 13.0

percent. Largest micas range from 100.0 to 250.0 microns long, with the average long axis being 193.8 microns.

Organics range from 3 to 10 percent, averaging 7.2 percent. Organic matter is concentrated in laminae, or results from rooting.

Pyrite is either absent or very rare, the greatest amount being 2 percent, with an average of 0.9 percent.

Siderite ranges from 2 to 14 percent, and averages 9.0 percent. Siderite occurs as euhedral rhombs 62.5 microns wide, and as very fine grains concentrated in small, nodule-like masses.

Silt, clay, and organic laminae are present in laminated siltstones. Silt and clay laminae commonly alternate. Silt laminae, 0.12 to 2.4 mm. thick, are composed of poorly sorted quartz grains, floating in a clay matrix. Reverse grading of the quartz grains is rare. Organic laminae consist of thin, parallel strands of translucent, reddish-orange, organic matter concentrated in laminae 0.08 to 1.0 mm. thick. Clay laminae, 0.12 to 2.4 mm. thick, are produced by well oriented clay minerals interspersed with fine silt and siderite. Most silt and clay laminae are even parallel, or discontinuous wavy parallel. Organic laminae are discountinuous wavy parallel. In all samples, contacts with the surrounding rock are gradational.

Clayshales: Clayshales are similar to claystones except for the presence of laminae, and much better clay mineral orientation. Fabric indices range from 0.12 to 0.19 (both good), and average 0.15 (good). This is the best orientation exhibited by any of the eight petrographic types.

Plate 2. Photomicrographs of: A) claystone, B) clay-shale, C) mudstone, D) mudshale, E) siltstone, F) laminated siltstone, G) organic shale, and H) sideritic shale.

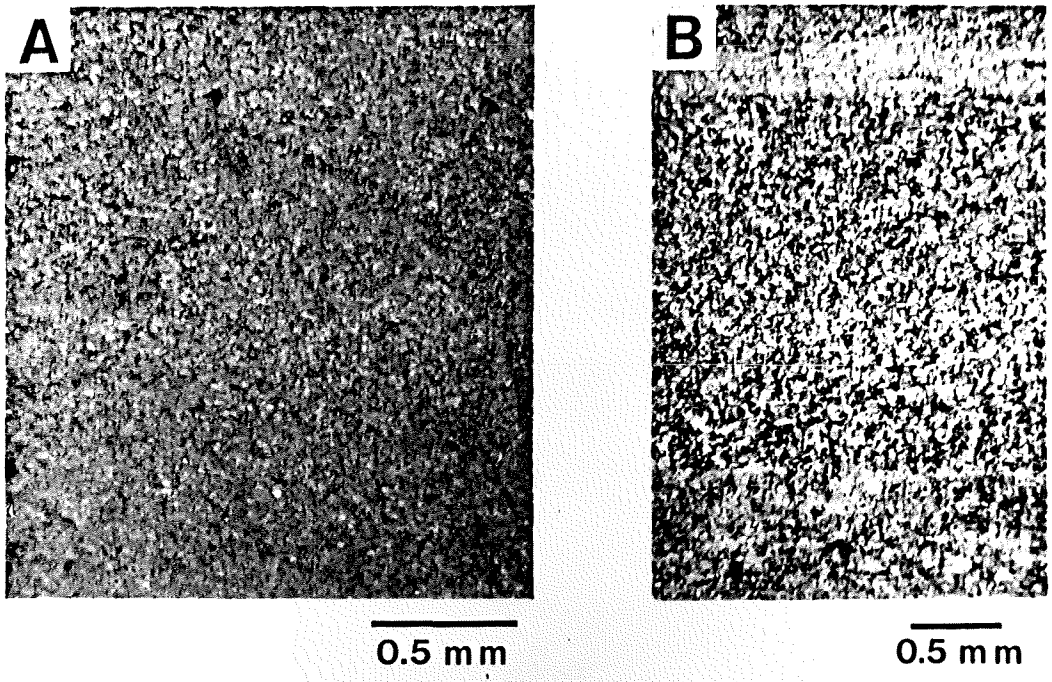
A
0.5 mm
B
0.5 mm
C
0.5 mm
D
0.5 mm

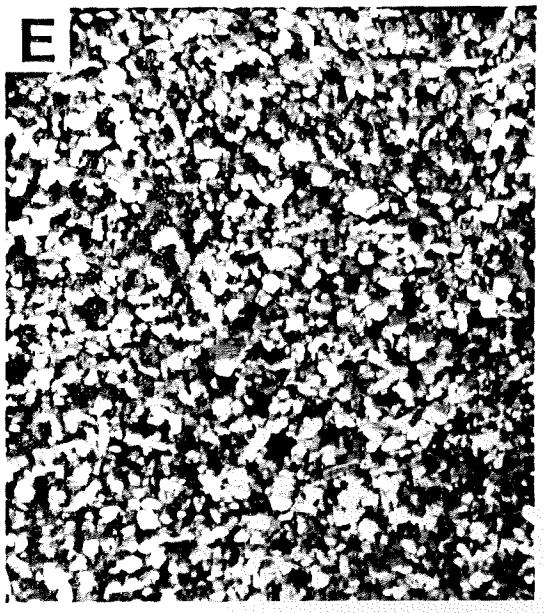

0.5 mm

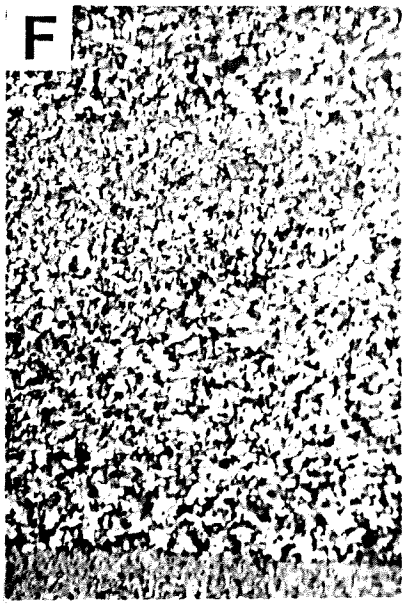

0.5 mm

.15 mm

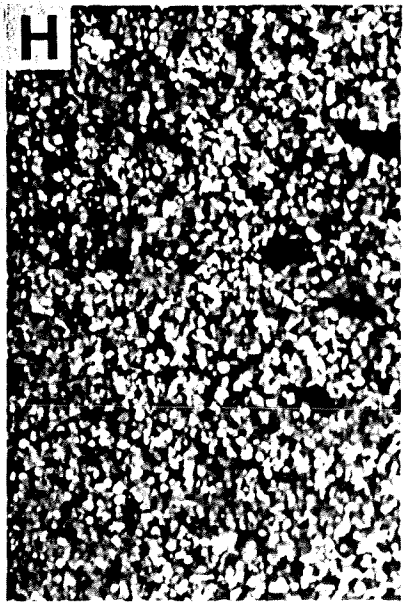

.05 mm

Organic, sideritic, and clay laminae are present in clayshales. Clay laminae, up to 0.2 mm. thick, consist of well oriented, pure clay layers. Organic laminae, 0.1 to 0.9 mm. thick, are characterized by elongate strands of organic matter, along with interspersed clay, and poorly sorted quartz grains. Sideritic laminae, 0.1 to 0.7 mm. thick, result from concentrations of abundant siderite, combined with silt and clay. Organic laminae are even parallel, or discontinuous wavy parallel. Clay laminae are even parallel, and sideritic laminae are discontinuous wavy parallel. Contacts with the surrounding matrix are gradational.

Sideritic Shales: Clay content varies from 22 to 78 percent, while quartz and feldspar range from 1 to 33 percent. As indicated by these values, sideritic shales may have the textures of silts, muds, or clays.

Siderite ranges from 17 to 22 percent, averaging 19.8 percent. Elongate, nodule-like patches, parallel to bedding are common, and subhedral to euhedral crystals, as large as 45 microns, are rare. Siderite occurs as nodules, laminae, cements, and very fine, disseminated grains.

Although the classification does not require laminae for this shale type, most samples do contain either organic or sideritic laminae, often occurring together. Organic laminae are thin, 0.01 to 0.3 mm., discontinuous wavy parallel, and composed of long, stringy, organic matter. Sideritic laminae, 1.2 to 5.0 mm. thick, are commonly discontinuous wavy parallel. Both types have gradational contacts with the surrounding rock.

Organic Shales: These shales would normally be classified as claystones, but organic material is unusually abundant (20 percent or greater), making them quite distinctive, and easily differentiated from other claystones.

Total organics vary from 24 to 31 percent, averaging 27.5 percent. Opaque, amorphous organics occur as very fine, disseminated grains. Both the opaque material and the translucent, reddish-orange material form long strands (5 mm.), which are contorted and bent in a completely random fashion. In other instances, the organics form thick, 0.04 to 2.4 mm., discontinuous wavy parallel laminae. Contacts with the surrounding matrix are sharp.

DEPOSITIONAL ENVIRONMENT

Throughout Pennsylvanian time, deltas deposited a thick, clastic wedge of sediments in eastern Kentucky (Rice et al., 1979, p. F-14; Wanless, 1975, p. 40). In the Pocohontas Basin, deposition was greatly influenced by the growth faults associated with the Paint Creek Fault Zone. The increase in basin subsidence, created by these faults, produced not only thicker sedimentary accumulations, but also concentrated deposition in a smaller area, allowing similar environmental units to stack vertically, one upon another (Ferm, 1974, p. 93). Vertically stacked upper delta plain deposits, just west of the Vest Quadrangle, have been documented (Cobb et al., 1981; Dever, 1971). These previous interpretations, support this author's conclusion that an upper delta plain environment extended across the Vest Quadrangle

during Middle Pennsylvanian time, and accounted for sediments over 100 meters thick, an interval extending from the Haddix Coal to the Skyline Coal (Fig. 6).

The upper delta plain is one of three commonly accepted environments in the delta complex, lying between the lower delta plain and the alluvial plain, as shown in Fig. 7 (Donaldson, 1979; Ferm et al., 1971). Thick, interdistributary bayfill shale sequences, and distributary mouth bar sands dominate lower delta plain deposits, while distributary channel sands (primarily point bar deposits), and thin, floodplain shales characterize the alluvial plain. The upper delta plain contains elements common to both the lower delta plain and the alluvial plain, including shallow interdistributary bays and distributary channels.

Lithologies existing in the upper delta plain are discussed in greater detail on the following pages, with special emphasis on the interdistributary bayfill shales. Features characterizing the several, upper delta plain facies identified in the three cores described for this study (Appendix V) have been summarized from the works of Horne and Ferm (1976), Flores and Arndt (1979), and Donaldson (1979).

Distributary Channels: Sand is much more abundant than shale in the upper delta plain, ranging in thickness from 15 to 24 meters, and extending from 2 to 11 km. laterally. Such massive, linear, lenticular sand bodies developed as distributary channels migrated across the delta, allowing point bar deposits to coalesce and stack upon each other.

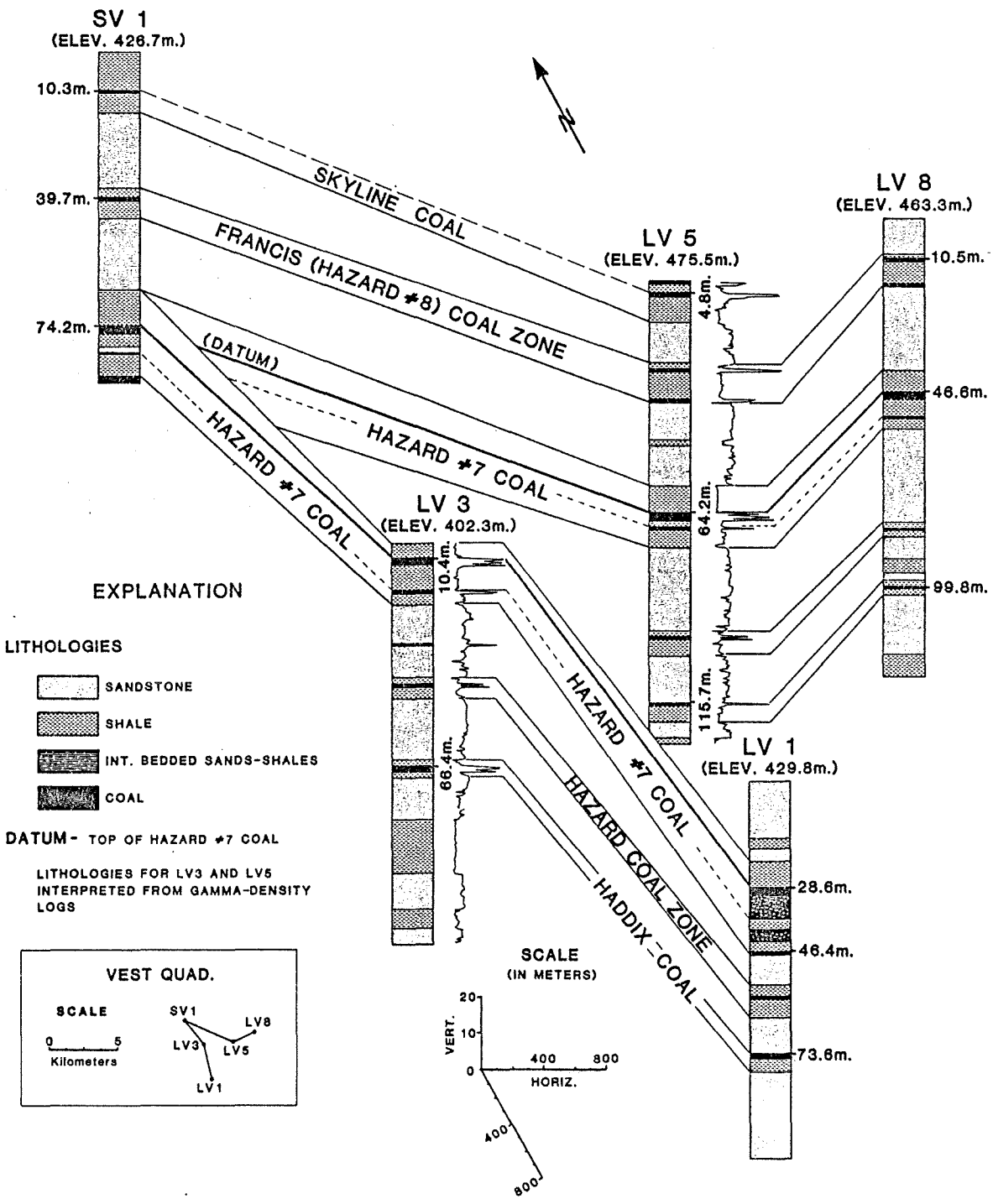

Figure 6. Correlation of fine-grained units associated with the major coal seams in the Breathitt Formation. Figs. 8-10 describe the shales surrounding the Hazard coals in greater detail.

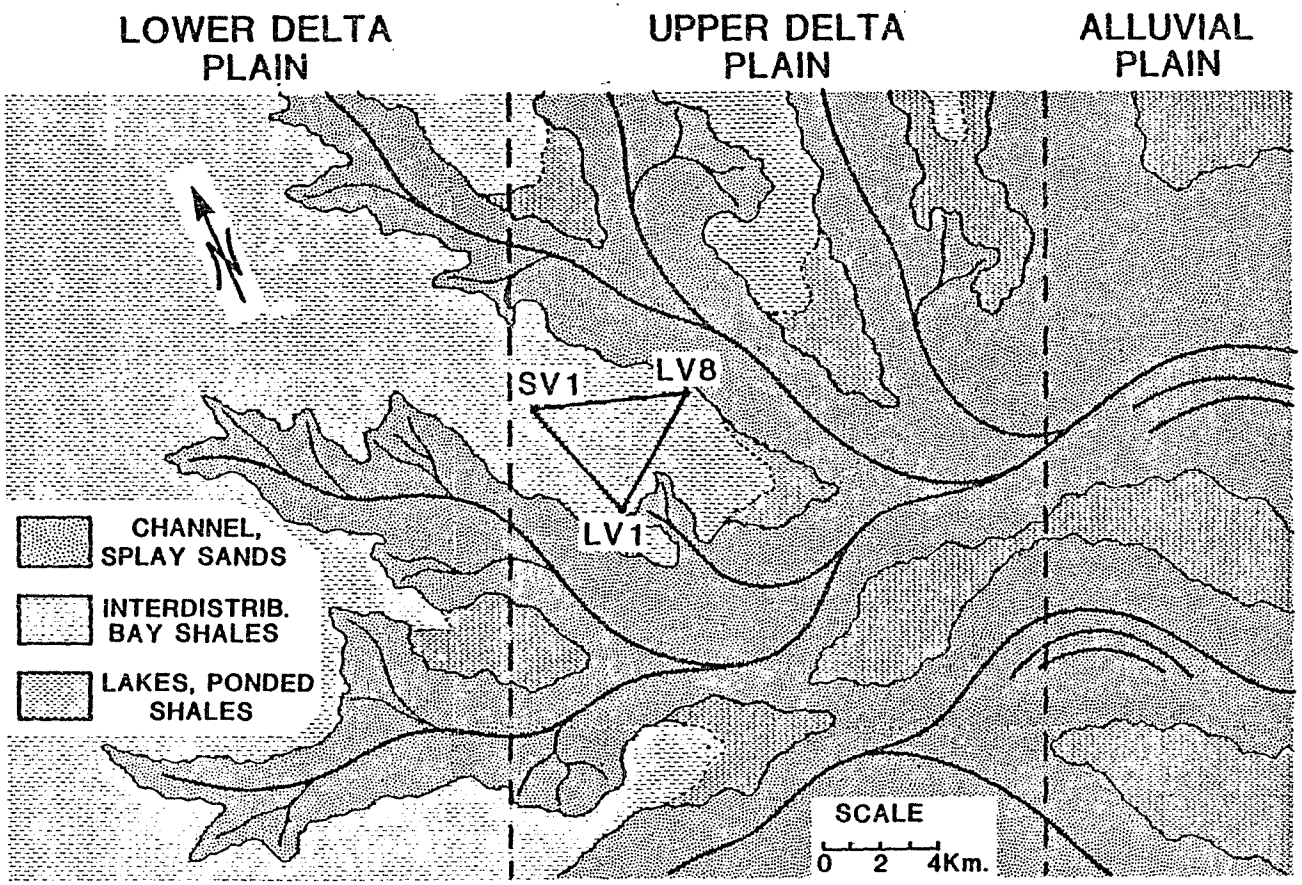

Figure 7. Three, major depositional environments found in a delta complex with the approximate location of the study area, at the time the bayfill shales associated with the Hazard No. 7 Coal were being deposited, also shown (modified from Ferm et al., 1971, Fig. 2).

These sands are medium to coarse grained, lithic graywackes or arkoses. Gravel lags of siderite nodules, shale clasts, and coal spars are found near the channel's scoured base. Grain size decreases upward, as the bedding changes from festoon, cross-laminae or cross-beds in the lower portions, to smaller scale cross-laminae and planar bedding in the upper portions. Rippled, partially rooted, sandstones and siltstones cap the channel deposits.

The fine to medium grained, lithic graywacke sandstones, described in this study, occur in units up to 20 meters thick, the result of several, vertically stacked point bars from the same progradational cycle (Donaldson, 1979, p. 125). However, because the distributary channels were constantly migrating across each other, the complete fining upward cycle is seldom preserved. The finer grain size indicates deposition nearer the lower reaches of the upper delta plain.

Interdistributary Bays: The area between distributary channels is referred to as an interdistributary bay, whether the water body is open or closed to the sea (Elliot, 1974, p. 612). Used in this sense, the term includes both the upper delta plain's shallow bays, and shallow lakes. In this study, the only distinction made between the two is based on lateral extent. Bays range from 3 to 8 km. wide, while lakes occupy less than a 3 km. area.

A single bayfill deposit is 1 to 8 meters thick, with shale being the dominant lithology. The upward coarsening sequence of fine-grained sediments begins with claystone or seatearth, at the

base, followed by coal, and then shale with numerous plant fossils and rare, freshwater pelecypods. Further seaward, but still in the upper delta plain, marine or brackish water faunas, and burrowing become more evident. Siltstones from adjacent levees, and sporadic crevasse splay sands aid in filling the bay. Coal swamps develop once the bays fill sufficiently to allow land plants to take hold.

Levees: Located adjacent to channels, these deposits can be as thick as 8 meters. Both thickness and grain size decrease away from the channel. Poorly sorted, crudely laminated, partially rooted silts and silty sands characterize levee deposits.

Crevasse Splays: These usually lobe-shaped sand bodies occur as discrete, coarse beds in the interdistributary bayfill shales (Elliot, 1974, p. 613). Internally, splay sands are distinguished by convolute and small scale cross laminae in the lower portions, changing to parallel laminae and climbing ripples near the top. Major splays enter the bay through breaches in the levee system. Thinner sand bodies are deposited near the bay margins by overbank flooding.

Shales are the most poorly described lithology in the upper delta plain, bayfill deposits. This study's detailed petrographic analysis provides the first in-depth look at the compositional variations existing in these 'dark gray' shales. Although many interesting shale attributes were revealed through this analysis, only a few were selected to demonstrate the complex, vertical and lateral relationships

existing in bayfill sediments. The characteristics chosen include clay percent, bedding type (laminated vs. massive), and the presence of rooting and siderite. These features are all graphically displayed for the bayfills surrounding the Hazard Coal Zone, the Hazard No. 7 Coal, and the Hazard No. 8 Coal Zone in Figs. 8, 9 A+B, and 10, respectively.

As these figures illustrate, the bayfill shales do not display the steady decrease in clay percent expected in a 'coarsening upward' delta sequence. Instead, the amount of clay fluctuates in lithologies ranging from clays to silts, which may be either laminated or massive. Siderite also appears to behave unpredictably, being virtually absent in some cases (Fig. 10), while being quite common in others (Fig. 9B). Rooting is restricted to seatearths and levees, though at times it is notably absent from the latter.

To explain the lithologic changes in and across these bays, it is necessary to first determine where the three sampled cores are located in relation to the delta complex, as a whole. One possible interpretation is shown in Fig. 7. This setting places core LV8 near a major distributary channel, core LV1 near a crevasse splay, and core SV1 in the central region of an interdistributary bay. Remembering that growth faults in this region caused similar depositional environments to stack vertically, a setting such as this (or very similar to it) applies equally well to the bays developed around all the Hazard coals. Brachiopods, found in the thicker shales overlying the Hazard No. 7 Coal, indicate that deeper, more brackish to marine bays were

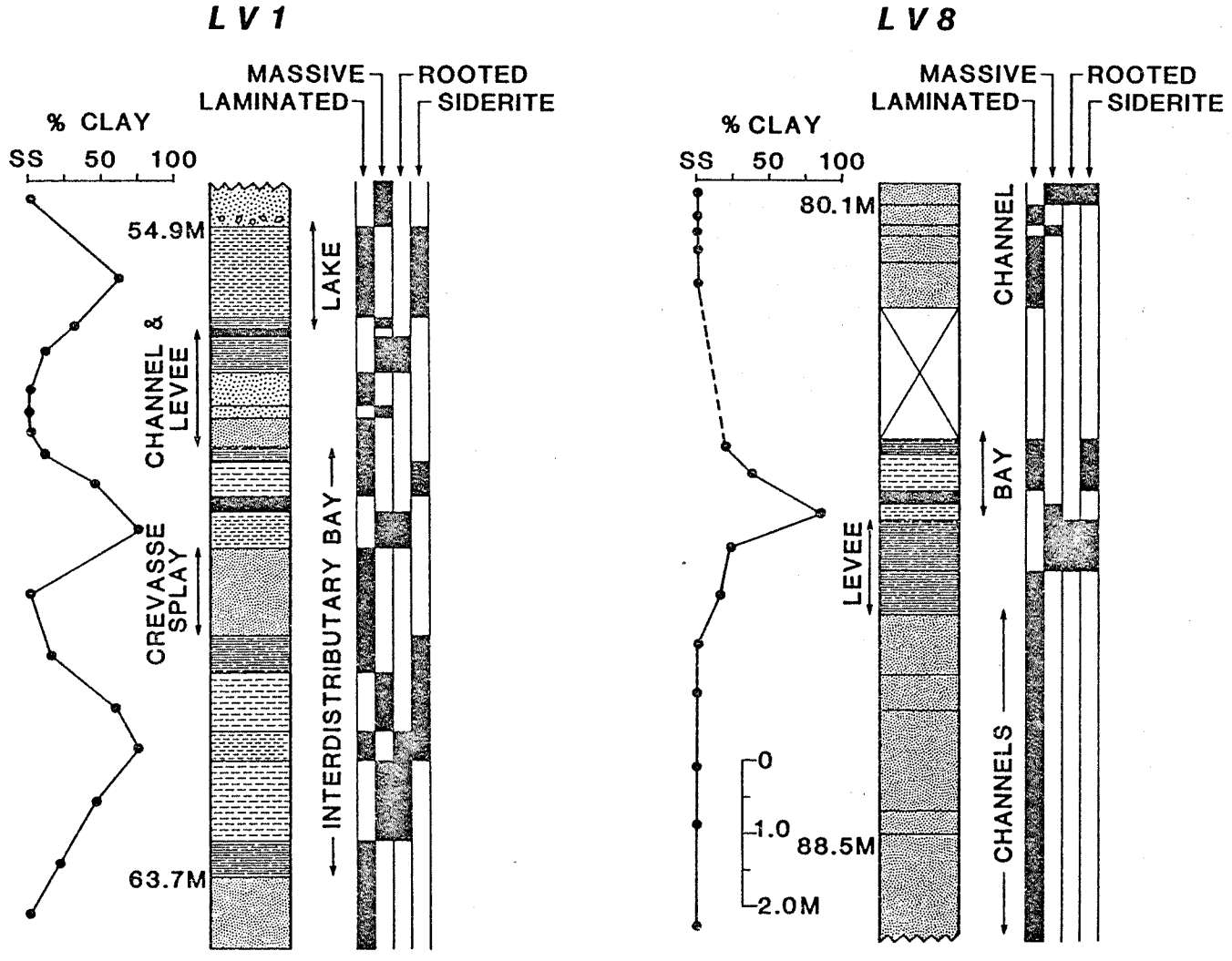

Figure 8. Bayfill deposits surrounding two, thin coals in the Hazard Coal Zone. Figs. 8-10 provide interpretations of depositional environment, and graphically illustrate variations in shale composition and selected shale attributes. Lithic symbols are explained in Appendix V.

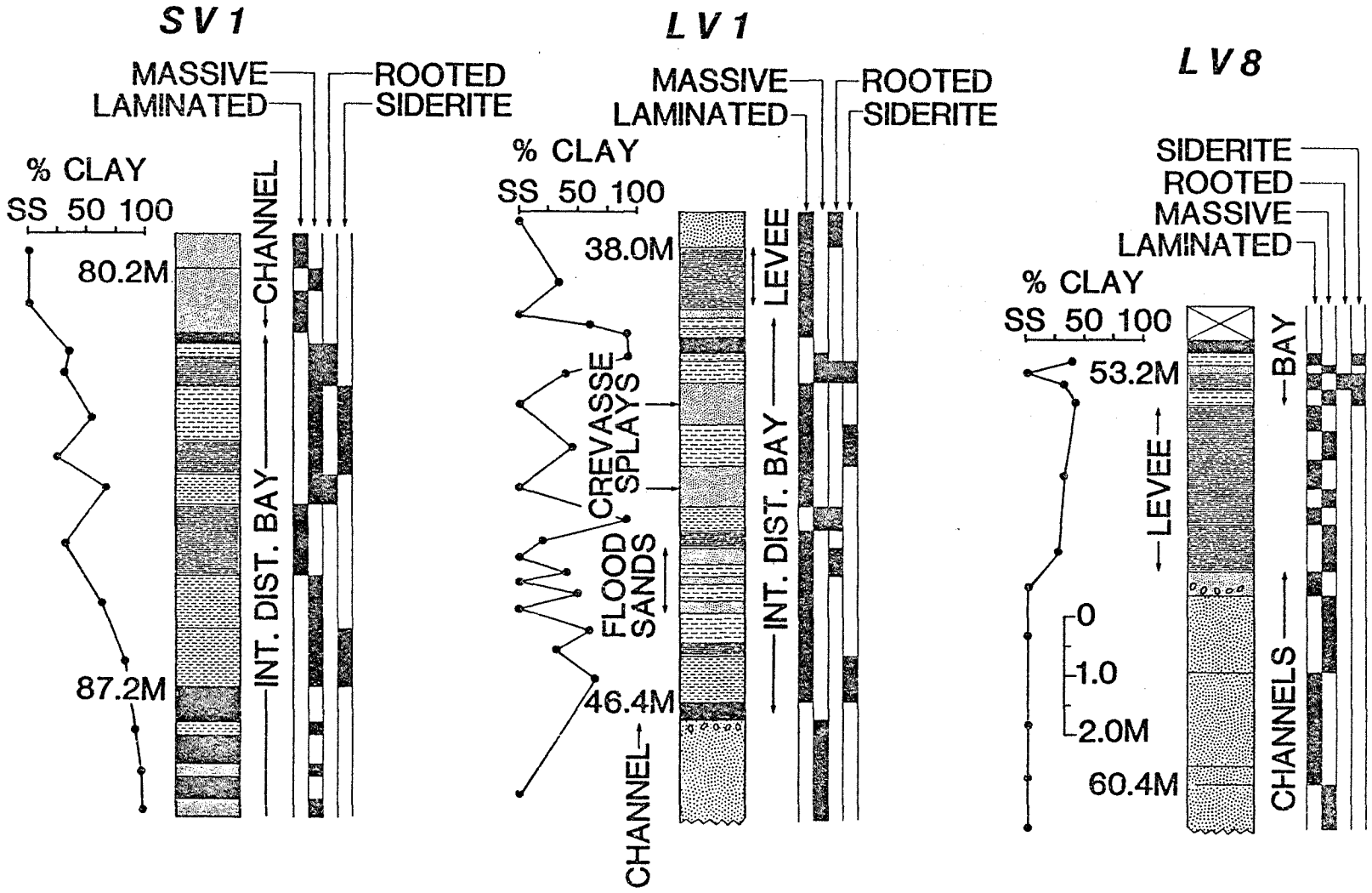

Figure 9A. Bayfill deposits surrounding a thin, but continuous, unnamed coal associated with the Hazard No. 7 Coal and a discontinuous, triple-seam coal, at the top of the Hazard Coal Zone.

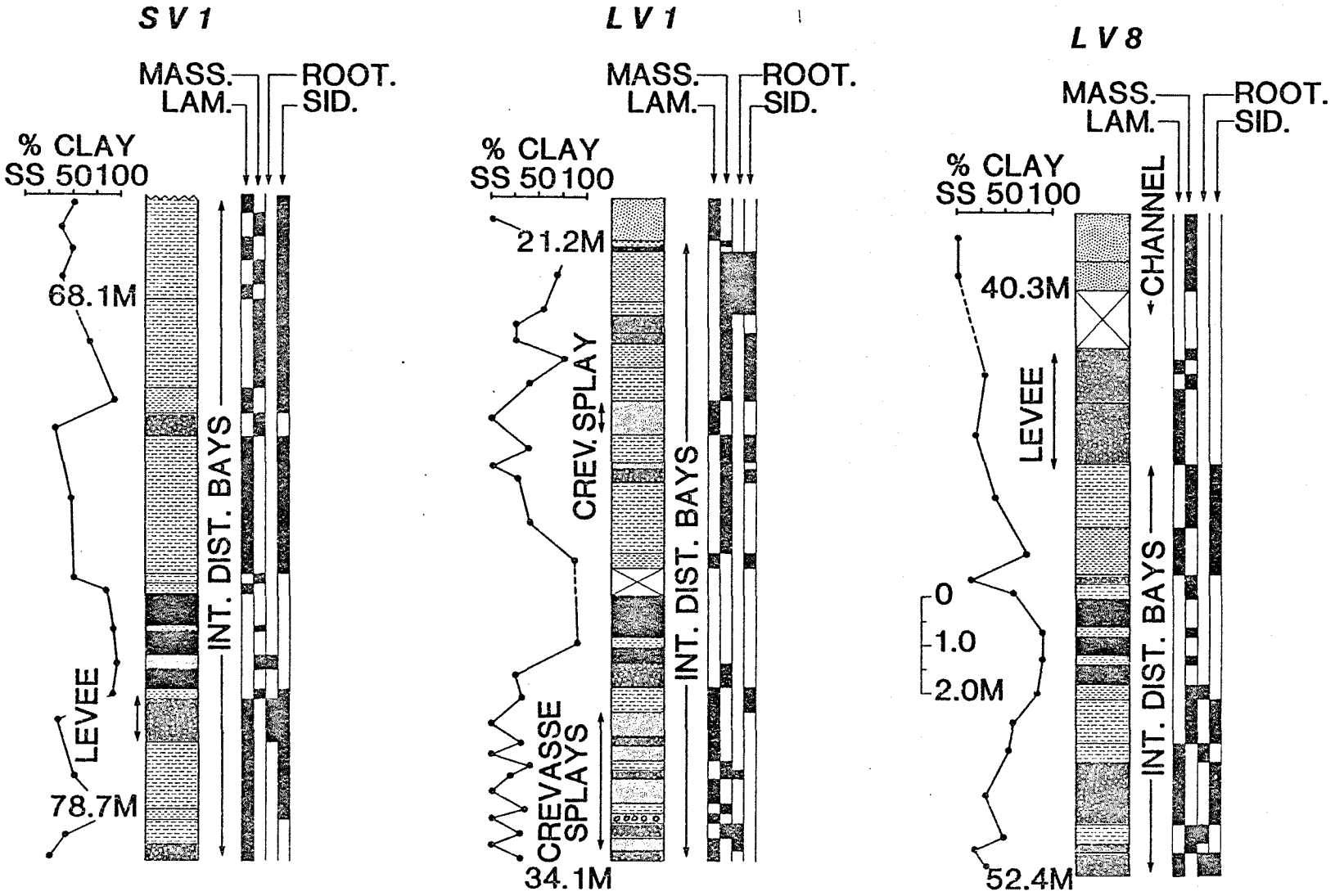

Figure 9B. Bayfill deposits associated with the thick, triple-seam, Hazard No. 7 Coal.

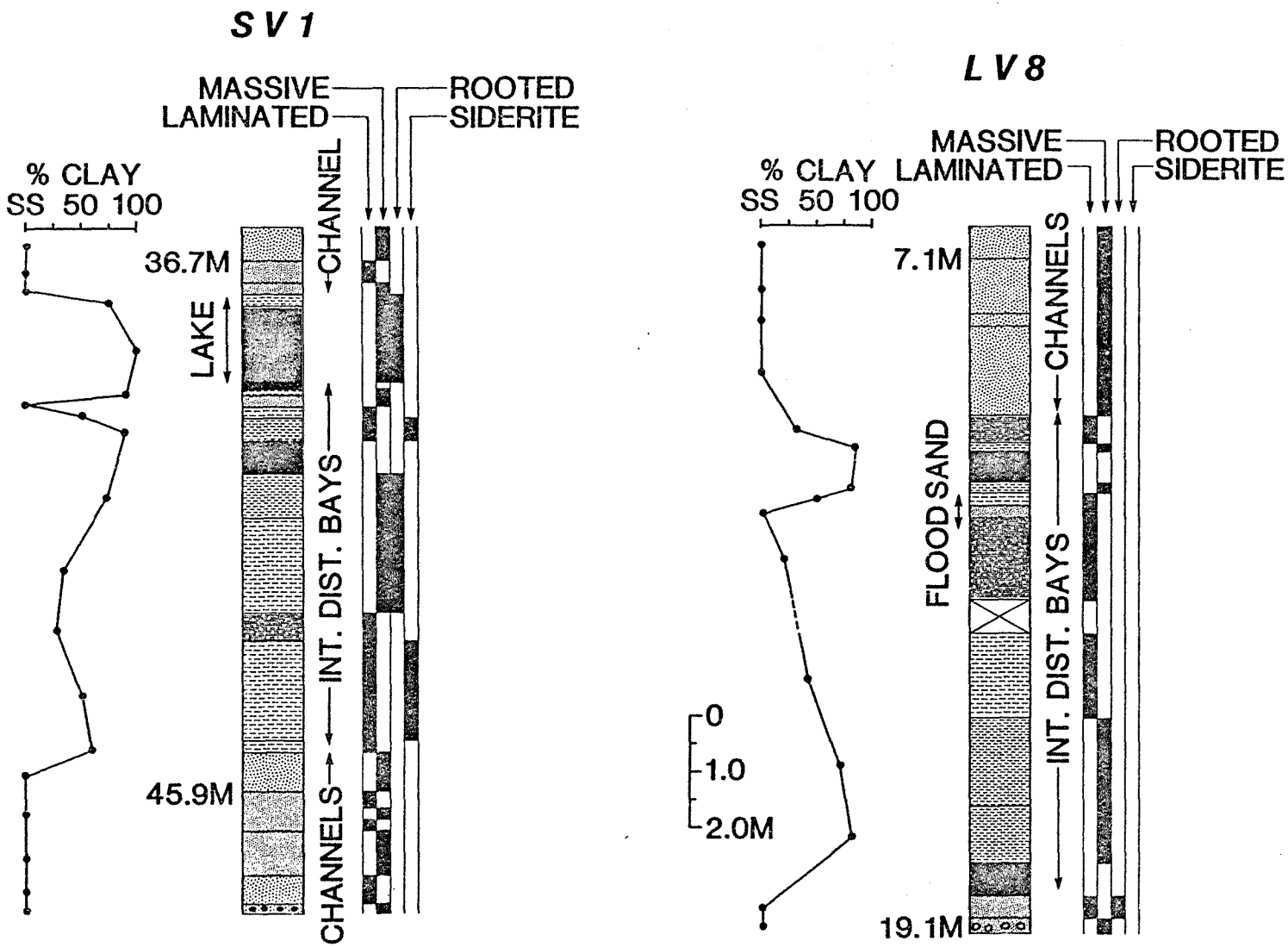

Figure 10. Bayfill deposits associated with two, thick coals in the Hazard No. 8 Coal Zone.

forming at this time, probably in response to a slight transgression of the seas.

The fluctuation in clay percent can then be attributed to numerous, crevasse splays injecting sands into the bays near shore, and a finer silt fraction which reached far out into the bays. The end result is that the normal coarsening upward trend is frequently disrupted across the entire bay. Subsidence, created as the underlying shales compact, also helps explain the fluctuation in clay percent. As the bays fill, a thin (1 to 3 meter), coarsening upward sequence of clays, muds, and silts is produced. If and when subsidence occurs, a similar sequence will begin developing directly above the previous one, again resulting in an apparently erratic change in clay percent, as in core SV1 (Figs. 9 A+B). Subsidence also permits organic matter to accumulate over long periods in the same area, conditions necessary to produce thick, minable coals such as the Hazard No. 7 and Hazard No. 8.

Abundant, clay-rich, laminated shales suggest that quiet, undisturbed waters existed in these bays, at least, between interruptions caused by crevasse splays. This low energy environment would allow the slow deposition needed to produce clay laminae (Spears, 1976, p. 724). When laminae either fail to develop or are destroyed, massive shales result. Massive underclays are thought to form when, 1) suspended clays undergo massive flocculation upon contacting more saline waters, 2) dewatering inhibits the normal reorientation of clay floccules under load, or 3) laminae are disrupted by root penetration (Wanless, 1969, p. 137). The remaining, massive bayfill shales most

likely resulted from rooting, along with other forms of bioturbation.

The irregularly bedded silts which have been interpreted as levees in Figs. 9 A+B, lack the characteristic rooting common to levee deposits. However, the cores may have penetrated the levees' subaqueous portions. These poorly drained areas support water tolerant, non-woody vegetation (Flores and Arndt, 1979, p. 119), which may be less likely to leave rooting traces.

Siderite nodules, laminae, and cements are found throughout the bayfill shales, but become much more common in core SV1. To explain this distribution, conditions favoring siderite production must be explored. In ancient shales, siderite is the product of early diagenesis, resulting when iron is mobilized in an organic-rich, reducing, diagenetic environment with high pH (7 to 8), and low Eh (0 to -2) (Blatt et al., 1980, p. 575; Baganz et al., 1975, p. 184). One must assume that these conditions were more prevalent in the thick, clays and muds deposited further seaward (in the vicinity of core SV1). A detailed geochemical study is required to verify such a general observation, and would add new insights into siderite distribution in upper delta plain, bayfill shales.

SLAKE DURABILITY

A process known as 'slaking' causes many earth materials to disintegrate or crumble when exposed to water or air. The slake durability test measures a rock's resistance to such physical decomposition over relatively short time periods. Although chemical and physical weather-

ing are long term processes, the test does simulate short term weathering effects on clay-rich rocks, by subjecting samples to accelerated climatic slaking events (alternate wet and dry phases). Simultaneous sieving determines the amount of slake induced, grain size reduction. Predicted slake durabilities are important not only for immediate engineering considerations, but also because slaking creates increased surface areas, which may accelerate the long term weathering effects.

Engineers often use slake durability test results to aid in planning and designing highway embankments (Stollar, 1976; Wood and Deo, 1975), but shale decomposition is also a concern in coal mining operations. Conlin (1954) used slake durability to characterize good and poor coal mine roof rock, a questionable application, because so many other geologic factors (fracture systems, faults, bedding planes and joints, gas and water pressures in overlying strata) produce potential roof hazards, as well (Overbey et al., 1973). However, the ability to predict slaking characteristics can be quite beneficial in strip mining, where shales may compose a large part of the removed overburden. To meet the Kentucky Bureau of Surface Mining requirements for a durable rock fill, 80 percent of the total overburden material, must have slake durability indices greater than 90 percent, conditions very much dependent on how the shales slake.

Testing Procedure: The standard apparatus for testing slake durability consists of several (2 to 4), wire mesh drums, which rotate at 20 revolutions per minute, in troughs filled with the slaking fluid. Franklin and Chandra (1972) more completely describe the device, and

discuss the many factors influencing the test results. Unfortunately, no standard technique for conducting the test exists. This analysis uses one, 60 minute cycle and oven-dried material, a highly regarded procudure for differentiating Pennsylvanian shales based on slaking characteristics (Hopkins and Gilpin, 1982).

All 47 samples examined petrographically were subjected to the slake durability test, as were several samples assigned rock names by macroscopic examination. Each sample was divided into approximately 8 equidimensional pieces, and then oven-dried at 110° C., for twelve hours. They were then carefully weighed, with 300-400 grams considered an ideal, initial (before testing) weight. After inserting the weighed samples, the apparatus was filled with tap water at 25° C., and operated for exactly one hour. Upon completing the test, the samples were removed from the drums, dried for another twelve hours, and finally weighed. The slake durability index (SDI) was calculated as follows:

$$SDI = 100\ Weight_{(final)} / Weight_{(initial)}$$

These values are accurate to the nearest 0.1 percent. Slaking processes effect shales in different ways, almost completely disintegrating some samples, while leaving others relatively intact (Plate 3). Appendix II tabulates the slake durability test results, and notes the physical appearance of the samples following the test.

IDENTIFYING AND INTERPRETING THE ESSENTIAL VARIABLES

Defining the relationship between shale petrology and slake dura-

Plate 3. Appearance of samples following the slake durability test: A) SDI = 31.3%, B) SDI = 46.5%, C) SDI = 75.3%, and D) SDI = 98.5%.

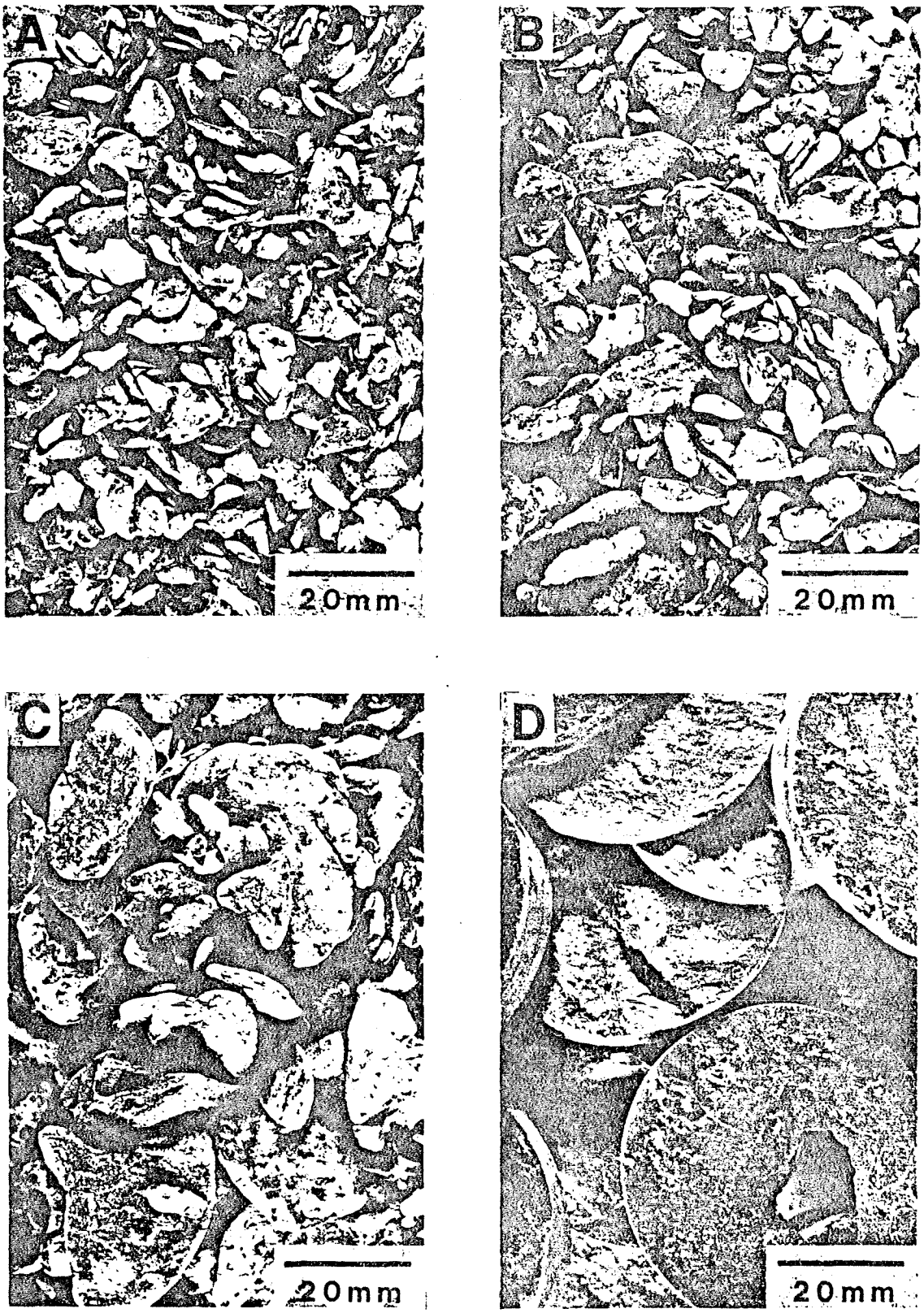
A
20mm
B
20mm
C
20mm
D
20mm

bility requires isolating the most significant variables effecting durability, from the eleven observed shale attributes. The ways in which each variable, or combinations of these variables could effect the slaking process are numerous, creating such a complex problem that statistical analyses must be utilized to find a solution. Multiple linear regression and the discriminant function can explain such multivariate data, both estimating slake durability, and suggesting which shale characteristics most directly influence this property.

Multiple Regression as described by Davis (1973, p. 413-430), Crow et al. (1960, p. 169-182), and Krumbein and Graybill (1965, p. 391-400), predicts the value of a dependent variable y, based on any number of independent (known) variables x_1, x_2, ..., x_k, using the general equation:

$$y = a + b_1x_1 + b_2x_2 + \ldots + b_kx_k$$

The partial regression coefficients b_1, b_2, ..., b_k, and the constant a, are estimated from the given data. Percentage of the total variance of y, explained by any independent variable, is determined by squaring that variable's partial correlation coefficient r, and multiplying by one hundred. This value, 100 r^2, is the highest for the most significant variable in the regression equation, and lower for the other variables as they become less important. In a stepwise analysis, the most significant variable is entered into the equation first followed, in order, by the less significant varables, constantly improving the correlation, but by progressively smaller amounts, as each is added.

"Multiple Regression" a program from the SPSS package (Kim and

Kohout, 1975, p. 320-367) analyzed the effect eleven petrographic characteristics (the independent variables x_1 to x_{11}, see Table 7), obtained from each of the 47 shale samples, had on slake durability (the dependent variable y). The results are summarized in Table 7. Two shale attributes, clay percent and average clay mineral orientation, are clearly the most significant variables, accounting for 52.7 percent of the total variance. All the remaining variables combined, explain only an additional 10 percent of the total variance. Errors between predicted slake durability indices and the actual values (Appendix III), indicate that the derived regression equation does not reliably explain the slaking behavior of the examined shales. Classifying the shales as either durable (SDI's greater than 90 percent), or slakable (SDI's less than 90 percent) might prove more efficient, and is readily accomplished by a discriminant function.

A discriminant function, discussed by Krumbein and Graybill (1965, p. 359-367), Davis (1973, p. 442-456), and Shimp et al. (1969, p. 567-574), assigns an individual sample, possessing several observed characteristics x_1, x_2, ..., x_k, to one of two or more predetermined groups. The function:

$$z = a + a_1x_1 + a_2x_2 + \ldots + a_kx_k$$

transforms all the observed characteristics from one sample, into a single discriminant score (z), with the constants a, a_1, a_2, ..., a_k, computed to maximize the separation between the various groups. As exemplified below, group membership is determined by the position of a sample's z-score along the line defined by the discriminant function.

TABLE 7

SUMMARY OF MULTIPLE LINEAR REGRESSION RESULTS

INDEPENDENT VARIABLES	b	100 r^2	100 r^2 CHANGE
Clay Percent, x_1	-0.8441	37.508	37.508
Clay Orientation, x_2	-40.2336	52.739	15.231
Carbonate Percent, x_3	0.6893	55.555	2.816
Lamination, x_4	3.9032	57.452	1.897
Burrowing, x_5	13.5390	58.522	1.070
Pyrite Percent, x_6	-3.3270	59.969	1.448
Average Quartz Size, x_7	-0.4558	62.006	2.037
Rooting, x_8	-5.5117	62.826	0.820
Mica Percent, x_9	0.2366	62.948	0.122
* Quartz Percent, x_{10}	-	-	-
* Organic Percent, x_{11}	-	-	-
Constant, a	142.9973		

Multiple Correlation Coefficient, R = 0.7934

* Insignificant, not included in computation.

This study requires a discriminant function yielding the maximum separation between durable and slakable shales. Clay percent (x_1) and clay orientation (x_2), the two most significant shale attributes predicting slake durability indices, were used in "Discriminant Analysis", an SPSS program (Klecka, 1975, p. 434-467), examining their effectiveness as discriminating variables. The discriminant function computed is:

$$z = 5.5074 - 0.0556\ x_1 + 11.9276\ x_2\ .$$

The F ratio for this discriminant function is F=14.50, exceeding the critical F value at the 99 percent confidence level $F_{(2,44)}$ =5.15. Accordingly, clay percent and clay orientation combined, significantly discriminate between durable and slakable shales.

To classfy a sample, the centers of the durable group (Z_1) and the slakable group (Z_2), along the discriminant function, must first be calculated by substituting the group mean values for clay percent ($\bar{x}_{1,1}$, $\bar{x}_{1,2}$) and clay orientation ($\bar{x}_{2,1}$, $\bar{x}_{2,2}$) into the above equation:

$$Z_1 = 5.5074 - 0.0556\ \bar{x}_{1,1} + 11.9276\ \bar{x}_{2,1}$$

$$= 5.5074 - 0.0556\ (43.7037) + 11.9276\ (0.2004) = -0.6872$$

$$Z_2 = 5.5074 - 0.0556\ \bar{x}_{1,2} + 11.9276\ \bar{x}_{2,2}$$

$$= 5.5074 - 0.0556\ (62.1500) + 11.9276\ (0.2490) = 0.9181$$

The discriminant index (Z_0) the point dividing the durable and slakable groups, is the midpoint between Z_1 and Z_2,

$$Z_0 = (Z_1 + Z_2)/2$$

$$= (-0.6872 + 0.9181)/2 = 0.1154$$

If the z-score of a sample is greater than Z_0, the shale is classified

as slakable, whereas, if z is less than Z_0, it is classified as durable (see Fig. 11 for examples of this classifying procedure).

Calculated z-scores, for the 47 samples in this study (Appendix IV), correctly classify 37 samples (79 percent) as durable or slakable. As z-score distributions demonstrate (Fig. 12), the classification is improved by incorporating the remaining nine variables, x_3 to x_{11} (refer to Table 7), into the function. However, this much more complicated equation increases the efficiency only 10 percent, correctly classifying 42 samples (89 percent). The best discriminant function is one requiring the least number of variables to assign an unknown sample to the correct group at some predetermined level of acceptance. For this reason, the function using clay percent and clay orientation is considered superior to one needing all eleven variables.

A plot of clay percent versus clay mineral orientation, for the tested samples, graphically displays the discriminant analysis results (Fig. 13). The distribution of points indicates that shales with more than 40 percent clay and clay orientations exceeding 0.20 (fair to poor) are, usually, slakable. Separating the two shale groups, is a line drawn normal to the direction of maximum slope of the discriminant function, passing through the midpoint between the slakable and durable group means. Another way to position this line involves evaluating the discriminant function at the discriminant index, Z_0:

$$Z_0 = 0.1154 = 5.5074 - 0.0556\ x_1 + 11.9276\ x_2$$

All samples with x_1 and x_2 values satisfying this equation must, by definition, fall directly between the two groups, somewhere along the

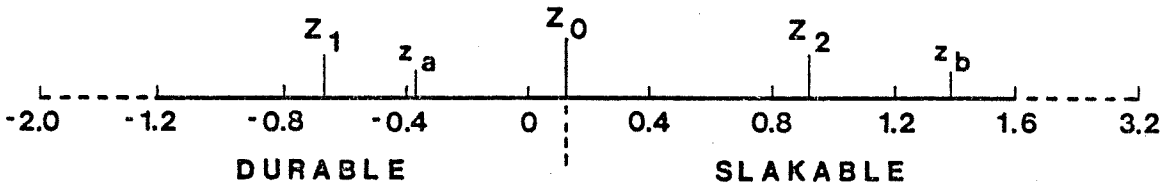

Z_1 = DURABLE GROUP MEAN Z_2 = SLAKABLE GROUP MEAN

Z_0 = DISCRIMINANT INDEX

Examples

A) For a sample with clay percent = 49 and clay mineral orientation = 0.20:

$z_a = 5.5074 - (0.0556)(49) + (11.9276)(0.20) = -0.3979$

z_a is less than Z_0, a DURABLE shale.

B) For a sample with clay percent = 83 and clay mineral orientation = 0.19:

$z_b = 5.5074 - (0.0556)(83) + (11.9276)(0.19) = 1.3736$

z_b is greater than Z_0, a SLAKABLE shale.

Figure 11. Use of z-scores and the discriminant function in classifying samples as durable or slakable.

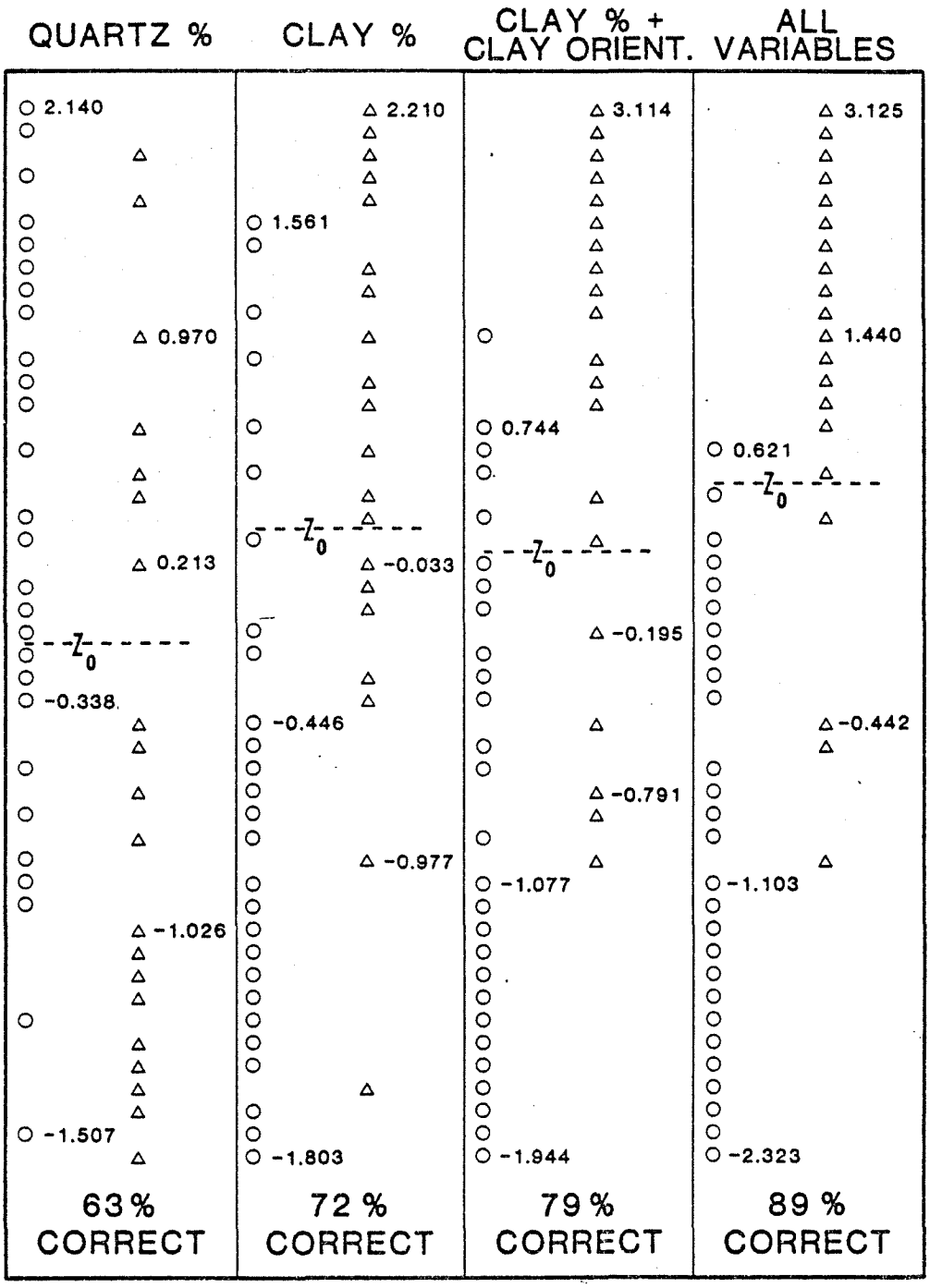

Figure 12. z-score distributions showing the effect different variables and combinations of variables have on the discriminant function's ability to distinguish slakable (triangles), from durable (circles) shales. Selected values of the discriminant are shown, along with the position of the discriminant index, Z_0.

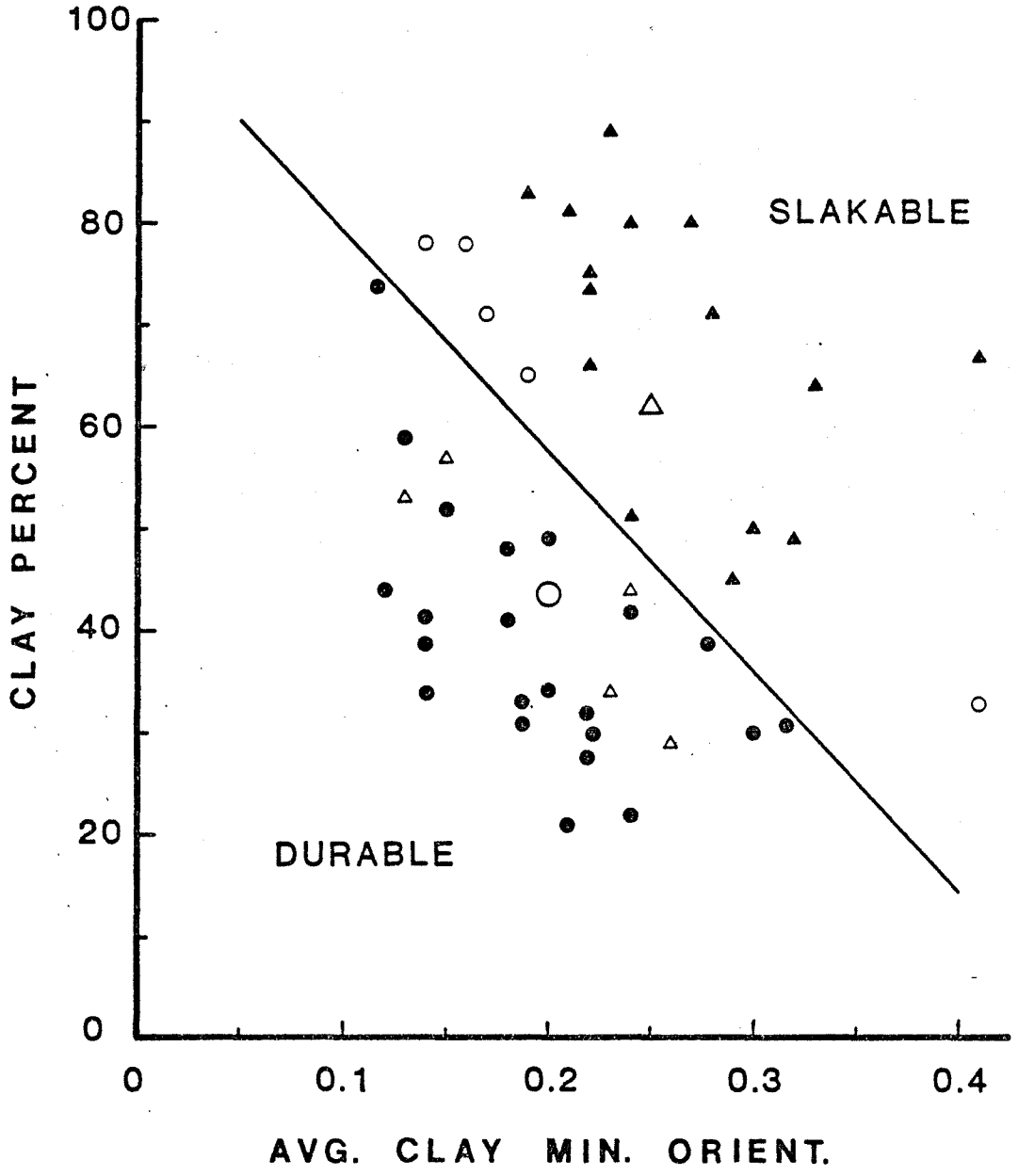

Figure 13. Plot of average clay mineral orientation vs. clay percent for the tested samples, showing the line of separaration between the durable and slakable shale groups, as determined by the discriminant function. Closed circles and triangles represent durable and slakable samples, respectively. Open symbols represent incorrectly classified samples. Group means for the durable group (large open circle), and the slakable group (large open triangle) are also shown.

line of separation. Any two such samples, define the line.

Taylor and Spears (1970) attribute slaking to two major processes: intra-particle expansion or swelling of clay minerals, especially smectite, and air-breakage associated with capillary pressures. Air-breakage, described by Olivier (1979, p. 262), results when capillary action draws fluid into a dessicated shale, trapping and compressing the air previously in the pores. This causes the mineral skeleton to fail along the weakest plane, exposing new surfaces to similar occurrences. The following discussion examines the effect abundant clay and poor clay mineral orientation have on the above two processes.

As clays and clay-sized particles become more abundant in a shale, pore spaces correspondingly diminish in size. The inverse relationship between pore radius and capillary pressure (Taylor and Spears, 1970, p. 498), allows these smaller pores to create greater capillary pressures, promoting air-breakage and subsequent slaking. Abundant mixed-layer clay (illite-smectite), present throughout the coal measure shales studied, further enhances slaking. Smectite, when expanded, produces unequal local pressures in the shale matrix, eventually breaking down the rock (Van Eekhout, 1976, p. 63). This process is more effective in clay-rich shales, with proportionately higher amounts of smectite.

Porosity is critical to the slaking process, as previously suggested. Poor clay mineral orientation results in increased porosity (Gipson, 1966, p. 896; Heling, 1970, p. 258), providing more opportunities for capillary pressure and air-breakage to destroy a shale. A comparison between flocculated and dispersed clays, demonstrates the

effect clay mineral orientation has on porosity (Fig. 14). Unless intense overburden pressures significantly alter ancient shale fabrics, the more porous, random fabric present in flocculated clays, should also exist in poorly oriented shales. The scanning electron microscope, which permits direct observation of clay mineral orientation (O'Brien, 1970; Barrows, 1980), was used to verify this hypothesis. Several samples, with widely differing slake durability indices, were examined with the SEM. Shales with low SDI's and poor orientations, displayed the porous, random fabric found in flocculated clays, while shales with higher SDI's and good orientations, appeared similar to dispersed clays (Plate 4). These observations confirm the important control clay mineral orientation has on porosity and slake durability.

DURABILITY CLASSIFICATION FOR SHALES

Present durability classifications usually require results from several, different engineering tests (Chapman et al., 1976; Wood and Deo, 1975; Olivier, 1979), a time consuming process. However, as just demonstrated, petrographic criteria can predict the outcome of the slake durability test, suggesting that a geologically oriented shale classification might also serve as a durability classification. Such a combination, would permit slake durability predictions to be made by carefully inspecting a shale sample, while still in the field.

The field classification used in this study, utilizes the two most significant variables in predicting slake durability. Obviously, clay percent plays a major role in classifying shales, while clay mineral

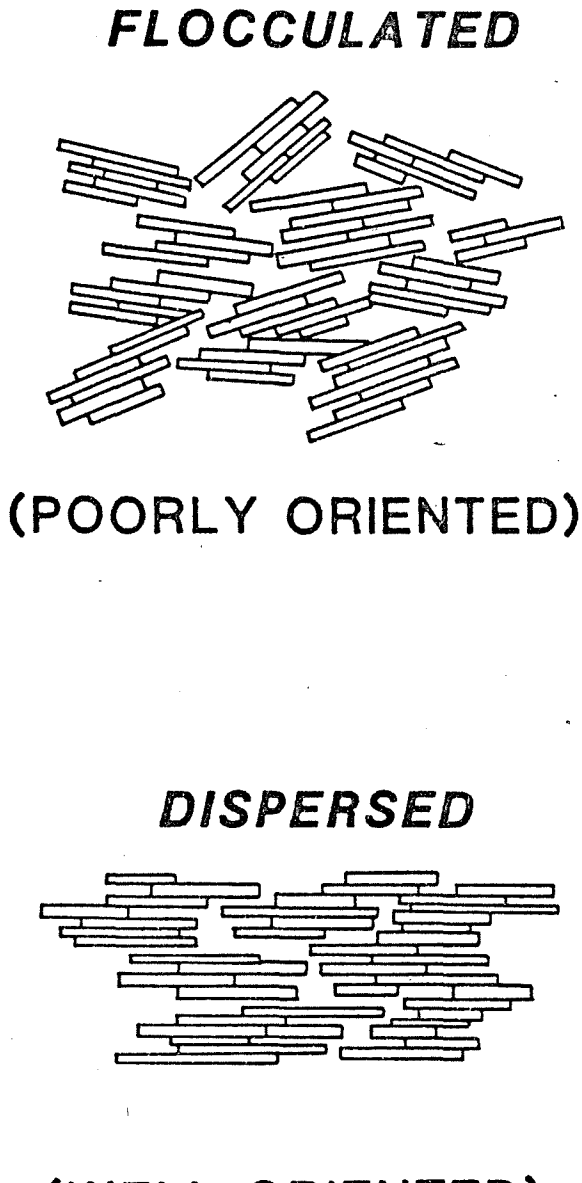

Figure 14. Model relating flocculated clays to poorly oriented shales, and dispersed clays to well oriented shales, demonstrating the effect orientation has on controlling porosity (modified from Moon, 1972, Fig. 7).

Plate 4. SEM photos of shale samples showing: A) poorly oriented clays viewed parallel to bedding, B) poorly oriented clays viewed perpendicular to bedding, C) well oriented clays viewed parallel to bedding, and D) well oriented clays viewed perpendicular to bedding.

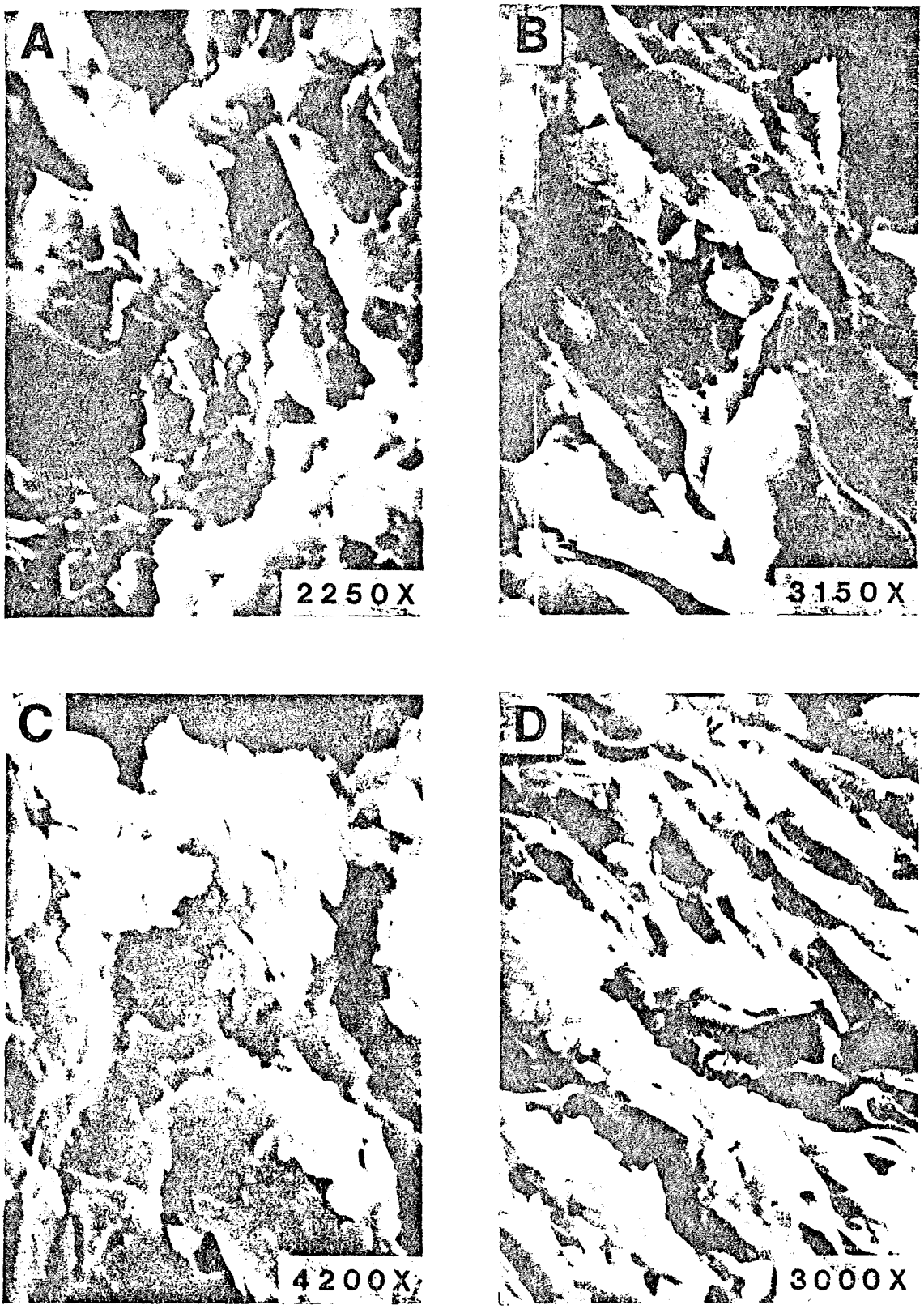
A
2250X
B
3150X
C
4200X
D
3000X

orientation is, indirectly, related to the presence or absence of laminae. The following discussion, based on SDI's obtained from samples within each of the eight shale classes (Table 8), examines this classification's ability to differentiate between slakable and durable shale lithologies.

Claystones and organic shales are slakable. Both lithologies contain abundant clay, and have random shale fabrics (FI's from 0.21 to 0.41). SDI's range from 2.8 to 75.3 percent, with only one sample having an anomalously high SDI of 89 percent.

Clayshales are durable, if the laminae are well developed and consist of alternating clay and silt layers or siderite. SDI's range from 89.5 to 92.7 percent, when such laminae are present. If the laminae are wavy discontinuous parallel, and organic-rich, SDI's tend to be very low, ranging from 49.5 to 76.8 percent.

Mudshales, sideritic shales, siltstones, and laminated siltstones are all durable types. SDI's range from 90.8 to 98.6 percent. Only two exceptions were encountered, a mudshale with an SDI of 81.1 percent, and a siltstone with an SDI of 73.7 percent.

Mudstones are the most difficult to assign relative durabilities, having SDI's between 44.4 and 98.0 percent. Even the distinction noticed in thin section between clay-rich muds (clay greater than 50 percent), and silt-rich muds (clay less than 50 percent) fails to efficiently separate these samples into either durable or slakable types.

Except for mudstones, which necessitate further engineering tests,

TABLE 8

SHALE TYPES WITH ASSOCIATED SLAKE DURABILITY INDICES

	SAMPLE	SDI
CLAYSTONES	SV1-8	58.5
	SV1-13	55.0
	SV1-25A	31.3
	SV1-37	89.0
	SV1-39	75.3
	LV8-3	34.7
	LV8-9	2.8
	LV8-16	68.2
	LV1-6	51.1
	LV1-33	64.8
CLAYSHALES	SV1-12	76.8
	SV1-23	98.5
	LV8-10	49.5
	LV8-14	93.8
	LV1-30	92.7
MUDSTONES	SV1-1	44.4
	SV1-3	76.4
	SV1-14	92.3
	SV1-17	98.0
	SV1-19	94.0
	SV1-23	94.9
	SV1-33	83.6
	LV8-13	96.0
	LV8-15	94.1
	LV8-17	94.1
	LV8-19	84.5
	LV8-21	96.2
	LV8-38	77.7
	LV1-1	95.3
	LV1-7	94.2
	LV1-11	95.2
	LV1-13	96.4
	LV1-37	75.8
	LV1-41	84.1
MUDSHALES	SV1-15	93.3
	SV1-16	81.1
	SV1-18A	94.9
	SV1-22	96.4
	SV1-28	96.6
	LV8-6	94.1
	LV8-25	94.3
	LV1-16	93.6
SILTSTONES	SV1-21	93.9
	SV1-32	96.6
	SV1-32A	73.7
	SV1-34	94.9
	LV8-12	95.5
	LV8-22	95.8
LAMINATED SILTSTONES	SV1-14A	96.0
	SV1-26	94.1
	SV1-27	98.6
	SV1-30	94.3
	SV1-36	93.0
	LV8-30	95.0
	LV8-42	96.3
	LV1-34	96.5
ORGANIC SHALES	SV1-10	46.5
	SV1-25	63.5
	SV1-40	70.7
SIDERITIC SHALES	SV1-20	92.6
	LV1-12	96.5
	LV1-14	93.1
	LV1-31	98.5

the field classification shows definite promise as a durability classification for Pennsylvanian, coal measure shales (Table 9).

CONCLUSIONS

1. Shales of Hazard age, in the Vest Quadrangle, were deposited in shallow, upper delta plain, interdistributary bays. Crevasse splays frequently interrupted the prevailing, quiet water sedimentation, common to this depositional environment. Eight identified shale lithologies, reflect the compositional variation in and across these bayfill deposits.
2. Detailed shale petrology aids in the interpretation of slake durability. Multiple linear regression indicates that two shale attributes, clay percent and clay mineral orientation, exert the most influence on slake durability.
3. A discriminant function, using clay percent and clay mineral orientation as the discriminating variables, successfully differentiates slakable from durable shales, correctly classifying 79 percent of the tested samples.
4. The field classification, used in this study, functions as a durability classification, except for mudstones. Mudstones display a wide variety of compositions and slaking characteristics, not predictable by simple field examination.

TABLE 9

RELATION OF FIELD CLASSIFICATION TO DURABILITY

% CLAY SIZE CONSTITUENTS	0-32	33-65	66-100
MASSIVE	DURABLE	SLAKABLE OR DURABLE	SLAKABLE
LAMINATED	DURABLE	DURABLE	DURABLE
> 15% SIDERITE	DURABLE		
> 20% ORGANICS	SLAKABLE		

SUGGESTIONS FOR FURTHER STUDY

Shales with more diverse compositions, obtained from different depositional environments, need to be examined. This approach will better determine the effect clay mineralogy and environment of deposition have on the engineering properties of shales.

REFERENCES

Baganz, B.P., J.C. Horne, and J.C. Ferm, 1975, Carboniferous and Recent Mississippi Lower Delta Plains - A Comparison: Trans.-Gulf Coast Assoc. Geol. Soc., v. 25, p. 183-191.

Barrows, M. H., 1980, Scanning Electron Microscope Studies of Samples from the New Albany Shale Group: Scanning Electron Microscopy, I, SEM Inc., AMF O'Hare, Il. 60666, p. 579-585.

Biscaye, P.E., 1965, Mineralogy and Sedimentation of Recent Deep Sea Clay in the Atlantic Ocean and Adjacent Seas and Oceans: Geol. Soc. Amer. Bull., v. 76, p. 803-832.

Blatt, H., G.V. Middleton, and R.C. Murray, 1980, Origin of Sedimentary Rocks, 2nd Edition: Prentice-Hall, Englewood Cliffs, N.J., 782 p.

Broadhead, R.F., and P.E. Potter, 1980, Petrology of the Devonian Gas-Bearing Shale Along Lake Erie: U.S. Dept. of Energy, Morgantown, West Virginia, 49 p.

Chapman, D.R., L.E. Wood, C.W. Lovell, and W.J. Sisiliano, 1976, A Comparative Study of Shale Classification Tests and Systems: Assoc. Eng. Geol. Bull., v. 13, p. 247-266.

Chen, P., 1977, Table of Key Lines in X-ray Powder Diffraction Patterns of Minerals in Clays and Associated Rocks: Ind. Geol. Survey Occasional Paper 21, 67 p.

Cobb, J.C., D.R. Chestnut, N.C. Hester, and J.C. Hower, 1981, Coal and Coal-Bearing Rocks of Eastern Kentucky: Ann. Field Trip, Geol. Soc. Amer. Coal Division, Ky. Geol. Survey, 97 p.

Cole, R.D., and M.D. Picard, 1975, Primary and Secondary Sedimentary Structures in Oil Shale and Other Fine-grained rocks, Green River Formation (Eocene), Utah and Colorado: Utah Geol., v. 2, p. 49-67.

Conlin, R.R., 1954, A Geologic Study of the Coal Mine Roof Strata of the Herrin (No. 6) Coal Bed Near Virden, Illinois: M.S. Thesis, University of Illinois, 45 p.

Crow, E.L., F.A. Davis, and M.W. Maxfield, 1960, Statistics Manual: Dover Publications, Inc., New York, 288 p.

Curtis, C.D., S.R. Lipshie, G. Oertel, and M.J. Pearson, 1980, Clay Orientation in Some Upper Carboniferous Mudrocks, Its Relationship to Quartz Content and Some Inferences About Fissility, Porosity,

and Compactional History: Sedimentology, v. 27, p. 333-339.

Danilchik, W.D., and H.A. Waldrop, 1978, Geologic Map of the Vest Quadrangle, Eastern Kentucky: U.S. Geol. Survey Geol. Quad. Map GQ-1441.

Davis, J.C., 1973, Statistics and Data Analysis in Geology: John Wiley and Sons, Inc., New York, 530 p.

Dever, G.R., Jr., 1971, Guide to the Geology Along Interstate Highway 64 and the Mountain Parkway, Lexington to Wolfe County, Kentucky, in Smith, G.E., G.R.Dever, Jr., J.C. Horne, J.C. Ferm, and P.W. Whaley, Depositional Environments of Eastern Kentucky Coals: Ann. Field Conf., Geol. Soc. Amer., Coal Division, Ky. Geol. Survey, p. 2-22.

Donaldson, A.C., 1979, Depositional Environments of the Upper Pennsylvanian Series, in Englund, K.J., H.H. Arndt, and W. Henry, Eds., Proposed Pennsylvanian Stratotype Virginia and West Virginia: Ninth Int. Cong. Carboniferous Geol. and Strat. Field Trip No. 1, Amer. Geol. Institute Selected Guidebook Series No. 1, p. 123-136.

Elliot, T., 1974, Interdistributary Bay Sequences and Their Genesis: Sedimentology, v. 21, p. 611-622.

Ferm, J.C., J.C. Horne, J. P. Swinchatt, and P.W. Whaley, 1971, Carboniferous Depositional Environments in Northeastern Kentucky: Field Guide, Ann. Spring Field Conf., Geol. Soc. Ky., 30 p.

_____,1974, Carboniferous Environmental Models in Eastern United States and Their Significance, in Briggs, G., Ed., Carboniferous of the Southeastern United States: Geol. Soc. Amer. Spec. Paper 148, p. 79-96.

Flores, R.M., and H.H. Arndt, 1979, Depositional Environments of Middle Pennsylvanian Series in Proposed Pennsylvanian System Stratotype, in Englund, K.J., H.H. Arndt, and W. Henry, Eds., Proposed Pennsylvanian Stratotype - Virginia and West Virginia: Ninth Int. Cong. Carboniferous Geol. and Strat. Field Trip No. 1, Amer. Geol. Institute Selected Guidebook Series No. 1, p. 115-122.

Franklin, J.A., and R. Chandra, 1972, The Slake Durability Test: Int. Jour. Rock Mech. Min. Sci., v.9, p. 325-341.

Gipson, M., 1965, Application of the Electron Microscope to the Study of Particle Orientation and Fissility in Shale: Jour. Sed. Petrology, v. 35, p. 408-414.

_____, 1966, A Study of the Relations of Depth, Porosity, and Clay

Mineral Orientation in Pennsylvanian Shales: Jour. Sed. Petrology, v. 36, p. 888-903.

Heling, D., 1970, Microfabrics of Shales and Their Rearrangement by Compaction: Sedimentology, v. 15, p. 247-260.

Hester, N.C., 1977, Upper Member of the Breathitt Formation, in Dever, G.R., Jr., and others, Stratigraphic Evidence for Late Paleozoic Tectonism in Northeastern Kentucky: Field Trip Guidebook Amer. Assoc. Petroleum Geologists, Eastern Sec., Ann. Mtg., Ky. Geol. Survey, p. 38-43.

Hopkins, T.C., and B.C. Gilpin, 1982, Identification of Kentucky Shales: Research Report, University of Kentucky, in Press.

Horne, J.C., and J.C. Ferm, 1976, A Field Guide to Carboniferous Depositional Environments in the Pocohontas Basin, Eastern Kentucky and Southern West Virginia: University of South Carolina, Dept. of Geology, 129 p.

Hosterman, J.W., and P.J. Loferski, 1978, Preliminary Report on the Clay Mineralogy of the Upper Devonian Shales in the Southern and Middle Appalachian Basin: U.S. Geol. Survey Open File Report, 78-1084, 26 p.

Johns, W.D., R.E. Grim, and W.F. Bradley, 1954, Quantitative Estimations of Clay Minerals By Diffraction Methods: Jour. Sed. Petrology, v. 24, p. 242-251.

Kazi, A., 1975, Quantitative Fabric Analysis of Drammen Clay Using X-ray Diffraction Technique: Jour. Sed. Petrology, v. 45, p. 883-890.

Kim, J., and F.J. Kohout, 1975, Multiple Regression Analysis, Subprogram Regression, in Nie, N.H., and others, SPSS - Statistical Package for the Social Sciences, 2nd Edition: McGraw-Hill Book Co., New York, p. 320-367.

Kinter, E.B., and S. Diamond, 1965, A New Method for Preparation and Treatment of Oriented-Aggregate Specimens of Soil Clays for X-ray Diffraction Analysis: Soil Science, v. 81, p. 111-120.

Klecka, W.R., 1975, Discriminant Analysis, in Nie, N.H., and others, SPSS - Statistical Package for the Social Sciences, 2nd Edition: McGraw-Hill Book Co., New York, p. 434-467.

Krumbein, W.C., and F.A. Graybill, 1965, An Introduction to Statistical Models in Geology: McGraw-Hill, New York, 475 p.

Lewan, M., 1978, Laboratory Classification of Fine-Grained Sedimentary

Rocks: Geology, v. 6, p. 745-748.

Lundegarde, P.D., and N.D. Samuels, 1980, Field Classification of Fine-Grained Sedimentary Rocks: Jour. Sed. Petrology, v. 50, p. 781-787.

Meade, R.H., 1961, X-ray Diffractometer Methods for Measuring Preferred Orientations in Clays: U.S. Geol. Survey Prof. Paper 424 B, p. 273-276.

Moon, C.F., 1972, The Microstructure of Clay Sediments: Earth Science Reviews, v. 8, p. 303-321.

O'Brien, N.R., 1970, The Fabric of Shale - An Electron Microscope Study: Sedimentology, v. 15, p. 229-246.

Odom, E.I., 1967, Clay Fabric and Its Relation to Structural Properties in Mid Continent Pennsylvanian Sediments: Jour. Sed. Petrology, v. 37, p. 610-623.

Olivier, H.J., 1979, A New Engineering - Geological Rock Durability Classification: Engineering Geology, v. 14, p. 255-279.

Overbey, W.K., C.A. Komar, J. Pasini III, 1973, Predicting Probable Roof Fall Areas in Advance of Mining by Geological Analysis: Bureau of Mines, Health and Safety Research Program, Tech. Prog. Report 70, 17 p.

Pettijohn, F.J., 1975, Sedimentary Rocks, 3rd Edition, Harper and Row, New York, 628 p.

Picard, M.D., 1971, Classification of Fine-Grained Sedimentary Rocks: Jour. Sed. Petrology, v. 41, p. 179-195.

Potter, P.E., J.B. Maynard, and W.A. Pryor, 1980, Sedimentology of Shale: Springer-Verlag, New York - Heidelberg - Berlin, 303 p.

Rice, C.L., E.G. Sable, G.R. Dever, Jr., and T.M. Kehn, 1979, Kentucky, in The Mississippian and Pennsylvanian (Carboniferous) Systems in the United States: U.S. Geol. Survey Prof. Paper 1110 A-L, p. FI-32.

_____, 1981, The Stratigraphic Framework of the Pennsylvanian Rocks in Eastern Kentucky, in Cobb, J.C., and others, Coal and Coal Bearing Rocks of Eastern Kentucky: Ann. Field Trip, Geol. Soc. Amer. Coal Division, Ky. Geol. Survey, p. 2-5.

Shimp, N.F., J. Witters, P.E. Potter, and J.A. Schleicher, 1969, Distinguishing Marine and Freshwater Muds: Jour. of Geology, v. 77, p. 566-580.

Smith, G.E., 1971, Introduction to Depositional Environments of Eastern Kentucky Coals in Smith, G.E., G.R. Dever, Jr., J.C. Horne, J.C. Ferm, and P.W. Whaley, Depositional Environments of Eastern Kentucky Coals: Ann. Field Conf., Geol. Soc. Amer., Coal Division, Ky. Geol. Survey, p. 1-2.

Spears, D.A., 1976, The Fissility of Some Carboniferous Shales: Sedimentology, v. 23, p. 721-725.

_____, 1980, Towards a Classification of Shales: Jour. Geol. Soc. London, v. 137, p. 125-129.

Stollar, R.L., 1976, Geology and Some Engineering Properties of Near Surface Pennsylvanian Shales in Northeastern Ohio: M.S. Thesis, Kent State University, 40 p.

Taylor, R.K., and D.A. Spears, 1970, The Breakdown of British Coal Measure Rocks: Int. Jour. Rock Mech. Min. Sci., v. 7, p. 481-501.

Tchalenko, J.S., A.D. Burnett, and J.J. Hung, 1971, The Correspondence Between Optical and X-ray Measurements of Clay Particle Orientation in Clays: Clay Minerals, v. 9, p. 47-70.

Tourtelot, H.A., 1960, Origin and Use of the Word "Shale": Amer. Jour. Sci., Bradley Vol., v. 258-A., p. 335-343.

Van Eekhout, E.M., 1976, The Mechanisms of Strength Reduction Due to Moisture in Coal Mine Shales: Int. Jour. Rock Mech. Min. Sci., v. 13, p. 61-67.

Wanless, H.R., J.R. Baroffio, and P.C. Trescott, 1969, Conditions of Deposition of Pennsylvanian Coal Beds, in Dapples, E.C., and M.E. Hopkins, Eds., Environments of Coal Deposition: Geol. Soc. Amer. Spec. Paper 114, p. 105-142.

_____, 1975, Appalachian Region, in McKee, E.D., and E.J. Crosby, Coordinators, Introduction and Regional Analysis of the Pennsylvanian System, Pt. 1 of Paleotectonic Investigations of the Pennsylvanian System in the United States: U.S. Geol. Survey Prof. Paper 853, p. 17-62.

Wood, L.E., and P. Deo, 1975, A Suggested System for Classifying Shale Materials for Embankments: Assoc. Eng. Geol. Bull., v. 12, p. 39-55.

APPENDICES

APPENDIX I

PETROLOGY OF BREATHITT FORMATION COAL MEASURE SHALES

Part A. Counted Samples

SAMPLE	DEPTH (meters)	SHALE TYPE	QUARTZ + FELDSPAR	CLAY	MICA	ORGANICS	PYRITE	CARBONATE	OTHERS	ROOTED	BURROWED
			Core #10-714 (SV1), Starfire Coal Co., Vest Quadrangle								
SV1-1	10.86	Mudstone	48	44	6	tr	-	1	tr	-	-
SV1-3	12.29	Mudstone	44	35	16	-	1	3	1	-	-
SV1-8	16.24	Claystone	11	71	9	8	tr	tr	-	-	-
SV1-10	38.44	Org. Shale	4	64	2	24	6	-	-	yes	-
SV1-13	40.57	Claystone	15	74	6	4	1	-	-	yes	yes
SV1-14A	43.00	Lam. Siltstone	32	32	15	10	2	9	-	-	-
SV1-16	45.03	Mudshale	16	57	16	9	1	tr	tr	-	-
SV1-17	65.38	Mudstone	40	33	13	4	2	8	-	-	-
SV1-18A	66.62	Mudshale	28	49	13	5	tr	4	tr	-	-
SV1-19	69.06	Mudstone	14	65	12	6	1	2	-	-	-
SV1-20	70.13	Sid. Shale	1	78	tr	2	1	17	tr	-	-
SV1-22	71.88	Mudshale	20	48	15	10	1	6	-	-	-
SV1-25A	76.22	Claystone	5	89	2	3	1	-	-	yes	-
SV1-32	81.80	Siltstone	54	30	12	1	3	-	-	yes	yes
SV1-32A	82.05	Siltstone	37	29	23	8	3	-	-	yes	-
SV1-33	82.36	Mudstone	13	53	14	6	1	13	-	-	-
SV1-36	84.28	Lam. Siltstone	41	30	18	8	1	2	-	yes	-
SV1-39	86.58	Claystone	tr	81	4	6	tr	8	-	-	-
SV1-40	89.12	Org. Shale	2	66	tr	31	tr	-	-	yes	-
			Core #8 (LV8), Leeco Coal Co., Vest Quadrangle								
LV8-3	11.10	Claystone	4	80	7	8	tr	tr	-	yes	-
LV8-6	14.10	Mudshale	22	41	18	13	1	5	-	-	-
LV8-9	17.40	Claystone	7	80	4	4	4	tr	tr	-	-
LV8-10	38.52	Clayshale	3	83	4	6	3	tr	tr	-	-
LV8-12	41.90	Siltstone	37	29	12	5	2	14	1	-	-

APPENDIX I - Part A.

SAMPLE	DEPTH (meters)	SHALE TYPE	QUARTZ + FELDSPAR	CLAY	MICA	ORGANICS	PYRITE	CARBONATE	OTHERS	ROOTED	BURROWED
			Core #8 (LV8), Leeco Coal Co., Vest Quadrangle								
LV8-13	44.70	Mudstone	34	39	15	6	1	5	-	-	-
LV8-14	45.60	Clayshale	10	74	8	4	1	2	1	-	yes
LV8-17	48.79	Mudstone	12	59	15	12	1	1	-	-	-
LV8-19	51.36	Mudstone	26	50	15	5	3	tr	tr	yes	-
LV8-21	53.82	Mudstone	26	42	16	9	tr	6	tr	-	-
LV8-22	55.06	Siltstone	44	31	13	4	tr	7	tr	-	-
LV8-25	83.63	Mudshale	18	34	27	9	1	11	-	-	-
LV8-38	100.05	Mudstone	30	51	14	3	2	-	-	yes	-
LV8-42	122.42	Lam. Siltstone	41	31	10	3	tr	14	tr	-	-
			Core #9 (LV1), Leeco Coal Co., Vest Quadrangle								
LV1-1	15.58	Mudstone	33	34	14	5	2	11	1	-	-
LV1-6	21.60	Claystone	8	67	9	7	7	2	-	yes	yes
LV1-7	22.44	Mudstone	25	52	15	4	3	1	-	-	-
LV1-11	25.58	Mudstone	25	41	20	6	3	5	-	-	-
LV1-12	26.09	Sid. Shale	33	22	15	6	2	22	-	-	-
LV1-13	26.57	Mudstone	28	39	17	7	3	5	1	-	-
LV1-14	27.80	Sid. Shale	5	71	2	2	tr	19	tr	-	-
LV1-16	30.83	Mudshale	42	33	13	3	3	5	1	-	-
LV1-30	46.11	Clayshale	10	78	3	7	-	2	-	-	-
LV1-31	55.69	Sid. Shale	10	44	14	8	3	21	-	-	-
LV1-33	58.86	Claystone	5	75	6	12	2	-	-	yes	-
LV1-34	60.57	Lam. Siltstone	51	21	9	8	-	11	-	-	-
LV1-37	62.50	Mudstone	32	45	20	tr	1	1	tr	-	-
LV1-41	77.05	Mudstone	30	49	14	4	2	-	1	yes	-

APPENDIX I - CONTINUED

Part B. Samples Classified Based on Estimated Clay Percent

SAMPLE	DEPTH (meters)	SHALE TYPE	CLAY	SAMPLE	DEPTH (meters)	SHALE TYPE	CLAY
Core #10-714 (SV1), Starfire Coal Co., Vest Quadrangle							
SV1-2	12.11	Mudstone	60	SV1-24	74.00	Clayshale	83
SV1-4	13.17	Mudstone	60	SV1-25	75.55	Org. Shale	66
SV1-5	13.93	Clayshale	90	SV1-26	76.72	Lam. Siltstone	32
SV1-6	14.17	Mudstone	60	SV1-27	77.00	Lam. Siltstone	24
SV1-7	15.69	Clayshale	90	SV1-28	78.06	Mudshale	50
SV1-9A	37.25	Claystone	75	SV1-30	79.44	Lam. Siltstone	25
SV1-11A	39.11	Mudshale	50	SV1-31	81.46	Mudstone	33
SV1-12	39.32	Clayshale	90	SV1-34	83.10	Siltstone	24
SV1-14	41.37	Mudstone	33	SV1-35	83.40	Claystone	66
SV1-15	43.86	Mudshale	50	SV1-37	85.60	Claystone	66
SV1-21	70.64	Siltstone	16	SV1-38	86.10	Claystone	66
SV1-23	73.82	Mudstone	50				
Core #8 (LV8), Leeco Coal Co., Vest Quadrangle							
LV8-1	10.09	Lam. Siltstone	30	LV8-27	84.43	Siltstone	23
LV8-2	10.39	Claystone	85	LV8-28	85.12	Lam. Siltstone	16
LV8-4	11.30	Mudshale	50	LV8-30	92.49	Sid. Shale	75
LV8-5	12.20	Lam. Siltstone	16	LV8-31	92.99	Claystone	75
LV8-7	15.85	Claystone	70	LV8-32	93.76	Siltstone	25
LV8-8	17.05	Claystone	80	LV8-34	95.75	Mudstone	33
LV8-15	46.38	Mudstone	60	LV8-37	99.41	Clayshale	75
LV8-16	48.44	Claystone	83	LV8-39	116.26	Claystone	83
LV8-20	52.15	Lam. Siltstone	30	LV8-41	121.63	Siltstone	33
LV8-26	84.25	Claystone	83				

APPENDIX I - Part B.

SAMPLE	DEPTH (meters)	SHALE TYPE	CLAY	SAMPLE	DEPTH (meters)	SHALE TYPE	CLAY
Core #9 (LV1), Leeco Coal Co., Vest Quadrangle							
LV1-2	16.21	Mudshale	65	LV1-26	42.00	Mudshale	45
LV1-3	17.23	Clayshale	78	LV1-27	43.23	Claystone	90
LV1-5	17.74	Clayshale	75	LV1-29	45.76	Clayshale	66
LV1-9	23.32	Sid. Shale	58	LV1-31A	56.53	Siltstone	8
LV1-10	24.13	Mudstone	40	LV1-32	58.34	Mudshale	44
LV1-15	30.10	Siltstone	25	LV1-35	61.15	Mudstone	60
LV1-21	37.52	Clayshale	75	LV1-36	61.84	Clayshale	75
LV1-22	39.49	Lam. Siltstone	32	LV1-38	63.34	Lam. Siltstone	20
LV1-23	39.82	Mudshale	58	LV1-39	74.58	Claystone	90
LV1-25	40.67	Sid. Shale	33	LV1-42	77.73	Mudstone	33

APPENDIX II

SLAKE DURABILITY TEST RESULTS

SAMPLE	SHALE TYPE	INITIAL WEIGHT (grams)	FINAL WEIGHT (grams)	SDI	APPEARANCE AFTER TEST
SV1-1	Mudstone	398.3	179.2	45.0	completely fragmented
SV1-3	Mudstone	393.8	302.0	76.7	mostly intact, some fragments
SV1-8	Claystone	384.0	226.6	59.0	partly fragmented
SV1-10	Org. Shale	399.4	187.8	47.0	completely fragmented
SV1-12	Clayshale	382.1	294.2	76.8	mostly fragmented
SV1-13	Claystone	399.5	221.5	55.4	completely fragmented
SV1-14	Mudstone	361.2	333.8	92.4	mostly intact, some fragments
SV1-14A	Lam. Siltstone	370.1	355.4	96.0	intact, edges rounded
SV1-15	Mudshale	389.9	364.0	93.4	mostly intact, some fragments
SV1-16	Mudshale	347.8	282.7	81.3	completely fragmented
SV1-17	Mudstone	300.8	294.8	98.0	intact, edges rounded
SV1-18A	Mudshale	396.1	376.2	95.0	mostly intact, fissile
SV1-19	Mudstone	381.6	359.1	94.1	mostly intact, few fragments
SV1-20	Sid. Shale	378.8	351.1	92.7	mostly intact, few fragments
SV1-21	Siltstone	377.5	354.7	94.0	intact, edges rounded
SV1-22	Mudshale	375.0	361.7	96.4	mostly intact, few fragments
SV1-23	Mudstone	362.0	343.8	95.0	mostly intact, few fragments
SV1-24	Clayshale	264.1	260.4	98.6	intact
SV1-25	Org. Shale	293.8	188.2	64.1	completely fragmented
SV1-25A	Claystone	366.6	117.6	32.1	completely fragmented
SV1-26	Lam. Siltstone	362.0	340.8	94.2	intact, edges rounded
SV1-27	Lam. Siltstone	274.6	270.6	98.6	intact
SV1-28	Mudshale	367.5	355.2	96.6	intact, edges rounded
SV1-29	Lam. Siltstone	391.2	355.4	90.8	mostly intact, fissile
SV1-30	Lam. Siltstone	358.2	338.1	94.4	intact, edges rounded
SV1-32	Siltstone	360.7	348.6	96.6	intact, edges rounded
SV1-32A	Siltstone	260.2	192.8	74.1	partly fragmented

SAMPLE	SHALE TYPE	INITIAL WEIGHT (grams)	FINAL WEIGHT (grams)	SDI	APPEARANCE AFTER TEST
SV1-33	Mudstone	389.3	326.2	83.8	completely fragmented
SV1-34	Siltstone	388.8	369.1	94.9	intact, edges rounded
SV1-36	Lam. Siltstone	382.9	356.3	93.1	mostly intact, few fragments
SV1-37	Claystone	387.1	345.0	89.1	partly fragmented, fissile
SV1-39	Claystone	347.4	262.6	75.6	partly fragmented
SV1-40	Org. Shale	365.1	259.3	71.0	completely fragmented
LV8-3	Claystone	147.2	53.7	36.4	completely fragmented
LV8-6	Mudshale	352.8	332.2	94.2	intact, edges rounded
LV8-9	Claystone	385.0	14.7	3.8	disintegrated
LV8-10	Clayshale	388.5	194.3	50.0	completely fragmented
LV8-12	Siltstone	383.2	366.4	95.6	intact, edges rounded
LV8-13	Mudstone	387.1	371.8	96.1	intact, edges rounded
LV8-14	Clayshale	391.7	367.5	93.8	partly fragmented, fissile
LV8-15	Mudshale	371.0	349.2	94.1	intact, edges rounded
LV8-16	Claystone	353.8	242.8	68.6	mostly fragmented
LV8-17	Mudstone	376.1	354.1	94.2	mostly intact, few fragments
LV8-19	Mudstone	382.5	323.8	84.4	mostly fragmented
LV8-20	Lam. Siltstone	384.9	365.8	95.0	intact, edges rounded
LV8-21	Mudstone	387.6	373.2	96.3	mostly intact, few fragments
LV8-22	Siltstone	376.4	360.8	95.9	intact, edges rounded
LV8-24	Siltstone	313.7	287.1	91.5	intact, edges rounded
LV8-25	Mudshale	395.4	373.3	94.4	mostly intact, few fragments
LV8-38	Mudstone	363.6	283.5	78.0	partly fragmented
LV8-42	Lam. Siltstone	376.1	362.4	96.3	intact, edges rounded
LV1-1	Mudstone	376.0	358.5	95.3	intact, edges rounded
LV1-6	Claystone	392.9	203.0	51.7	mostly fragmented
LV1-7	Mudstone	390.1	367.7	94.3	mostly intact, few fragments
LV1-11	Mudstone	380.2	361.9	95.2	intact, edges rounded
LV1-12	Sid. Shale	372.1	359.2	96.5	intact, edges rounded
LV1-13	Mudstone	370.8	357.8	96.5	intact, edges rounded

SAMPLE	SHALE TYPE	INITIAL WEIGHT (grams)	FINAL WEIGHT (grams)	SDI	APPEARANCE AFTER TEST
LV1-14	Sid. Shale	383.3	357.4	93.2	intact, edges rounded
LV1-16	Mudshale	399.1	373.8	93.7	intact, edges rounded
LV1-30	Clayshale	392.5	364.4	92.8	partly fragmented, fissile
LV1-31	Sid. Shale	389.2	383.4	98.5	intact
LV1-33	Claystone	359.8	234.6	65.2	completely fragmented
LV1-34	Lam. Siltstone	332.3	320.9	96.6	intact, edges rounded
LV1-37	Mudstone	356.6	271.4	76.1	partly fragmented
LV1-41	Mudstone	397.0	334.4	84.2	mostly fragmented

APPENDIX III

SLAKE DURABILITY INDICES PREDICTED BY MULTIPLE LINEAR REGRESSION

SAMPLE	ACTUAL SDI	PREDICTED SDI	RESIDUAL
SV1-1	45.0	75.5	-30.5
SV1-3	76.7	87.2	-10.5
SV1-8	59.0	65.2	-6.2
SV1-10	47.0	45.3	1.7
SV1-13	55.4	71.6	-16.2
SV1-14A	96.0	99.1	-3.1
SV1-16	81.3	84.8	-3.5
SV1-17	98.0	90.0	8.0
SV1-18A	95.0	88.7	6.3
SV1-19	94.1	75.6	18.5
SV1-20	92.7	74.0	18.7
SV1-22	96.4	94.6	1.8
SV1-25A	32.1	38.9	-6.8
SV1-32	96.6	85.9	10.7
SV1-32A	74.1	87.0	-12.9
SV1-33	83.8	94.9	-11.1
SV1-36	93.1	99.4	-6.3
SV1-39	75.6	65.8	9.8
SV1-40	71.0	71.7	-0.7
LV8-3	36.4	53.0	-16.6
LV8-6	94.2	90.3	3.9
LV8-9	3.8	48.4	-44.6
LV8-10	50.0	58.4	-8.4
LV8-12	95.6	91.5	4.1
LV8-13	96.1	88.0	8.1
LV8-14	93.8	86.8	7.0
LV8-17	94.2	84.6	9.6
LV8-19	84.4	66.5	17.9
LV8-21	96.3	90.3	6.0
LV8-22	95.9	91.1	4.8
LV8-25	94.4	115.5	-21.1
LV8-38	78.0	68.0	10.0
LV8-42	96.3	97.0	-0.7
LV1-1	95.3	93.9	1.4
LV1-6	51.7	52.2	-0.5
LV1-7	94.3	78.3	16.0
LV1-11	95.2	89.6	5.6
LV1-12	96.5	108.5	-12.0
LV1-13	96.5	91.2	5.3
LV1-14	93.2	85.7	7.5
LV1-16	93.7	75.1	18.6
LV1-30	92.8	72.4	20.4
LV1-31	98.5	106.4	-7.9
LV1-33	65.2	54.5	10.7
LV1-34	96.6	108.6	-12.0
LV1-37	76.1	80.2	-4.1
LV1-41	84.2	69.8	14.4

APPENDIX IV

DISCRIMINANT FUNCTION CLASSIFICATION OF SHALE SAMPLES AS DURABLE OR SLAKABLE, USING CLAY PERCENT AND CLAY MINERAL ORIENTATION.

SAMPLE	ACTUAL GROUP	PREDICTED GROUP	Z SCORE
SV1-1	Slakable	Durable	-0.1947
SV1-3	Slakable	Durable	-0.8151
SV1-8	Slakable	Slakable	1.7858
SV1-10	Slakable	Slakable	1.9924
SV1-13	Slakable	Slakable	1.2372
SV1-14A	Durable	Durable	-1.4593
SV1-16	Slakable	Durable	-0.5443
SV1-17	Durable	Durable	-1.4036
SV1-18A	Durable	Durable	-0.3934
SV1-19	Durable	Slakable	0.3782
SV1-20	Durable	Slakable	0.7443
SV1-22	Durable	Durable	-0.6876
SV1-25A	Slakable	Slakable	2.1917
SV1-32	Durable	Durable	-0.2586
SV1-32A	Slakable	Durable	-0.7914
SV1-33	Slakable	Durable	-1.0056
SV1-36	Durable	Durable	-1.2128
SV1-39	Slakable	Slakable	1.5077
SV1-40	Slakable	Slakable	0.7918
LV8-3	Slakable	Slakable	2.1677
LV8-6	Durable	Durable	-1.0774
LV8-9	Slakable	Slakable	1.8099
LV8-10	Slakable	Slakable	1.3805
LV8-12	Durable	Durable	-1.2685
LV8-13	Durable	Durable	0.0040
LV8-14	Durable	Durable	0.0445
LV8-17	Durable	Durable	-0.6715
LV8-19	Slakable	Slakable	0.8550
LV8-21	Durable	Durable	-0.3061
LV8-22	Durable	Durable	-1.1572
LV8-25	Durable	Durable	-1.9443
LV8-38	Slakable	Slakable	0.1951
LV8-42	Durable	Durable	0.0356
LV1-1	Durable	Durable	-1.2287
LV1-6	Slakable	Slakable	3.1137
LV1-7	Durable	Durable	-0.8227
LV1-11	Durable	Durable	-1.5545
LV1-12	Durable	Durable	-1.4198
LV1-13	Durable	Durable	-1.6659
LV1-14	Durable	Slakable	0.4738
LV1-16	Durable	Slakable	1.2205
LV1-30	Durable	Slakable	0.5057
LV1-31	Durable	Durable	-1.6260
LV1-33	Slakable	Slakable	1.2929
LV1-34	Durable	Durable	-1.7140
LV1-37	Slakable	Slakable	0.4573
LV1-41	Slakable	Slakable	1.3079

Discriminant Index, Z_0 = 0.1154

APPENDIX V

SAMPLED CORE DESCRIPTIONS

EXPLANATION

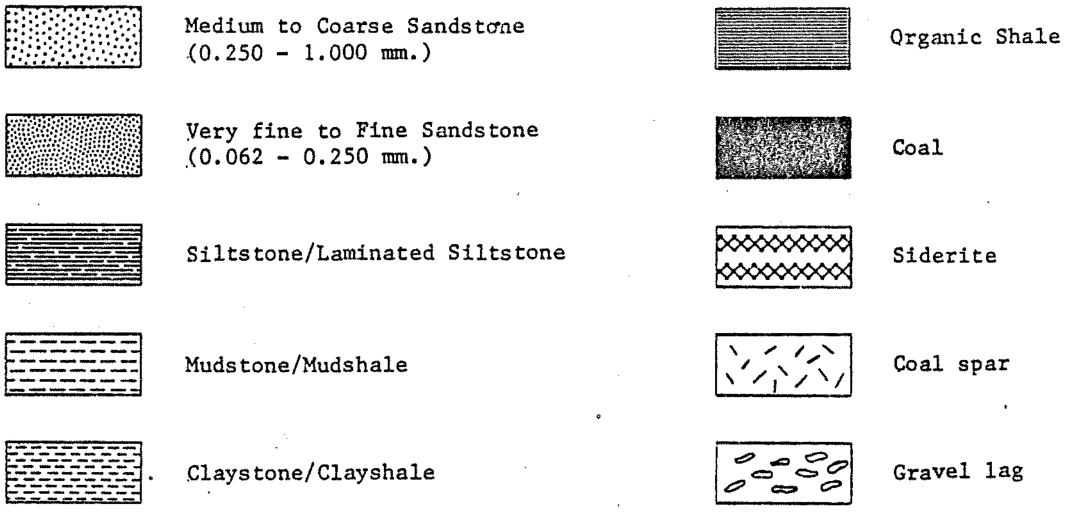

Scale: 50 mm. = 1 meter

Note

Colors described after coating with oil.

Laminae described according to Cole and Picard (1975), see Fig. 3.

Sorting refers to the quartz and feldspar fraction.

Coals were absent in several cases. Thicknesses were determined from driller's logs, data from the Kentucky Geological Survey, or gamma-density logs.

All contacts are gradational, unless otherwise noted.

All rock units drawn to scale except for sandstones thicker than 1.10 meters.

Core #10-714 (SV1), Starfire Coal Co., carter coordinates 22-L-77, 100' FSL x 1200' FEL, elev. 1400', Vest Quadrangle, Knott County, Kentucky.

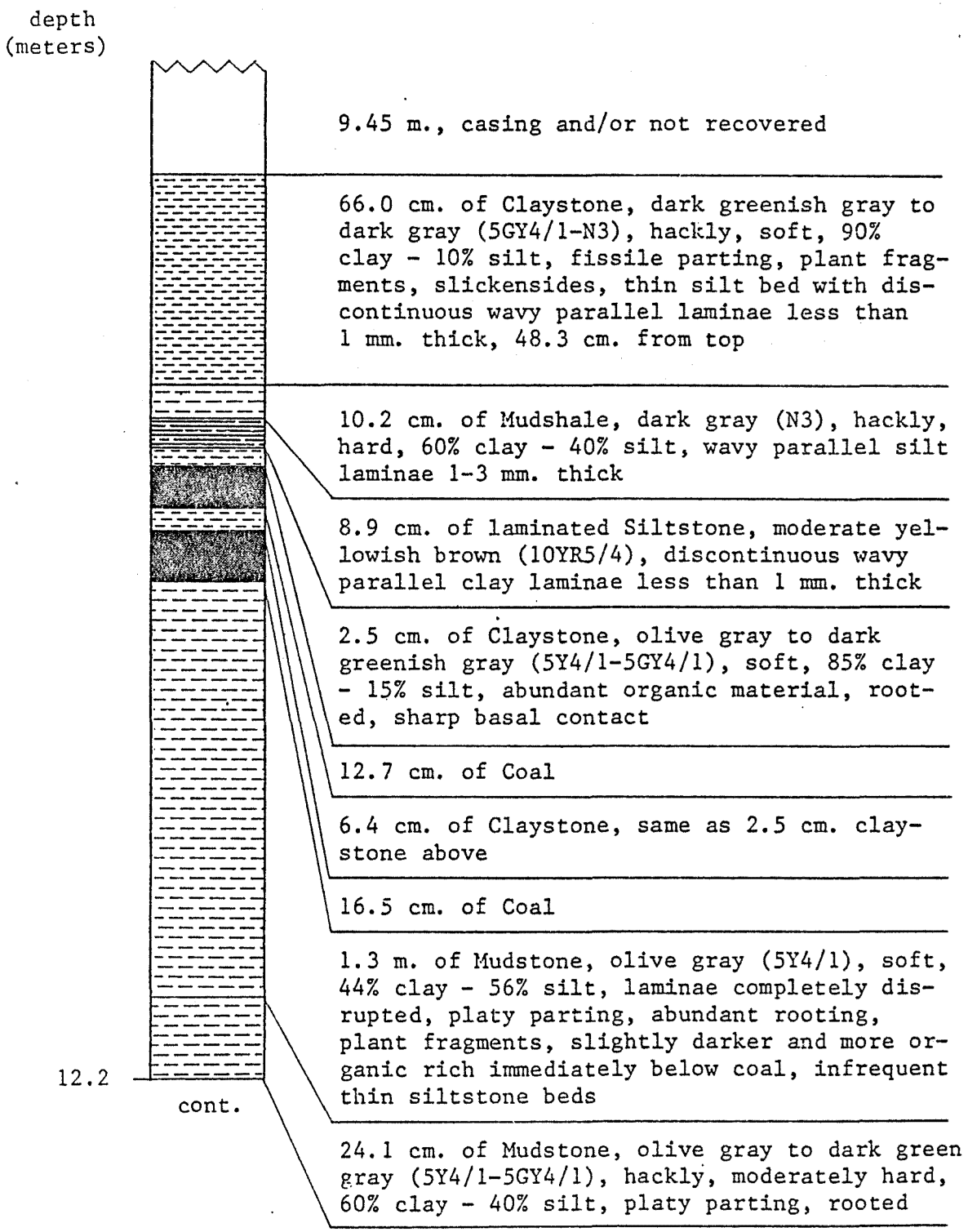

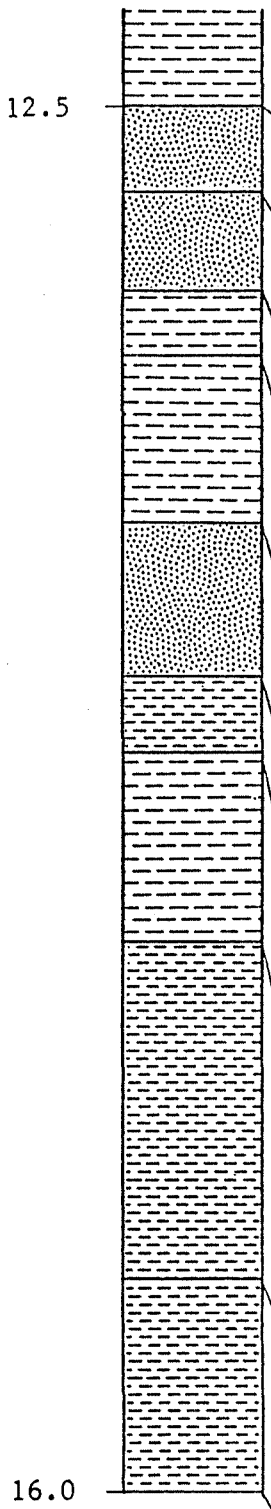

12.5

25.4 cm. of Mudstone, olive gray to dark greenish gray (5Y4/1-5GY4/1), hackly, moderately hard, 60% clay - 40% silt, platy parting, rooted

21.6 cm. of fine Sandstone, greenish gray (5GY6/1) at top, light olive gray (5Y6/1) at base, average grain size .125-.177 mm., very well sorted, even parallel laminae

24.1 cm. of very fine Sandstone, greenish gray (5GY6/1), average grain size .088-.125 mm., very well sorted, infrequent laminae in upper 5 cm.

16.5 cm. of Mudstone, medium dark gray (N4), 55% clay - 45% silt, silt decreases toward base, even parting surfaces

43.2 cm. of Mudstone, dark gray (N3), brittle to hackly fracture, moderately hard, 60% clay - 40% silt, platy parting with even surface, sparse mica

38.1 cm. of fine Sandstone, dark greenish gray to dark gray (5GY4/1-N3), average grain size .125-.177 mm., very well sorted, cross laminated

20.3 cm. of Clayshale, dark greenish gray to dark gray (5GY4/1-N3), brittle, hard, 90% clay - 10% silt, even parallel color (siderite) laminae 2 mm. thick, approximately 5% siderite

48.3 cm. of Mudstone, dark gray (N3), brittle, hard, 60% clay - 40% silt, silt decreases towards base, flaggy parting, sparse plant fragments, sharp basal contact

86.3 cm. of Clayshale, dark gray to dark greenish gray (N3-5GY4/1), hackly, moderately hard, 90% clay - 10% silt, even discontinuous parallel laminae, fissile parting with fairly even surface

16.0

cont.

53.3 cm. of Clayshale, medium dark gray (N4), hard, 90% clay - 10% silt, even parallel color (siderite) laminae 1-2 mm. thick, fissile parting, plant fragments, sharp basal contact

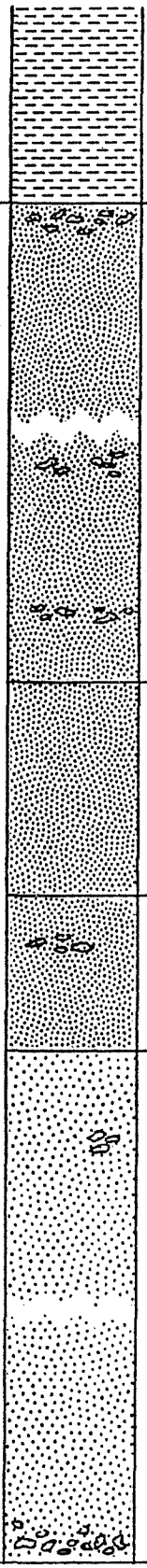

53.3 cm. of Claystone, moderate olive brown (5Y4/4), hackly, moderately hard, 71% clay - 29% silt, infrequent even parallel siderite and organic laminae 1 mm. thick, striking color contrast

16.5

2.9 m. of massive, fine to medium Sandstone, light gray (N7), average grain size .177-.250 mm. in upper 2.0 m., .350-.500 mm., in lower 0.9 m., well sorted, clay clasts at top, at 1.9 m., and at 2.1 m., rare thin even parallel laminae in lower 0.9 m., basal 15.2 cm. is fractured

55.9 cm. of cross-laminated, fine Sandstone, light gray (N7), average grain size .177-.250 mm., very well sorted, laminae 3 mm. thick

43.2 cm. of cross-bedded, fine Sandstone, light gray (N7), average grain size .177-.250 mm., clay clasts at 17.8 cm.

4.1 m. of massive, medium Sandstone, light gray (N7), average grain size .177-.350 mm., coarsening downward, moderately sorted, infrequent clay clasts, rare cross-laminae, basal 1.1 m. fractured, gravel lag at base

24.5

cont.

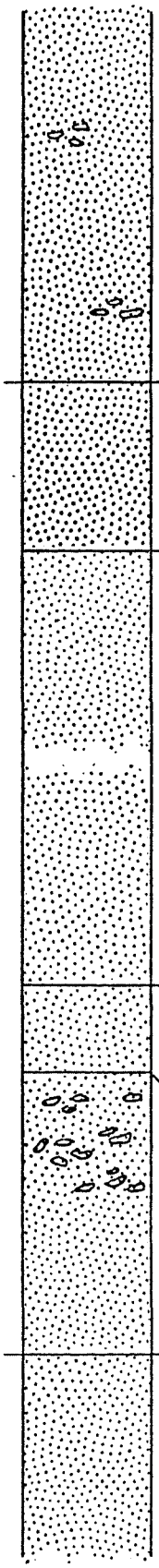

99.1 cm. of massive, medium Sandstone, light gray (N7), average grain size .177-.350 mm., coarsening downward, moderately sorted, infrequent cross-laminae and clay clasts

25.5

47.0 cm. of cross-laminated, medium sandstone, grayish orange (10YR7/4), average grain size .250-.350 mm., moderately sorted, thin organic rich laminae

1.6 m. of massive, medium Sandstone, light gray (N7), average grain size .177-.350 mm., moderately sorted, isolated cross-laminae, clay clast at 67.1 cm.

24.1 cm. of massive, medium Sandstone, light gray (N7), average grain size .250-.350 mm., moderately sorted, rare thin even parallel laminae

78.7 cm. of massive, medium Sandstone, yellowish gray (5Y8/1), average grain size .250-.350 mm., moderately sorted, upper 35.6 cm. fracturedwith abundant clay clasts, lower 15.2 cm., fractured

28.6

1.6 m. of massive, medium Sandstone, light gray (N7), average grain size .250-.500 mm., moderately sorted

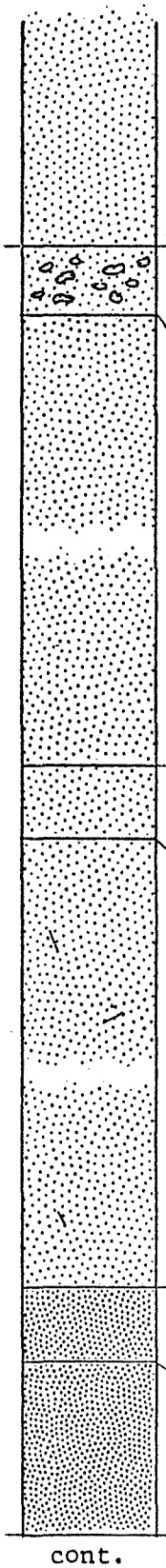

30.2

17.8 cm. of medium Sandstone with rippled coal spar, clay clasts, yellowish gray (5Y8/1), average grain size .250-.350 mm., moderately sorted

1.4 m. of rippled Sandstone, light gray (N7), average grain size .177-.250 mm. in upper 22.9 cm., .250-.350 mm. to base, very well to well sorted, laminae become less abundant toward base

20.3 cm. of cross-laminated, medium Sandstone, light gray (N7), average grain size .250-.350 mm.,moderately sorted

1.2 m. of massive, medium Sandstone, light gray (N7), average grain size .250-.350 mm., moderately sorted, rare coal spars

20.3 cm. of cross-laminated, fine Sandstone, light gray (N7), average grain size .177-.250 mm., coaly organic rich laminae

48.3 cm. of massive, fine Sandstone, light gray (N7), average grain size .177-.250 mm., very well sorted

33.9

cont.

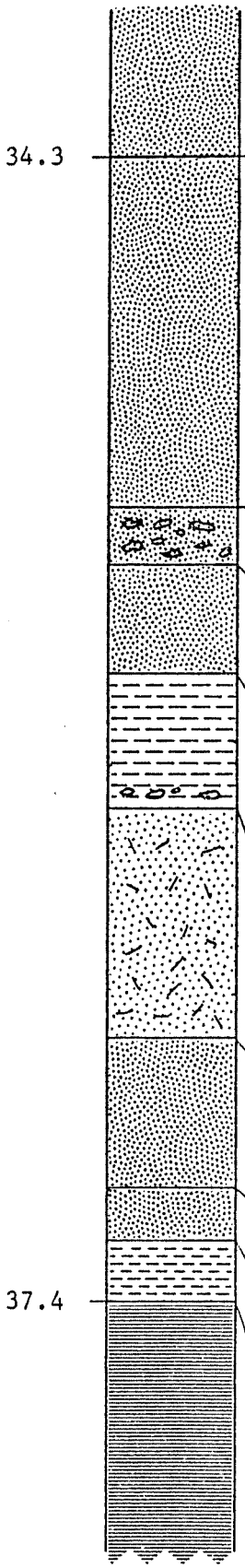

40.6 cm. of laminated, fine Sandstone, light gray (N7), average grain size .177-.250 mm., very well sorted, organic rich even parallel laminae

34.3

95.2 cm. of massive, fine Sandstone, light gray (N7), average grain size .177-.250 mm., well sorted, isolated even parallel laminae

15.2 cm. of massive, fine Sandstone with large clay clasts and siderite pebble, average grain size .177-.250 mm., well sorted

30.5 cm. of cross-laminated, fine Sandstone, light gray (N7), average grain size .177-.250 mm., very well sorted, cross-laminated coal spars

35.6 cm. of Mudshale, dark greenish gray (5GY4/1), hard, 50% clay - 50% silt, cross-laminated with wavy, convolute laminae, followed by 2.5 cm. of siltstone with clay clasts and siderite nodules, slickensides, plant fragments

61.0 cm. of medium Sandstone with randomly oriented, abundant, large coal spars, average grain size .250-.350 mm., moderately sorted

40.6 cm. of rippled, fine Sandstone, average grain size .177-.250 mm., moderately sorted, rippled coal spars

37.4

14.0 cm. of massive, fine Sandstone, light gray (N7), average grain size .125-.177 mm., very well sorted, rooted

15.2 cm. of Claystone, medium dark gray to dark greenish gray (N4-5GY4/1), hackly, hard, 75% clay - 25% silt, slickensides, plant fragments, rooting, mica

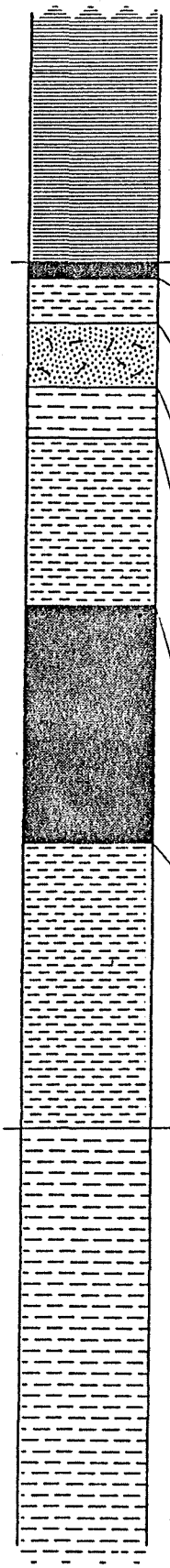

1.4 m. of Organic Shale, medium dark gray (N4), hackly, hard, 64% clay - 36% organics, lamination destroyed, rooted, slickensides

38.8

2.5 cm. of Coal

11.4 cm. of Clayshale, grayish black (N2), hackly, hard, 90% clay - 10% organics, wavy parallel coal spar less than 1 mm. thick

15.2 cm. of fine Sandstone, average grain size .177-.250 mm., moderately sorted, with slumped shale and coal spar

14.0 cm. of Mudshale, medium dark gray (N4), 50% clay - 50% silt, wavy parallel silt laminae 1-2 mm. thick, minor bioturbation, sand bed 2.5 cm. thick, .177-.250 mm.

45.7 cm. of Clayshale, top is dark gray (N3) base is grayish black (N2), hackly, even parallel siderite laminae 3 mm. thick, discontinuous wavy parallel near base, fissile parting

66.0 cm. of Coal

74.9 cm. of Claystone, greenish gray to dark greenish gray (5GY6/1-5GY4/1), hackly, soft, 73% clay - 27% silt, rooted, slickensides, dark green glauconite-like grains .710 mm.

41.0

1.7 m. of Mudstone, gradational color change from dark greenish gray (5GY4/1) at top to dark gray (N3) at base, hackly, hard, 33% clay - 67% silt, platy parting, plant fragments, rooted, trace siderite, mica

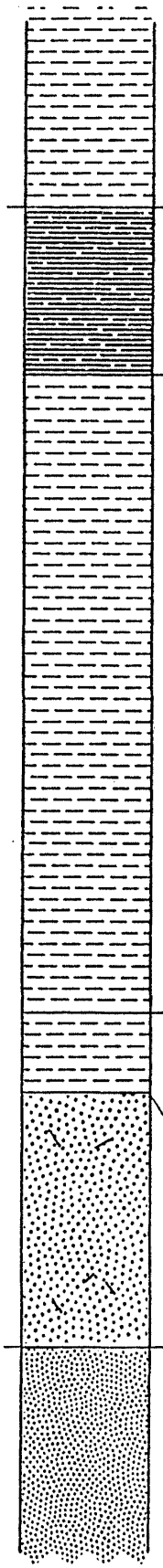

42.8

45.7 cm. of laminated Siltstone, medium gray (N4), 32% clay - 68% silt, even parallel silt laminae 1 mm. thick, flaggy parting

1.8 m. of Mudshale, dark gray (N3), brittle, hard, 50% clay - 50% silt, even discontinuous parallel silt laminae less than 1 mm. thick, flaggy parting, siderite and organic laminae 1 mm. thick increase in lower 68.6 cm., plant fragments

20.3 cm. of Mudshale, dark gray to dark greenish gray (N3-5GY4/1), hackly, hard, 60% clay - 40% silt, even parallel silt and clay laminae 1-4 mm. thick, sand bed at 10 cm., erosive basal contact

72.4 cm. of massive, medium Sandstone, yellowish gray (5Y8/1), average grain size .177-.350 mm., well sorted, occasional coal spar

45.9

73.7 cm. of rippled, fine Sandstone, yellowish gray (5Y8/1), average grain size .125-.250 mm., well sorted, becomes massive at 25.4 cm. for 22.9 cm., rare coal spars

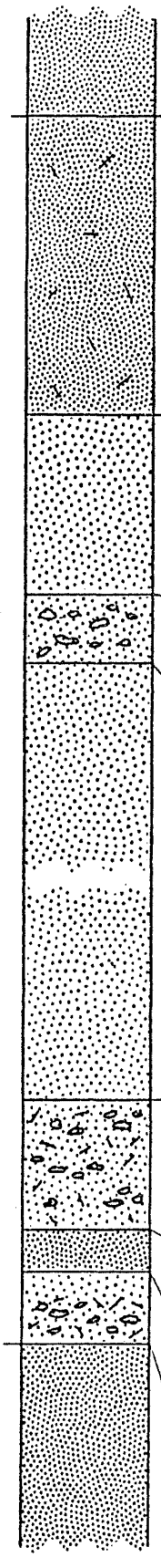

46.7

81.3 cm. of massive, fine Sandstone, very light gray (N8), average grain size .177-.250 mm., very well sorted, infrequent coal spars

49.5 cm. of cross-laminated, medium Sandstone, grayish black to yellowish gray (N2-5Y8/1), average grain size .250-.350 mm., moderately sorted, laminae less than 5 mm. apart in upper 20.3 cm., becoming cross-bedded toward base

19.1 cm. of massive, medium Sandstone, yellowish gray (5Y8/1), average grain size .350-.500 mm., moderately sorted, with abundant clay clasts

2.0 m. of massive, medium Sandstone, yellowish gray (5Y8/1), average grain size .350-.500 mm., moderately sorted, rare coal spars

35.6 cm. of massive, medium Sandstone, yellowish gray (5Y8/1), average grain size .177-.350 mm., moderately sorted, with clay clasts and coal spars

11.4 cm. of laminated, fine Sandstone, very light gray (N8), average grain size .177-.250 mm., well sorted, organic rich laminae 6 mm. thick

50.8

19.1 cm. of massive, medium Sandstone, yellowish gray (5Y8/1), average grain size .250-.350 mm., very well sorted, clay clasts and coal spars abundant in lower 10.2 cm.

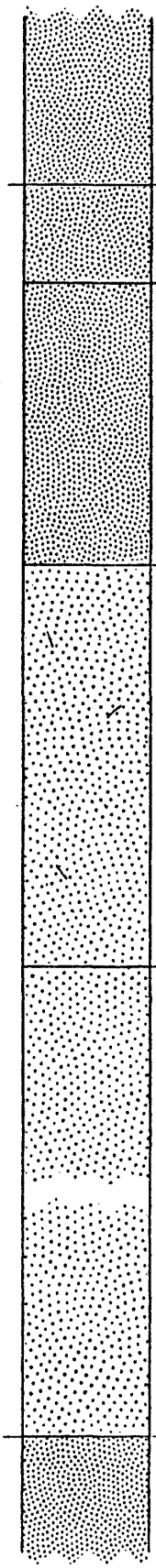

91.4 cm. of massive, fine Sandstone, very light gray (N8), average grain size .177-.250 mm., very well sorted

51.7

25.4 cm. of cross-laminated, fine Sandstone, as above

78.7 cm. of massive, fine Sandstone, as above with 3.8 cm. of rippled coal spar 30.5 cm. from base

1.1 m. of generally massive, medium Sandstone, light gray (N7), average grain size .250-.350 mm., well sorted, rare coal spars, alternating with 4 cross-laminated units 7.6 to 22.9 cm. thick

2.4 m. of massive, medium Sandstone, light gray (N7), average grain size .250-.350 mm., size increases downward, well sorted, isolated thin ripple laminae

56.3

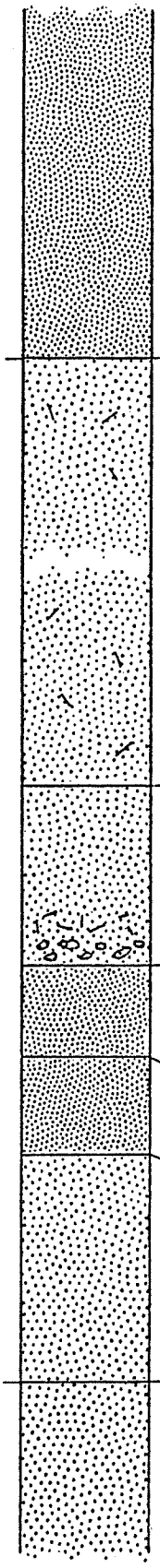

1.3 m. of rippled, fine Sandstone, light gray (N7), average grain size .177-.250 mm., well sorted, rare coal spar, 38.1 cm. of massive sand at 76.2 cm.

57.6

1.6 m. of massive, medium Sandstone, light gray (N7), average grain size .250-.350 mm., very well sorted, infrequent ripple laminae and coal spars

48.3 cm. of rippled, medium Sandstone, as above, with large coal spars, clay clasts, and siderite pebbles in basal 10.2 cm.

25.4 cm. of massive, fine Sandstone, light gray (N7), average grain size .177-.250 mm., well sorted

25.4 cm. of rippled, fine Sandstone, as above

61.0 cm. of massive, medium Sandstone, light gray (N7), average grain size .250-.350 mm., well sorted, large coal spar 5 mm., thick 8.9 cm. from base

60.8

71.1 cm. of cross-laminated, medium Sandstone, light gray (N7), average grain size .250-.350 mm., well sorted, laminae 2 mm. thick, 20.3 cm. of massive sand at 81.3 cm.

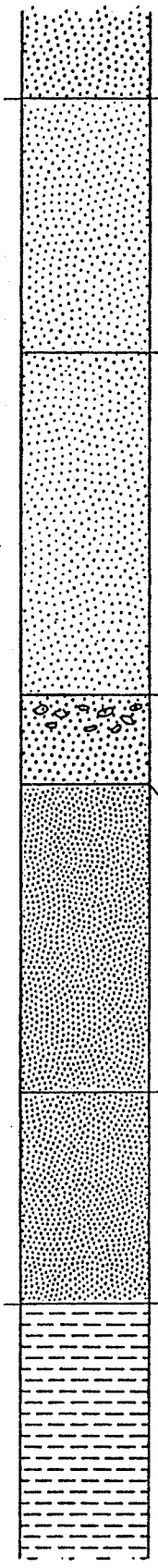

61.5

68.6 cm. of rippled, medium Sandstone, similar to previous unit

95.2 cm. of massive, medium Sandstone, light gray (N7), average grain size .250-.350 mm., very well sorted

25.4 cm. of medium Sandstone, light gray (N7), with clay clasts in upper 10.2 cm., followed by cross-laminae and rippled coal spar to base, average grain size .250-.350 mm., moderately sorted

86.4 cm. of rippled, fine Sandstone, light gray (N7), average grain size .177-.250 mm., very well sorted

55.9 cm. of massive, fine Sandstone, light gray (N7), average grain size .177-.250 mm., very well sorted, with 3.8 cm. of rippled coal spar 15.2 cm. from base

64.8

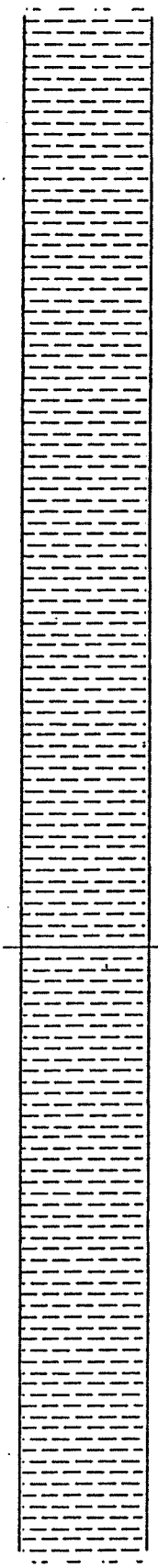

3.3 m. of alternating Mudshale and Mudstone, olive gray to dark greenish gray (5Y4/1-5GY4/1), hard, with plant fragments, mica, iron staining (siderite). Mudstones contain 33% clay - 67% silt. Mudshales contain 49% clay - 51% silt, with even discontinuous parallel silt laminae 1-2 mm. thick, rare bioturbation, silt content and laminae thickness decrease toward base.

9 units were differentiated, the 5 mudshale units range from 7.6 cm. to 1.1 m. thick, the 4 mudstone units range from 6.4 cm. to 36.8 cm. thick

68.1

1.8 m. of Mudstone, dark greenish gray (5GY4/1), hard, 65% clay - 35% silt, slabby parting, siderite, plant fragments

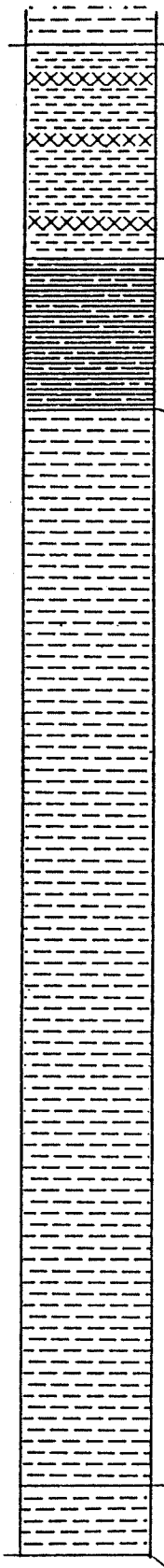

69.9

55.9 cm. of Sideritic Shale, grayish black (N2), hackly, 78% clay - 5% silt - 17% siderite, slabby parting, small siderite nodules 1x5 mm.

40.6 cm. of Siltstone, medium gray to dark greenish gray (N5-5GY4/1), laminae destroyed by bioturbation, brachiopods, silt decreases toward base

2.9 m. of Mudshale, dark gray (N3), hackly, 48% clay - 52% silt, discontinuous wavy parallel silt and organic laminae 1 mm. thick, plant fragments, mica, siderite

17.8 cm. of Mudstone, olive black (5Y2/1), hackly, hard, 50% clay - 50% silt, churned (bioturbated), flaggy parting

74.0

cont.

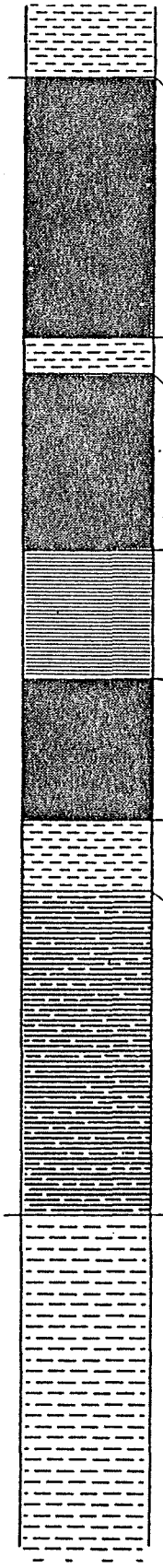

74.2

20.3 cm. of Clayshale, olive black (5Y2/1), hackly, hard, 83% clay - 17% silt, even parallel color laminae 1-2 mm. thick, flaggy parting, sharp basal contact

69.8 cm. of Coal

10.2 cm. of Claystone, grayish black (N2), hackly, soft, 90% clay - 10% organics, slickensides, coal fragments

50.8 cm. of Coal

33.0 cm. of Organic Shale, grayish black (N2), hackly, soft, 66% clay - 2% silt - 32% organics, rooted

39.4 cm. of Coal

20.3 cm. of Claystone, medium dark gray (N4), hackly, soft, 90% clay - 10% silt, slickensides, rooted

87.6 cm. of laminated Siltstone, medium gray (N5), blocky, 32% clay - 68% silt, wavy parallel silt and organic laminae 1-2 mm. thick in upper 67.3 cm., wavy discontinuous clay laminae less than 1 mm. thick in lower 20.3 cm., horizontal burrow, plant fragments, rooting, disseminated siderite

77.3

1.4 m. of Mudshale, dark greenish gray (5GY4/1), hackly, hard, 50% clay - 50% silt, wavy parallel silt laminae 2-3 mm. thick, slabby parting, plant fragments, mica, siderite

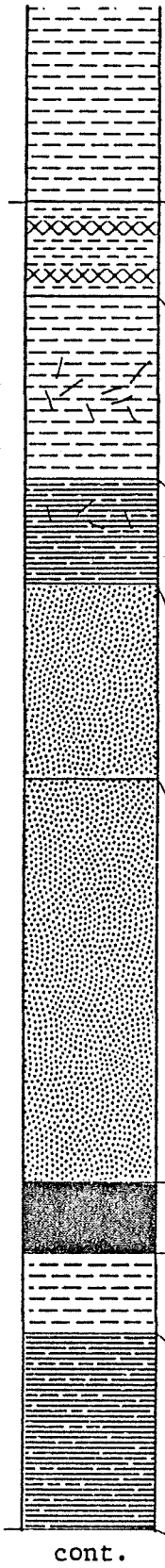

78.7

25.4 cm. of Sideritic Shale, olive black (5Y2/1), hackly, hard, 70% clay - 11% silt - 19% siderite, discontinuous wavy parallel organic laminae less than 1 mm. thick, blocky parting, siderite nodules, plant fragments

48.3 cm. of Mudshale, medium dark gray (N4), hard, 40% clay - 60% silt, discontinuous wavy parallel laminae less than 1 mm. thick, slickensides, coal spar, plant fragments

27.9 cm. of laminated Siltstone, olive gray to medium dark gray (5Y4/1-N4), hard, 25% clay - 75% silt, even parallel silt and clay laminae 1-4 mm. thick, silt increases toward base, plant fragments, coal spar, rare siderite

50.8 cm. of laminated, very fine Sandstone, light gray (N7), average grain size .088-.177 mm., very well sorted, with even parallel organic laminae

1.1 m. of fine Sandstone, light gray (N7), average grain size .177-.250 mm., well sorted, upper 35.6 cm. massive, lower 71.1 cm. rippled with organic rich wavy laminae

16.5 cm. of Coal

21.6 cm. of Mudstone, dark greenish gray (5GY4/1), hackly, hard, 33% clay - 67% silt, slickensides, plant fragments, rooted

52.1 cm. of Siltstone, medium light gray to greenish gray (N6-5GY6/1), hackly, 30% clay - 70% silt, disrupted laminae, slickensides, plant fragments, rooted

82.2

cont.

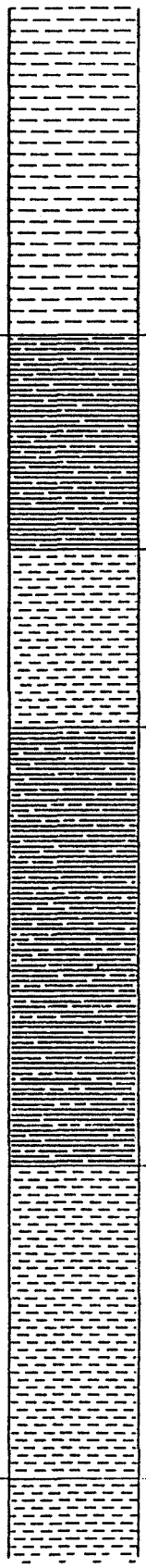

88.9 cm. of Mudstone, medium gray (N4), hackly, hard, 53% clay - 34% silt - 13% siderite, slabby parting, small siderite nodules, plant fragments.

83.1

58.4 cm. of Siltstone, medium light gray (N5), 24% clay - 71% silt - 5% siderite, discontinuous wavy parallel clay laminae in lower 33.0 cm., plant fragments

49.5 cm. of Claystone, medium gray (N4), hackly, hard, 66% clay - 34% silt, slabby parting, 3 mm. clay clasts, rooting, trace siderite

1.2 m. of laminated Siltstone, dark gray (N3), 30% clay - 70% silt, discontinuous wavy silt and clay laminae 1-2 mm. thick, flaggy parting, plant fragments

90.2 cm. of Claystone, dark gray (N3), hackly, hard, 66% clay - 34% silt, rare very thin, discontinuous parallel laminae, clay increases to 90% between 43.2 and 57.2 cm., plant fragments, slickensides

86.3

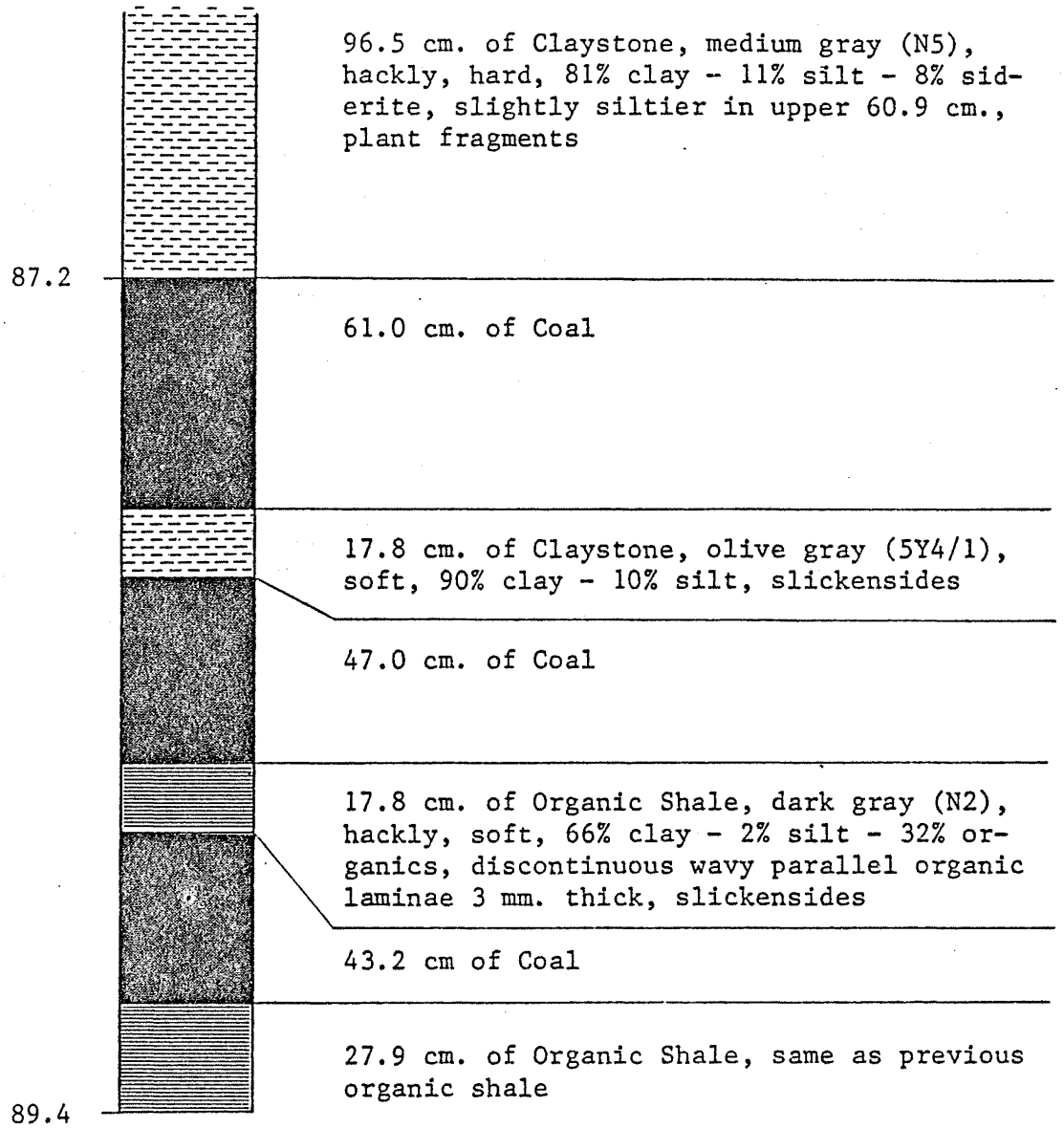
96.5 cm. of Claystone, medium gray (N5), hackly, hard, 81% clay - 11% silt - 8% siderite, slightly siltier in upper 60.9 cm., plant fragments
87.2
61.0 cm. of Coal
17.8 cm. of Claystone, olive gray (5Y4/1), soft, 90% clay - 10% silt, slickensides
47.0 cm. of Coal
17.8 cm. of Organic Shale, dark gray (N2), hackly, soft, 66% clay - 2% silt - 32% organics, discontinuous wavy parallel organic laminae 3 mm. thick, slickensides
43.2 cm of Coal
27.9 cm. of Organic Shale, same as previous organic shale
89.4

Core #9A (LV1), Leeco Coal Co., carter coordinates 15-K-78, 1400' FNL x 1600' FWL, elev. 1410', Vest Quadrangle, Knott County, Kentucky.

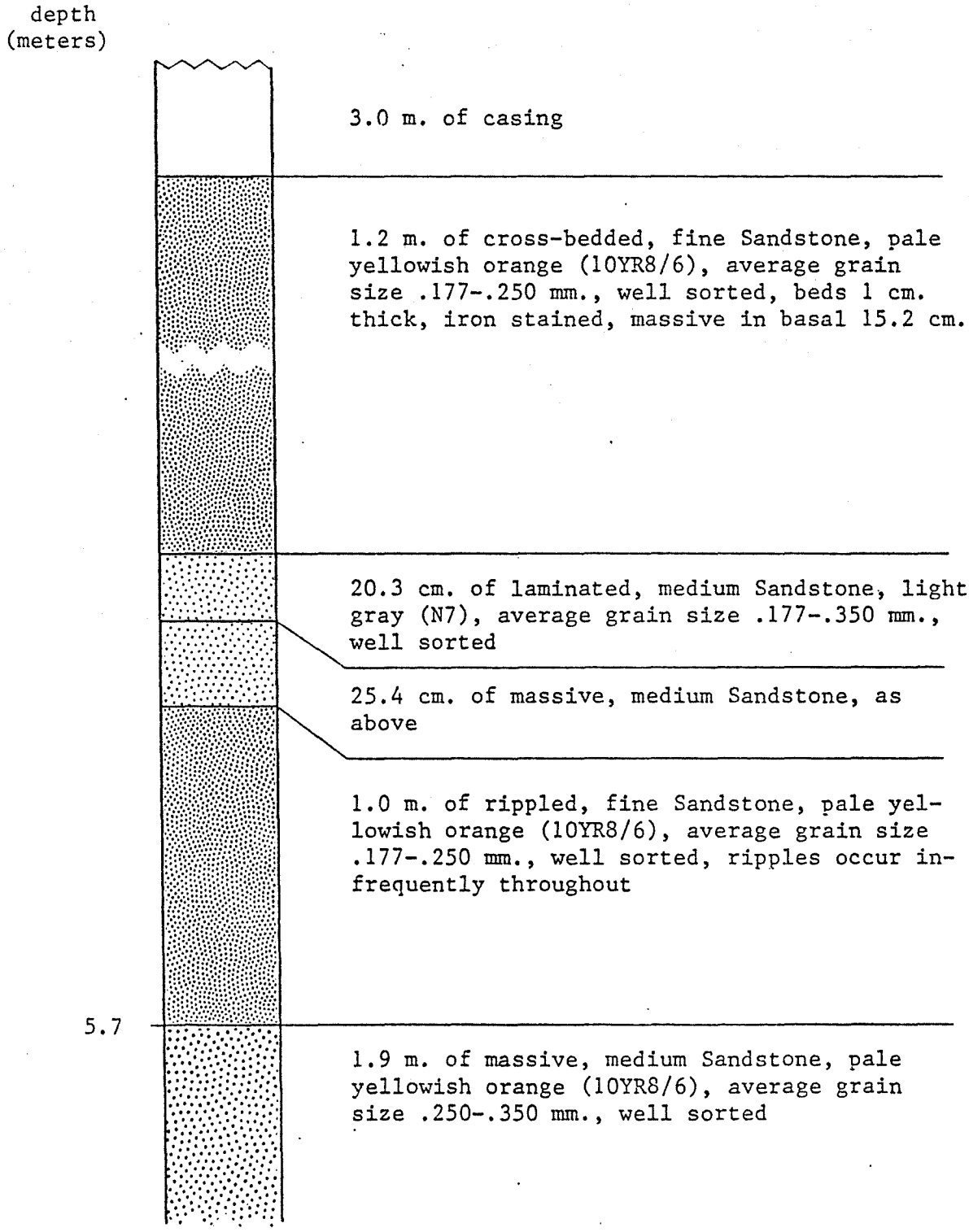

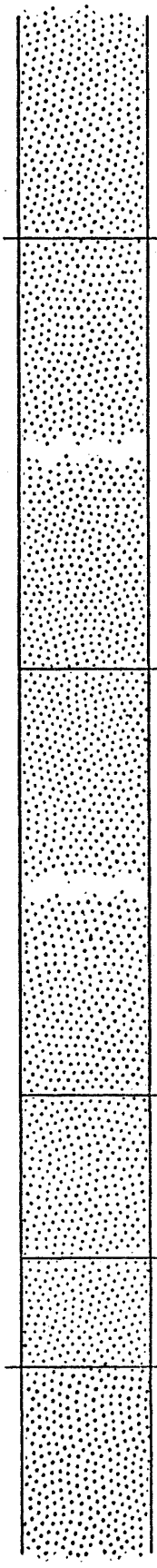

7.6

1.5 m. of cross-bedded, medium Sandstone, pale yellowish orange (10YR8/6), average grain size .177-.350 mm., moderately sorted, ripples in upper 20.3 cm.

1.4 m. of massive, medium Sandstone, pale yellowish orange (10YR8/6), average grain size .250-.350 mm., moderately sorted, very infrequent ripples

45.7 cm. of cross-bedded, medium Sandstone, pale yellowish orange (10YR8/6), average grain size .177-.350 mm., well sorted, becoming rippled in lower 15.2 cm.

30.5 cm. of massive, medium Sandstone, as above

11.2

78.7 cm. of rippled, medium Sandstone, as above, with clay clasts up to 1.5 cm. long, and organic rich ripple laminae in basal 21.6 cm., 17.8 cm. of massive sand 20.3 cm. from top

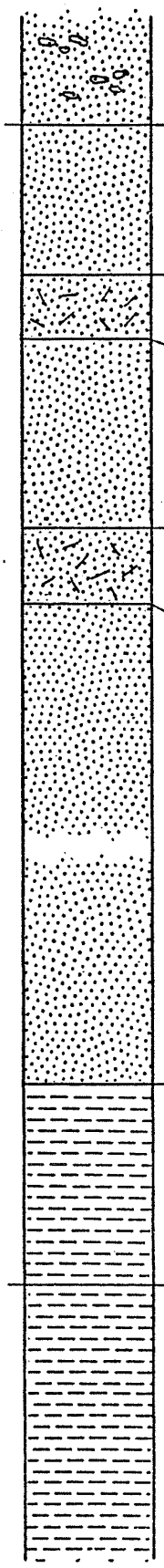

12.0

40.6 cm. of massive, medium Sandstone, pale yellowish orange (10YR8/6), average grain size .250-.350 mm., very well sorted

17.8 cm. of massive, medium Sandstone, light gray (N7), with coal spars

52.1 cm. of cross-laminated to laminated, medium Sandstone, light gray (N7), average grain size .250-.350 mm., very well sorted

20.3 cm. of massive, medium Sandstone, light gray (N7), with coal spars

2.2 m. of cross-laminated and rippled, medium Sandstone, light gray (N7), laminae become more abundant and organic rich toward base, average grain size .177-.350 mm., moderately sorted

59.7 cm. of Mudstone, medium gray (N5), hard, 34% clay - 55% silt - 11% siderite, plant fragments

16.1

94.0 cm. of Mudshale, dark gray (N3), hard, 65% clay - 35% silt, even parallel organic and silt laminae 1-2 mm. thick, laminae slightly inclined

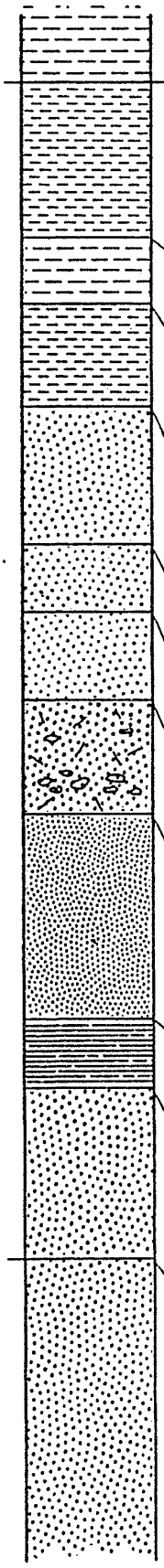

17.1

43.2 cm. of Clayshale, dark gray to dark greenish gray (N3-5GY4/1), hackly, moderately hard, 78% clay - 22% silt, wavy parallel to even parallel clay and siderite laminae 1 mm. thick, clay laminae disrupted by large pyrite nodules (6-15 mm.), abundant plant fragments

17.8 cm. of Mudshale, dark gray (N3), hard, 50% clay - 50% silt, even parallel silt laminae 1-2 mm. thick, sand in top 2.5 cm.

27.9 cm. of Clayshale, dark gray (N3), moderately hard, 75% clay - 25% silt, even parallel organic laminae 1-2 mm. thick, slightly inclined, rare siderite

38.1 cm. of massive, medium Sandstone, light gray (N7), average grain size .250-.350 mm., very well sorted

19.1 cm. of rippled, medium Sandstone, as above

25.4 cm. of massive, medium Sandstone, as above, becoming laminated in basal 5.1 cm.

30.5 cm. of rippled, medium Sandstone, as above, with clay clasts and coal spars

58.4 cm. of massive, fine Sandstone, light gray (N7), top 7.6 cm. laminated, average grain size .177-.250 mm., moderately sorted

19.1 cm. of laminated Siltstone, medium light gray (N6), 16% clay - 74% silt+sand - 10% organics, wavy parallel laminae, average grain size of sand .177-.250 mm.

20.3

47.0 cm. of rippled, medium Sandstone with abundant clay clasts, light gray (N7), average grain size .250-.350 mm., well sorted

90.2 cm. of rippled, medium Sandstone, light gray (N7), average grain size .250-.350 mm., very well sorted

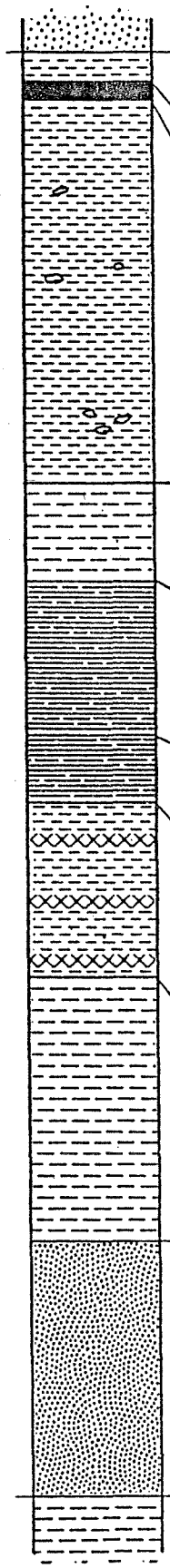

21.2

6.4 cm. of Claystone, dark gray (N3), brittle, moderately hard, 80% clay - 20% silt, slickensides

2.5 cm. of Coal

1.1 m. of Claystone, medium gray to dark greenish gray (N5-5GY4/1), 67% clay - 31% silt - 2% siderite, rare discontinuous silt laminae, slickensides, rooting, clay clasts, plant fragments

25.4 cm. of Mudstone, dark greenish gray (5GY4/1), hard, 52% clay - 47% silt - 1% siderite, rooted, very rare burrows

43.2 cm. of interbedded Mudstone/Siltstone, medium gray (N5), approximately 25% clay - 75% silt in siltstone, beds up to 6 cm. thick, rare bioturbation

15.2 cm. of Siltstone, dark greenish gray (5GY4/1), laminae destroyed (churned), siderite nodules

50.8 cm. of Sideritic Shale, dark greenish gray (5GY4/1), hard, 58% clay - 22% silt - 20% siderite, silt decreases toward base, siderite in nodules and disseminated grains, abundant plant fragments

73.7 cm. of Mudstone, medium gray (N5), hard, 40% clay - 50% silt - 10% siderite, siderite in nodules and diffuse laminae

73.7 cm. of rippled, fine Sandstone, dark greenish gray (5GY4/1), average grain size .088-.250 mm., well sorted, infrequent siderite nodules

25.2

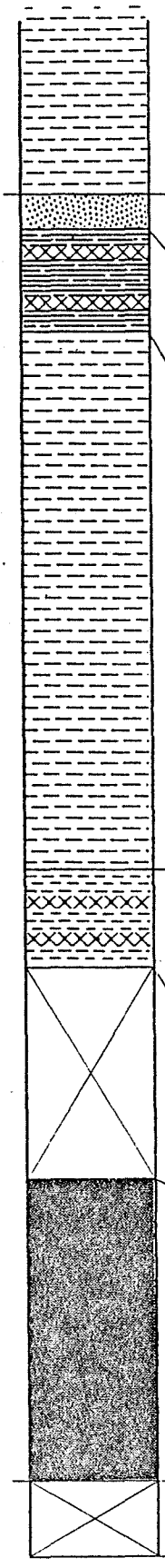

62.2 m. of Mudstone, dark greenish gray (5GY4/1), 40% clay - 55% silt - 5% siderite, even parallel organic and siderite laminae 2 mm. thick, small burrows, plant fragments, erosive basal contact

25.9

8.9 cm. of rippled, fine Sandstone, light gray (N7), average grain size .177-.250 mm., very well sorted

27.9 cm. of Sideritic Shale, dark greenish gray (5GY4/1), 22% clay - 56% silt - 22% siderite, infrequent plant fragments

1.5 m. of Mudstone, medium gray (N3), hard, 39% clay - 61% silt, even parallel organic laminae 1-2 mm. thick, infrequent siderite laminae, abundant plant fragments and leaf impressions, 8.9 cm. of siltier mudshale at 1.1 m.

29.2 cm. of Sideritic Shale (clayshale), dark gray to dark greenish gray (N3-5GY4/1), hackly, moderately hard, 71% clay - 10% silt - 19% siderite, discontinuous wavy parallel siderite laminae, abunadant plant fragments, sparse coal spar

57.9 cm., missing, logged as 39.6 cm. of (324) dark gray, massive, sandy shale, followed by 18.3 cm. of (124), dark gray shale

87.6 cm. Coal

29.5

21.6 cm., missing, logged as (127), dark gray fire clay

cont.

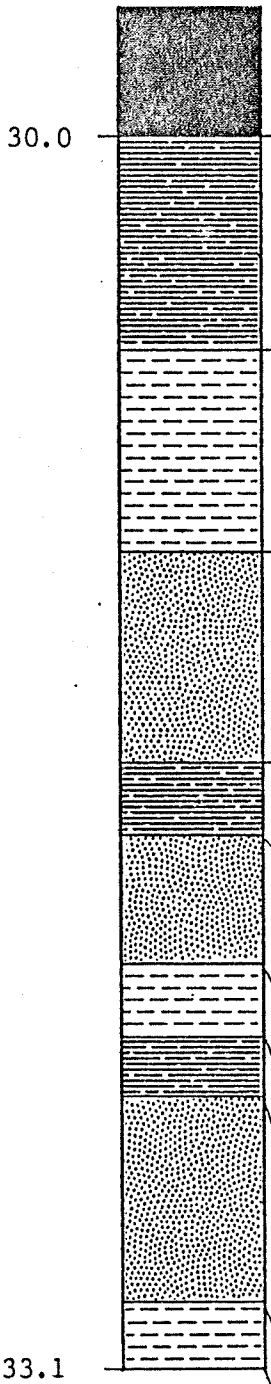

31.8 cm. of Coal

30.0

53.3 cm. of Siltstone, dark greenish gray (5GY4/1), 25% clay - 75% silt+sand, sand averages .088-.125 mm., abundant plant fragments

52.1 cm. of Mudshale, dark gray (N3), 33% clay - 63% silt - 4% siderite, discontinuous wavy parallel clay laminae 1-3 mm. thick, small horizontal burrows, slickensides, plant fragments

53.3 cm. of rippled, fine Sandstone, light gray (N7), average grain size .125-.177 mm., very well sorted, sparse bioturbation

16.5 cm. of laminated Siltstone, dark greenish gray (5GY4/1), 30% clay - 70% silt, even parallel silt laminae 2 mm. thick increasing in abundance downward, sparse bioturbation

34.3 cm. of cross-laminated, very fine Sandstone, light gray (N7), average grain size .088-.125 mm., laminae approximately 2 mm. thick, slightly inclined to parallel, clay laminae increase toward base

17.8 cm. of Mudstone, dark gray to medium dark gray (N3-N4), brittle to hackly, hard, 40% clay - 60% silt, abundant plant fragments

14.0 cm. of Siltstone, medium gray (N5), 20% clay - 80% silt, rooting, plant fragments

33.1

cont.

50.8 cm. of cross-laminated, fine Sandstone, light gray (N7), average grain size .125-.177 mm., very well sorted

16.5 cm. of Mudstone, medium gray to dark greenish gray (N5-5GY4/1), hard, plant fragments

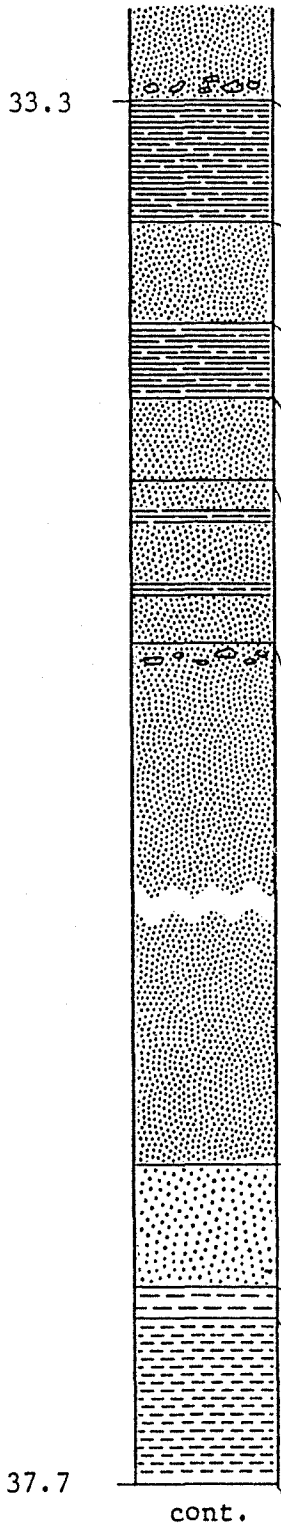

33.3

22.9 cm. of cross-laminated, fine Sandstone, light gray (N7), average grain size .125-.177 mm., very well sorted, infrequent rooting, clay clasts at base

30.5 cm. of Siltstone, dark gray (N3), 30% clay - 70% silt, rooted

26.7 cm. of laminated, fine Sandstone, average grain size .177-.250 mm., very well sorted, infrequent rooting

17.8 cm. of laminated Siltstone, dark gray (N3), 32% clay - 68% silt, even parallel sandy (.177-.250 mm.) laminae

20.3 cm. of fine Sandstone, light gray (N7), average grain size .177-.250 mm., rippled in upper 2.5 cm., massive for next 10.2 cm., then cross-bedded to base, beds 1 cm. thick

40.6 cm. of fine Sandstone interbedded with Siltstone, light gray to dark gray (N7-N3), beds up to 5.1 cm. thick, steeply inclined (slump), rare siderite, erosive basal contact

2.2 m. of cross-laminated, fine Sandstone, light gray (N7), average grain size .177-.250 mm., very well sorted, laminae 1-5 mm. thick, clay clasts in upper 7.6 cm.

30.5 cm. of massive, medium Sandstone, light gray (N7), average grain size .250-.350 mm., moderately sorted, erosive basal contact

7.6 cm. of Mudstone, dark gray (N3), hard, 60% clay - 40% silt, plant fragments, mica

37.7

cont.

40.6 cm. of Clayshale, dark greenish gray (5GY4/1), soft, 75% clay - 20% silt - 5% siderite, discontinuous wavy parallel organic laminae, siderite nodules, plant fragments, erosive basal contact

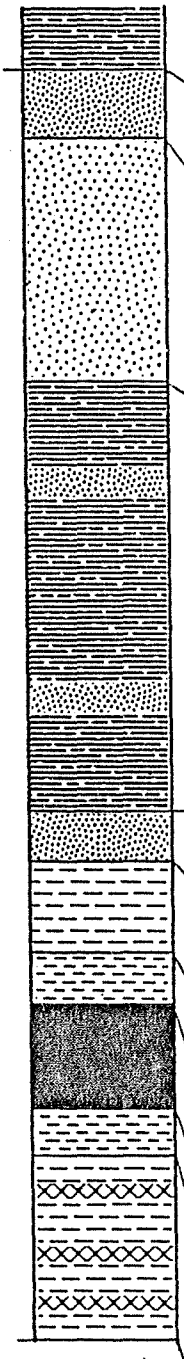

37.8

15.2 cm. of Siltstone, olive gray (5Y4/1), hackly, 20% clay - 80% silt, rooted, plant fragments, slickensides at base

16.5 cm. of rippled, very fine Sandstone, medium dark gray (N4), average grain size .177-.250 mm., rare bioturbation

62.2 cm. of laminated, medium Sandstone, light olive gray (5Y6/1), average grain size .250-.350 mm., moderately sorted, upper 36 cm. abundantly rooted

1.1 m. of laminated Siltstone with interbedded Sandstone, dark greenish gray (5GY4/1), 33% clay - 67% silt+sand, even parallel laminae 1-5 mm. thick, rare plant fragments

12.7 cm. of laminated, fine Sandstone, light gray (N7), average grain size .177-.250 mm., very well sorted

21.6 cm. of Mudshale, dark gray (N3), hard, 60% clay - 40% silt, even discontinuous parallel silt laminae 1 mm. thick, disseminated pyrite

12.7 cm. of Clayshale, medium gray (N5), changing to grayish black (N2) at base, soft, 90% clay - 10% silt, even parallel clay laminae 1-5 mm. thick

25.4 cm. of Coal

41.0

cont.

12.7 cm. of Claystone, olive gray (5Y4/1), hackly, 90% clay - 10% silt, plant fragments, slickensides

45.7 cm. of Sideritic Shale (mudstone with interbedded very fine sand .088-.125 mm.), dark greenish gray (5GY4/1), 33% clay - 52% silt - 15% siderite, rooted, sharp basal contact

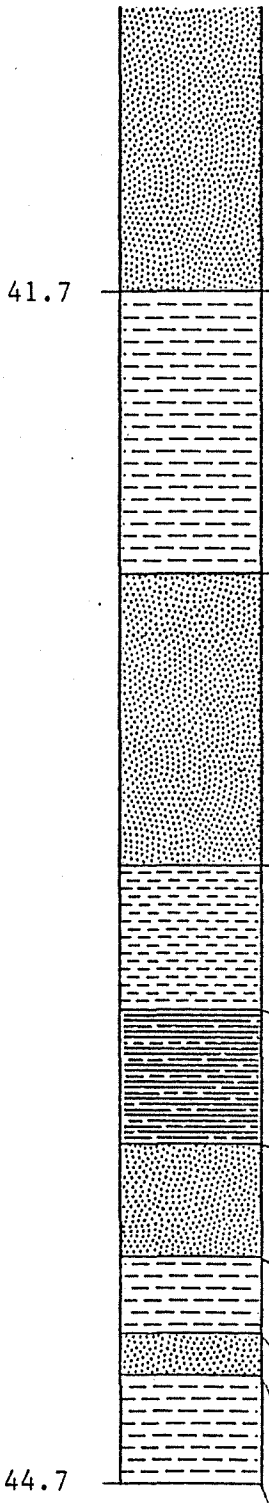

72.4 cm. of rippled, fine Sandstone, light gray (N7), average grain size .177-.250 mm., very well sorted

41.7

71.1 cm. of Mudshale, dark gray (N3), hard, 45% clay - 50% silt - 5% siderite, even parallel siderite, organic, and silt laminae 1-4 mm. thick, plant fragments, rare bioturbation

73.7 cm. of rippled, fine Sandstone, light gray (N7), average grain size .125-.250 mm., well sorted, 12.7 cm. of cross-lamination beginning at 30.5 cm.

38.1 cm. of Claystone, dark gray (N3), hackly, 90% clay - 10% silt, abundant plant and woody fragments, rooting, slickensides, flaggy parting

33.0 cm. of laminated Siltstone, light gray (N7), 20% clay - 80% silt, discontinuous wavy parallel laminae

29.2 cm. of rippled, very fine Sandstone, light gray (N7), average grain size .088-.125 mm., very well sorted, rooted at base

17.8 cm. of Mudshale, medium gray (N5), hard, 40% clay - 60% silt, wavy parallel laminae less than 1 mm. thick, rooted

44.7

cont.

10.2 cm. of rippled, fine Sandstone, light gray (N7), average grain size .177-.250 mm., very well sorted

26.7 cm. of Mudshale, dark gray (N3), hard, 50% clay - 50% silt, wavy parallel laminae 1 mm. thick, flaggy to slabby parting

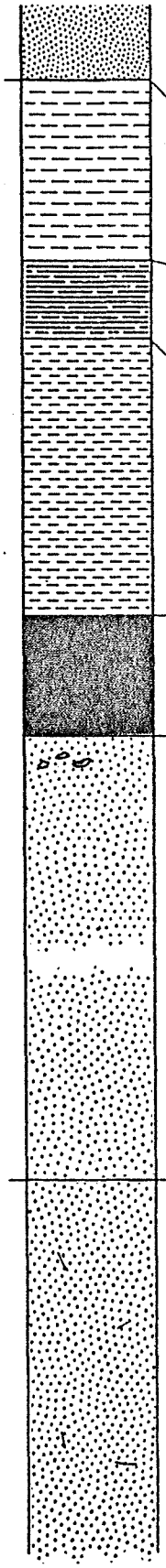

44.9

20.3 cm. of cross-laminated, fine Sandstone, medium light gray (N6), average grain size .125-.177 mm., very well sorted, laminae 1 mm. thick

49.5 cm. of Mudshale, medium gray (N5), hard, 60% clay - 40% silt, even parallel laminae 1-5 mm. thick

21.6 cm. of laminated Siltstone, medium dark gray (N4), 32% clay - 68% silt, even discontinuous parallel silt laminae 1 mm. thick

78.7 cm. of Clayshale, dark gray (N3), moderately soft, fines downward from 66% clay - 34% silt to 78% clay - 15% silt - 7% organics, even parallel clay laminae 1-3 mm. thick, siderite bands, plant fragments, slickensides at base, very even parting surface

30.5 cm. of Coal

2.0 m. of massive, medium Sandstone, light gray (N7), average grain size .250-.350 mm., moderately sorted, clay clasts at 15.2 cm.

48.7

2.8 m. of rippled and cross-laminated, medium Sandstone, light gray (N7), average grain size .250-.350 mm., moderately sorted, laminae 1-2 mm. thick, 1 massive bed, infrequent coal spar

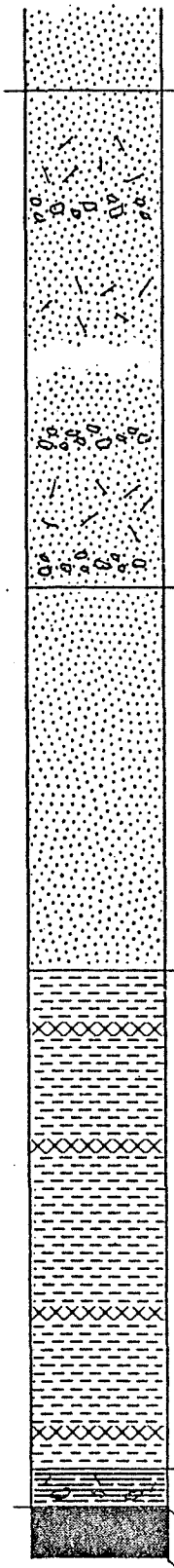

51.5

2.4 m. of massive, medium Sandstone, with abundant coal spars, light gray (N7), average grain size .250-.350 mm., poorly sorted, pebbles (siderite), clay clasts, several gravel lag deposits

1.0 m. of massive, medium Sandstone, with rare ripples, pebbles, and coal spar, average grain size .350-.500 mm., moderately sorted, erosive basal contact

1.3 m. of Sideritic Shale (clayshale), medium gray (N5), moderately hard, 44% clay - 21% siderite - 8% organics - 27% silt, even parallel organic laminae 2 mm. thick, abundant siderite nodules, plant fragments, rare coal spar

56.3

6.4 cm. of Siltstone, grayish black (N2), 30% clay - 70% silt, coal spars and clay clasts

cont.

10.7 cm. of Coal

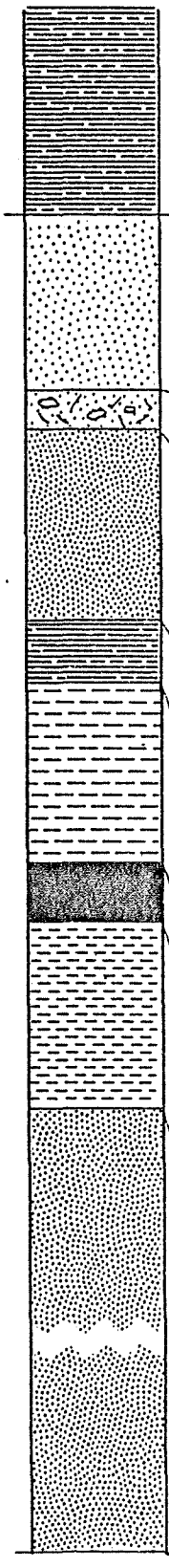

54.6 cm. of Siltstone, greenish gray (5GY6/1), 8% clay - 92% silt+sand, laminae destroyed by abundant rooting, rare vertical burrows, sand averages .088-.125 mm.

57.0

45.7 cm. of medium Sandstone with interlaminated shale, light gray (N7) and dark gray (N3), average grain size .250-.350 mm., shale laminae are wavy parallel 2-3 mm. thick, rare oblique burrows, 60% ss. - 40% sh.

8.9 cm. of massive, medium Sandstone, with coal spar and clay clasts, average grain size .250-.350 mm., well sorted

50.8 cm. of fine Sandstone with interlaminated shale, light gray (N7) and dark gray (N3), average grain size .125-.250 mm., very well sorted, shale laminae are wavy parallel 1-3 mm. thick, 65% ss. - 35% sh., rare rooting and siderite

15.2 cm. of Siltshale, medium gray to light olive gray (N5-5GY6/1), 10% clay - 90% silt, wavy parallel laminae less than 1 mm. thick, becomes sandy at base .125-.177 mm., erosive basal contact

47.0 cm. of Mudshale, dark gray to medium dark gray (N3-N4), soft, 44% clay - 51% silt - 5% siderite, even parallel silt and siderite laminae 1-3 mm. thick, plant fragments

16.2 cm. of Coal

49.5 cm. of Claystone, medium gray (N5), moderately soft, 75% clay - 19% silt - 6% organics, wavy parallel organic laminae less than 1 mm. thick, rooted, slickensides, coarsening downward

1.2 m. of fine Sandstone with interlaminated shale, light gray (N7) and dark gray (N3), average grain size .177-.250 mm., well sorted, wavy parallel organic laminae, shale becomes dominant toward base

60.5

cont.

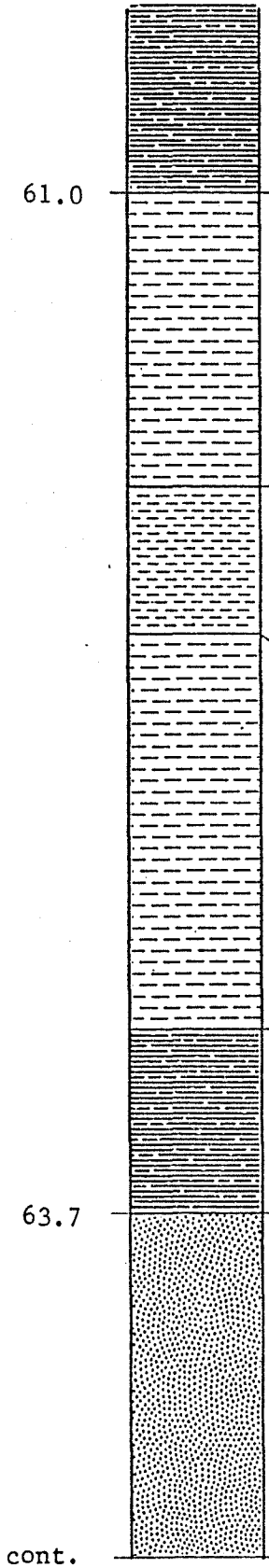

50.8 cm. of laminated Siltstone, light gray (N7), 16% clay - 8% organics - 76% silt, discontinuous wavy parallel organic laminae 1 mm. thick, disseminated siderite, (flaser bedding)

61.0

79.2 cm. of Mudstone, medium gray (N5), hard, 60% clay - 40% silt, slabby parting with even surface, disseminated siderite

40.6 cm. of Clayshale, dark gray (N3), hackly, soft, 75% clay - 20% silt - 5% siderite, even parallel siderite and organic laminae 1-3 mm. thick, plant fragments, rooting, slickensides

1.1 m. of Mudstone, light olive gray (5Y4/1), 45% clay - 55% silt, large clay pebble 1.5 x 3.0 cm., becomes sandy toward base, rooted

45.7 cm. of laminated Siltstone, light gray (N7), 20% clay - 80% silt+sand, discontinuous wavy parallel organic laminae, sand averages .125-.177 mm.

63.7

96.5 cm. of rippled, fine Sandstone, light gray (N7), average grain size .125-.177 mm., very well sorted

cont.

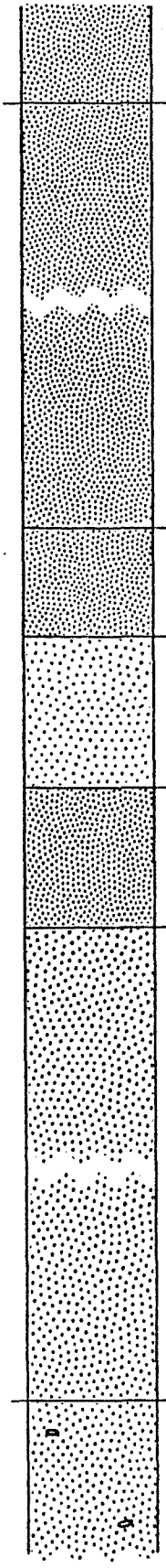

25.4 cm. of laminated, fine Sandstone, light gray (N7), average grain size .177-.250 mm., well sorted

65.0

1.2 m. of rippled, fine Sandstone, as above, very well sorted

29.2 cm. of massive, fine Sandstone, as above, moderately sorted

41.9 cm. of cross-laminated, medium Sandstone, light gray (N7), average grain size .250-.350 mm., well sorted, laminae 3 mm. thick

41.9 cm. of massive, fine Sandstone, light gray (N7), average grain size .177-.250 mm., well sorted

2.1 m. of cross-laminated to cross-bedded, medium Sandstone, light gray (N7), average grain size .350-.500 mm., moderately sorted

69.4

62.2 cm. of rippled, medium Sandstone, light gray (N7), average grain size .250-.350 mm., well sorted, very infrequent clay clasts

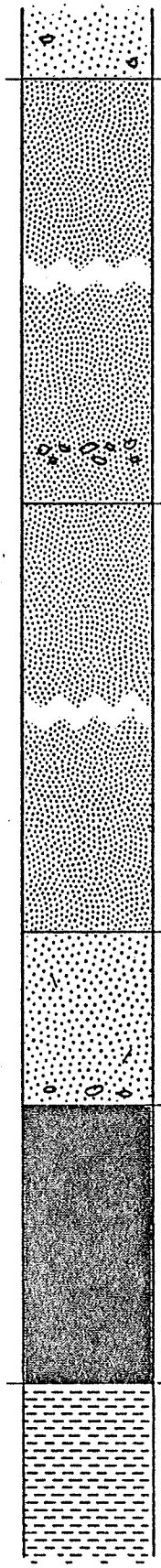

70.0

1.7 m. of massive, fine Sandstone with clay clasts and coal spars at 1.3 m., light gray (N7), average grain size .177-.250 mm., moderately sorted

1.5 m. of cross-bedded, fine Sandstone, as above, beds 1 cm. thick

47.0 cm. of massive, medium Sandstone, light gray (N7), average grain size .250-.350 mm., moderately sorted, rare coal spars and clay clasts near base

76.2 cm. of Coal

74.4

69.8 cm. of Claystone, dark greenish gray (5GY4/1), soft, 90% clay - 10% silt, clays appear to swell, rooted

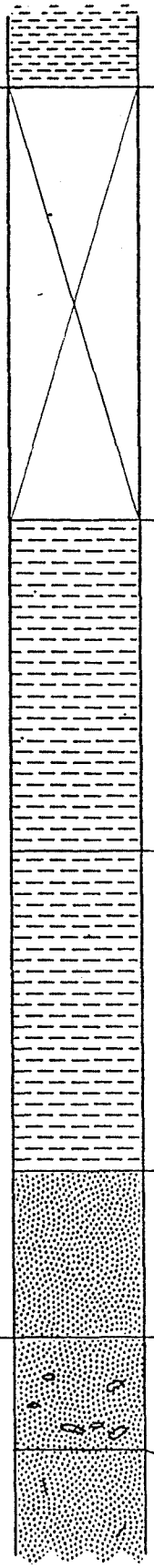

75.2

1.2 m., missing, logged as (547), rooted, gray sandstone

91.4 cm. of Mudstone, medium gray to olive gray (N5-5Y4/1), hackly, hard, 49% clay - 51% silt, clay decreases toward base, abundant rooting, plant fragments

90.2 cm. of Mudstone, olive black (5Y2/1), hard, 33% clay - 62% silt - 5% disseminated siderite, slightly darker than above unit

47.0 cm. of rippled, fine Sandstone, light gray (N7), average grain size .125-.177 mm., very well sorted

78.6

30.5 cm. of massive, fine Sandstone with shale rip-up clasts and infrequent ripples, average grain size .177-.250 mm., very well sorted

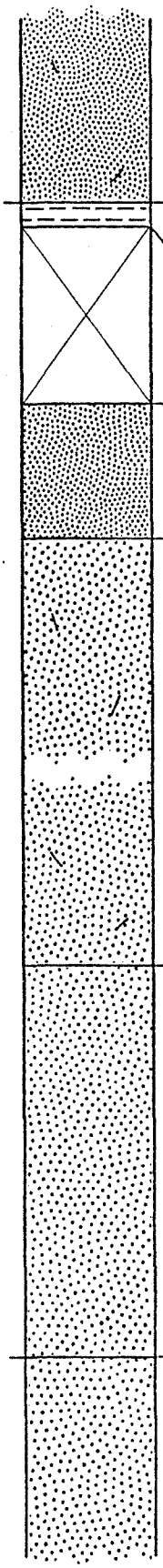

80.0 cm. of rippled, very fine Sandstone, light gray (N7), average grain size .088-.125 mm., very well sorted, infrequent coal spars

79.7

3.8 cm. of Mudshale, dark gray (N3), hard, 65% clay - 35% silt, even parallel laminae 1 mm. thick

48.0 cm., missing, logged similar to above unit

38.1 cm. of rippled, fine Sandstone, light gray (N7), average grain size .177-.250 mm., well sorted

1.7 m. of cross-laminated to cross-bedded, medium Sandstone, light gray (N7), average grain size .250-.350 mm., moderately sorted, very infrequent coal spars

1.1 m. of massive, medium Sandstone, as above, well sorted

83.4

62.2 cm. of cross-bedded, medium Sandstone, as above, beds up to 2.5 cm. thick

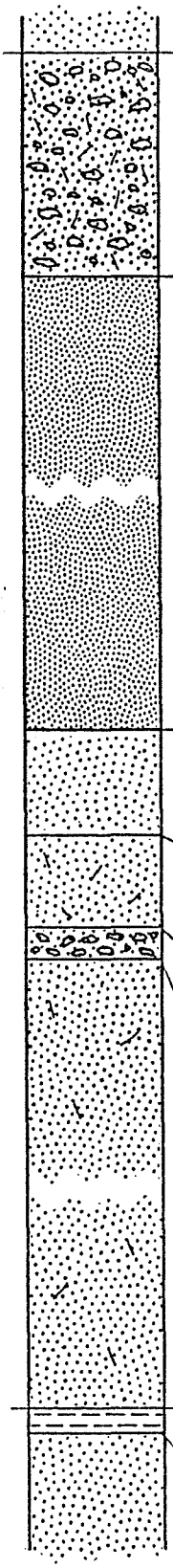

84.1

61.0 cm. of massive, medium Sandstone with abundant coal spars, siderite pebbles, and shale clasts, poorly sorted

1.5 m. of rippled, fine Sandstone, light gray (N7), average grain size .177-.250 mm., well sorted

27.9 cm. of medium Sandstone with rippled coaly laminae, average grain size .250-.350 mm., well sorted, rare siderite nodules

24.1 cm. of massive, medium Sandstone, light gray (N7), average grain size .350-.500 mm., well sorted, infrequent coal spars

6.4 cm. of massive, medium Sandstone with abundant clay clasts, average grain size .250-.350 mm., moderately sorted

1.2 m. of massive, medium Sandstone with infrequent coal spars, light gray (N7), average grain size .250-.350 mm., very well sorted

88.0

6.4 cm. of Mudshale, dark gray (N3), moderately hard, 40% clay - 60% silt, wavy parallel laminae, plant fragments

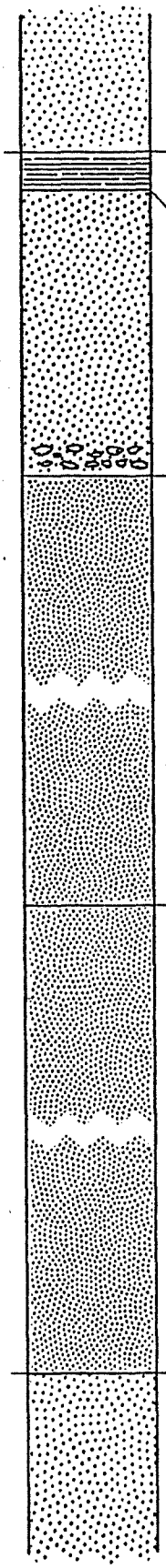

66.0 cm. of massive, coarse Sandstone with coal spars, light gray (N7), average grain size .500-.710 mm., well sorted

88.7

8.9 cm. of laminated Siltstone, olive black (5Y2/1), convolute laminae

81.3 cm. of medium Sandstone with rippled coaly laminae, pebbles and shale clasts near base, average grain size .250-.350 mm., well sorted

1.5 m. of massive, fine Sandstone, light gray (N7), average grain size .177-.250 mm., very well sorted, infrequent cross-laminae and ripples

2.1 m. of rippled, fine Sandstone, as above

93.2

99.1 cm. of massive, medium Sandstone, light gray (N7), average grain size .350-.500 mm., well sorted

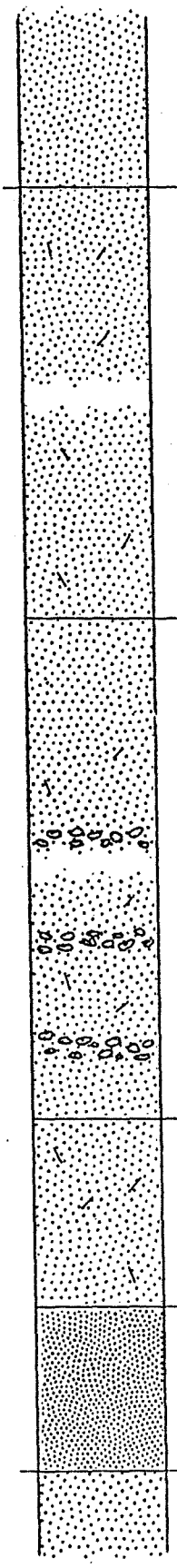

94.2

1.9 m. of massive, medium Sandstone with infrequent coal spars and cross-laminae, average grain size .250-.350 mm., well sorted

3.6 m. of massive, medium Sandstone with infrequent coal spars, shale clasts and siderite pebbles at 2.0 m., 2.6 m., and 3.0 m., average grain size .177-.350 mm., moderately sorted, grain size increases downward

50.8 cm. of rippled, medium Sandstone, light gray (N7), average grain size .350-.500 mm., well sorted, very infrequent coal spars

47.0 cm. of massive, fine Sandstone, light gray (N7), average grain size .177-.250 mm., moderately sorted

100.6

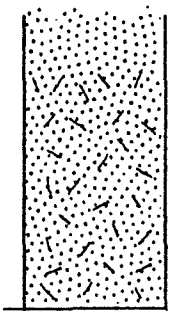

101.6

94.0 cm. of medium Sandstone with rippled coaly laminae in upper 33.0 cm., coal spars throughout remainder, average grain size .250-.350 mm., moderately sorted

Core #8 (LV8), Leeco Coal Co., carter coordinates 3-K-78, 1400' FNL x 1800' FWL, elev. 1520', Vest Quadrangle, Knott County, Kentucky.

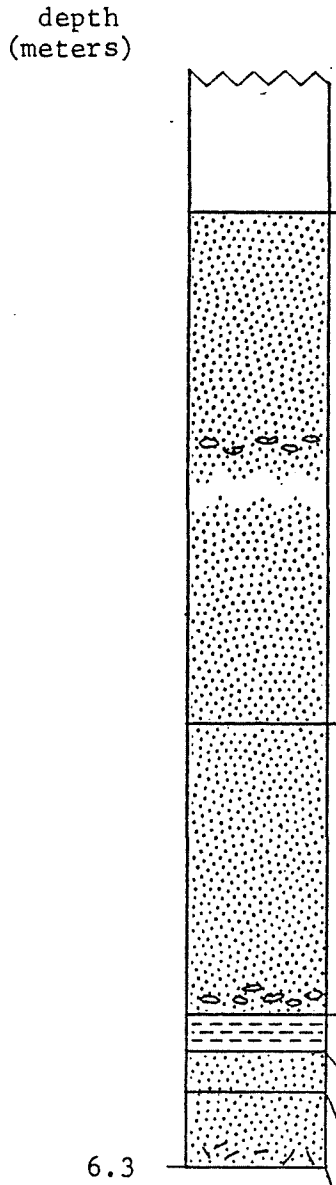

3.0 m., casing

2.2 m. of massive, medium Sandstone with frequent even parallel lamine, grayish orange (10YR7/4), average grain size .250-.350 mm., moderately sorted, laminated units 10-15 cm. thick, iron stained, small siderite pebbles at 91.4 cm.

76.2 cm. of massive, medium Sandstone, light gray (N7), average grain size .250-.350 mm., well sorted, with siderite pebbles in basal 15 cm. which is fractured

6.4 cm. of Claystone, dusky yellow green (5GY5/2), soft, 90% clay - 10% silt, completely fractured

7.6 cm. of cross-laminated, medium Sandstone, grayish orange (10YR7/4), average grain size .250-.350 mm., well sorted, appears weathered

17.8 cm. of laminated, medium Sandstone, light gray (N7), average grain size .250-.350 mm., very well sorted, laminae are organic rich less than 1 mm. thick, coal spars in basal 5cm.

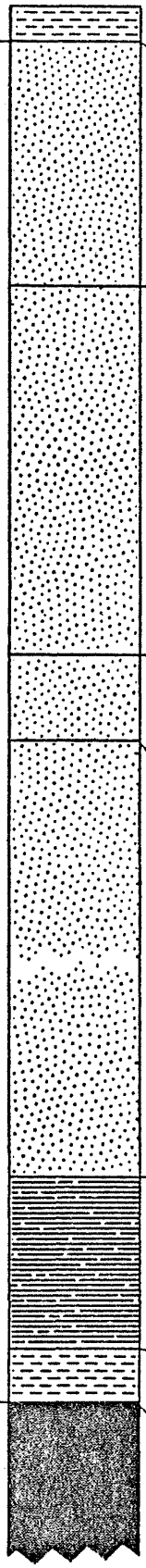

6.4

7.6 cm. of Claystone, medium gray (N5), hackly, moderately soft, 90% clay - 10% silt

66.0 cm. of massive, medium Sandstone with cross-laminae, light gray (N7), average grain size .250-.350 mm., moderately sorted, cross-laminated units 15 cm. thick, very infrequent ripples

1.0 m. of massive, medium Sandstone, light gray (N7), average grain size .250-.350 mm., moderately sorted, infrequent ripples

24.1 cm. of massive, medium Sandstone with abundant coal spars, average grain size .177-.350 mm., moderately well sorted, frequent ripple laminae

1.6 m. of massive, medium Sandstone, light gray (N7), average grain size .250-.350 mm., very well sorted, fining upward, rare cross-laminae less than 1 mm. thick, erosive basal contact

50.8 cm. of laminated Siltstone, dark greenish gray (5GY4/1), 30% clay - 70% silt, wavy parallel silt and very fine sand laminae 1 mm. thick, laminae become even parallel toward base, plant fragments, slickensides

10.5

11.4 cm. of Claystone, dark gray (N3), hackly, soft, 85% clay - 15% silt, plant fragments, slickensides

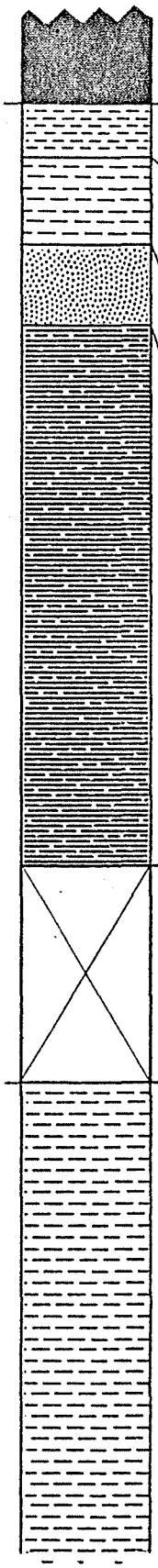

61.0 cm. of Coal

11.1

15.2 cm. of Claystone, dark gray (N3), hackly, moderately soft, 80% clay - 20% silt, abundant plant fragments

22.9 cm. of Mudshale, dark gray (N3), 50% clay - 50% silt, wavy parallel and discontinuous wavy parallel silt and color laminae 1-3 mm. thick, plant fragments, erosive basal contact

21.6 cm. of rippled, fine Sandstone, light gray (N7), average grain size .177-.250 mm., moderately sorted, woody fragment

1.5 m. of laminated Siltstone, dark gray (N3) and light gray(N7), wavy parallel silt and mud laminae 1-5 mm. thick (flaser), infrequent silt beds up to 2 cm. thick about 30 cm. from top, rare burrows

61.0 cm., missing

13.8

1.5 m. of Mudshale, dark greenish gray (5GY4/1), hackly-brittle, hard, 41% clay - 59% silt, discontinuous wavy parallel silt laminae 1-2 mm. thick, flaggy to slabby parting, plant fragments, rare bioturbation (horizontal burrows)

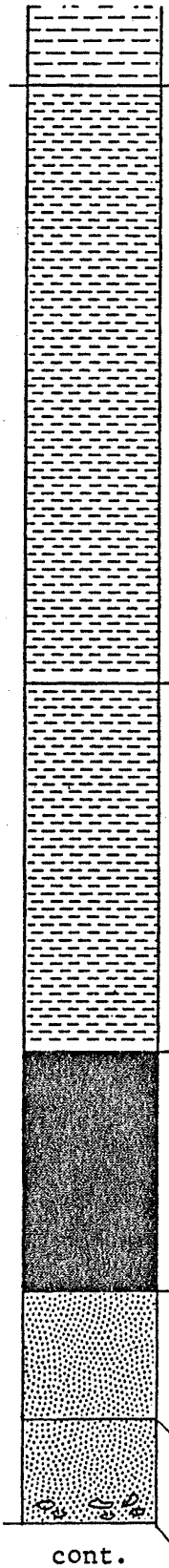

15.3

1.6 m. of Claystone, medium gray (N5), hackly, hard, 70% clay - 30% silt, very rare even discontinuous parallel silt laminae, slabby parting, plant fragments

1.0 m. of Claystone, grayish black (N2), brittle-hackly, soft, 80% clay - 15% silt - 5% pyrite, fabric laminae, flaggy to slabby parting

61.0 cm. of Coal

34.3 cm. of fine Sandstone, greenish gray (5GY6/1), average grain size .125-.250 mm., moderately sorted, organic rich ripple laminae in top 5 cm., remainder has considerable clay with plant fragments, rooting, slickensides

19.1

29.2 cm. of massive, fine Sandstone, medium gray (N5), average grain size .177-.250 mm., moderately sorted, large clay clasts in basal 8.9 cm., clasts up to 1x3 cm.

cont.

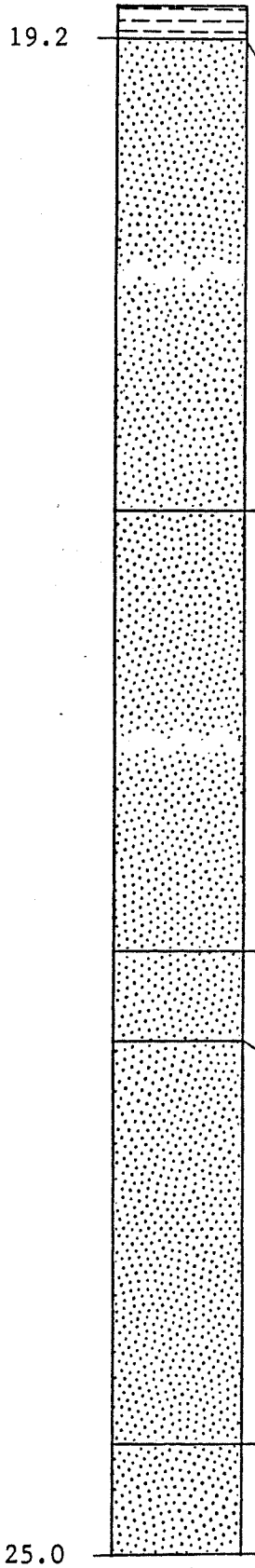

19.2

7.6 cm. of Mudshale, dark gray (N3), hard, 60% clay - 40% silt, even discontinuous parallel silt laminae, silt increasing toward base, rare burrowing

2.1 m. of massive, medium Sandstone, light gray (N7), average grain size .250-.350 mm., well sorted, rare coal spar and even parallel laminae in top 10 cm.

2.0 m. of massive, medium Sandstone, light gray (N7), average grain size .250-.350 mm., moderately sorted, infrequent ripple laminae

25.4 cm. of cross-laminated, medium Sandstone, light gray (N7), average grain size .250-.350 mm., well sorted

1.1 m. of massive, medium Sandstone, as above with infrequent ripple laminae

30.5 cm. of rippled, medium Sandstone, as above

25.0

cont.

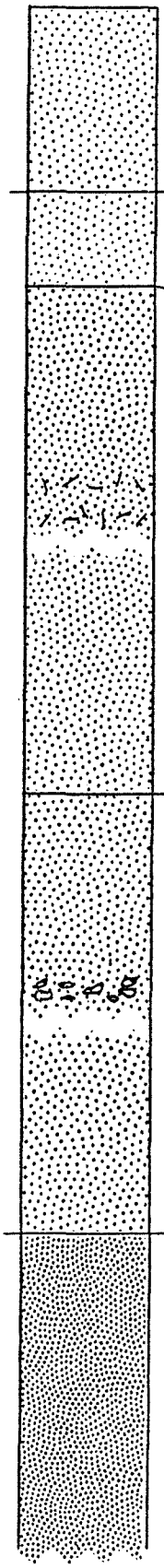

50.8 cm. of massive, medium Sandstone, similar to previous units

25.5

27.9 cm. of cross-bedded, medium Sandstone, as above, beds 1-3 cm. thick

3.4 m. of alternating rippled and massive, medium Sandstone, light gray (N7), average grain size .250-.350 mm., well sorted, 4 rippled units 33-68 cm. thick, 3 massive units 25-84 cm. thick, coal spar at 1.1 and 1.4 m.

1.8 m. of alternating cross-laminated and massive, medium Sandstone, light gray (N7), average grain size .250-.350 mm., well sorted, 3 cross-laminated units 17-46 cm. thick, 2 massive units 25-78 cm. thick, clay clasts at 50.8 cm.

31.0

5.8 m. of massive, fine Sandstone, light gray (N7), average grain size .177-.250 mm., well sorted, coarsening downward, infrequent ripple laminae

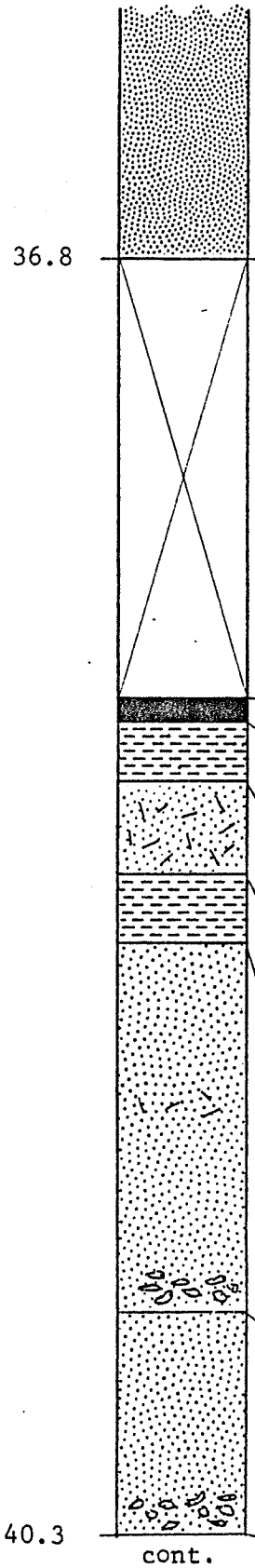

36.8

1.3 m., missing

5.0 cm. of Coal

12.7 cm. of Clayshale, medium gray (N5), hackly, 83% clay - 17% silt, discontinuous wavy parallel organic laminae, slickensides

24.1 cm. of rippled, medium Sandstone, medium dark gray (N4), average grain size .350-.500 mm., moderately sorted, rooted, coal spars

17.8 cm. of Clayshale, medium gray (N5), moderately hard, 83% clay - 17% silt, discontinuous wavy parallel organic laminae, rooting, slickensides, rare burrows

1.0 m. of massive, medium Sandstone, light gray (N7), average grain size .250-.350 mm., moderately sorted, large coal spars 45 cm. from top, large clay clasts and siderite pebbles in basal 12.7 cm.

61.0 cm. of massive, medium Sandstone, light gray (N7), average grain size .350-.500 mm., rippled in upper 5 cm., 10 cm. of cross-lamination, clay clasts and siderite pebbles in basal 12.7 cm.

40.3

cont.

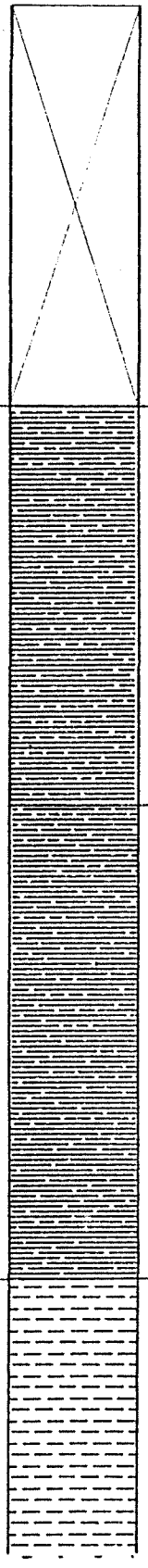

1.2 m., missing

41.5

1.1 m. of alternating Siltstone and laminated Siltstone, dark greenish gray (5GY4/1), blocky, 29% clay - 66% silt - 5% organics, 3 siltstone units 12-28 cm. thick, 2 laminated units 12-43 cm. thick, silt laminae are even parallel 1-3 mm. thick, rare burrows

1.3 m. of laminated Siltstone, dark greenish gray (5GY4/1), 20% clay - 80% silt, even discontinuous parallel silt to fine sand laminae 4-5 mm. thick, rare burrows

43.9

1.3 m. of Mudstone, dark greenish gray (5GY4/1), 39% clay - 55% silt - 6% siderite, infrequent silt laminae less than 1 mm. thick, plant fragments

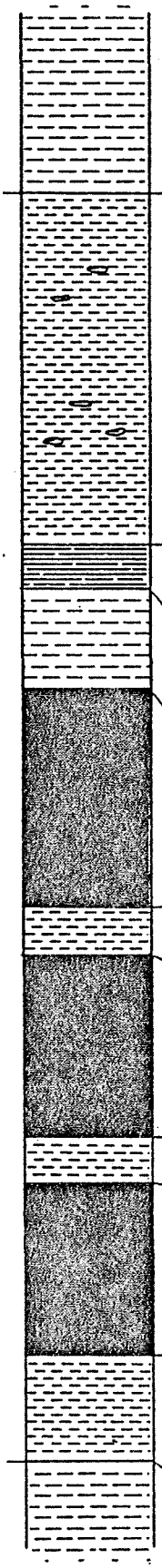

45.2

1.0 m. of Clayshale, medium dark gray (N4), hackly, hard, 74% clay - 22% silt - 4% organics, even discontinuous siderite laminae 1-2 mm. thick, small siderite nodules, plant fragments

12.7 cm. of Siltstone, medium gray (N5), 15% clay - 85% silt & fine sand (.088-.125 mm.), plant fragments

26.7 cm. of Mudstone, dark gray (N3), hackly, 60% clay - 40% silt, rare even parallel silt laminae 1 mm. thick

61.0 cm. of Coal

15.0 cm. of Claystone, missing

45.7 cm. of Coal

15.0 cm. of Claystone, missing

45.7 cm. of Coal

48.7

30.5 cm. of Claystone, medium dark gray (N4), hackly, 83% clay - 17% silt, fabric laminae, abundant plant fragments, rooted, slickensides

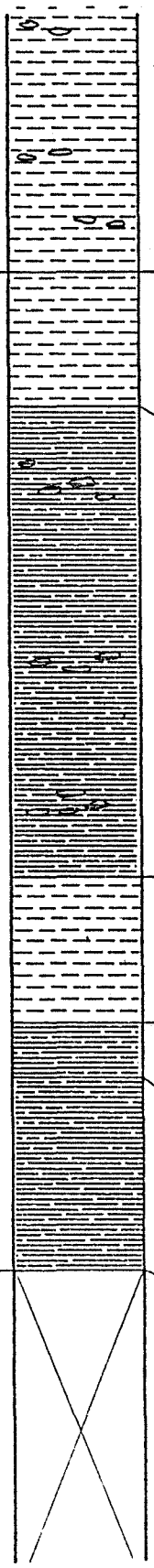

91.4 cm. of Mudstone, dark gray (N3), hackly, hard, 59% clay - 29% silt - 12% organics, even parallel silt laminae less than 1 mm. thick develop toward base, abundant plant fragments, siderite nodules, disseminated siderite

49.6

35.6 cm. of Mudshale, dark greenish gray (5GY4/1), hard, 55% clay - 45% silt, even parallel silt laminae 1 mm. thick, isolated siderite nodule, rooted

1.3 m. of laminated Siltstone, medium gray (N5), 30% clay - 70% silt, wavy parallel laminae 1-5 mm. thick, 35.6 cm. of siltstone beginning at 68.6 cm., siderite nodules

40.6 cm. of Mudstone, medium gray (N5), hard, 50% clay - 50% silt, extensively rooted, plant fragments, trace siderite

15.2 cm. of Siltstone, medium light gray (N6), 20% clay - 80% silt

53.3 cm. of laminated Siltstone, medium dark gray (N4), 30% clay - 70% silt, even discontinuous parallel clay laminae 1-5 mm. thick, rooting, siderite

52.4

83.8 cm., missing, including 22.8 cm. of coal

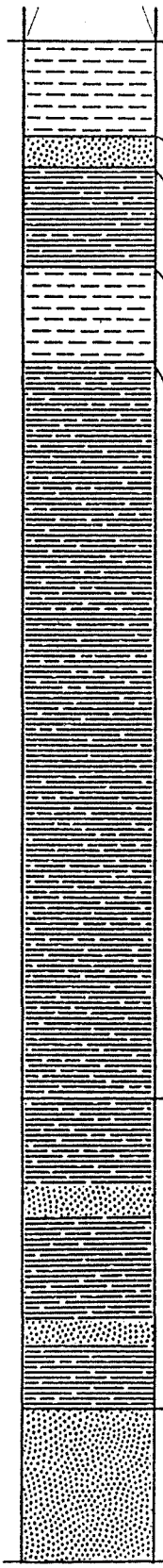

53.2

25.4 cm. of Mudshale, medium dark gray (N4), hard, siderite nodules and thin 1 cm. thick sand beds

6.4 cm. of massive, fine Sandstone, light gray (N7), average grain size .177-.250 mm.

25.4 cm. of laminated Siltstone, similar to 53.3 cm. unit previously described

25.4 cm. of Mudstone, dark gray (N3), hard, 42% clay - 53% silt - 5% siderite, isolated thin silt laminae

2.0 m. of alternating Siltstone and laminated Siltstone, similar to previous silt units, rare thin beds of fine sandstone, convolute laminae, 4 siltstone units 20-38 cm. thick, 4 laminated units 8-30.5 cm. thick

83.8 cm. of Siltstone with interbedded fine Sandstone, silts are similar to those previously described, sand beds range from 5-10 cm. thick, sands frequently rippled

40.6 cm. of rippled, fine Sandstone with clay clasts, light gray (N7), average grain size .125-.177 mm., 2.5 cm. of shale at base, erosive basal contact

57.3

cont.

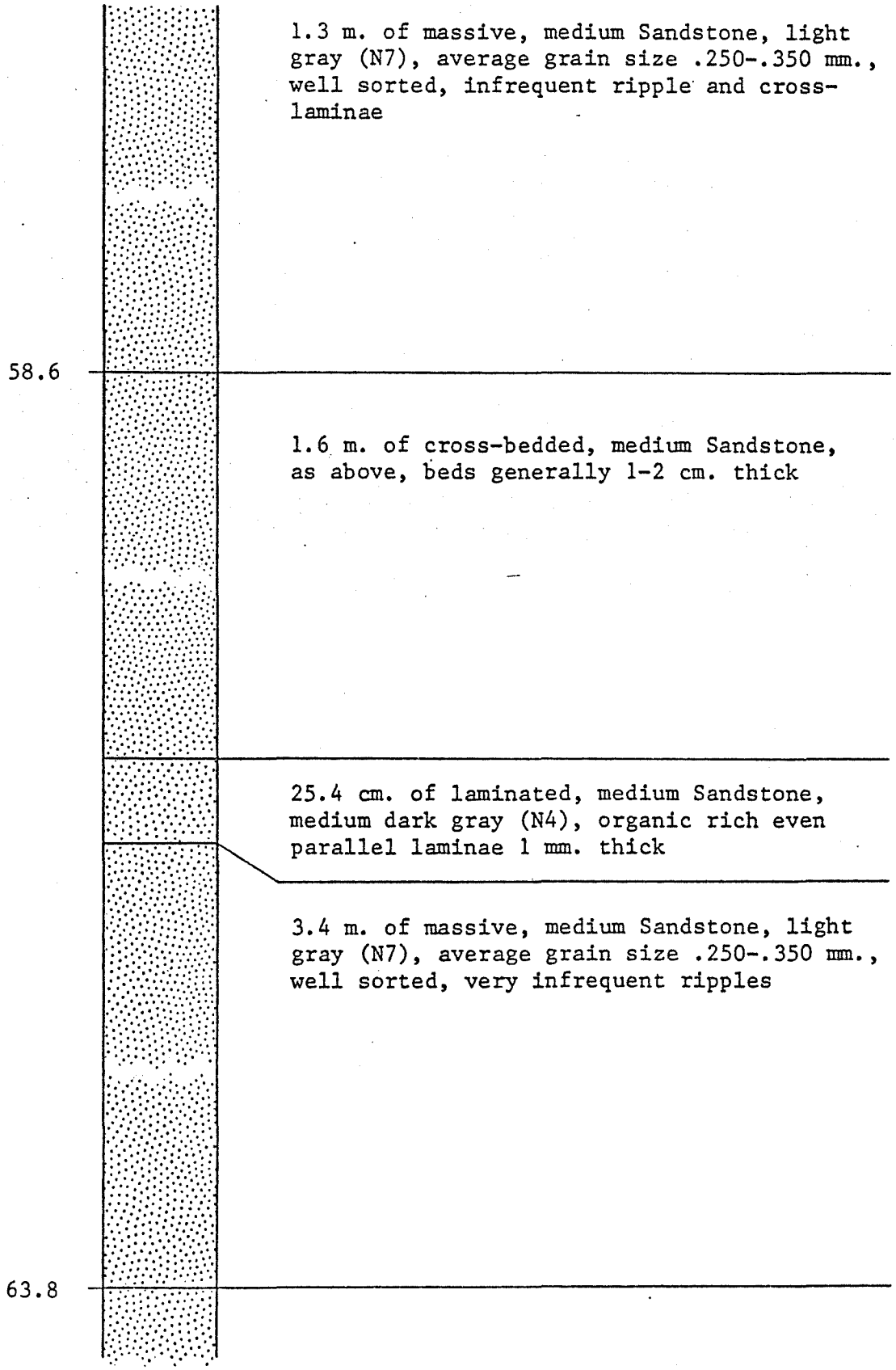
1.3 m. of massive, medium Sandstone, light gray (N7), average grain size .250-.350 mm., well sorted, infrequent ripple and cross-laminae
58.6
1.6 m. of cross-bedded, medium Sandstone, as above, beds generally 1-2 cm. thick
25.4 cm. of laminated, medium Sandstone, medium dark gray (N4), organic rich even parallel laminae 1 mm. thick
3.4 m. of massive, medium Sandstone, light gray (N7), average grain size .250-.350 mm., well sorted, very infrequent ripples
63.8

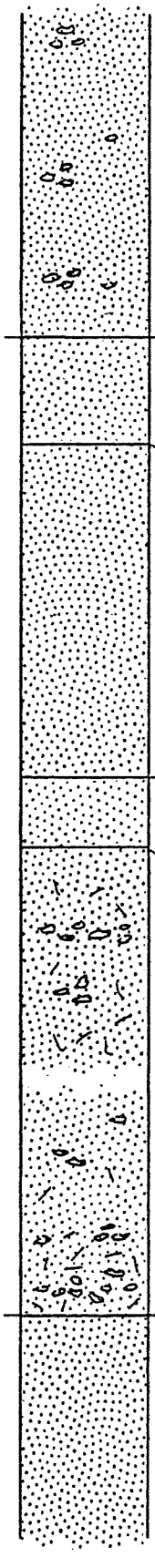

1.1 m. of massive, medium Sandstone, as above, with small clay clasts and siderite pebbles scattered throughout

64.9

30.5 cm. of cross-laminated, medium Sandstone, light gray (N7), average grain size .250-.350 mm., well sorted

91.4 cm. of massive, medium Sandstone, as above

20.3 cm. of rippled, medium Sandstone, as above with organic rich laminae

2.6 m. of massive, medium Sandstone with frequent coal spars and clay clasts, especially in basal 10 cm., light gray (N7), average grain size .250-.500 mm., moderately sorted

68.9

2.7 m. of massive, medium Sandstone, light gray (N7), average grain size .350-.500 mm., infrequent ripple and cross-laminae, siderite pebbles in basal 13 cm., rare coal spars

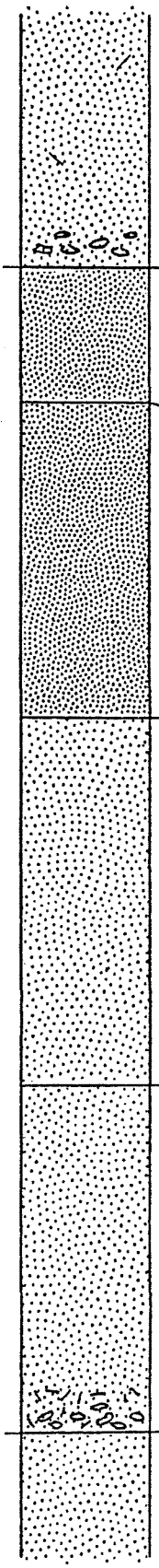

71.6

38.1 cm. of cross-laminated, fine Sandstone, light gray (N7), average grain size .177-.250 mm., well sorted, laminae 1-10 mm. thick

85.1 cm. of massive, fine Sandstone, light gray (N7), average grain size .125-.250 mm., well sorted

99.1 cm. of rippled and cross-laminated medium Sandstone, light gray (N7), average grain size .250-.350 mm., rippled in upper 15 cm., then becomes cross-laminated

99.1 cm. of massive, medium Sandstone, light gray (N7), average grain size .350-.500 mm., moderately sorted, infrequent coal spars throughout, pebbles, clay clasts, and coal spars abundant in basal 20 cm.

74.9

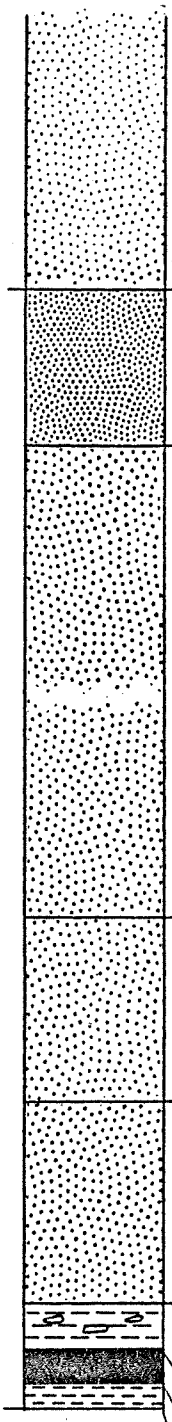

1.1 m. of rippled and massive, medium Sandstone, light gray (N7), average grain size .250-.350 mm., moderately sorted, rippled in upper 38 cm., remainder is massive

76.0

38.1 cm. of laminated, fine Sandstone, light gray (N7), average grain size .125-.250 mm., moderately sorted

1.9 m. of massive, medium Sandstone, light gray (N7), average grain size .350-.500 mm., moderately sorted, infrequent ripples

48.3 cm. of cross-bedded, medium Sandstone, as above, beds generally 2 cm. thick

50.8 cm. of massive, medium Sandstone, as above with sharp basal contact

79.4

cont.

10.2 cm. of Mudshale, grayish black (N2), hard, 50% clay - 50% silt, even parallel silt laminae less than 1 mm. thick, 12 mm. of coal, plant fragments, siderite nodules

8.0 cm. of Coal

2.5 cm. of Claystone, greenish gray (5GY6/1), soft, 80% clay - 20% silt, fractured, slickensides, rooting

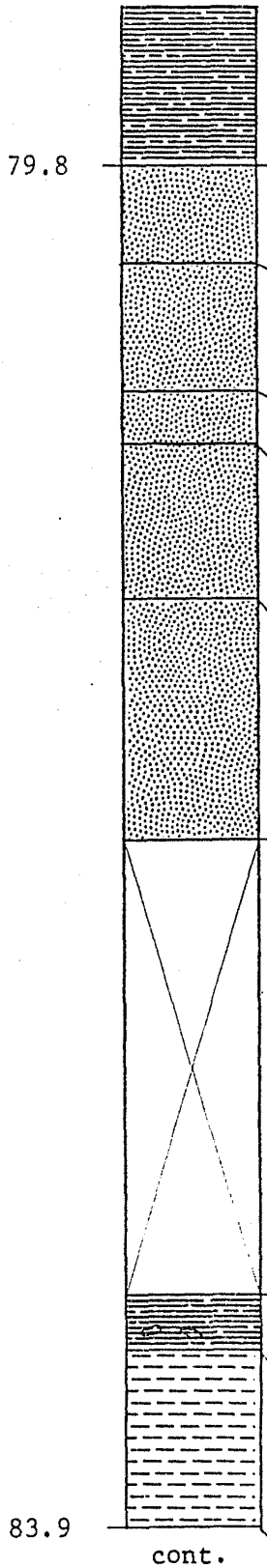

40.6 cm. of Siltstone, greenish gray (5GY6/1), 20% clay - 80% silt, fine sand toward base, rooted, oxidized around burrows and roots, siderite

79.8

26.7 cm. of massive, fine Sandstone, light gray (N7), average grain size .088-.125 mm., rooted, siderite

30.5 cm. of rippled, fine Sandstone, light gray (N7), average grain size .125-.177 mm., well sorted

10.2 cm. of massive, fine Sandstone, as above

40.6 cm. of laminated, fine Sandstone, medium dark gray (N4), average grain size .177-.250 mm., organic rich even parallel laminae 1-3 mm. thick

61.0 cm. of rippled, fine Sandstone, light gray (N7), average grain size .177-.250 mm., well sorted

1.8 m., missing

14.0 cm. of laminated Siltstone, greenish gray (5GY6/1), 20% clay - 80% silt, even discontinuous parallel laminae less than 1 mm. thick, siderite nodules

47.0 cm. of Mudshale, dark gray (N3), hard, 34% clay - 55% silt - 11% siderite, even parallel silt and siderite laminae 1-3 mm. thick, siderite nodule

83.9

cont.

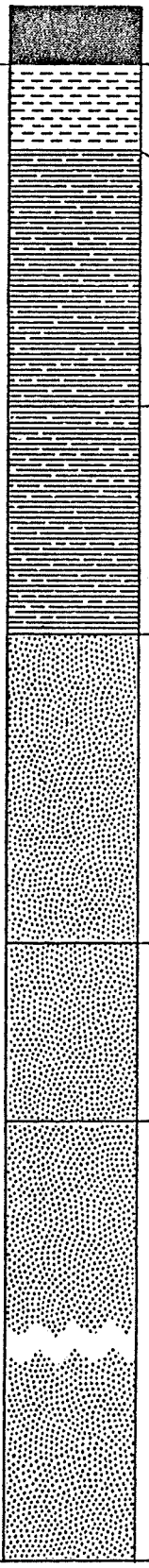

84.1

14.0 cm. of Coal

22.9 cm. of Claystone, medium gray (N5), hackly, soft, 83% clay - 17% silt, grains up to 3 mm. in diameter

67.3 cm. of Siltstone, medium light gray (N6), 23% clay - 67% silt - 10% siderite, rooted, burrows appear oxidized

62.2 cm. of laminated Siltstone, medium gray (N5), 16% clay - 84% silt, even parallel clay laminae 1-3 mm. thick

81.3 cm. of rippled, fine Sandstone, light gray (N7), average grain size .125-.177 mm., moderately sorted

45.7 cm. of laminated, fine Sandstone, medium dark gray (N4), average grain size .125-.177 mm., organic rich even parallel laminae less than 1 mm. thick

1.4 m. of rippled, fine Sandstone, light gray (N7), average grain size .125-.177 mm., rare coal spar

88.3

cont.

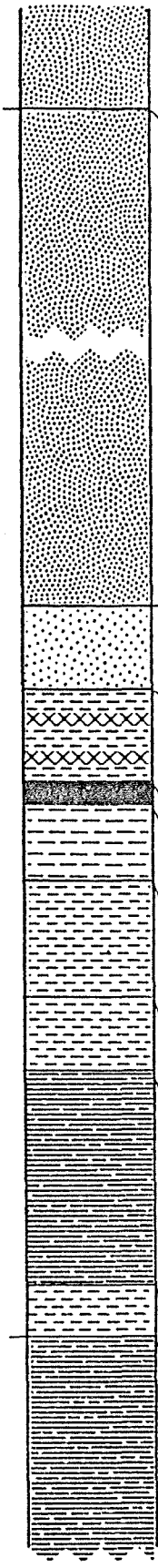

88.5

25.4 cm. of laminated, fine Sandstone, dark gray (N3), average grain size .125-.177 mm., organic rich even parallel laminae 1-3 mm. thick

3.7 m. of laminated, fine Sandstone, light gray (N7), average grain size .177-.250 mm., well sorted, even parallel laminae 2 mm. to 4 cm. thick

24.1 cm. of cross-laminated, medium Sandstone, light gray (N7), average grain size .250-.350 mm., very well sorted, laminae 3 mm. thick

24.1 cm. of Sideritic Shale (clayshale), dark gray (N3), hard, 75% clay - 5% silt - 20% siderite, even discontinuous siderite laminae 4 mm. thick, also contains siderite nodules, plant fragments

3.8 cm. of Coal

21.6 cm. of Mudstone, dark gray (N3), hard, 40% clay - 60% silt, interbedded claystone 2 cm. thick

31.8 cm. of Claystone, dark gray (N3), hackly, hard, 75% clay - 25% silt, mottled, rooted

19.1 cm. of Claystone, olive gray (5Y4/1), hackly, soft, 70% clay - 30% silt, contains grains up to 3 mm. in diameter

94.2

61.0 cm. of Siltstone, olive gray (5Y4/1), 25% clay - 70% silt - 5% disseminated siderite, infrequent silt laminae

11.4 cm. of Claystone, light olive gray (5Y6/1), soft, similar to 19.1 cm. unit above

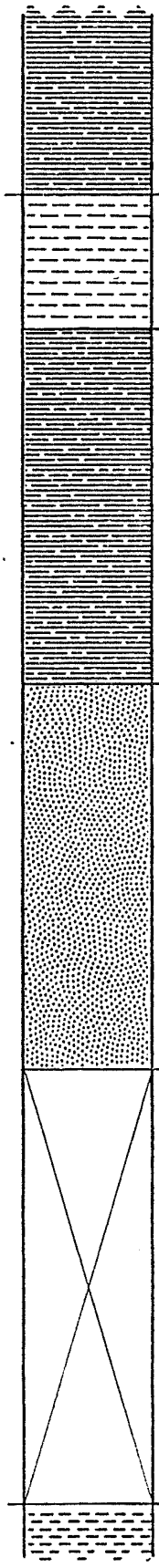

1.1 m. of Siltstone, olive gray (5Y4/1), 20% clay - 80% silt, siderite, sand grains .088-.125 mm., 15.2 cm. of even discontinuous parallel laminae less than 1 mm. thick at 49.5 cm.

95.3

35.6 cm. of Mudstone, dark greenish gray (5GY4/1), hard, 33% clay - 67% silt, rooted, siderite nodules

1.0 m. of laminated Siltstone, dark gray (N3), 20% clay - 80% silt, discontinuous wavy parallel laminae 2-3 mm. thick, siderite nodules and bands in basal 15 cm., rooted, very little clay in upper 30 cm.

1.1 m. of interbedded rippled, fine Sandstone and Siltstone, medium gray (N5), sand averages .125-.177 mm., entire unit consists of 60% ss. - 40% sh., 4 siltstone units range from 5-8 cm. thick

1.2 m., missing

99.0

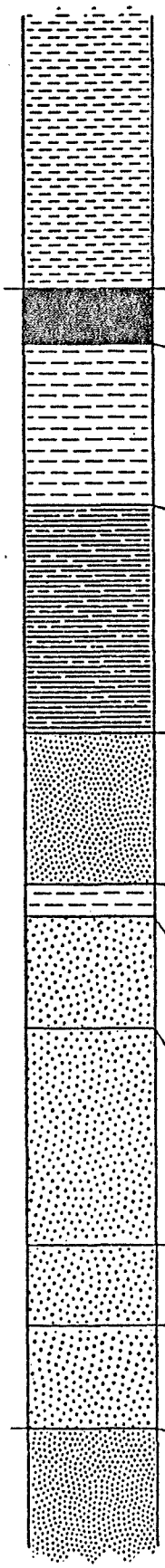

88.9 cm. of Clayshale, medium dark gray (N4), hackly, hard, 75% clay - 5% silt - 20% siderite, even parallel siderite laminae 3 mm. thick, abundant plant fragments

99.8

15.2 cm. of Coal

44.5 cm. of Mudstone, dark gray (N3), becoming olive gray (5Y4/1), hackly, hard, 51% clay - 49% silt, abundant plant fragments, rooted, slickensides

62.2 cm. of Siltstone, olive gray (5Y4/1), 80% silt and sand - 20% clay, sand averages .088-.125 mm., infrequent even parallel silt laminae in basal 7.6 cm.

45.7 cm. of rippled, fine Sandstone, light gray (N7), average grain size .177-.250 mm., very well sorted

6.4 cm. of Mudshale, dark gray (N3), hard, 60% clay - 40% silt, even discontinuous parallel silt laminae, erosive basal contact

30.5 cm. of massive, medium Sandstone, light gray (N7), average grain size .250-.350 mm., well sorted, rooted

61.0 cm. of rippled, medium Sandstone, as above

20.3 cm. of massive, medium Sandstone, as above

29.2 cm. of rippled, medium Sandstone, light gray (N7), average grain size .350-.500 mm., moderately sorted

103.0

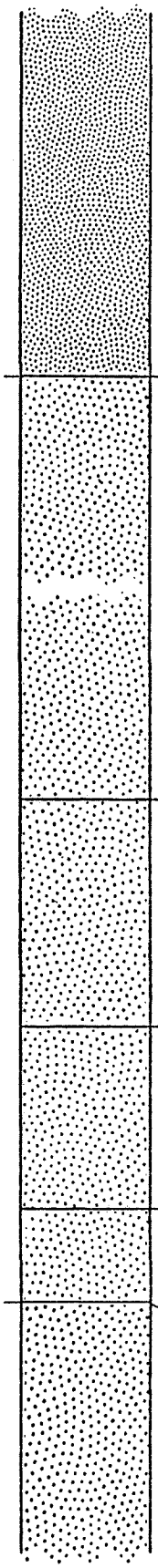

2.5 m. of massive, fine Sandstone, light gray (N7), average grain size .177-.250 mm., well sorted, infrequent ripple laminae, rare coal spars, basal 7.6 cm. fractured

105.5

1.4 m. of massive, medium Sandstone, light gray (N7), average grain size .250-.350 mm., well sorted, infrequent ripples

61.0 cm. of cross-laminated, medium Sandstone, as above, 5 cm. of rippled coal spar at 15 cm.

50.8 cm. of massive, medium Sandstone, as above, with rare ripple laminae

108.3

25.4 cm. of medium Sandstone with abundant rippled coal spars, average grain size .250-.350 mm., moderately sorted

1.1 m. of massive, medium Sandstone, light gray (N7), average grain size .250-.350 mm., moderately sorted

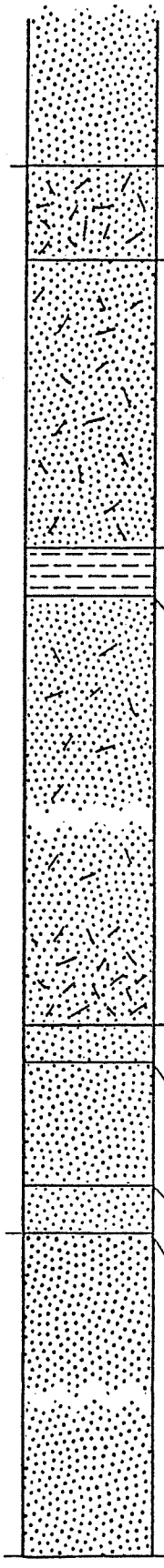

109.4

25.4 cm. of rippled, medium Sandstone, as above, with abundant coal spars

80.0 cm. of massive, medium Sandstone, as above, with frequent coal spars, siderite near base

12.7 cm. of Mudstone, medium dark gray (N4), hard, 65% clay - 35% silt, siderite nodules up to 5 cm. long, plant fragments, sharp basal contact

1.4 m. of massive, medium Sandstone, light gray (N7), average grain size .250-.350 mm., moderately sorted, siderite, frequent coal spars becoming larger and more abundant near base

10.2 cm. of laminated, medium Sandstone, dark gray (N3), average grain size .250-.350 mm., moderately sorted, even parallel organic rich laminae 2-3 mm. thick

35.6 cm. of massive, medium Sandstone, as above

112.5

10.2 cm. of laminated, medium Sandstone, dark gray (N3), similar to 10.2 cm. unit above

1.9 m. of cross-bedded, medium Sandstone, light gray (N7), average grain size .250-.350 mm., well sorted, beds 1-4 cm. thick

cont.

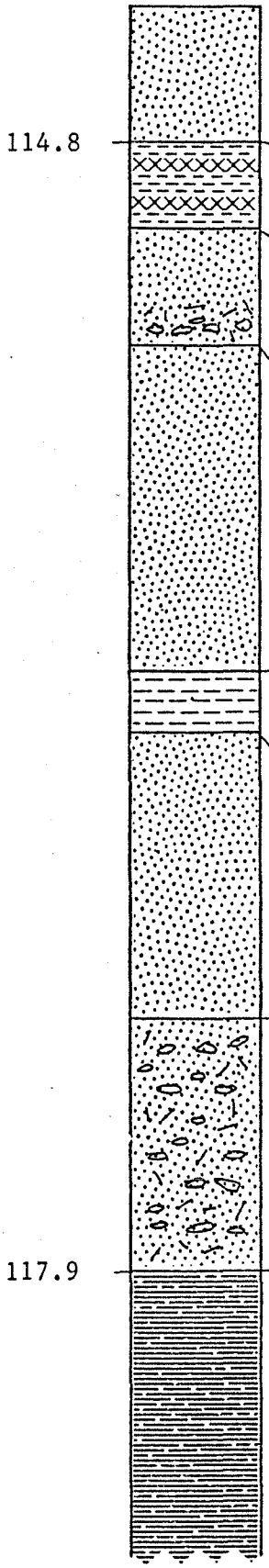

114.8

38.1 cm. of massive, medium Sandstone, light gray (N7), average grain size .350-.500 mm., moderately sorted, siderite pebbles and clay clasts, erosive basal contact

22.9 cm. of Sideritic Shale (claystone), hard, medium gray (N5), 80% clay - 5% silt - 15% siderite, large siderite nodules

30.5 cm. of massive, medium Sandstone, light gray (N7), average grain size .250-.350 mm., moderately sorted, rare clay clasts, siderite pebbles and coal spar at base

90.2 cm. of cross-bedded, medium Sandstone, as above, beds up to 3 cm. thick

16.5 cm. of Mudstone, dark gray (N3), hard, 65% clay - 35% silt, rare convolute laminae, slickensides

76.2 cm. of massive, medium Sandstone, light gray (N7), average grain size .250-.350 mm., moderately sorted, single large siderite pebble

71.1 cm. of massive, medium Sandstone, as above, with abundant large siderite pebbles and coal spars

117.9

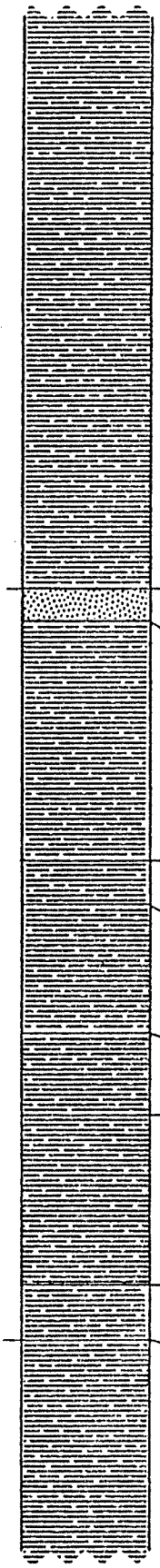

2.4 m. of laminated Siltstone, dark gray (N3), 31% clay - 69% silt, even parallel graded silt laminae 1-5 mm. thick, isolated siderite bands, 3 very fine (.088-.125 mm.) sand beds 2.5 cm. thick, clay infrequently as high as 60%

120.3

7.6 cm. of massive, fine Sandstone, light gray (N7), average grain size .125-.250 mm.

66.0 cm. of laminated Siltstone, same as 2.4 m. unit above

10.2 cm. of Siltstone, similar to above without laminae

35.6 cm. of laminated Siltstone, same as 2.4 m. unit above

25.4 cm. of Siltstone, as above

45.7 cm. of laminated Siltstone, as above

122.3

15.2 cm. of Siltstone, as above

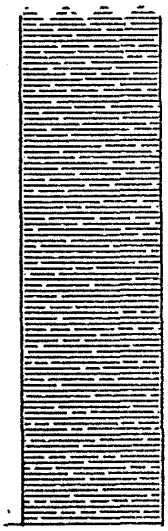

1.9 m. of laminated Siltstone, similar to previous 2.4 m. unit

124.2

In addition to these described cores, geophysical logs from the following locations, aided in correlation:

Hole #3 (LV3), Leeco Coal Co., carter coordinates 1-K-77, 600' FSL x 300' FEL, elev. 1320', Vest Quadrangle, Knott County, Kentucky.

Hole #5 (LV5), Leeco Coal Co., carter coordinates 4-K-78, 1700' FSL x 1100' FWL, elev. 1560', Vest Quadrangle, Knott County, Kentucky.

Hole #7 (LV7), Leeco Coal Co., carter coordinates 4-K-78, 500' FNL x 200' FEL, elev. 1520', Vest Quadrangle, Knott County, Kentucky.

Hole #9 (LV9), Leeco Coal Co., carter coordinates 3-K-78, 2900' FNL x 1400 FWL, elev. 1560', Vest Quadrangle, Knott County, Kentucky.

VOLUME V:

COMPARISON OF MECHANICAL PROPERTIES OF FOUR TYPES OF SANDSTONES DESCRIBED BY FERM'S CLASSIFICATION

by

Joseph G. Turner, III
University of Kentucky
Lexington, Kentucky

June 1983

Volume V of Acquisition, Storage, and Classification of Engineering and Geological Data for Surface-Mine Design and Reclamation under Grant Number ~~G5195018~~ or G1195018, September 1979.

G1105068

Prepared for the University of Kentucky Institute for Mining and Minerals Research Title III Program.

ACKNOWLEDGMENTS

I would like to thank Professor Fred Wright, Department of Mining Engineering, for giving me the opportunity to conduct my research in the Mining Laboratory; Professor Kot Unrug, Department of Mining Engineering, for his valuable assistance and encouragement; and Professor Nicholas Rast, Department of Geology, for his suggestions and comments while proof reading this thesis. And a special note of thanks to Edward Thompson, Mining Laboratory Supervisor, for his technical assistance and suggestions.

TABLE OF CONTENTS

LIST OF FIGURES

LIST OF TABLES

CHAPTER 1.0

PURPOSE OF THESIS

The candidate used rock cores of Breathitt Formation sandstone described by Ferm's classification. It was found that the sandstone was not a homogeneous unit but a combination of different types of sandstone. The purpose of the thesis was to determine if the different types of sandstone in the Breathitt Formation as indicated by Ferm's classification have different mechanical properties. Thus the comparison of the mechanical properties of each sandstone was attempted by means of uniaxial compression testing. The elastic properties compared are Young's modulus (E) and Poisson's ratio (ν) for each sandstone. The compressive strength of each sandstone will be presented but not evaluated due to the large amount of variation with each sample set.

CHAPTER 2.0

INTRODUCTION

The process of fracturing in sandstone is complicated since the stress field induced in the sandstone may not be uniform. Such non-uniform stress state can be caused by the mineral composition and/or texture of the sandstone. These features of the sandstone may inhibit or induce fracture.

The fracture process in granular aggregates have been defined in two fields of engineering, soil mechanics and rock mechanics. In soil mechanics the grain is assumed to be unbreakable and any deformation of the grain is a resultant of strain from elastic deformation. Failure in bulk aggregates is because unbroken grains slide past one another. This explanation of fracture is sufficient for granular media under low stress conditions but in rock mechanics this explanation is inadequate. In rock mechanics the grains are under additional constraints through higher confining pressures and stronger, stiffer cements. In rock mechanics the fracture process is studied by the evaluation of the stress across the boundaries of the grains, neglecting the individual contribution of each grain in the medium, and assuming an uniform state of stress.

Using the assumption of uniform stress throughout the granular media, experiments are conducted to determine mechanical properties. One experiment commonly used to determine mechanical properties is the uniaxial compression test. This test involves a sample to be axially loaded with no confining pressure prior to failure. During this test, measurements of deformation are recorded at equal stress intervals to obtain a stress-strain curve. From this curve two relationships of stress to strain can be derived--Young's modulus (E) and Poisson's ratio (ν). Young's modulus is a ratio of stress in a body to the corresponding strain. Poisson's ratio is the ratio of lateral expansion to longitudinal contraction during uniaxial testing. Values of Poisson's ratio and Young's modulus of the rock give an indication of the strength and compressibility. These properties are usually dependent upon the magnitude of the applied stress, grain and twin boundaries, the misfit of different types of grains and their orientation in relation to the applied stress, and various types of "microcracks" and "pores" present in the rock. The definition of "pore" is a nearly equidimensional intergranular space between sediments, while "microcracks" refers to cleavages in the mineral grains and partings at originally intact grain boundaries. The effects of microcracks and pores need to be differentiated in that; a pore is independent of the applied stress and may reach static equilibrium without closing while a microcrack at low

stress can remain open until the stress is increased and the microcrack will close. These pores and microcracks have an important role in the fracturing process since they tend to raise the stress above the applied or regional stress field. Upon closing (microcracks) the rock becomes elastically stiffer, causing Young's modulus and Poisson's ratio to increase.

2.1.0 Griffith's Theory of Failure

In this thesis the explanation of fracture initiation is based upon Griffith's theory of failure. Griffith (1920) introduced an energy argument to calculate the tensile strength of material. His energy approach uses surface energy as a measure of the local cohesive strength of the material. This principle is based on the minimum potential energy of a system. A crack will propagate if the sum of the three terms are zero or negative:

1. The surface energy of the new crack surface created.

2. The change in the elastic strain energy of the body.

3. The change in the potential energy of the loading system.

This sum represents a change in the Gibb's potential and the energy criterion is equivalent to requiring the Gibbs potential to be minimized. In his energy balance theory Griffith (1924) postulated that failure would occur when

applied stress induces tensile stress at or near the tip of an unfavorably oriented crack from a population of randomly oriented cracks. The crack will propagate when the tensile stress component reaches a critical stress, σ_c, that will overcome the molecular cohesive strength of the material. Griffith assumed that the cracks were of cylindrical shape with a flattened cross-section at the ends of negligible width and he dealt with the two-dimensional problem in the plane of this cross-section by using the classical theory of linear elasticity to calculate the local stress distribution around a crack (Paterson, 1978, p. 53).

In the application of Griffith's theory to the compressive stress state major difficulties arise. Griffith assumed that the crack propagated in a plane. He failed to recognize other energy absorption processes in crack spreading such as plastic deformation in the vicinity of the crack tip due to high stresses, proliferation of microcracking by relaxation of internal stresses, and acoustic and thermal losses (Paterson, 1978, p. 56). Griffith applied his energy approach to a stationary crack. To extend the energy treatment to a moving crack, kinetic energy must be accounted. Kinetic energy of the material on one side of the new crack surface set in motion relative to the other will be absorbed thus setting the upper limit to the crack velocity. Thus crack extention can no longer be assumed to remain in one plane and calculation of energy changes cannot be made without the determination of the

direction of crack extension (Brace and Bombolakis, 1963). A crack of negligible width under a compressive stress will tend to close and it cannot be assumed that the crack faces are not loaded. A crack of negligible width implies that the radius of the curvature at the crack tip is effectively zero and the maximum stress is infinite in the elasticity calculation (Paterson, 1978, p. 54). Thus the region affected is negligibly small and the radius of the curvature of the crack cannot be smaller than atomic or molecular dimensions. Under this condition no contribution to energy change can result from any relaxation of the elastic stress field during crack extension that would result in displacement of opposite crack faces towards one another.

McClintock and Walsh (1962) modified Griffith's hypothesis for crack closure. In Fig. 1a an element of rock is loaded by the maximum and minimum principal stresses σ_1 and σ_3 (compression is defined as negative). The normal stress acting upon the crack surface is denoted by σ_n oriented at angle θ and frictional shear on the crack surface is denoted by τ_f. Fig. 1b is the equivalent stress, where the magnitudes of the stress components normal and parallel to the crack surface are found from Mohr's circle:

$$\sigma_{xx} = \frac{\sigma_1 + \sigma_3}{2} + \frac{\sigma_1 + \sigma_3}{2} \cos 2\theta \qquad (1)$$

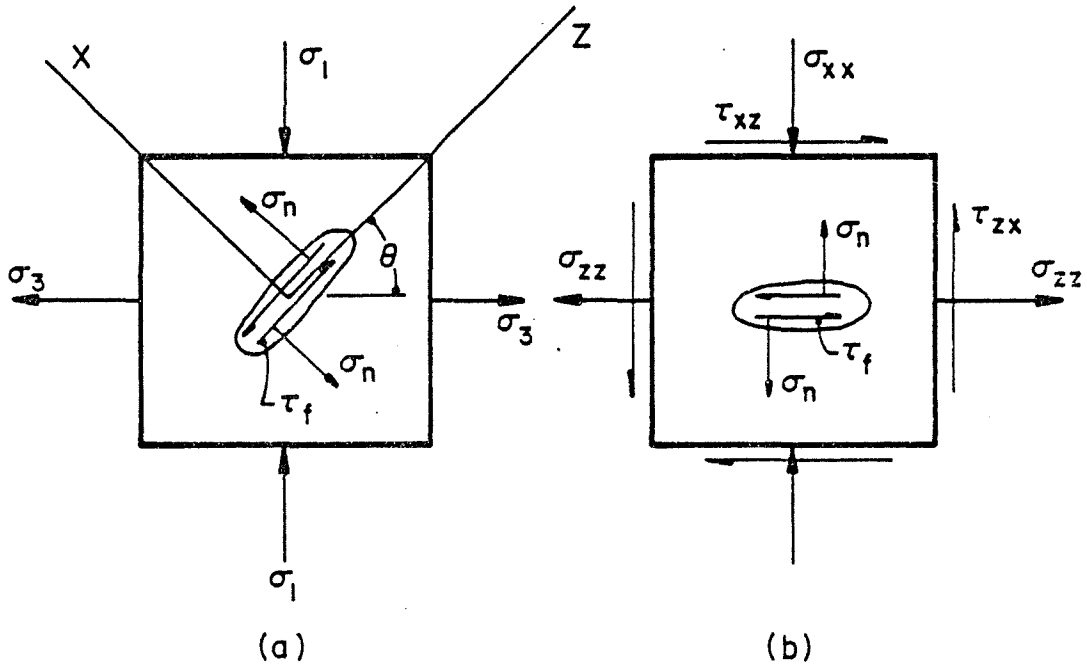

Fig. 1. Stress Components Referred to Principal Axes and and to Axes of Crack (after McClintock and Walsh, 1962).

$$\tau_{xz} = \frac{\sigma_1 - \sigma_3}{2} \sin 2\theta \qquad (2)$$

The normal stress on the crack faces, σ_n, is assumed to be a function of only the applied stress normal to the crack, σ_{xx}. The assumption for the relationship between σ_n and σ_{xx} is due to that the applied stress σ_{xx} must reach a critical value, σ_c, to close the crack at least at the ends and after closure of the crack any increase in σ_{xx} causes an increase in σ_n (McClintock and Walsh, 1962). The relationship between σ_{xx} and σ_n is:

$$\begin{aligned} \sigma_n &= 0 \text{ for either } \sigma_{xx} > 0 \text{ or } |\sigma_{xx}| < |\sigma_c| \\ \sigma_n &= \sigma_{xx} - \sigma_c \text{ for } |\sigma_{xx}| \geq |\sigma_c| \end{aligned} \qquad (3)$$

The frictional shear stress, $_f$, is found by assuming that for the crack to grow, a frictional stress must be overcome. The latter is proportional to the existing normal stress:

$$\sigma_f = -\mu \sigma_n \text{ for } \sigma_{xx} > \sigma_f \qquad (4)$$

(negative sign required due to compression is negative)

Once the stresses on the crack surface are related to the applied stress, analysis based on Griffith's hypothesis can be used except that the additional stresses on the crack face are also considered. Thus for each value of θ and each point around the periphery of the crack, local stresses due to the stresses at infinity and those acting

on the surface of the crack are found. The maximum value of this stress for the most stressed point on the crack with the least favorable orientation is found and equated to the corresponding value of pure tension (McClintock and Walsh, 1962).

Murrell (1964) developed a similar theory to McClintock and Walsh (1962) and Murrell and Digby (1970) extended the theory by applying a three dimensional state of stress to the problem of crack closure. Murrell and Digby (1970) carried out calculations on an isotropic brittle solid of the Griffith's type subjected to a homogeneous, uniform but arbitrary triaxial state of stress at infinity. It was assumed that the cracks were flattened ellipsoidal cavities and were closed under applied stress. Murrell and Digby (1970) concluded that their treatment of crack closure in a three dimensional stress state is similar to that of the two dimensional stress state found earlier by McClintock and Walsh (1962) and Murrell (1964). Fracture initiation is shown to be independent of the intermediate principal stress. Thus in either biaxial or triaxial stress systems when the cracks are closed, the initiation of failure is goverened by:

$$(\sqrt{1 + \mu^2} - \mu)\ (\sigma_1 - \sigma_3) = \alpha' T_o \sqrt{1 + \sigma_c / T_o} + 2\mu\ (\sigma_3 - \sigma_c) \qquad (5)$$

equivalent Mohr envelope

$$\tau = \frac{\alpha'}{2} T_o \sqrt{1 + \sigma_c/T_o} + \mu(\sigma_n - \sigma_c) \qquad (6)$$

σ_1 and σ_3 are the greatest and least principal stresses and τ and σ_n are the maximum shear stress and the normal stress on the plane of the crack in which failure initiates. This plane contains the intermediate stress axis, σ_2, and is inclined at an angle θ to the σ_1 axis. μ is the coefficient of friction on the crack faces and σ_c is the critical stress needed to close the crack. α' is a function of Poisson's ratio, ν, and the axial ratios of the crack. T_o is the uniaxial tensile stress induced on the crack.

2.2.0 Coulomb Criterion of Failure

Coulomb (1773) made extensive research in friction and suggested shear failure of rocks had a shear stress tending to cause failure across a plane resisted by the cohesion of the material and by a constant times the normal stress across the plane. This is represented by:

$$|\tau| = \tau_o + \mu\sigma \quad \text{or}$$
$$|\tau| - \mu\sigma = \tau_o \qquad (7)$$

σ and τ are the normal and shear stresses across the plane, τ_o is the inherent shear strength of the shear strength of the material and μ is the coefficient of internal friction. This relationship can be expressed in terms of a Mohr diagram by a straight line envelope:

$$|\tau| = \tau_o + \sigma\tan\phi \qquad (8)$$

Tanϕ in this expression cannot be directly interpreted as the coefficient of friction in a real physical sense but it can be identified with a real coefficient of friction in the modified Griffith theory of failure.

The intermediate stress is not involved in Coulomb's criterion of failure just as in Griffith's criteria. The value of the intermediate stress will not affect the brittle fracture strength but in the direction of intermediate stress two possible conjugate planes of fracture may pass through making an angle $\frac{1}{4}\pi - \frac{1}{2}\phi$ with the direction of maximum stress (Jaeger and Cook, 1969, p. 91). Anderson (1942) used this assumption for his theory of faulting. Faults are geologic fractures of rock in which relative displacement occurs along the plane of fracture. Fracture takes place along one or both of the conjugate planes which pass through the direction of the intermediate stress, equally inclined at angles of less than 45° to the direction of the greatest principal stress. Assuming that the earth is a free surface, one of the principal stresses at the surface must be normal to it and it is reasonable to also assume that one principal stress is vertical at moderate depths. Assuming this there are three cases of faulting: thrust faulting, strike-slip faulting, and normal faulting (Fig. 2). In thrust faulting the least principal stress, σ_3, is vertical and faulting may take place on

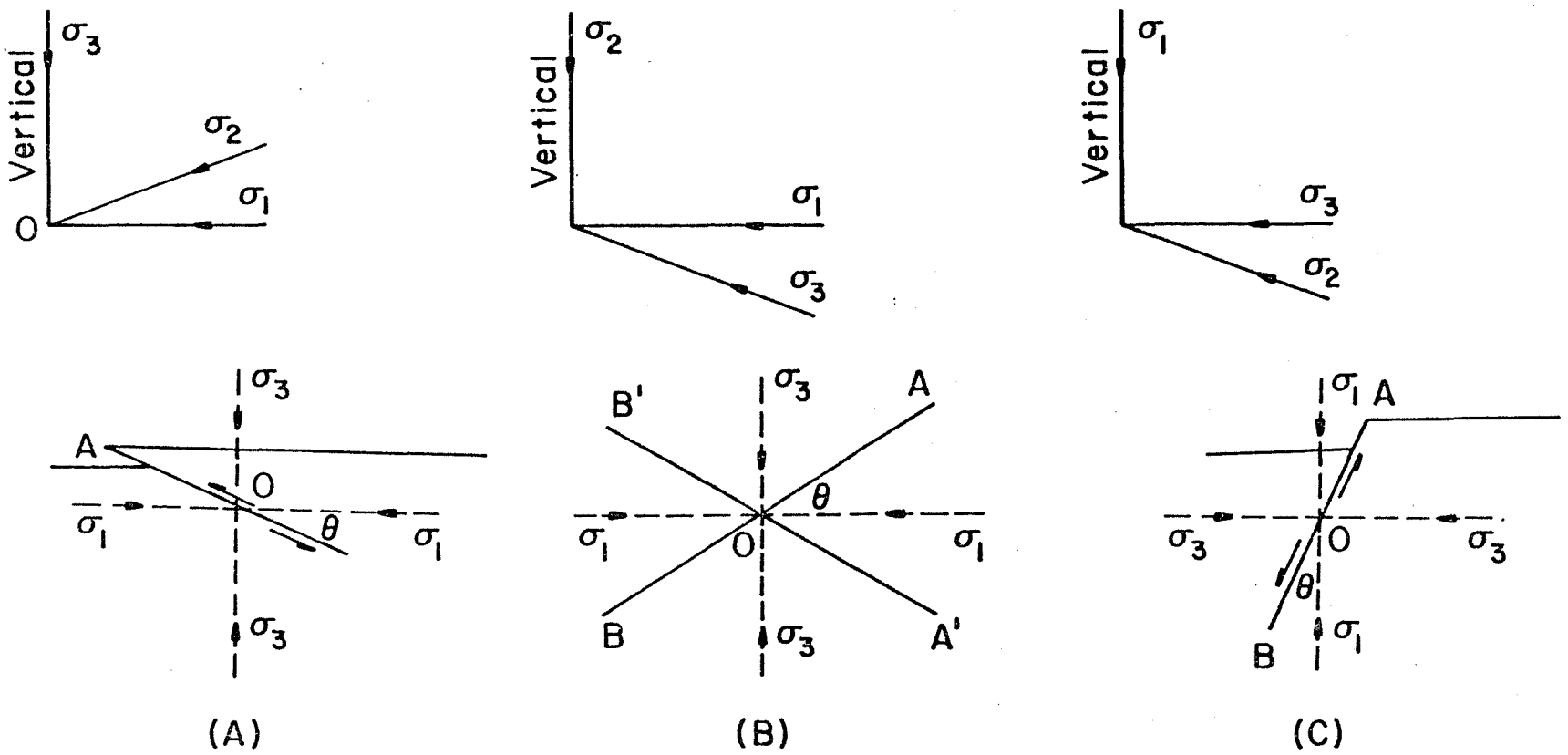

Fig. 2. Diagram of three types of faulting discussed by Anderson (1942). (A) Thrust faulting. (B) Strike-slip faulting. (C) Normal faulting. (After Jaeger and Cook, 1969, p. 401).

either of two planes inclined at $\theta < 45°$ to the horizontal. Strike-slip faulting has the intermediate stress, σ_2, vertical, with failure occuring on either two vertical planes passing through $0\tau_2$ and inclined at angle $\theta < 45°$ to $0\sigma_1$. Normal faulting occurs when the greatest principal stress is vertical, σ_1, and failure may occur on either of two planes inclined at $\theta < 45°$ to the vertical.

2.3.0 Ferm's Classification

The candidate used four types of sandstone from the Breathitt Formation of the Hazard coal district of eastern Kentucky (Fig. 3). The sandstone were described in terms of the Ferm's classification (Ferm and Melton, 1979) which utilizes a three digit system.

2.3.1 Description of Ferm's Classification

Ferm's classification is used to describe Pennsylvanian sedimentary rocks from the Appalachian Basin of eastern Kentucky. This classification employs a three digit system instead of the traditional descriptive classification. The first digit that ranges from one to nine, describes the rock type by grain size. The second digit may describe either the sand components, color, or fossil content. The third place digit describes any sedimentary features present. The term flat (FLT) or rippled (RIP) may follow the description if shale or sandstone streaks are present. If the streaks are horizontal and parallel, the term flat is used and if the streaks are

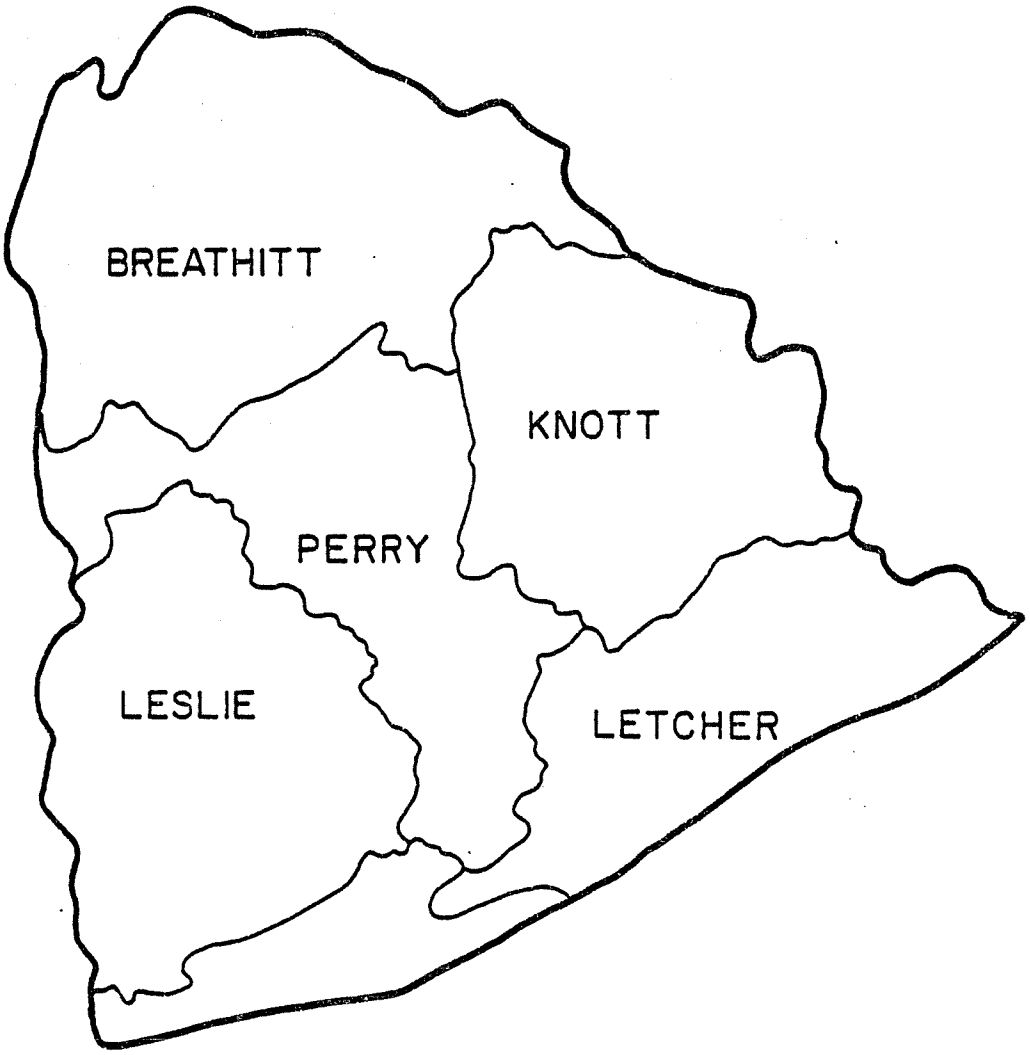

Fig. 3 Hazard Coal District of Eastern Ky

CHAPTER 3.0

PREVIOUS WORK

Griffith flaws have now been widely accepted and attributed to grain boundaries. Brace (1963) states that fractures may start at grain boundaries and that "Griffith's cracks or flaws" might lie within grain boundaries. Brace and Bombolakis (1963) stated that for rock sample size usually studied experimentally in the laboratory, "Griffith's cracks" are probably grain boundaries, in larger masses a similar role is assumed by joints, faults, and other discontinuities. Hoek and Bieniawski (1965) suggested that the inherent cracks from which fracture propagates are also contained within grain boundaries. Paterson (1963) found that internal stresses arising from anisotropy of thermal expansion or linear compressibility can be expected to give rise to microcracks along grain boundaries even in monomineralic rocks. Hundley-Goff and Moody (1980) found that cracks that grew during their grain sliding experiments were due to surface defects that were unfavorably oriented with regard to the local stress field. These defects include surface pits, grain boundaries, dislocation networks, and preexisting cracks produced during machining.

wavy the term rippled is used.

The sandstones thus studied in the thesis are 541, 544, 543RIP, and 543FLT. A 541 is a cross-bedded gray sandstone, 544 is a massive gray sandstone, 543RIP is a gray sandstone with shale streaks rippled and 543FLT is the same as 543RIP except that the streaks are lying flat. The choice of these four types of sandstone was based on personal observation of abundance of samples and intact core length.

2.4.0 General Geology

The Pennsylvanian strata of eastern Kentucky form a thick clastic wedge that thickens in a southeastward direction towards the axis of the Appalachian Basin. The axis of the Appalachian trough trends southeast and is generally parallel to the strike of Pine and Cumberland mountains. This area was the site of shallow water deposition strongly influenced by the rapidly subsiding Appalachian trough. Within this trough the Breathitt Formation of lower to middle Pennsylvanian age was deposited.

The Breathitt Formation was formed in lower and upper delta-plain environments; tidal flats, interdistributary bays, swamps, and shallow anastomosing stream channels. These environments are indicated by fluvial siltsone and sandstone, lagoonal shale, bayfill sequences, seat rock, flint clay, coal, and marine and nonmarine

limestone. The Breathitt Formation is not readily divisible into lithological units due to no single bed persisting across the entire basin. Subdivision of the formation is based upon the recognition of coal and marine beds or zones. Further investigations of the Breathitt Formation indicate that it can be divided into two units where the lower unit is shale dominant and the upper sandstone dominant.

The sandstones of the Breathitt Formation are generally less massive and resistant than the orthoquartzites of the underlying Lee Formation which intertongues with the Breathitt Formation. The sandstone appears to be stacked deposits of shallow anastomosing streams and are argillaceous and micaceous. The sandstones can be classified as subgraywackes (Folk, 1974) as it is shown in the petrographic report.

3.1.0 Grain Boundaries

The presence of "Griffith flaws" within grain boundaries and the composition and texture of the rock can give an indication of the physical properties. Sandstones generally consist of grains separated by matrix or cement. Studies on individual grains have shown that large, clear, well rounded grains are stronger than smaller angular grains or those showing lamellae or strain shadows (Borg and Maxwell, 1956; Maxwell, 1960). In practice it has been noted that finer grain aggregates are stronger than the coarser grain ones because finer grained aggregates have more surface area in which forces may act upon (Trash, 1959).

The positioning of critical contacts depends primarily on sorting, packing, grain shapes, and the boundary load conditions applied to the aggregate (Gallagher et al., 1974). Gallagher and others (1974) tested two-dimensional arrays of plastic and rock discs, and three-dimensional arrays of glass beads and found that extension-fracture criterion is dependent on packing but independent of the grain size and material. Gallagher and others (1974) also concluded that microfracture and contact line orientations are related to the orientations and relative magnitudes of boundary loads and to the packing arrangement, size, sorting, and dominant grain shapes in the aggregate. Other microfracture orientations have a tendency to be subparallel to the direction of the greatest

boundary compressive load and cluster at orientations that depend on size, sorting, dominant grain shape and packing arrangement of the aggregate. Fractures that form at the low-magnitude concentrations at single load points tend to become stable at a short distance into the grain and they are not likely to penetrate the entire grain (Gallagher et al., 1974). At or near contacts, maximum stress differences are very high; thus fracturing seems most likely to initiate here than anywhere else in the grain.

3.2.0 Cement

The role of cement bonding the grains would influence the orientation of microfractures. Assuming this, the influence of packing, sorting, shape, and confining pressures are reduced in comparison with uncemented aggregates (Gallagher et al., 1974). Cement in sandstone will also cause the orientation of microfracture to be homogeneous in distribution.

The strength of the cement will affect the strength of the cemented aggregate. If the strength of the cement is equal or greater than the material strength of the grain, the macroscopic fracture will pass through the cemented matrix and individual grains that lie along the same fracture plane. This can be observed in orthoquartzites and metaquartzites. If the cement is weaker than the grain material, macroscopic fracture will tend to go around individual grains due to the cement failing

before the grains. Friedman and Logan (1970) stated elastic strains locked in the aggregates cemented while under load can further influence the subsequent mechanical behavior of the aggregate. In aggregates cemented while not under load, subsequent boundary loads are transmitted from grain to grain as in uncemented aggregates although some of the applied load is transmitted by the cement and rigid movement of grains before and after fracture are inhibited (Gallagher et al., 1974). Thus grains of cemented aggregates are more highly stressed at their centers than at margins and stress distribution under applied load are more uniform not only in individual grains but for the entire aggregate.

CHAPTER 4.0

UNIAXIAL COMPRESSION TEST

The uniaxial compression test involves the use of a cylindrical specimen axially loaded between two platens of the testing machine. This test is used in the determination of the compressive strength of the unconfined material. The results obtained are not dependent on the properties of the rock alone but also upon the external factors of the testing machine. These factors of the specimen and testing machine complicate the results of the uniaxial compression test. The internal factors of the specimen that contribute to the difficulty in determining the compressive strength are mineral characteristics of the components, grain size, porosity, and internal defects. The external factors are contact friction between machine platens and specimen, specimen geometry, rate of loading, and moisture.

The stress distribution in the specimen will be non-uniform due to end effects and elastic mismatch of the specimen and the testing machine, however this non-uniformity can stay in acceptable limits when certain preparation standards are met. As the specimen is compressed between the platens it will expand laterally as it shortens due to "Poisson's effect." But the frictional

constraints between the specimen and platens prevent this expansion, thus the specimen is not in a state of uniaxial compression at the ends of the specimen. The coefficient of friction between the specimen and platens is dependent upon the nature of the contact surfaces. Correction for this effect has attempted by other researchers (Hast, 1943; Jenkins, 1958; Lunborg, 1968; Brady, 1971) through the introduction of a weak pad between the platen and specimen (e.g., parafin, rubber, cardboard). The result was the reduction of friction between the platen and specimen, and uniform load, but usually lower ultimate strength.

Sample shape or geometry will influence results of tests especially in compression. Cylindrical specimens are preferred since less preparation time is needed and stress distribution in them is symmetrical about the axis (Vutukuri et al., 1974). Length (L) to diameter (D) ratios are critical in compression testing. Pforr and Rosetz (1966) studied the effect of L/D ratios for uniaxial compression testing on salt samples. Their studies showed an increase of compressive strength with a decrease in the L/D ratio (Fig. 4). Specimens with small L/D ratios have a stress distribution that will tend to become triaxial and the specimen will exhibit a high compressive strength. If the L/D ratio is high the sample will fail due to elastic instability. Thus samples with a medium range of L/D will have uniform stress distribution and elasticially stable behavior. L/D = 2 is recommended, assuring close to

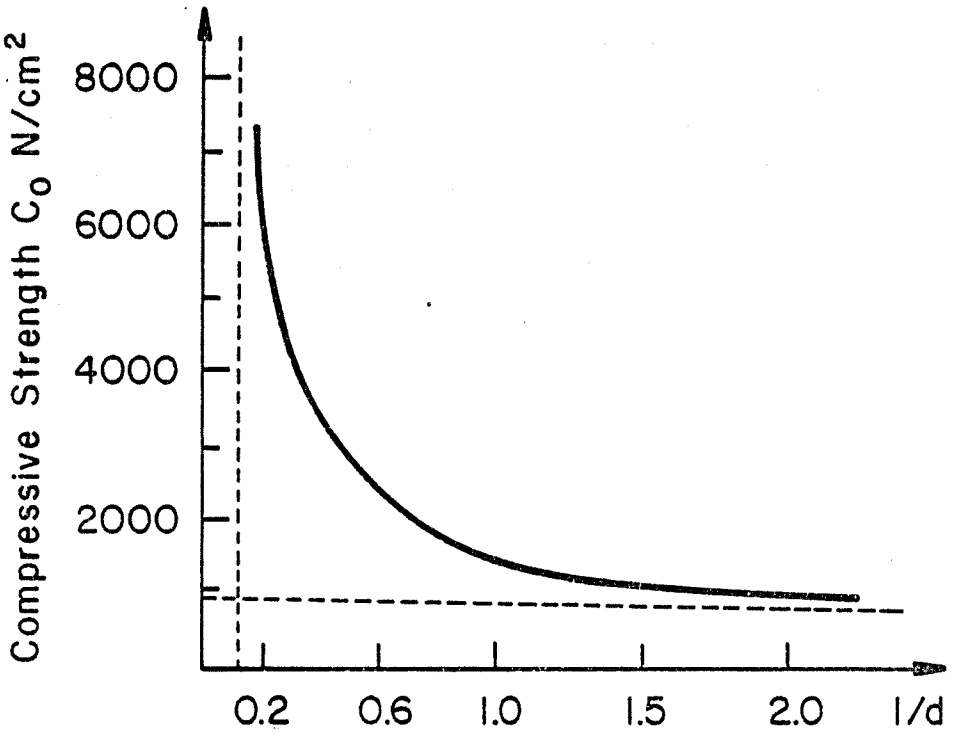

Fig. 4. Influence of slenderness factor (L/D) on compressive strength (Salt samples). (After Pforr and Rosetz, 1966).

uniaxial state of stress in the vicinity of the mid-length of the sample.

The compressive strength is also dependent upon the rate of loading. As the rate of loading increases the compressive strength will increase. In dynamic loading tests such as impact and sonic testing, the compressive strength value will be several times higher as compared to those results of static loading (e.g., uniaxial compressive test). This higher compressive strength value is due to the increased build up of strain within the sample that will cause an abrupt and violent failure.

The moisture content in the specimen will influence the compressive strength. Bauer (1979) found that rock samples, that have not been protected to preserve the natural moisture, can lose up to 70 percent of the natural moisture content within days. He also concluded that as the natural moisture content decreases, compressive strength will increase. Burshtein (1969) studied the effect of moisture content on the compressive strength of sandstone. He found that with a 4 percent increase in moisture content, the sandstone will lose half of its compressive strength (Fig. 5).

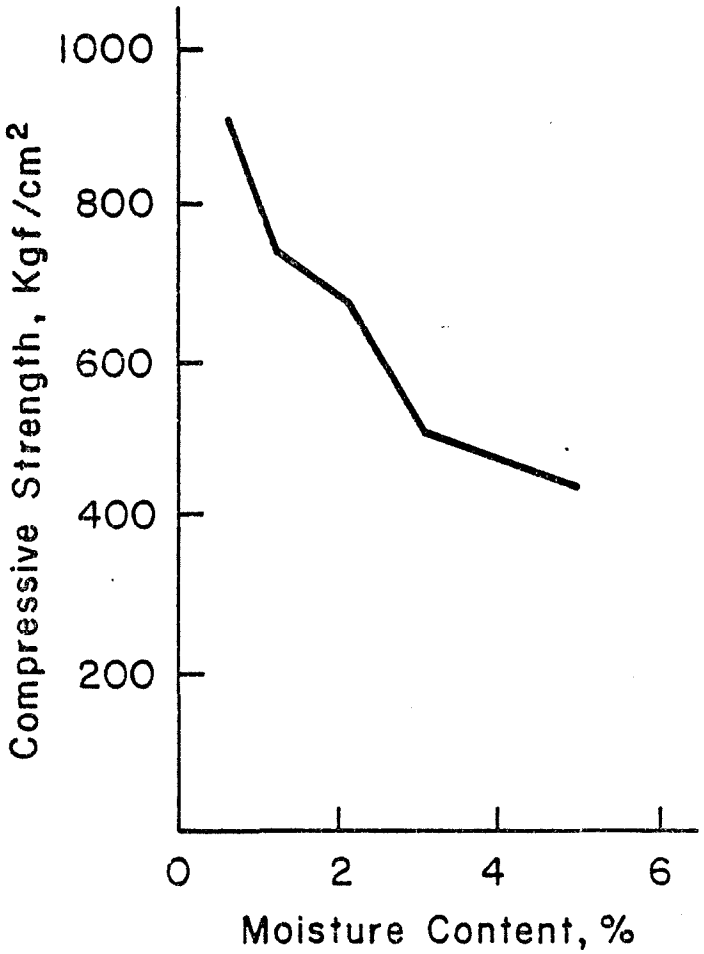

Fig. 5. Compressive strength versus moisture content for sandstone (After Burshtein, 1969).

CHAPTER 5.0

BRITTLE BEHAVIOR OF ROCK

A material is considered to be brittle if its ability to resist load rapidly decreases with increasing deformation. Many rocks exhibit brittle behavior and it is characterized by the stress-strain curve (Fig. 6 and 7). The stress-strain behavior in compression prior to macrofracturing can be divided into four stages. These four stages are:

1. Closing of some cracks
2. Linear elasticity
3. Stable fracture propagation
4. Unstable fracture propagation

In the first stage of the stress-strain curve, nearly all pores and microcracks will close under very little stress. This is evident by the upward concavity of the curve. During this stage if the stress is released, pores and microcracks will reopen with little or no deformation, thus it is a reversable process. Poisson's ratio, ν, in this stage initially decreases until all the pores close or reach static equilibrium. At this point with all of the microcracks and pores closed or statically equalized, the sample will become elastically stiff. Young's modulus, E, will be increasing after the microcrack closure. The

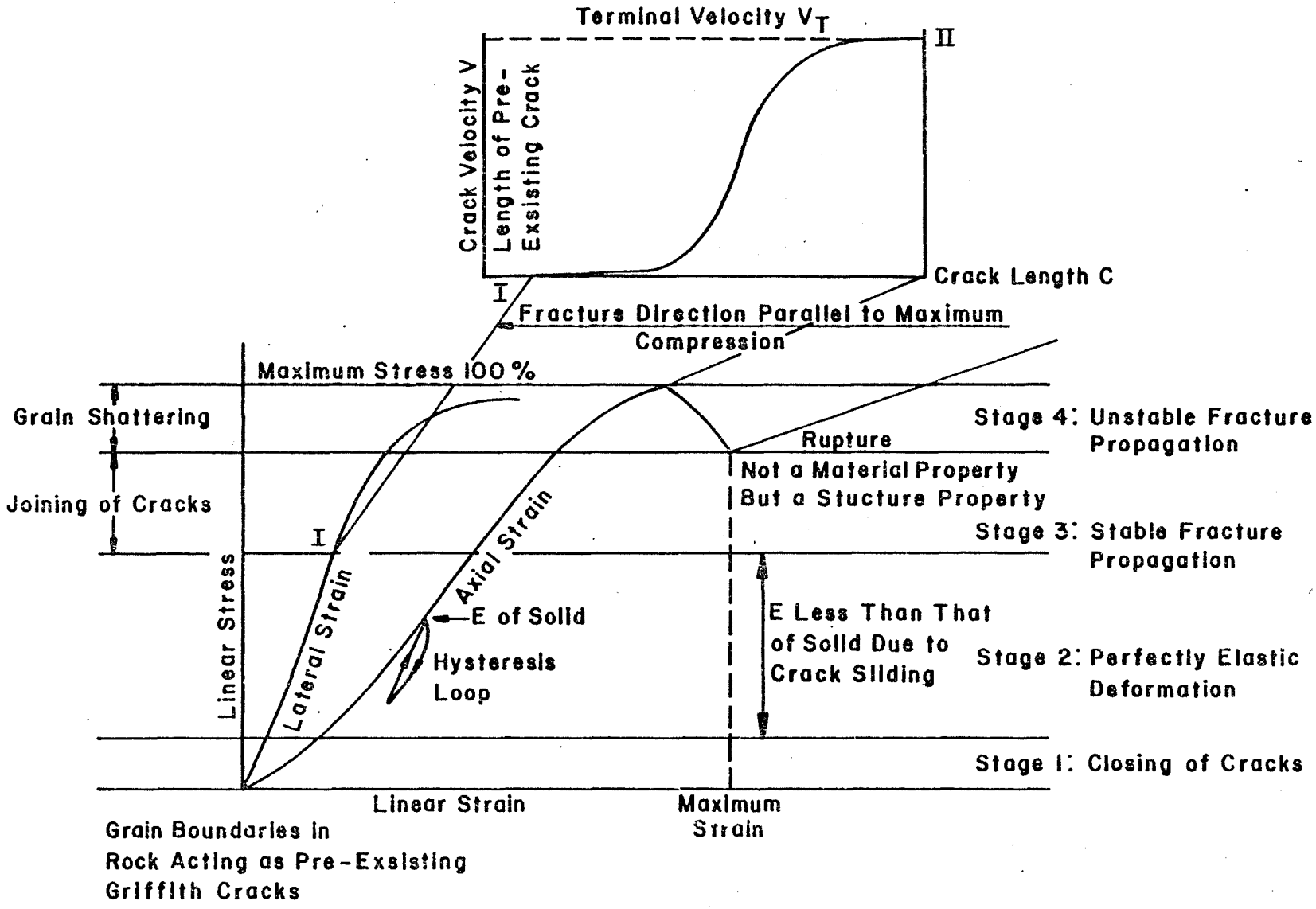

Fig. 6. Mechanism of brittle fracture of rock in uniaxial compression (After Bieniawski, 1967).

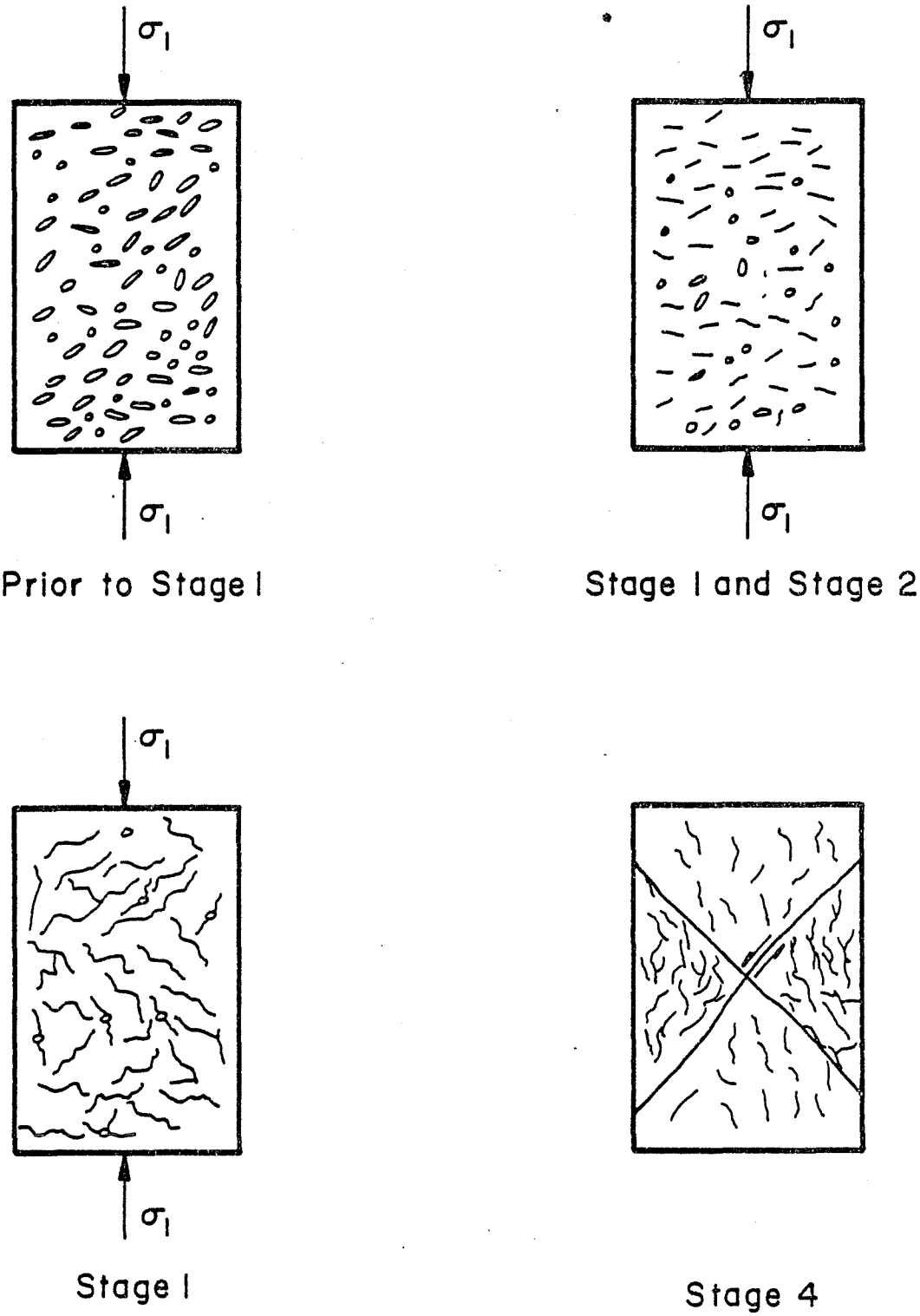

Fig. 7. Cross-sectional view of rock core during the four stages of uniaxial compression.

volumetric strain, $\frac{\Delta V}{V}$, is increasing with the change in volume, ΔV, and the volume, V, remaining constant. The second stage is the beginning of linear elasticity. As the load is increased, E and ν will remain constant, but E will be less than that of an ideal solid due to crack sliding, elastic deformation of pores and grains initiate here. Thus the microcracks and pores during this stage cannot be reopened and are irreversable. If the sample was unloaded to zero stress, it would follow a different path as compared to the loading cycle, this is called a hysteresis loop. This occurs if more work is done by the sample during loading than is done during unloading so that energy is dissapated in the body during a cycle of loading and unloading (Jaeger and Cook, 1969, p. 76). Volumetric strain is still increasing. The third stage is the departure from linear elastic state, marking Griffith's criteria. During this period cracks are starting to propagate in a stable manner in the direction of maximum compressive stress. Microcracks that are inclined 45° from the principal stress are the most favorably oriented and crack initation is likely to begin here. The crack propagation only extend in limited amounts in response to given increments of stress and may join together but do not form macroscopic cracks. E is still constant and ν is starting to increase due to lateral expansion. In stage four, the crack propagation becomes unstable. The velocity at which the crack may propagate through the

sample increases until it reaches its terminal velocity for that media. The cracks at this stage split up and join with other cracks at random. Grains within the sample are shattering as the sample approaches rupture. E is decreasing as evident in the negative slope on the curve and ν is still increasing. At rupture the microcracks form together a macrofracture network and an audible noise can be heard upon rupture as the sample releases energy from the induced stress.

CHAPTER 6.0

LOADING EQUIPMENT AND PROCEDURE

The compressive stress state induced on the samples was produced by a Riehle Testing machine with a 300,000 pound (136,000 kg) capacity and variable control rate of load (Fig. 8). Loading rate of samples were governed by the use of the Riehle dial gauge and stopwatch. The dial gauge measured the amount of pounds produced by the testing machine. The variable control of load rate was timed over a 20 second period and an uniform load rate of 1,000 lbs/sec (454 kg/sec) could be established. Stress on the sample was measured by a Daytronic Model 170B pressure transducer.

6.1.0 Sample Preparation

The sandstone samples were wet diamond cut with a L/D ratio of 2:1. These samples were precision ground on a DoAll surface grinder using V-blocks and parallel bars. Samples were checked for parallelism on a Soil Test dial gauge and were found to be parallel near 0.002 inch (0.005 cm), all dimensions and weight were recorded after this procedure to obtain the specific gravity of each sandstone group (Table 1).

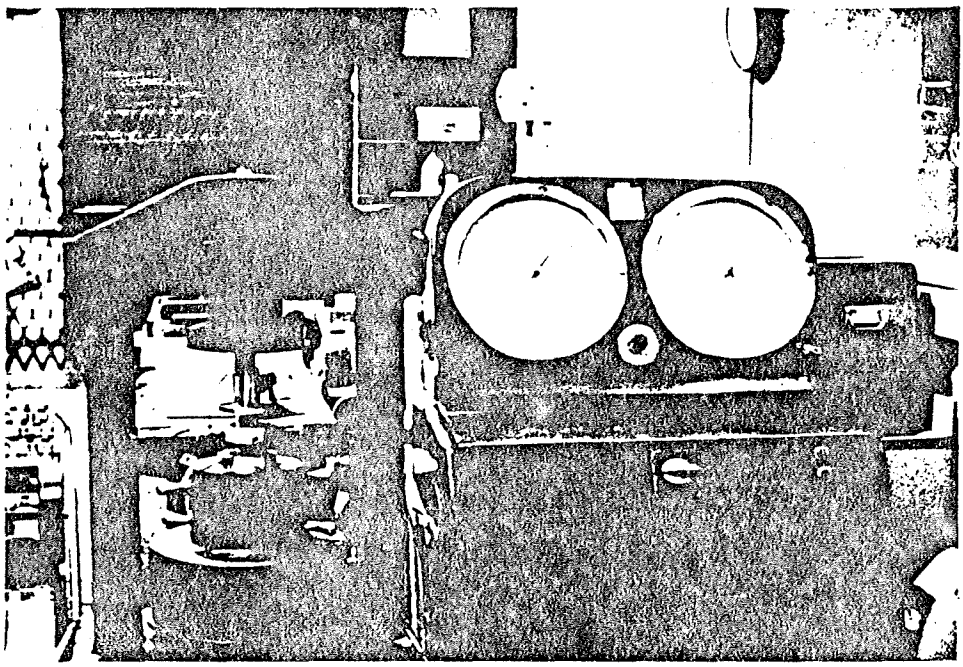

Fig. 8. Photograph of Riehle Testing Machine with LVDT setup.

TABLE 1

SPECIFIC GRAVITY OF SANDSTONES

Ferm Class.	Specific Gravity lb/in^3	kg/cm^3	Standard Dev.
543RIP	0.0884	2.44	0.0029
543FLT	0.0889	2.46	0.0009
541	0.0867	2.39	0.0013
544	0.0877	2.42	0.0013

6.2.0 Deformation Measurements with Strain Gages

Strain measurements in the lateral and longitudinal direction during compressive stress was measured by means of strain gages of 1/2 inch gage length. Gates were mounted on eight samples using M-600 adhesive under manufacturers instructions. Four gages were mounted on each sample, with two gages in the longitudinal direction and two gages in the lateral direction. The gages were separated 90° from one another. As the load was applied to the sample, readings from the strain gages were measured on four P-350 strain indicator boxes. Readings were made at an equal stress interval and loading rate.

6.3.0 Deformation Measurements with LVDTs

Measurements of lateral and longitudinal deformation under compressive stress was made by using six LVDTs (Linear Variable Differential Transducers). To measure lateral deformation four LVDTs (X-axis, Y-axis) were mounted in an adjustable aluminum holding ring separated 90° apart. Longitudinal deformation (Z-axis) was measured by two LVDTs mounted in the upper platen (Fig. 9).

The LVDT consists of two secondary coils, one primary coil and a magnetic core. An AC excitation voltage is passed through the primary coil which induces an AC voltage in the two secondary coils. Output voltage from the secondary coils is dependent upon the relative position of the magnetic core to the secondary coils. If the core

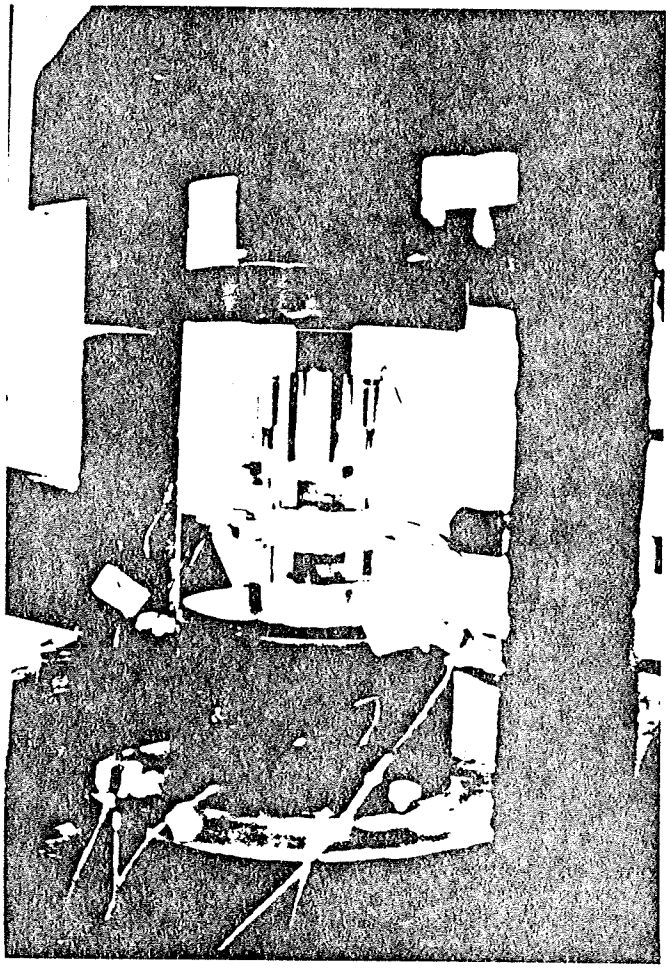

Fig. 9. LVDT apparatus in between loading platens of Riehle Testing machine.

is positioned between the two secondary coils no voltage is induced, the null position. Thus any displacement of the core will cause a voltage output. The LVDT system was chosen due to it provides a high sensitivity range of displacement due to deformation and it is reusable unlike the strain gage.

The lateral LVDTs are placed against the sample and are zeroed to the null position. The LVDT is held in the aluminum ring holder by set screws and may be adjusted. The longitudinal LVDTs located in the upper platen are held by set screws and are zeroed against two vertical pins mounted to the lower platen. The signal from each LVDT and the pressure transducer (stress moniter) is amplified in a Valydyne Model MC1 amplifier. The LVDT sensitivity may be controlled by adjusting the coarse and fine gain settings. The signals after amplification are brought together in a LVDT interface box. This device adds together the signals received from two LVDTs on the same linear axis and averages them together to produce a single signal. The four signals are plotted on two Y-Y-X recorders that generates four stresses--strain curves simultaneously; two lateral strain (X and Y axes) versus stress and two longitudinal strain (Z-axis) versus stress (Fig. 10).

6.4.0 Calibration of Equipment

The stress-strain curve equipment was calibrated by using an isotropic solid with known physical properties. A

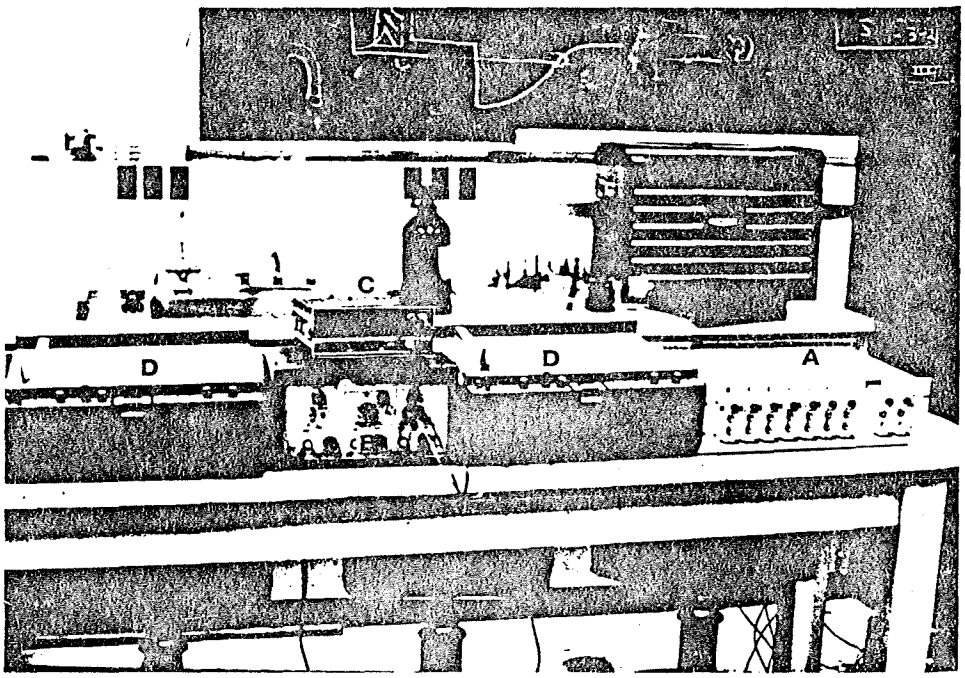

Fig. 10. LVDT stress-strain curve recording equipment. A: Valydyne Model MC1 Amplifier. B: LVDT interface box. C: Digital voltmeter. D: Y-Y-X plot graphing machines.

cylindrical specimen of aluminum with a length to diameter ratio of 2:1 was used. Mounted to the aluminum specimen were four strain gages. Two gages were mounted in the longitudinal direction and two gages were mounted in the lateral direction separated 90° from one another. The aluminum specimen was placed in the LVDT setup and was loaded at an uniform rate and measurements were made at equal stress intervals. A comparison of the Young's modulus and Poisson's ratio obtained from the strain gages and LVDTs was made to find if any difference in the loading system using LVDTs exists.

CHAPTER 7.0

PLATEN DEFORMATION

Results from the LVDTs versus the strain gages show a 23 percent difference in Young's modulus and a 2.3 percent difference in Poisson's ratio. The differences in values from the LVDTs and strain gages in the longitudinal direction is the result of platen deformation. As the load is applied to the specimen the platens are deformed around the specimen. As the load is increased, the penetration of the sample into the platens is stabilized and measurements taken from the LVDT will be greater than those of the strain gages. Since the LVDTs are not directly mounted to the specimen and are located away from it, the upper platen which holds the longitudinal LVDT will act like a cantilever beam. This cantilever beam will have a moment force due to the absence of a reaction force. The location of the reaction force is in the center of the platen directly under the sample. Because of the moment at the end of the platen, the platen will deflect downward causing the LVDT to record a higher deformation than normal. Thus the stress-strain curve from the LVDT will have a gentler slope compared to the strain gage curve. This is shown for aluminum, 544, 543RIP, 543FLT and 541 respectively in Figs. 11, 12, 13, 14, and 15.

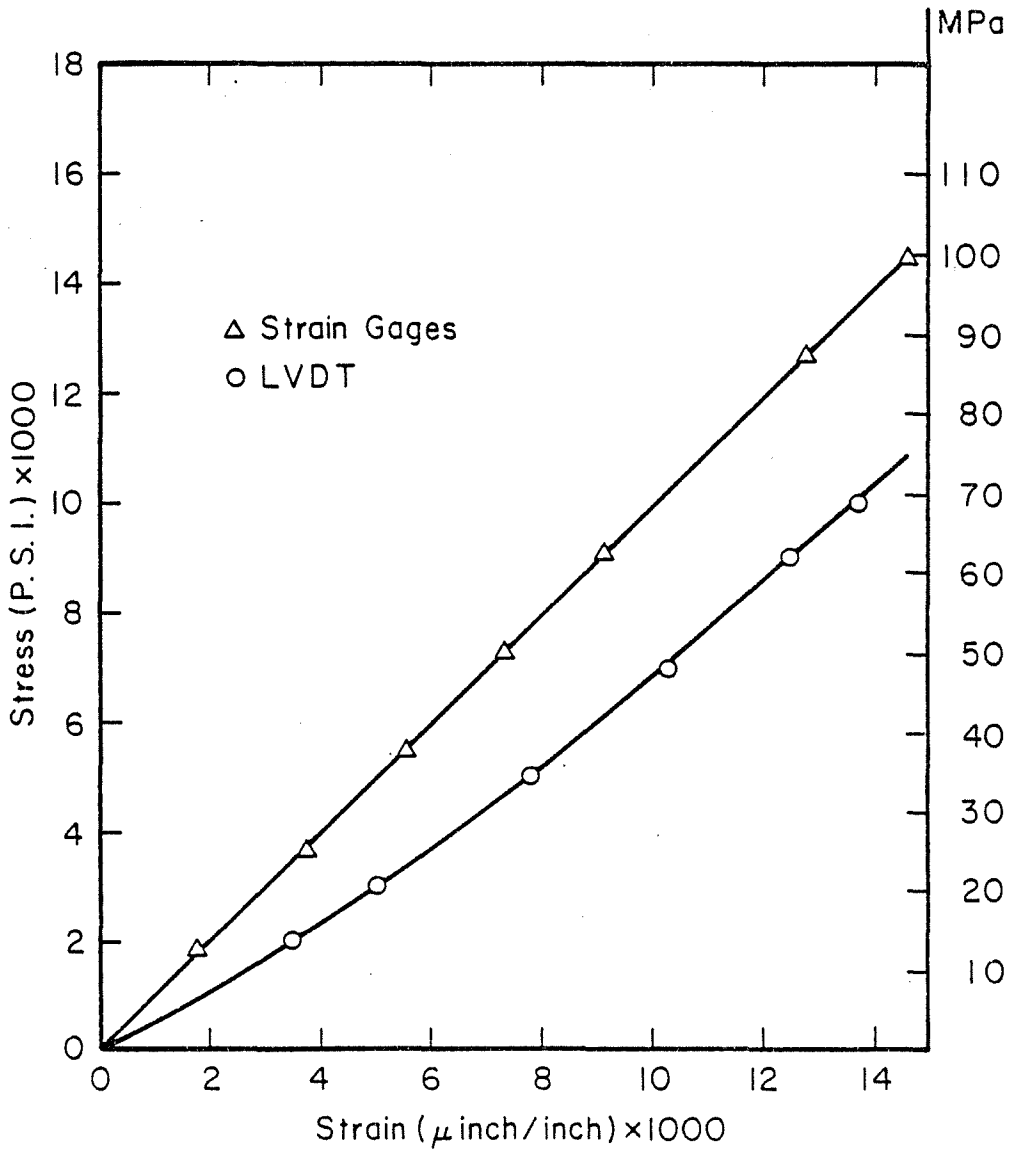

Fig. 11. Stress-strain curve (longitudinal direction) aluminum sample LVDT vs strain gages.

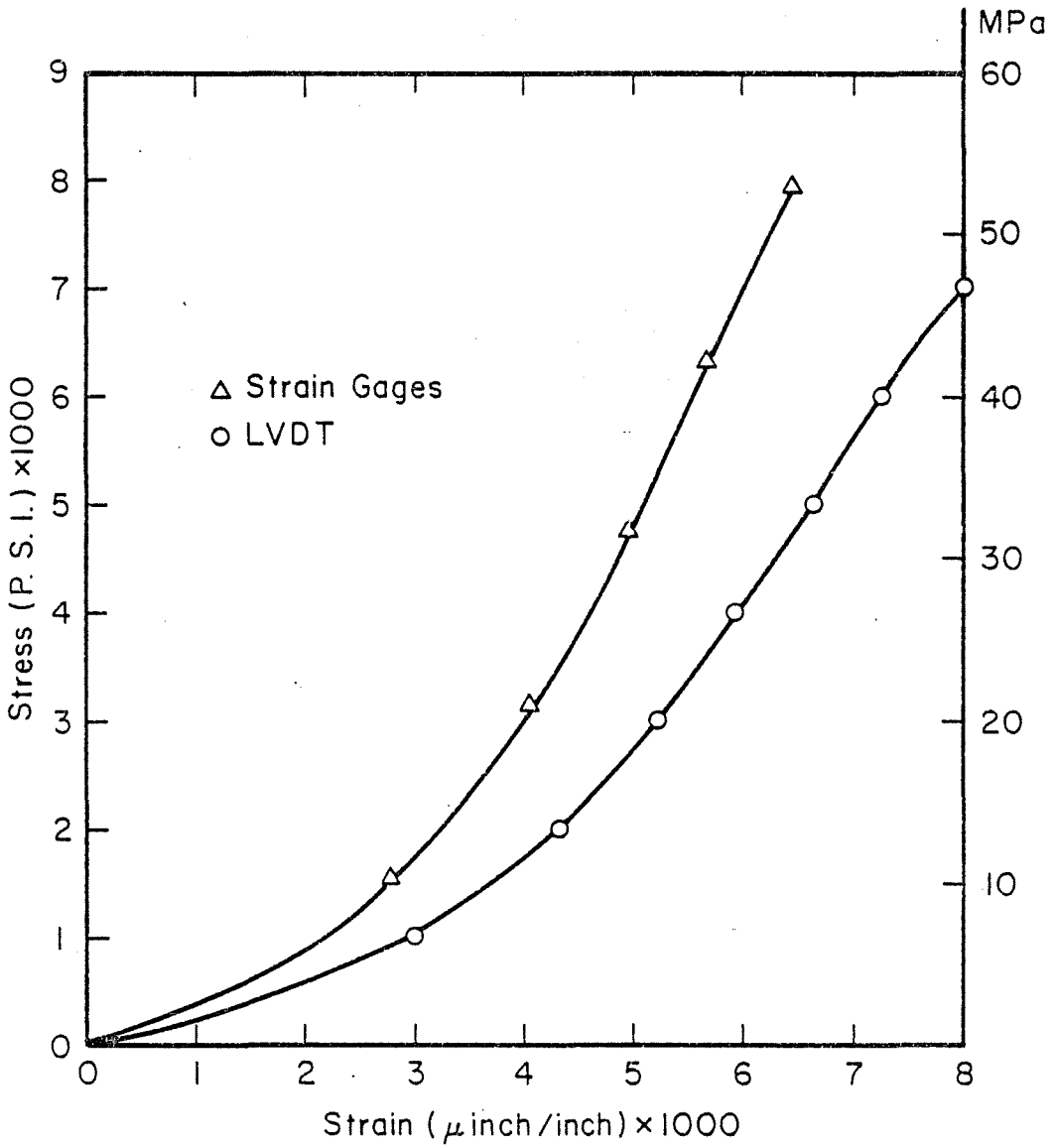

Fig. 12. Stress-strain curve (longitudinal direction) sample 30F 544 LVDT vs strain gages.

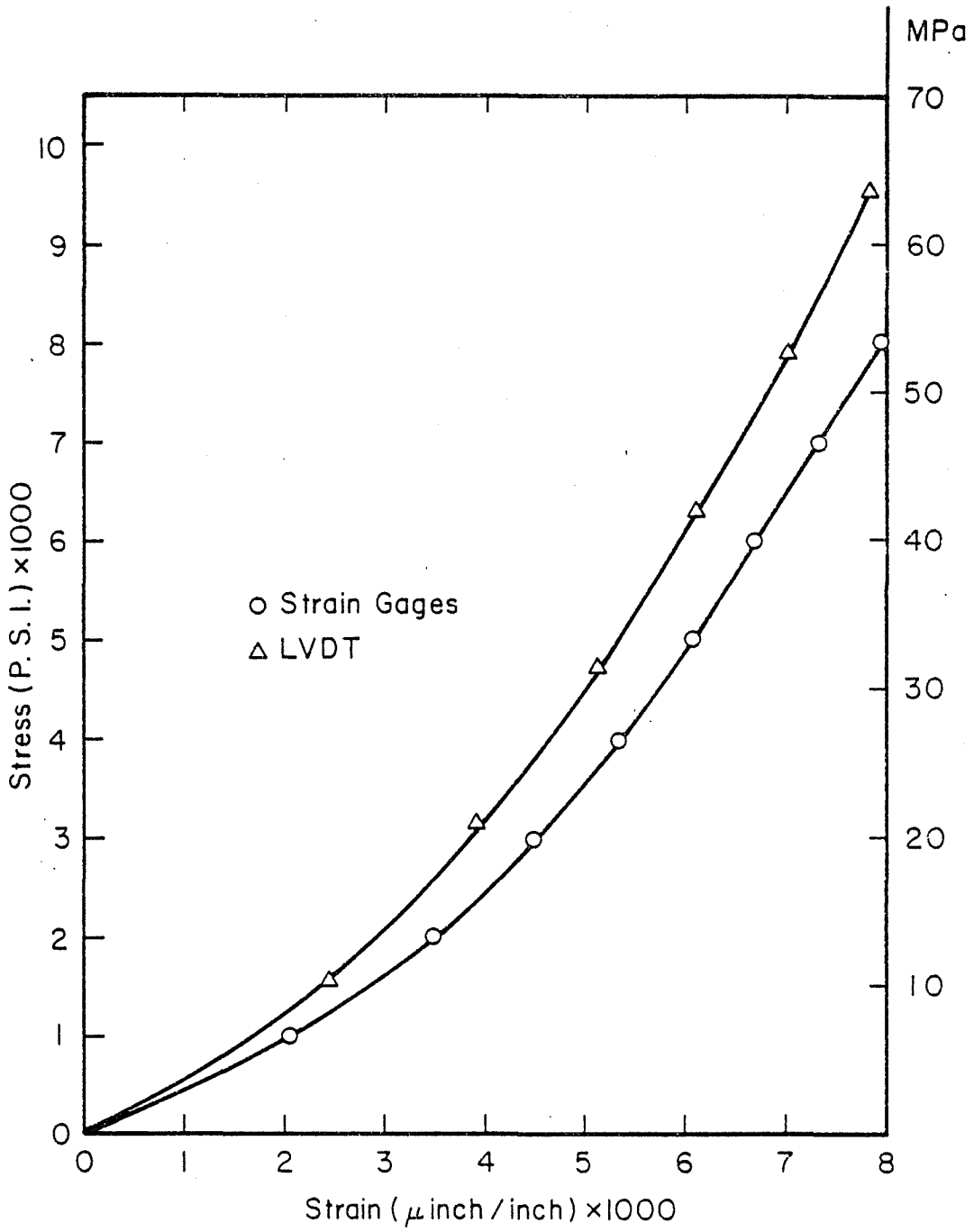

Fig. 13. Stress-strain curve (longitudinal direction) sample 3B 543RIP LVDT vs strain gages.

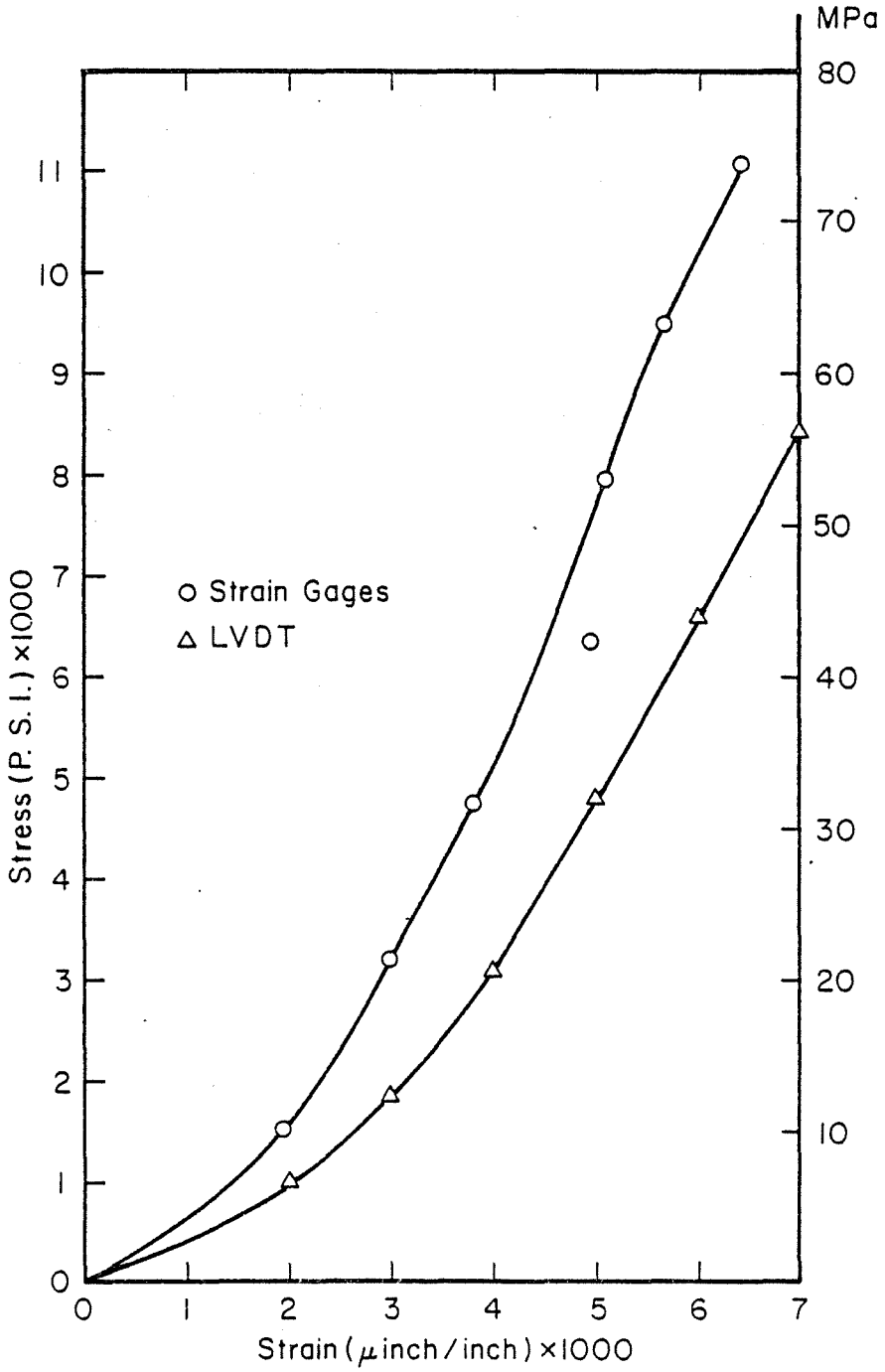

Fig. 14. Stress-strain curve (longitudinal direction) sample 92G 543FLT LVDT vs strain gages.

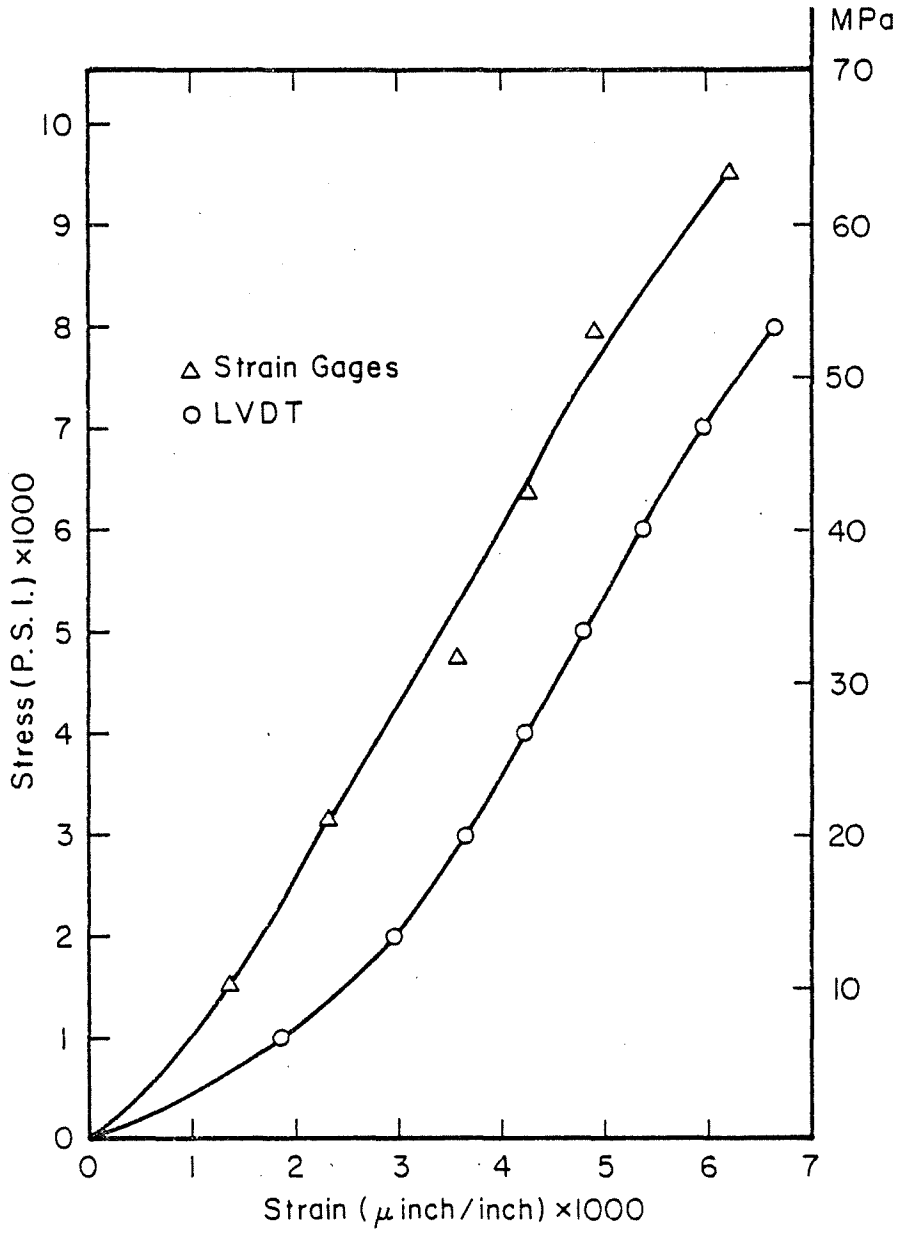

Fig. 15. Stress-strain curve (longitudinal direction) sample 117B 541 LVDT vs strain gages.

A platen deformation correction was attempted by using the same procedure as described by Agrawal (1979). Agrawal (1979) encountered platen deformation with his uniaxial compression experiments with shale, limestone, and aluminum. He attempted to correct the deformation by utilizing an equation to calculate the amount of deflection due to a load distributed over a circular area on the boundary of a semi-infinite solid. This equation was taken from Timoshenko (1934) and is given by:

$$\delta AVE = \frac{2mP\ (1 - \nu)}{E\sqrt{A}} \qquad (9)$$

δAVE is the average amount of deflection in inches, A is the area in square inches, E is the modulus of elasticity of the platen in P.S.I., m is a constant found to be equal to 1.0, ν is the Poisson's ratio of the platen and the multiplication of 2 is necessary since there are two platens. P is the load in pounds.

Agrawal (1979) calculated platen deformation at each load on the stress-strain curve using equation (9). He subsequently subtracted the calculated deformation from the observed deformation to obtain the actual deformation. The candidate has attempted to use Agrawal's suggestion for platen correction but has had no success in reproducing a correction factor. Another approach was to compare the buckling of the platen to a die penetrating a plate causing a deflection of the plate. This attempt also failed. The

reason for the failure in finding a correction factor is due to the platen deflection caused by sample penetration is very small and very difficult to empirically calculate or reproduce. Possibly the only solution for this problem would be to mount strain gages on the upper platen and record the amount of strain occuring during the compression test. This procedure was not carried out due to the lack of additional machinery necessary to record this phenomenon, therefore no attempt will be made to correct this error, but it is noted that it exists.

CHAPTER 8.0

PETROLOGY

Thin sections were made on rock samples prior to and after testing and were petrographically compared by the candidate. The rocks are subgraywackes (Folk, 1974) and can be subdivided into four different lithologic units according to Ferm's classification (1979). They are as follows: 541, 544, 543RIP, and 543FLT.

Grain size analysis and petrographic examination was accomplished on each thin section. All four types of sandstone were similar in mineral composition. The presence of feldspars, rock fragments, high amount of matrix material, and recrystallized minerals indicate that these sandstones are subgraywackes (Table 2). The fabric of the sandstone consisted of interlocking grains caused by quartz overgrowths (Fig. 16). The grain size differed in all four types and is shown in Table 3. The grains are subangular with long sutured contacts between grains and matrix. The grains are well to moderately sorted with no preferred orientation. The grain material may be considered isotropic even though deformation on the scale of individual grains are anisotropic (Walsh, 1965). Quartz and feldspar were the main minerals with acessory minerals of muscovite, biotite, calcite, and limonite in small

TABLE 2

RESULTS FROM PETROGRAPHIC EXAMINATION

Ferm Class.	Sorting	Mode (μ)	Shape	Constituents			Terrigenous Comp.			
				Terr	Ortho	Allo	Qtz	Rf	Mica	FsPAR
543FLT	WELL	200	SA	97.0	1.0	2.0	93	5	1	1
543RIP	MOD	125	SA	97.0	1.0	2.0	90	6	3	1
544	WELL	300	SA	98.0	1.0	1.0	94	5	½	½
541	WELL	95	SA	94.0	5.0	1.0	75	20	5	TR

SA = Subangular
μ = Micrometer
TR = Trace
RF = Rock Fragments

(After Weinheimer, 1980)

Fig. 16. Photomicrograph of a quartz grain with secondary quartz overgrowth. Iron oxide coats the original shape of the quartz grain. Cross-nichols. x20

TABLE 3

COMPARISON OF GRAIN SIZE OF FOUR SANDSTONES

Ferm Classification	Grain Size		Standard Dev.
	mm	inch	
541	0.177	0.007	0.172
543FLT	0.101	0.004	0.047
543RIP	0.343	0.014	0.127
544	0.386	0.015	0.100

quantities. Small amounts of sericite and chlorite were also noted. The cement consists of cryptocrystalline quartz and was confirmed by a negative reaction to dilute hydrochloric acid and low birefringence of the material.

From the petrographic examination the following conclusion is made. Secondary quartz overgrowths indicate that these sandstones had porosity and permeability. Later these pores were filled by precipitated quartz forming interlocking grains. The porosity of the sandstone was also changed by compaction. This can be seen in the presence of bent micas around grains (Fig. 17). Quartz overgrowths and the compaction of matrix around these grains fill all pore space thus there appears to be no porosity. The low porosity of the sandstone samples indicate that these samples would be elastically stronger and stiffer as compared to samples with higher porosity.

Fig. 17. Photomicrograph of bent mica around grains before uniaxial compression testing. Cross-nichols. x8

CHAPTER 9.0

RESULTS

The results of the uniaxial compression test for the four types of sandstone are given on Table 4 and 5. Ten samples for each type of sandstone were tested and Young's modulus and Poisson's ratio were calculated at 50 percent of the compressive strength.

The Poisson's ratio found for the four types of sandstone are very similar to one another, indicating that the compressibility are equal to one another. The high Poisson's ratio value indicates that there is little or no porosity within the sandstone groups. The petrographic examination confirms these findings in that no compositional differences in the sandstones is identified to justify different compressibilities and no apparent porosity was found in the thin sections.

The petrographic study of the deformed samples shows deformation of the grains. The most prevelant phenomenon is shattered grains. Fig. 18 shows a grain that has been shattered due to deformation. The reason for the destruction of the grain is due to the grain experiencing a moment of force and it was inhibited to rotate. The rotational movement of the grain was blocked by matrix material, and closed microcracks and pores. Eventually the

TABLE 4

RESULTS FROM UNIAXIAL COMPRESSION TEST

Sample No.	Ferm Class.	E PSI x10^6	E MPa x10^4	ν	Co PSI	Co MPa
117E	541	1.56	1.07	0.32	7700	54.14
117F	541	1.66	1.15	0.62	7400	52.03
117C	541	1.70	1.18	0.34	7800	54.84
173	541	1.16	0.80	0.48	5500	38.67
117B	541	2.29	1.58	0.39	9549	67.14
207	541	3.42	2.35	0.41	13956	98.12
124B	541	2.20	1.52	0.21	9603	67.51
194A	541	3.81	2.63	0.36	22000	154.68
194B	541	2.97	2.06	0.30	14852	104.42
117D	541	1.75	1.21	0.35	9800	68.90
3C	543RIP	1.48	1.02	0.44	11100	78.04
3A	543RIP	1.53	1.06	0.33	1090	7.66
90D	543RIP	1.53	1.06	0.45	6950	48.86
90A	543RIP	1.50	1.03	0.38	5080	35.71
90E	543RIP	1.36	0.94	0.48	5910	41.55
141B	543RIP	2.69	1.85	0.11	12453	87.55
141A	543RIP	3.04	2.10	0.05	12775	89.82
3B	543RIP	1.62	1.12	0.33	12783	89.87
90C	543RIP	1.58	1.10	0.42	8100	56.95

TABLE 4--(continued)

Sample No.	Ferm Class.	E PSI x10^6	E MPa x10^4	ν	Co PSI	Co MPa
90B	543RIP	1.53	1.06	0.50	7200	50.62
92B	543FLT	1.53	1.06	0.25	8200	57.65
92C	543FLT	1.66	1.15	0.28	8800	61.87
92A	543FLT	1.81	1.26	0.34	9800	68.90
92H	543FLT	1.80	1.26	0.45	10200	71.71
127C	543FLT	2.44	1.69	0.37	10000	70.31
127A	543FLT	2.67	1.84	0.36	12275	86.30
92G	543FLT	2.38	1.64	0.36	11140	78.32
92D	543FLT	1.66	1.15	0.35	9900	69.60
92E	543FLT	1.75	1.21	0.35	9500	66.79
92F	543FLT	1.90	1.31	0.34	9700	68.20
30A	544	1.15	0.79	0.44	6200	43.59
30C	544	1.18	0.81	0.30	6400	44.99
30E	544	1.40	0.97	0.44	7300	51.32
30D	544	1.53	1.06	0.41	7400	52.02
30B	544	1.43	0.99	0.48	7300	51.32
93B	544	1.72	1.20	0.35	7195	50.58
153B	544	2.82	1.94	0.15	15660	110.10
153	544	1.95	1.34	0.32	12118	85.20

TABLE 4--(continued)

Sample No.	Ferm Class.	E PSI x10^6	E MPa x10^4	ν	Co PSI	Co MPa
30F	544	1.79	1.24	0.37	9597	67.47
93A	544	1.79	1.24	0.25	8600	60.46

TABLE 5

AVERAGE OF MECHANICAL PROPERTIES

Ferm Class.	Elastic Properties Average			Standard Dev.	
	E		ν	E	ν
	PSI x10^6	MPa x10^4			
541	2.25	1.55	0.38	0.875	0.108
543FLT	1.96	1.36	0.35	0.390	0.053
543RIP	1.79	1.23	0.35	0.579	0.153
544	1.68	1.16	0.35	0.482	0.010

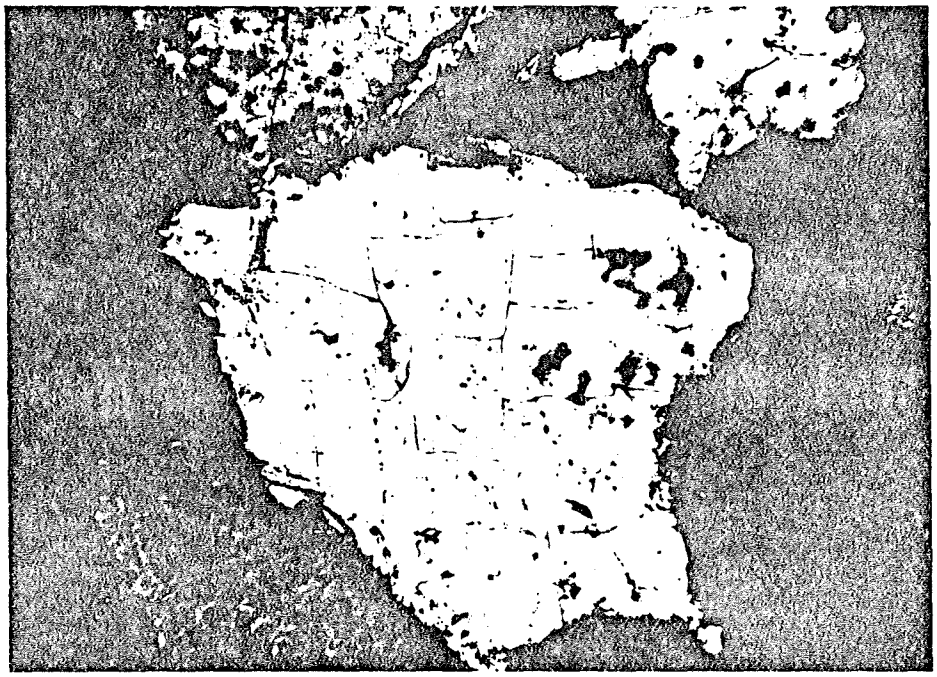

Fig. 18. Photomicrograph of shattered quartz grain after uniaxial compression test. Cross-nichols. x20

force was sufficiently high to overcome the molecular cohesion of the quartz and feldspar grains, thus shattering. Other minerals in the sandstone showed signs of strain lamellae and twinning due to high stress on the sample.

Young's modulus is an indicator of the material's physical strength. The Young's moduli for the sandstones vary considerably with respect to one another. The 541 sandstone exhibited the highest modulus, followed by 543FLT, 543RIP, and 544. Although the composition of the sandstone were similar, the major difference was the grain size. Although the 541 had a larger grain size than 543FLT, it had the highest modulus. This due to the 541 having no shale streaks. 543FLT modulus was similar to 541 but the streaks of shale caused the modulus of the sample to be lower. It has been noted that if a material consists of two different sized grains, the overall modulus would be lower than that of a material that consists of single sized grains. At the boundary of the different sized grains a weak zone or plane of failure exists. Failure is most likely to initiate here than anywhere else in the sample. The 543RIP is similar to the 543FLT in composition but differ in grain size. The 543RIP has a larger grain size than the 543FLT, thus with the larger grain size, it has a lower modulus. Finally the 544 is a coarse grained, massive sandstone with no shale streaks. The reason for its low modulus is due to its large grain size as compared to the other. The large grain

size will have less surface area for the stress to act on and stress is not as easily transmitted grain to grain to reach a static equilibrium as in finer grained aggregates. The larger grains will reach a critical stress necessary to initiate fracture before the finer grains due to the concentration of stress at the point of grain to grain contact. Thus the larger grained sandstone will fail first before the finer grained sandstone with the same loading rate.

CHAPTER 10.0

CONCLUSIONS

From the experimental data the following conclusions have been derived:

1. The determination of Young's modulus and Poisson's ratio of the sandstones studied indicate that there are at least four mechanically different types of sandstone within the Breathitt Formation.

2. The compressibility of the four sandstones as measured by their Poisson's ratios were nearly identical.

3. The high value of the Poisson's ratio for the four types of sandstone indicate that there is little porosity in them. This is verified by the petrograghic examination.

4. Young's modulus of the four sandstones show that the finer grained material has better elastic properties and higher strength than the coarse material.

5. The mechanical data found on the four sandstones could be used for engineering and geologic work but further investigation is necessary to enlarge the experimental data base.

BIBLIOGRAPHY

1. Agrawal, A. K., 1979, Determination of t
Constants of coal mine shales, Unpub
University of Kentucky, 82 p.

2. Anderson, E. M., 1942, The Dynamics of Fa
Dyke Formation with Application to Br
ed., Edinburgh, Oliver and Boyd, p. 1

3. Bauer, R. A., 1979, The Loss of Natural M
Content and its effect on the Mechani
Properties of some Pennsylvanian shal
Illinois Basin, First Conference on G
Problems in the Illinois Basin, Southe
University, Carbondale, Illinois, 6 p.

4. Berg, Charles, A., 1965, Deformation of Fi
under High Pressure and Shear, Journal
Geophysical Research, v. 70, n. 14, p.

5. Bieniawski, Z. T., 1967, Mechanism of Briti
Fracture of Rock, National Mechanical E
Research Institute, Council for Scienti
Industrial Research, Pretoria, South Af

6. Borg, I., and Maxwell, J. C., 1956, Interpr
Fabrics of Experimentally Deformed Sand
Journal of Science, n. 254, p. 71-81.

7. Brace, W. F., and Riley, D. K., 1972, Stati
Deformation of 15 rocks to 30 Kb, Inter
Journal of Rock Mechanics and Mining Sc
9, p. 271-288.

8. Brace, W. F., 1961, Dependence of Fracture
rocks on Grain Size, Penn. State Univer
Mineral Industries Station, Bull., 79,

9. --- 1965, Relation of Elastic Properties of
Fabric, Journal of Geophysical Research
n. 22, p. 5657-5667.

10. --- 1965, Some new Measurements of Linear C
bility of rocks, Journal of Geophysical
v. 70, n. 2, p. 391-398.

11. Brace, W. F. and Bombolakis, E. G., 1963, A Note on Brittle Crack Growth, Journal of Geophysical Research, v. 68, n. 12, p. 3709-3713.

12. Brady, B. T., 1971, Effects of Inserts on the Elastic Behaviour of Cylindrical Materials Loaded between Rough End-plates, International Journal of Rock Mechanics and Mining Science, v. 8, n. 4, p. 357-369.

13. Burshtein, L. S., 1969, Effect of Moisture on the Strength and Deformability of Sandstone, Soviet Mining Science, n. 5, Sept.-Oct., p. 573-576.

14. Chilingarian, G. V., and Wolf, K. H., editors, 1976, Compaction of Coarse-grained Sediments: II Developments in Sedimentology, n. 18B, Amsterdam, Elseiver, 808 p.

15. Coulomb, C. A., 1773, Sur une Application des regles de Maximis et Minimis a quelques problemes de statique relatifs a l'Architecture, Academe Royale des Sciences, Memoires de Math. et de pysique par divers savans, 7, p. 393-382.

16. Dunn, D. E., LaFountain, L. J., and Jackson, R. E., 1973, Porosity Dependence and Maechanism of Brittle Fracture in Sandstone, Journal of Geophysical Research, v. 78, n. 14, p. 2403-2417.

17. Dusseault, M. B., and Morgenstern, N. R., 1979, Locked Sands, Quarterly Journal of Engineering Geology, v. 12, p. 117-131.

18. Ettensohn, F. R., and Dever, G. R., editors, 1979, Carbiniferous Geology from the Appalachian Basin to the Illinois Basin through eastern Ohio and Kentucky, Field Trip No. 4, Ninth International Congress of Carboniferous Stratigraphy and Geology, University of Kentucky, Lexington, 293 p.

19. Ferm, J. C., and Melton, R. A., 1977, A Guide to Cored Rocks in the Pocahontas Basin, Carolina Coal Group, Department of Geology, University of South Carolina, Columbia, 90 p.

20. Folk, R. L., 1974, Petrology of Sedimentary Rocks, Austin, Texas, Hemphill Publishing Company, 170 p.

21. Friedman, M., and Logan, J. M., 1970, Influence of Residual Elastic Strain on the Orientation of Experimental Fractures in Three Quartzose Sandstones, Journal of Geophysical Research, v. 75, n. 2, p. 387-405.

22. Gallagher, J. J., Friedman, M., Handin, J., and Sowers, G. M., 1974, Experimental Studies Relating to Microfracture in Sandstone, Tectonophysics, v. 21, n. 3, p. 203-247.

23. Griffith, A. A., 1920, The Phenomena of Rupture and Flow in Solids, Transactions of the Royal Society, Philadelphia, Pennsylvania, ser. A 221, p. 163-198.

24. Griffith, A. A., 1924, Theory of Rupture, Proceedings of the First International Congress for Applied Mechanics, Delft, p. 55-63.

25. Hast, N., 1943, Measuring Stresses and Deformation in Solid Materials, Centraltrycheriet, Stockholm, Esselte ab.

26. Hoek, E., and Bieniawski, Z. T., 1965, Brittle Fracture Propagation in Rock under Compression, International Journal of Fracture Mechanics, v. 12, n. 3, p. 137-155.

27. Huang, W. T., 1962, Petrology, New York, McGraw-Hill Book Company, 480 p.

28. Hundley-Goff, E. M., and Moody, J. B., 1980, Microscopic Characteristics of Orthoquartzite from Sliding Friction Experiments, pt. I, Sliding Surface, Tectonophysics, v. 62, p. 279-299.

29. Jaeger, J. C., 1966, Brittle Fracture in Rock In: Failure and Breakage of Rock, Fairhurst, C., editor, New York, American Institute of Mining Engineers, p. 3-57.

30. Jaeger, J. C., 1969, Elasticity, Fracture and Flow, London, Methuen and Company Ltd., 180 p.

31. Jaeger, J. C., and Cook, N. G. W., 1969, Fundementals of Rock Mechanics, London, Methuen and Company Ltd., 513 p.

32. Jenkins, J. D., 1958, Discussion on Paper--Stress-Strain Relations and Breakage of Rocks--by Seldineath, Th. R., and Gamberg, J., Journal of the Proceedings of the Conference of Mechanical

Properties of Non-Metallic Brittle Materials, London, p. 102-103.

33. Koide, H., and Hoshino, K., 1979, Effect of Geological Compaction on the Deformation of Sedimentary Rocks, Proceedings of the 4th Congress of International Society of Rock Mechanics, v. 1.

34. Lajtai, E. Z., 1971, A Theoretical and Experimental Evaluation of the Griffith Theory of Brittle Fracture, Tectonophysics, v. 11, p. 129-158.

35. Lundborg, N., 1968, Strength of Rock-like Materials, International Journal of Rock Mechanics and Mining Sciences, v. 5, n. 5, p. 427-454.

36. Martin, R. J., and Durham, W. B., 1975, Mechanism of Crack Growth in Quartz, Journal of Geophysical Research, v. 80, n. 35, p. 4837-4844.

37. Maxwell, J. C., 1960, Experiments on Compaction of Sand, Geological Society of America, mem. 79, p. 105-132.

38. Murrell, S. A. F., 1964, The Theory of the Propagation of Elliptical Griffith Cracks under Various Conditions of Plane Strain or Plane Stress, pt. I, British Journal of Applied Physics, v. 15, p. 1195-1210.

39. Murrell, S. A. F., and Digby, P. J., 1970, The Theory of Brittle Fracture Initiation under Triaxial Stress Conditions, pt. I, Geophysical Journal of the Royal Astronomical Society, v. 19, p. 309-334.

40. McClintock, F. A., and Walsh, J. B., 1962, Friction on Griffith Cracks in Rocks under Pressure, Fourth U.S. Congress of Applied Mechanics, Berkely, 1962, American Society of Mechanical Engineers, New York, 1963, p. 1015-1021.

41. Obert, L., 1972, Brittle Fracture of Rock, In: Fracture, Liebowitz, H., editor, New York, Academic Press, v. 7, p. 93-156.

42. Paterson, M. S., 1963, Secondary Changes of Length with Pressure in Experimentally Deformed Rocks, Proceedings of the Royal Society, London, A 271, p. 57-87.

43. Paterson, M. S., 1978, Experimental Rock Deformation: The Brittle Field, In: Mineral and Rocks, v. 13, Berlin, Springer-Verlag, 254 p.

44. Pettijohn, F. J., 1975, Sedimentary Rocks, third ed., New York, Harper and Row Publishers, Inc., 628 p.

45. Pettijohn, F. J., Potter, P. E., and Siever, R., 1965, Geology of Sand and Sandstone, Indiana Geological Survey and Department of Geology, Indiana University, Bloomington, 205 p.

46. Pforr, H., and Rosetz, G. P., 1966, Ergebnisse und Erfahrungen bei Druckund Zugversuchen an Gesteinen des Kalibergbaus/Beitrag zum Festigkeitskatalog und zur Erfassung des Naturlichen Gesteinsverhaltens/., Freiberger Forschungsheft A376, VEB Deutscher Verlag fur Grundstoffindustrie, Leipzig, 1-123 p.

47. Pforr, H., 1973, Recommendations of International Bureau of Rock Mechanics for Determination of Geomechanical Parameters of Rocks and Rock Mass, VEB Deutcher Verlag fur Grundstoffindustrie, Lepzig, 115 p.

48. Rice, C. L., Sable, E. G., Dever, G. R., and Kehn, T. M., 1980, The Mississippian and Pennsylvanian (Carboniferous) Systems in Kentucky, ser. XI, Kentucky Geological Survey, University of Kentucky.

49. Scholz, C. H., 1968, Microfracturing and the Inelastic Deformation of Rock in Compression, Journal of Geophysical Research, v. 73, n. 4, p. 1417-1432.

50. --- 1968, Experimental Study of the Fracturing Process in Brittle Rock, Journal of Geophysical Research, v. 73, n. 4, p. 1447-1454.

51. Siever, R., 1959, Petrology and Geochemistry of Silica Cementation in Some Pennsylvanian Sandstones, In: Silica in Sediments, Special Publication, Society of Economic Palaeontologists and Mineralogists, Tulsa, n. 7, p. 56-79.

52. Simmons, Gene, and Brace, W. F., 1965, Comparison of Static and Dynamic Measurements of Compressibility of Rocks, Journal of Geophysical Research, v. 70, n. 22, p. 5649-5656.

53. Sneddon, I. N., and Lowengrub, M., 1969, Crack Problems in the Classical Theory of Elasticity, New York, John Wiley and Sons inc.

54. Timoshenko, S., 1934, Theory of Elasticity, New York, McGraw-Hill Book Company, Inc., 338 p.

55. Trashm P. D., 1959, Effect of Grain Size on Strength of Mixtures of Clay, Sand and Water, Bull. Geological Society of America, v. 70, p. 569-580.

56. Vutukuri, V. S., Lama, R. D., and Saluja, S. S., 1974, Handbook on Mechanical Properties of Rock, v. I, Clausthal, Germany, Trans Tech Publications, 280 p.

57. Walsh, J. B., 1965, The Effects of Cracks in Rocks on Poisson's Ratio, Journal of Geophysical Research, v. 70, n. 20, p. 5249-5257.

58. --- 1965, The Effect of Cracks on the Compressibility of Rock, Journal of Geophysical Research, v. 70, n. 2, p. 381-389.

59. --- 1965, The Effect of Cracks on the Uniaxial Compre-sion of Rocks, Journal of Geophysical Research, v. 70, n. 2, p. 399-411.

60. Walsh, J. B., and Brace, W. F., 1973, Mechanics of Rock Deformation, Rock Mechanics Symposium, American Society of Mechanical Engineers, Detroit, p. 1-24.

61. Weinheimer, R. L., 1980, Petrographic Report on KGS Cores JC8012 and Aguire, Unpublished Report, University of Cincinnati.

VOLUME VI:

VERTICAL SEQUENCE AND DIAGENESIS IN BREATHITT SANDSTONES OF EASTERN KENTUCKY

by

Roger L. Weinheimer
University of Cincinnati
Cincinnati, Ohio

June 1983

Volume III of Acquisition, Storage, and Classification of Engineering and Geological Data for Surface-Mine Design and Reclamation under Grant Number ~~G5195018~~ or G1195018, September 1979.
G 1105068

Prepared for the University of Kentucky Institute for Mining and Minerals Research Title III Program

ABSTRACT

Vertical variation of grain size, bedding thickness, bioturbation, sedimentary structures, lithology, and contact type are used to identify specific sandstone facies in three 1000 foot cores through the Breathitt Formation (Pennsylvanian) of eastern Kentucky. Facies identified include fluvial distributary, minor mouth bar/crevasse channel couplet, crevasse splay, bay-fill, and levee.

Standard and luminescent petrography is used to classify sandstones and characterize diagenetic relationships. Very fine to medium grained and very well to moderately sorted lithic subarkoses and lithic arkoses predominate and have been highly compacted and cemented by pore-filling kaolinite.

Comparison of facies with diagenetic relationships shows that all sands were uniformly subjected to the porosity reducing changes of compaction at depths greater than 5000 feet. In rare cases early ferroan calcite cementation occurred at shallow depths significantly reducing porosity and compaction. Later authigenic kaolinite cement occurred at great depth. Some of the coarsest sandstones, in channel facies, exhibited secondary porosity from the dissolution of detrital grains and interstitial cements.

TABLE OF CONTENTS

LIST OF FIGURES

LIST OF TABLES

LIST OF PLATES

LIST OF APPENDICES

INTRODUCTION

PURPOSE

Mining and reclamation in the Breathitt Formation of eastern Kentucky is complicated by the variability of its lithology. Ideally, one would like to be able to predict engineering properties from the geologic properties of a particular lithology. If we assume that diagenesis is an important factor in the prediction of engineering properties, then an understanding of the relationship between facies and diagenesis is valuable because facies are observable in the field. Hence, one could approximate the diagenetic properties. The primary purpose of this study is to explain the relationship between sandstone facies and their diagenetic properties in rocks taken from three cores through the Breathitt Formation.

The second objective of this study is to better document the vertical sequence of lithologies and the petrographic character of fluvio-deltaic sediments as represented by the Breathitt Formation.

LOCATION

Figure 1 shows the locations of the cores in Breathitt and Leslie counties of southeastern Kentucky. The U.S. Geologic Survey geologic quadrangle names and Carter coordinates for each core are as follows: C5, Noble Quad (GQ-1476), 5-L-76; C4, Guage Quad (GQ-1416), 17-M-77; and 1A, Cutshin Quad (GQ-1424), 19-G-74.

STRATIGRAPHY

The Breathitt Formation--middle Pennsylvanian--occurs in eastern

Figure 1 -- Location of cores used in this study (Southeastern Kentucky).

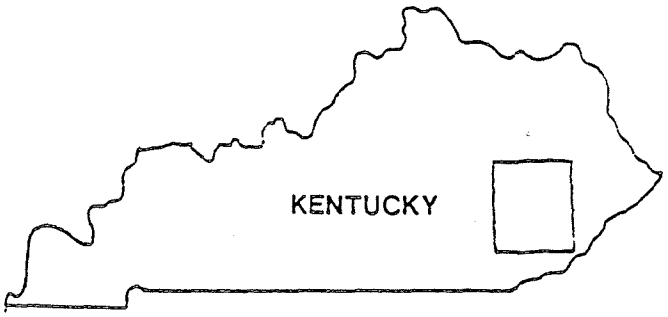

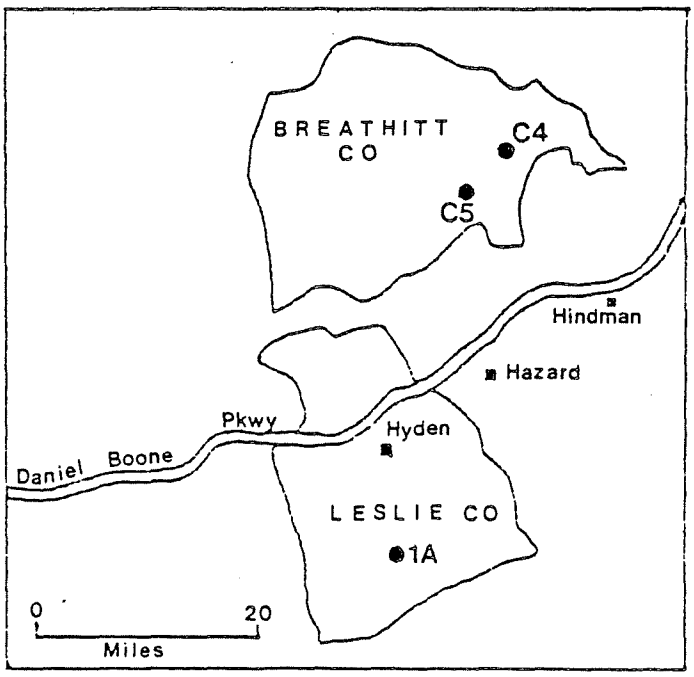

FIGURE 1

LOCATION OF STUDY

Kentucky in the Appalachian Plateau. Regionally, it dips very gently toward the east-southeast but appears horizontal in the road and stream cuts of the deeply incised Appalachian Plateau. These sediments represent the miogeosynclinal deposits associated with the Appalachian Geosyncline. They have not been disturbed by the compressive forces associated with the Appalachian orogeny, except in extreme southeastern Kentucky near the Pine Mountain Thrust Fault.

The Pennsylvanian rocks in eastern Kentucky consist principally of sandstone, siltstone, and shale and contain small amounts of limestone, ironstone, and coal (Huddle et al, 1963). Rocks of the Breathitt Formation are composed of nonmarine deltaic sediments deposited on the foreland of the Appalachian Basin. They were deposited subsequent to the Lee Formation of early Pennsylvanian age and are primarily Atokan and Des Moinesian equivalents or middle Pennsylvanian age (Cook and Bally et al, 1975). Table 1 shows the relationship of the formation to the other Pennsylvanian units in eastern Kentucky (Gardner, 1977).

The cores in this study were taken from the Breathitt Formation as determined by extensive geologic mapping done on 7½' quadrangles (Ping, 1977; Hinrichs, 1978; Lee et al, 1977). Cores C4 and C5 penetrate Breathitt Formation rocks from the Skyline Coal down to approximately the Whitesburg or Amburgy coals and represent the middle upper to lower middle Breathitt Formation. Core 1A penetrates the Breathitt Formation from the Whitesburg coal zone down to approximately the base of the formation and represents the lower middle to lower Breathitt Formation (Fig. 2).

Table 1--Pennsylvanian units of eastern Kentucky.

PENNSYLVANIAN STRATIGRAPHIC UNITS IN EASTERN KENTUCKY	
PENNSYLVANIAN	CONEMAUGH
	BREATHITT
	LEE

TABLE 1 - PENNSYLVANIAN UNITS OF EASTERN KENTUCKY

Figure 2 -- Schematic structural cross-section showing structural and stratigraphic relationships among the cores.

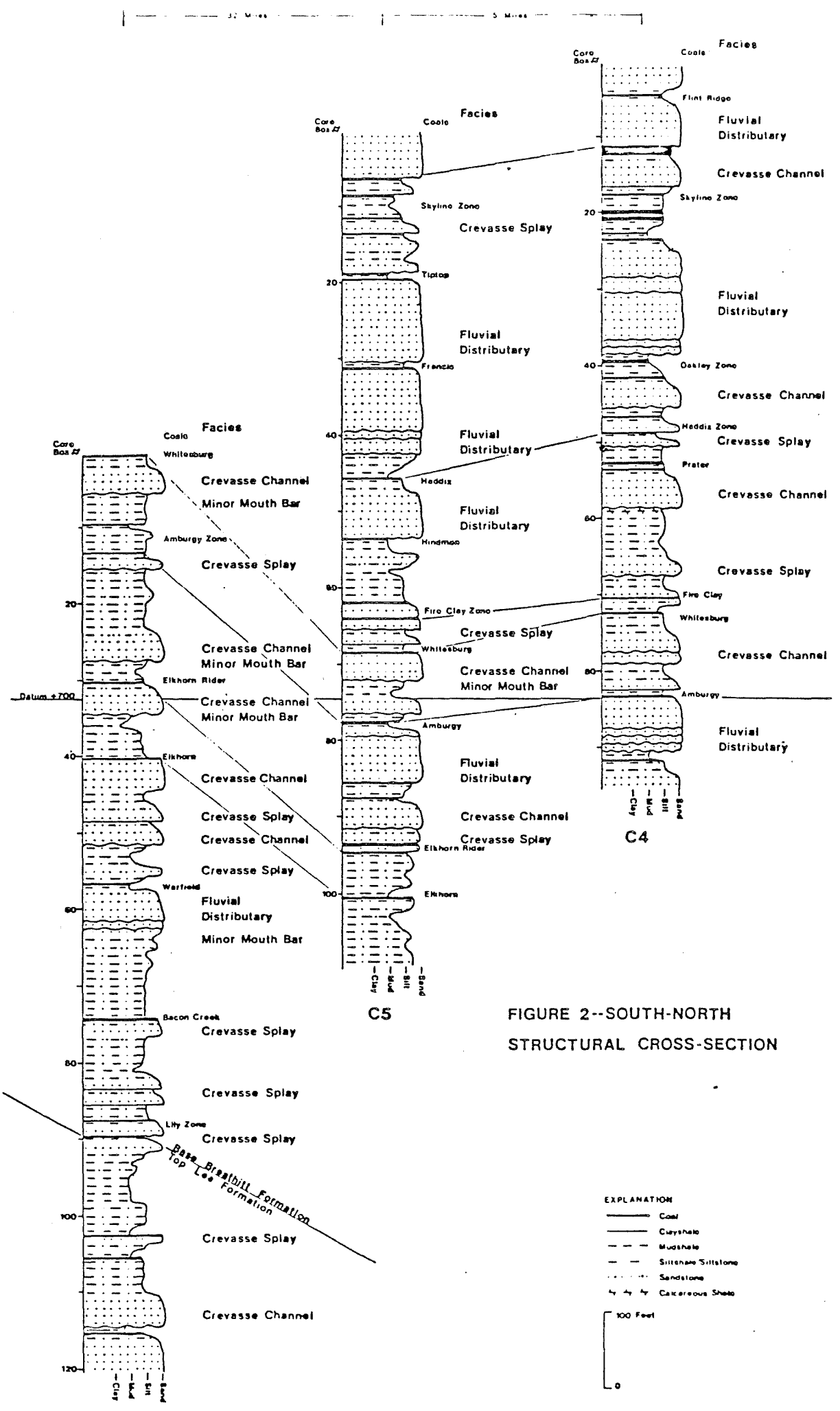

FIGURE 2--SOUTH-NORTH STRUCTURAL CROSS-SECTION

PREVIOUS WORK

Delta Facies

Much has been written on deltaic sedimentation and delta facies. Major studies of deltaic sediments are summarized in depth by Le Blanc (1975) and in a brief and concise style by Miall (1979). The Carboniferous Delta of eastern Kentucky has been studied extensively by John C. Ferm, John C. Horne, and many of their students. Their work, most recently documented in Horne and Ferm et al (1978), provides a basis for comparison of vertical sequences in this study to documented idealized sequences.

Diagenesis

Gardner (1977) is the only worker who has studied diagenesis of the Breathitt Formation in detail. He studied the Breathitt Formation in Floyd County, Kentucky to the east and northeast of my study area. Others have concentrated on petrographic classification, provenance, and petrographic properties statistically significant to environmental classification in Breathitt rocks (Ferm, 1962; Davis and Erlich, 1974; and Flores, 1978).

CONCLUSIONS

1. Three sandstone facies dominate. They are fluvial-distributary, crevasse channel, and crevasse splay.

2. Core 1A represents a lower delta plain environment dominated by crevasse channel and crevasse splay facies.

3. Cores C4 and C5 represent an upper delta plain environment dominated by fluvial distributary channel facies.

4. The diagenetic history of the rocks studied is dominantly one of porosity reduction and destruction.

5. Porosity was reduced by compaction at depths of over 5000 feet.

6. In rare cases early ferroan calcite cement prevented compaction.

7. Authigenic kaolinite cement occurred late at great depth effectively plugging pore spaces.

8. Porosity reduction by compaction and cementation is not controlled by facies whereas porosity production or secondary porosity appears to be facies related.

METHODS

CORE DESCRIPTION

This research is based largely on core description and thin section analysis. Three cores were described, each approximately 1000 feet long, from the middle-upper through the lower Breathitt Formation. Estimates of their stratigraphic range were determined by the geological mapping mentioned previously and by thickness measurements from the literature (Wanless, 1939; Huddle et al, 1963). Six parameters, based on one foot sample intervals, defined the vertical sequences observed in the core: lithology, grain size, bed thickness, bioturbation, sedimentary structures, and bed contacts. Table 2 shows the parameters with their numerical keys used in abbreviation. Use of these parameters provided a systematic approach to objective observation of the cores.

THIN SECTION ANALYSIS

Over 250 sandstone samples were taken from the three cores for analysis. These samples were subdivided into groups based on lithology and sedimentary structures. Representative samples from each group were chosen for thin section preparations. These totaled 20 per core or 60 in all.

The first set of slides made were from core C5. These were stained with Alizarin Red-S for carbonate mineral identification and were analyzed for grain size, based on 100 points per slide. Mineralogy was based on 200 points per slide. Textural and diagenetic properties other than packing were qualitatively described. Packing was quantita-

Table 2--Core description parameters.

Table 2--Core Description Parameters

Sedimentary Structures

I Laminations
- A. Parallel
- B. Lenticular
- C. Wavy

II Cross Laminations
- A. Simple
- B. Planar
- C. Trough

III Ripple Laminations
- A. Current
- B. Ripple-Drift
- C. Wave

IV Distorted Laminations
- A. Gas-heave
- B. Slump
- C. Recumbent Folds
- D. Convolute

V Scour and Fill

VI Erosional Truncation

Lithology

Clay

Mud

Silt

Sand

Grain Size

1.	62-88u	very fine
2.	88-125u	
3.	125-177u	fine
4.	177-250u	
5.	250-350u	medium
6.	350-500u	
7.	500-710u	coarse
8.	710-1000u	

Bedding Thickness

1.	Very thick	1m
2.	Thick	30-100cm
3.	Medium	10-30cm
4.	Thin	3-10cm
5.	Very Thin	1-3cm
6.	Thick laminations	0.3-1cm
7.	Thin laminations	0.3cm

Bioturbation

0.	No bioturbation	0%
1.	Sporadic Traces	1-5%
2.	Weakly Bioturbated	5-30%
3.	Moderately Bioturbated	30-60%
4.	Strongly Bioturbated	60-90%
5.	Very Strongly Bioturbated	90-99%
6.	Completely Bioturbated	100%

tively described for 18 samples from each of the facies represented in the study.

All 60 slides from the three cores were used to select a representative set of 18 samples for cathodoluminescent analysis. This set includes at least three samples from each of the facies interpreted in the cores. Photomicrographs of these samples were taken under cathodoluminescence. Textural and diagenetic properties were qualitatively interpreted from the cathodoluminescent properties of the samples. In addition scanning electron microscopy was used to identify clay mineralogy and authigenic minerals.

PRESENTATION OF DATA

VERTICAL SEQUENCES

Vertical sequences are those sequences within a core that are bounded above and below by coals. They may be anywhere from less than one foot to over 170 feet thick. In general, these sequences occur in one of six grain size patterns. They are: (1) coarsening upward, (2) coarsening upward followed by fining upward, (3) repeated coarsening upward, (4) fining upward, (5) repeated fining upward, and (6) repeated coarsening up/fining up. The following are descriptive definitions of the types of vertical sequences the author observed in cores from this study. This section does not include a genetic interpretation of the sequences. Genetic interpretation is examined later in "Discussion of Results."

Figure 3 is an explanation of the symbols used to describe sedimentary structures, special lithologies, grain size, and bioturbation types in the vertical sequences examined in this study. Depths are posted at the top and bottom of each sequence illustrated, and these can be converted to core-box number by dividing them by ten--because there are 10 feet of core per box. This will facilitate correlating the vertical sequence descriptions (Figs. 4-9, 13, 14, 16-20) with the whole core summary (Fig. 2).

(1) Coarsening Up

Coarsening upward sequences are characteristically thin, averaging only 21 feet thick (Fig. 4). They grade from a parallel laminated clayshale or mudshale through a parallel and lenticular laminated

Figure 3--Explanation of symbols used in vertical sequence diagrams.

CORE DESCRIPTION EXPLANATION

SEDIMENTARY STRUCTURES:

Laminations

- Parallel
- Wavy
- Lenticular

Cross-Laminations

- Simple
- Planar
- Trough

Ripple Laminations

- Current
- Ripple-Drift
- Wave

Other

- Distorted Laminations
- Massive Bedding

LITHOLOGY:

- Coal
- Coal Clasts
- Conglomerate

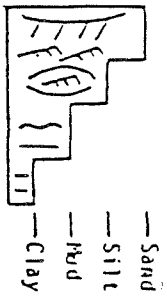

BIOTURBATION:

- Animal Burrow
- Rooting

Figure 4 -- Example of coarsening upward sequence from this study.

(1) COARSENING UPWARD SEQUENCE

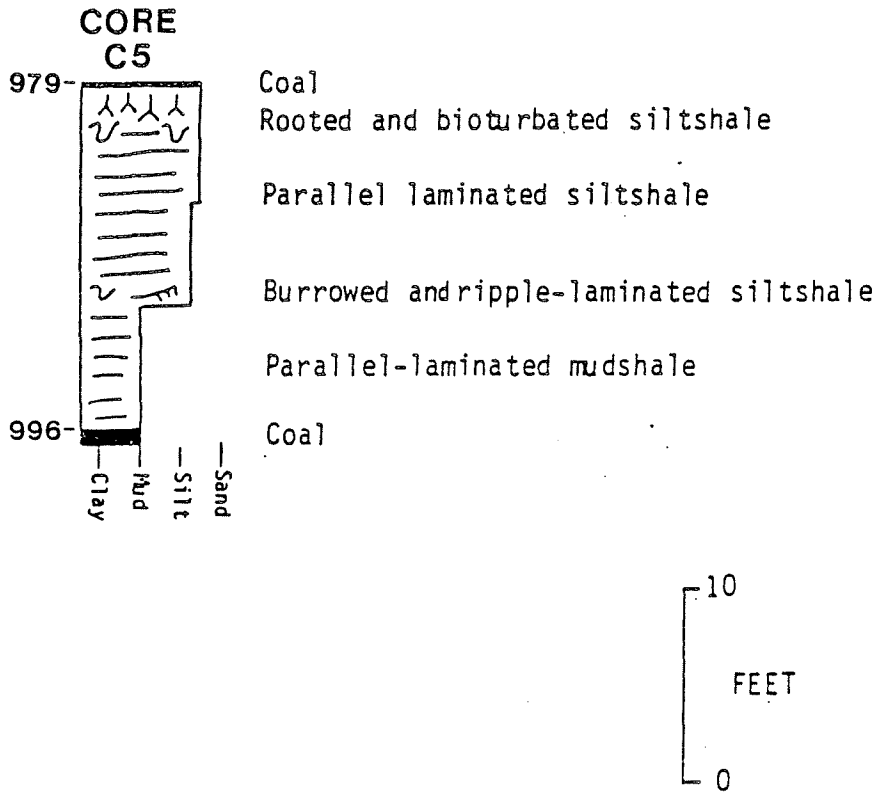

mudstone or siltstone to a wavy and ripple laminated siltstone and/or silty sandstone. Bioturbation is common in these sequences and is usually present to some degree--ranging from a trace to complete. The top of the sequence is rooted in all cases. Thin sandstone laminae in the coarsening upward sequence have gradational to sharp basal contacts.

(2) Coarsening Up/Fining Up

Coarsening upward/fining upward sequences have a basal section, characterized by the coarsening upward sequence previously described, which is directly overlain by a fining upward sequence. The overall sequence ranges from four feet to seventy-six feet thick and averages 17 feet in thickness (Fig. 5). The proportionate thickness of the two components varies from approximately 5:95 to 50:50 for the coarsening: fining ratio. The fining upward component of the sequence has a massive, crossbedded, or conglomeratic sandstone with a sharp to erosive basal contact. This grades upward with numerous erosional truncations through a medium to thick bedded sandstone with planar and trough crossbedding to a thin to very thin bedded sandstone with planar and ripple bedding. Bioturbation increases upward from no bioturbation in the basal and crossbedded sandstone to moderate bioturbation in the upper more thinly bedded sandstone and finally to complete bioturbation by rooting at the top of the sequence. Bedding thickness in this sequence ranges from thinly laminated, at the base of the coarsening upward component and the top of the fining upward component, to thickly bedded at the base of the fining upward component.

Figure 5 -- Example of coarsening upward/fining upward sequence from this study.

(2) COARSENING UPWARD/FINING UPWARD

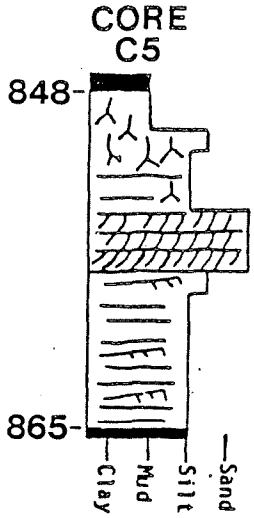

Coal

Rooted silt and mud

Parallel - laminated siltstone

Planar and trough crossbedded sandstone

Parallel and ripple-laminated siltshale and siltstone

Coal

10

FEET

0

(3) Repeated Coarsening Up

Few repeated coarsening upward sequences occurred in the cores examined. They average 16.7 feet thick (Fig. 6). Parallel and thinly laminated mudstones are at the base, and these grade into parallel, lenticular, and ripple laminated siltstone at the top. This pattern may be repeated or stacked 2 or 3 times in a particular sequence. Bioturbation is common throughout and is especially abundant at the tops of individual coarsening upward units within repeated coarsening upward sequences.

(4) Fining Up

Fining upwards sequences are abundant in these cores and average 51.1 feet thick (Fig. 7). They range in thickness between 3 and 147 feet. The base is characteristically a sharp to erosional contact with the underlying rocks which is overlain by massive, conglomeratic, or crossbedded fine to medium (125-350u) grained sandstone. Conglomerates are composed of subangular to subrounded cobbles and pebbles of siderite, mudrocks, and coal in a matrix of fine to medium sand. Erosional truncation is common in the basal portion of these sequences and is often marked by a conglomerate and/or clay drape. Massive and crossbedded sands, near the base, range from medium to thick bedded (30-100cm). Erosional truncation and massive bedding become less abundant upward in the middle of the sequence. The middle part of the sequence is mostly medium crossbedded, very fine to fine grained sandstones with minor amounts of ripple and planar bedded sandstones. Bedding thickness and grain size decrease upward toward the top of the sequence where

Figure 6 -- Example of repeated coarsening upward sequence from this study.

(3) REPEATED COARSENING UPWARD SEQUENCE

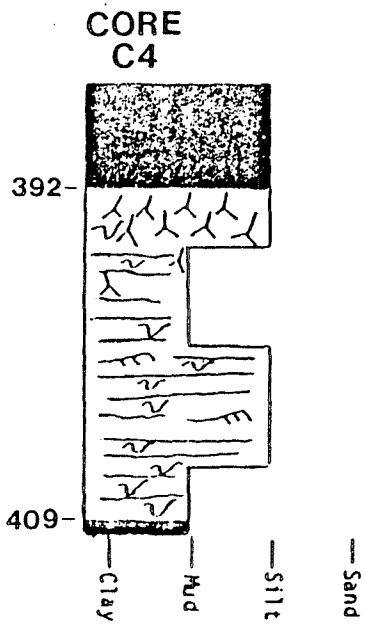

Coal

Rooted siltstone

Burrowed and rooted, parallel-laminated mudshale

Burrowed, parallel and ripple-laminated siltstone

Burrowed and parallel-laminated mudshale

Coal

10

FEET

0

Figure 7 -- Example of fining upward sequence from this study.

(4) FINING UPWARD SEQUENCE

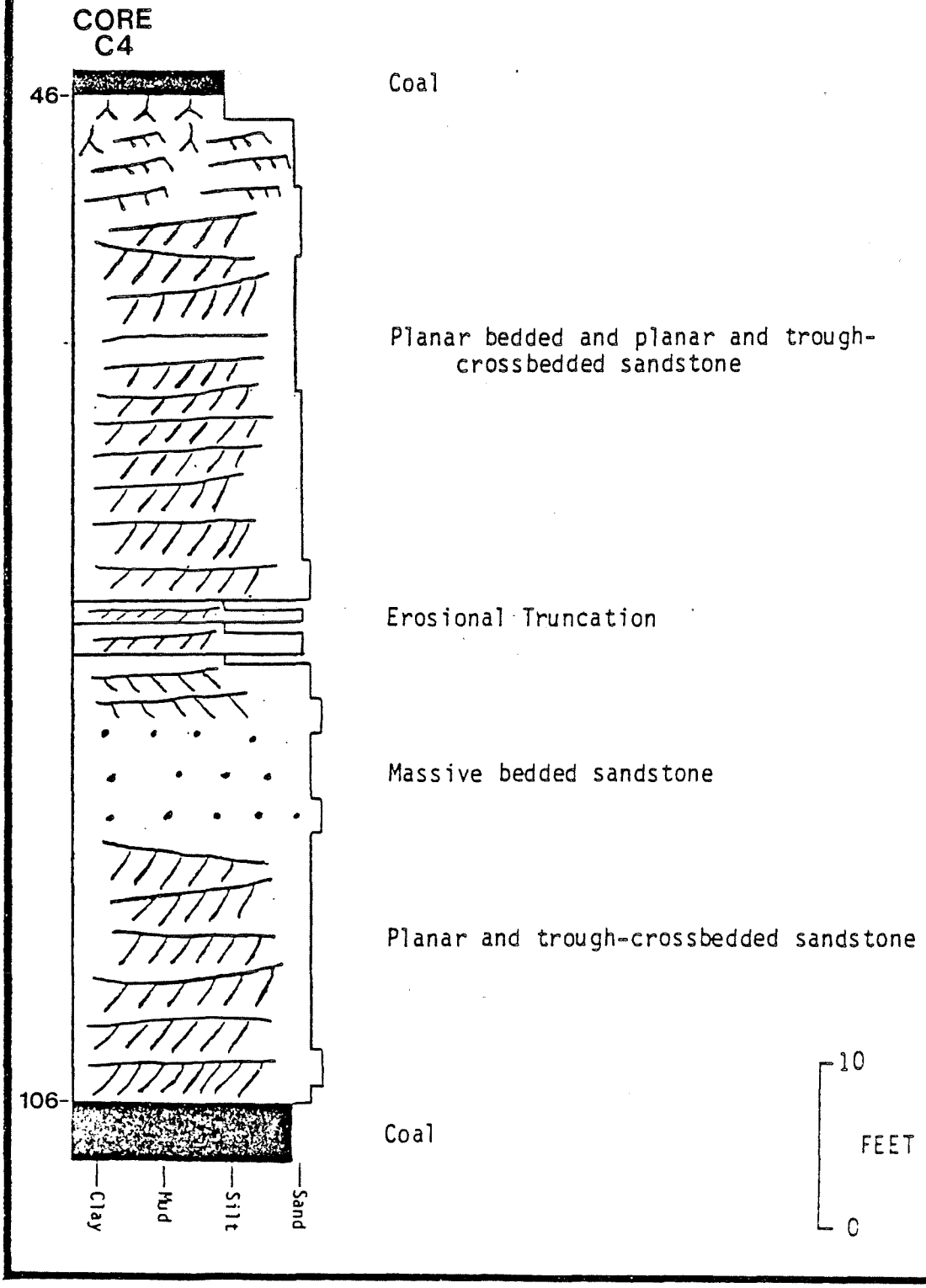

very fine (62-125u) grained, thin to very thin ripple, wavy, and small scale cross bedding dominates. Bioturbation is absent except in the very top part of the sequence and is usually in the form of plant rooting.

(5) Repeated Fining Up

Repeated fining upward sequences are fairly abundant, with an average thickness of 51.1 feet and a range of 10 to 98 feet thick (Fig. 8). These are comprised of several fining upward subsequences. These subsequences range from 2 to 30 feet thick. Moderate to complete bioturbation is common in the upper part of the individual subsequences.

(6) Repeated Coarsening Up/Fining Up

Repeated coarsening upward/fining upward sequences are abundant and average 103.5 feet thick with a thickness range of 29 to 175 feet (Fig. 9). They consist of two or more coarsening up/fining up subsequences similar to the coarsening upward/fining upward sequences previously described. These stacked subsequences usually have a thickly developed mudrock component--separating the subsequences--that in many cases is not heavily bioturbated. This mudrock component is commonly thin, parallel laminated siltshales, mudshales, and clayshales with siderite bands, and it reaches thicknesses of 30 feet or more.

The types of sequences described above comprise almost all of the types observed. There is a small percentage that doesn't fit neatly into any category described. These are either unusual combinations of the patterns described above or non-patterned. They represent less than 10% of all the core described.

Figure 8 -- Example of repeated fining upward sequence from this study.

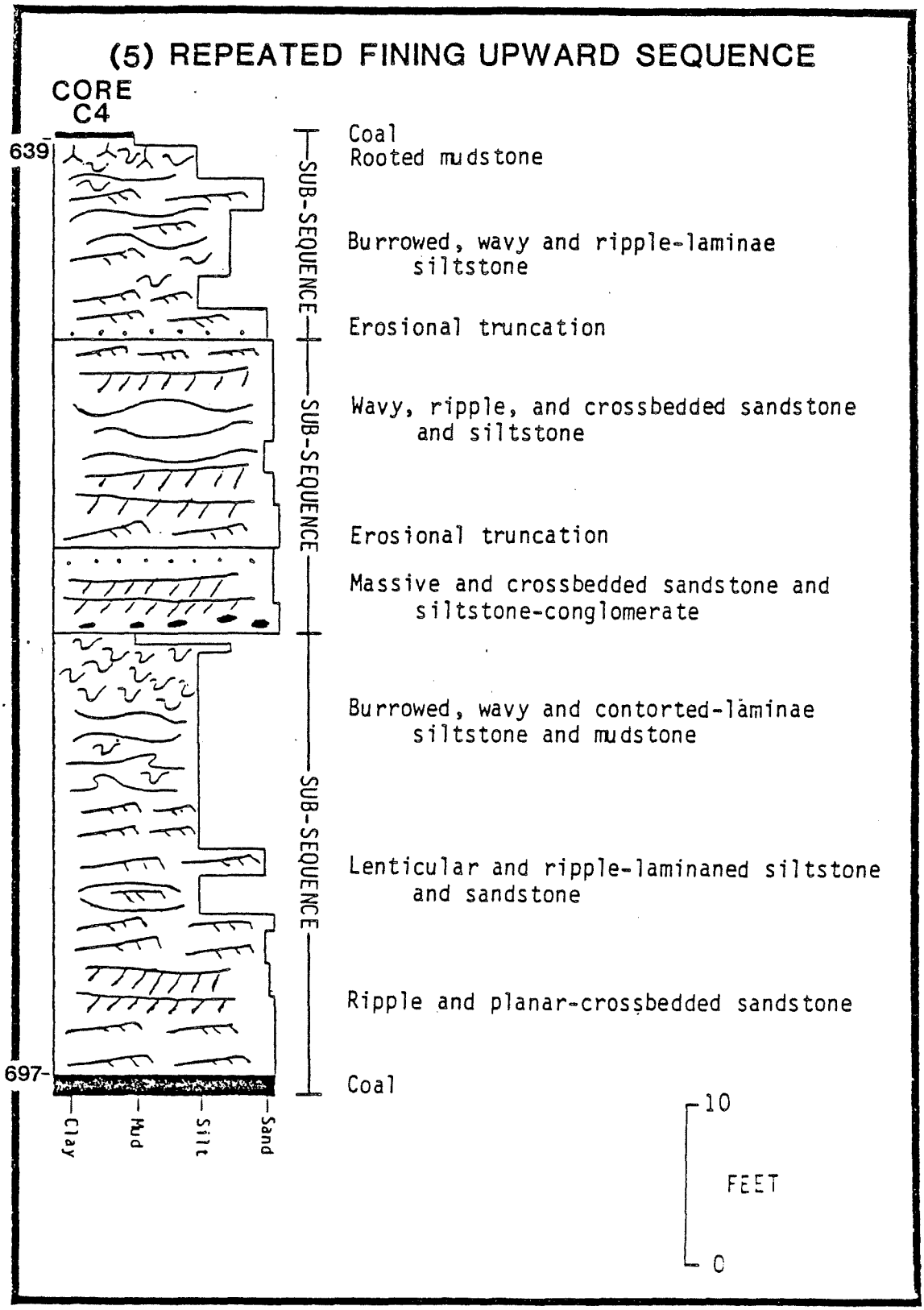
(5) REPEATED FINING UPWARD SEQUENCE
CORE
C4
639
697
SUB-SEQUENCE
SUB-SEQUENCE
SUB-SEQUENCE
Coal
Rooted mudstone
Burrowed, wavy and ripple-laminae siltstone
Erosional truncation
Wavy, ripple, and crossbedded sandstone and siltstone
Erosional truncation
Massive and crossbedded sandstone and siltstone-conglomerate
Burrowed, wavy and contorted-laminae siltstone and mudstone
Lenticular and ripple-laminaned siltstone and sandstone
Ripple and planar-crossbedded sandstone
Coal
Clay
Mud
Silt
Sand
10
FEET
0

Figure 9 -- Example of repeated coarsening upward/fining upward sequence from this study.

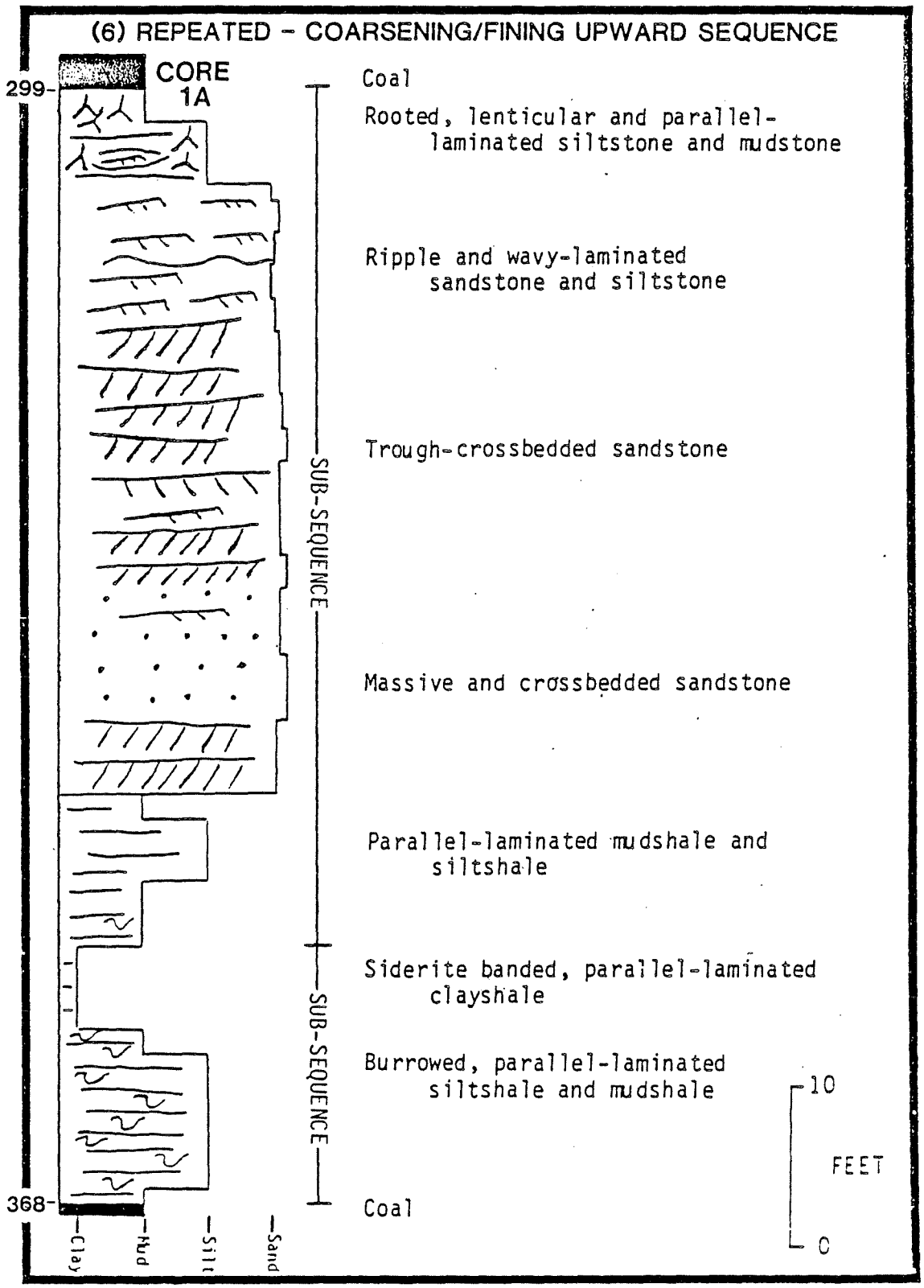
(6) REPEATED - COARSENING/FINING UPWARD SEQUENCE
CORE 1A
299-
368-
Coal
Rooted, lenticular and parallel-laminated siltstone and mudstone
Ripple and wavy-laminated sandstone and siltstone
Trough-crossbedded sandstone
Massive and crossbedded sandstone
Parallel-laminated mudshale and siltshale
Siderite banded, parallel-laminated clayshale
Burrowed, parallel-laminated siltshale and mudshale
Coal
SUB-SEQUENCE
SUB-SEQUENCE
10
FEET
0
Clay
Mud
Silt
Sand

PLAIN LIGHT PETROGRAPHY

Mineralogy

The eight constituents counted in each slide include quartz, feldspar, rock fragments, mica, orthochems, allochems, opaques, and heavy minerals. A description of each constituent follows. Table 3 is a summary of the constituent composition of the samples examined for mineralogy.

Quartz is the most abundant constituent. It ranges from 29.5 to 75.5 percent of the rock by volume and averages 47 percent. It is distributed uniformly throughout with only rare elongate grains having a preferred orientation subparallel to bedding. Quartz grains occur in sizes from silt to medium sand (40-400u). Shapes range between angular and subrounded. Overgrowths are rarely observed and, where they may be inferred, no diagnostic evidence exists to identify them. Bubbles and submicroscopic minerals form inclusions on some of the grains. The only alteration observed in quartz grains was replacement by ferroan calcite cement when the latter was abundant (Plates I and II).

Feldspar comprises between 6.5 and 25.0 percent of the rock by volume with an average of 17.3 percent. K-feldspar is the most abundant type with minor amounts of perthite and plagioclase also occurring. Feldspar distribution is uniform with no preferred orientation. Most grains were subangular to subrounded and were in the same size range as the detrital quartz. No overgrowths were observed, but sericitization was common to varying degrees. Alteration of feldspar includes replacement by ferroan calcite and/or kaolinite (Plate III). In general,

Table 3--Summary of mineralogic composition.

Table 3--Summary of Mineralogic Composition

Mineralogy	%							
Sample #	Qtz	F	RF	Mica	Ortho	Allo	Op	Heavy
C5-12	33.5	15.5	10.5	14.5	19.0	0.5	6.5	0
C5-6	36.5	14.0	10.0	6.0	22.0	1.0	7.5	3.0
C5-28	29.5	13.5	8.0	7.5	35.0	0	4.5	2.0
C5-16	33.0	20.5	16.0	7.5	17.5	0	5.0	0.5
C5-51	44.0	20.5	13.0	4.0	17.0	0	0.5	1.0
C5-64	38.5	22.5	16.5	5.0	15.5	0	1.5	0.5
C5-4	28.0	18.5	16.5	5.0	7.0	0.5	24.0	0.5
C5-62	36.5	24.0	11.5	9.0	17.5	0	0.5	1.0
C5-22	41.5	14.0	20.5	10.5	10.0	0	2.0	1.5
C5-71	51.0	25.0	12.0	0.5	6.5	0	5.0	0.
C5-11	46.5	22.0	9.5	5.5	14.0	0	2.0	0.5
C5-72	47.5	18.5	10.0	3.5	20.0	0	0.5	0
C5-39	62.5	13.0	18.0	4.5	1.5	0	0	0.5
C5-38	44.0	24.5	15.0	6.5	10.0	0	0	0
C5-15	36.5	18.5	14.0	11.0	17.5	0	2	0.5
C5-69	72.0	15.5	7.5	0	4.0	0	1	0
C5-55	67.0	16.0	9.5	2.0	5.5	0	0	0
C5-19	37.0	21.0	19.5	3.0	8.0	0	10.5	1.0
C5-14	75.5	12.5	6.0	2.0	4.0	0	0	0
C5-70	69.5	18.0	6.5	1.0	1.5	0	3.5	0
C4-42	35.5	10.5	1.0	4.0	46.5	0	2.0	0
1A-13	43.0	12.5	10.5	9.5	19.0	0	2.0	0
C4-3	72.5	6.5	12.5	1.5	7.0	0	0	0
Range	29.5-75.5	6.5-25.0	1.0-20.5	0-14.5	1.5-46.5	0-1.0	0-24.0	0-3.0
Avg.	47.0	17.3	11.9	5.4	(23.0)12.7	0.1	3.5	0.5

Plate I -- (A) Plain light view (30X) of a 350-500u, very well sorted, subarkose. (B) Same field of view under crossed nicols showing replacement of quartz and feldspar by ferroan calcite (center), which has since been partially dissolved, and abundant long and suture grain contacts. Sample #C5-70.

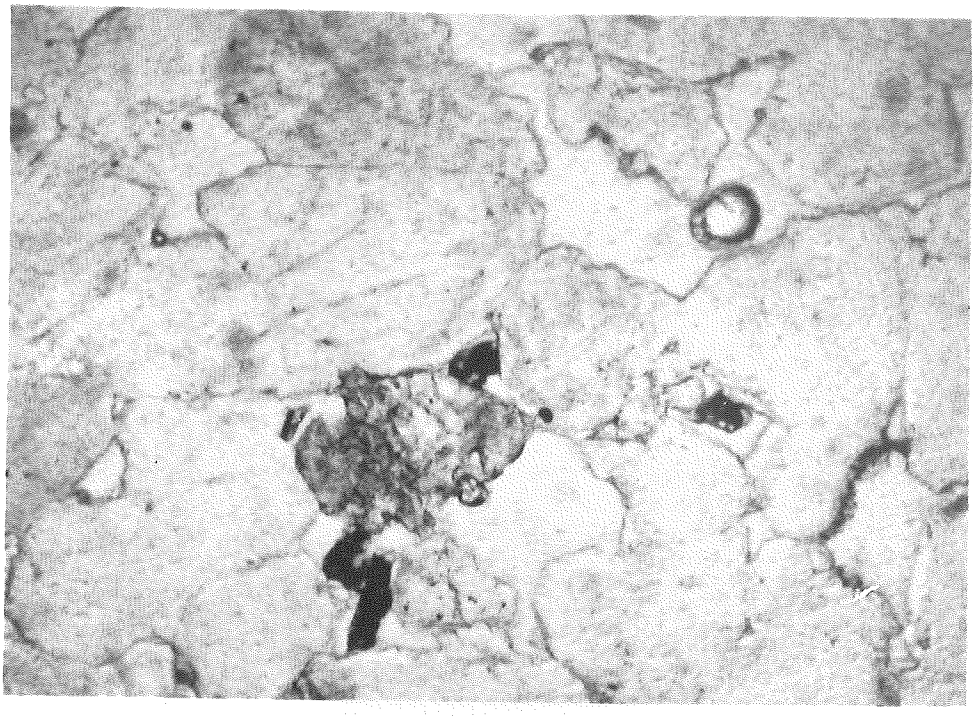

IA

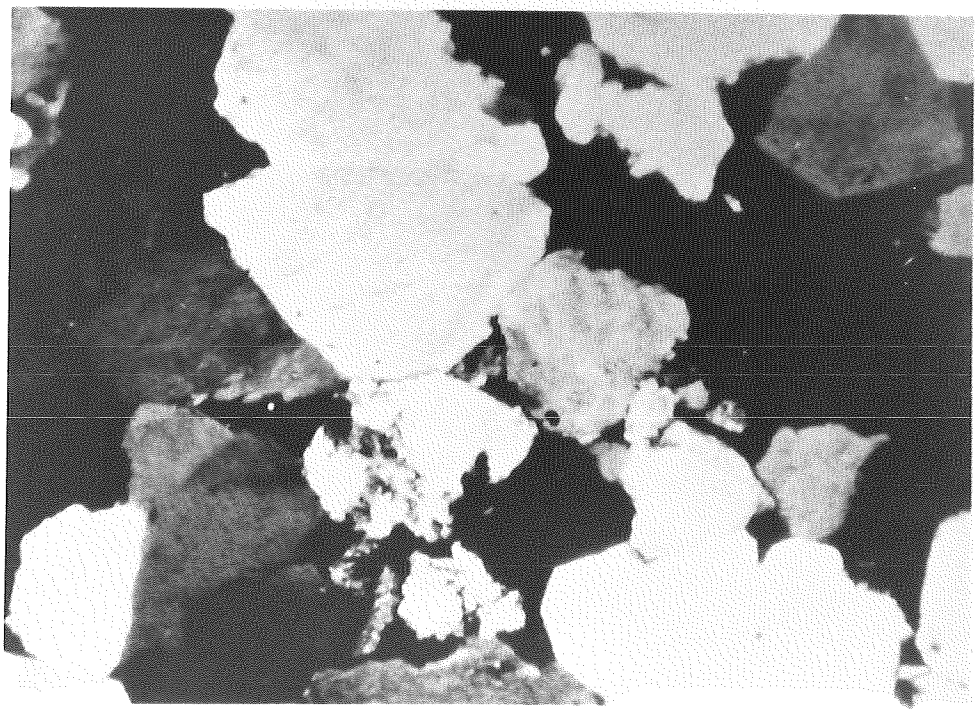

IB

Plate II--(A) Plain light view (30X) of a 350-500u, very well sorted, subarkose showing a detrital dolomite grain surrounded by ferroan calcite cement that also replaces some of the quartz and feldspar along grain boundaries. (B) Same sample but different field of view under cathodoluminescence showing authigenic character of kaolinite (royal blue) pore-filling suggested by pure, monomineralic composition, hydraulic inequivalence to framework grains, and undeformed occurrence. Sample #C5-14.

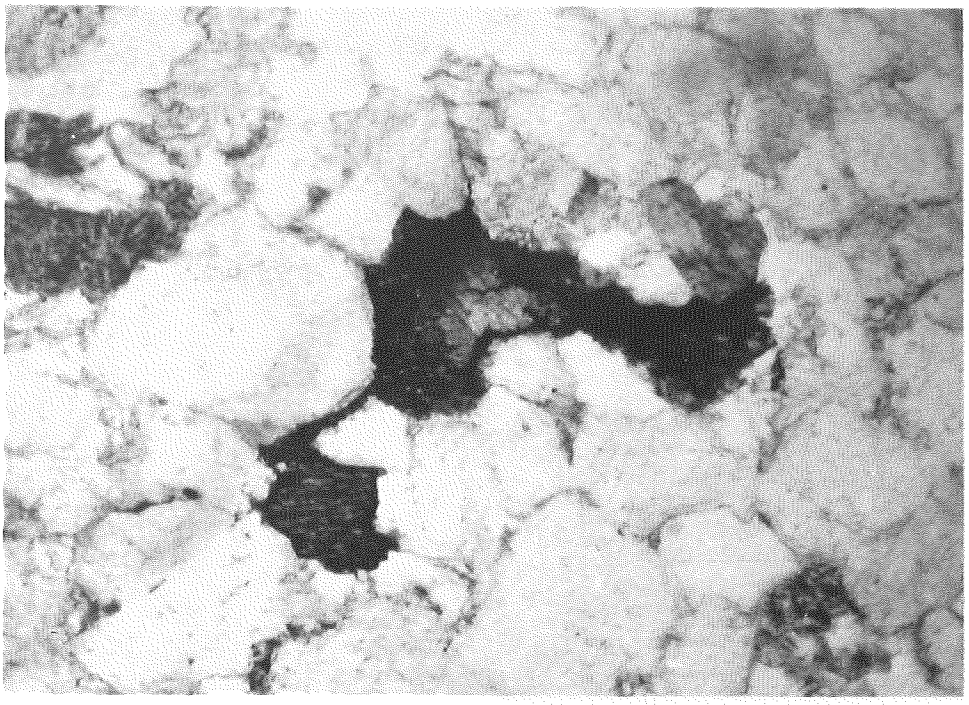

II A

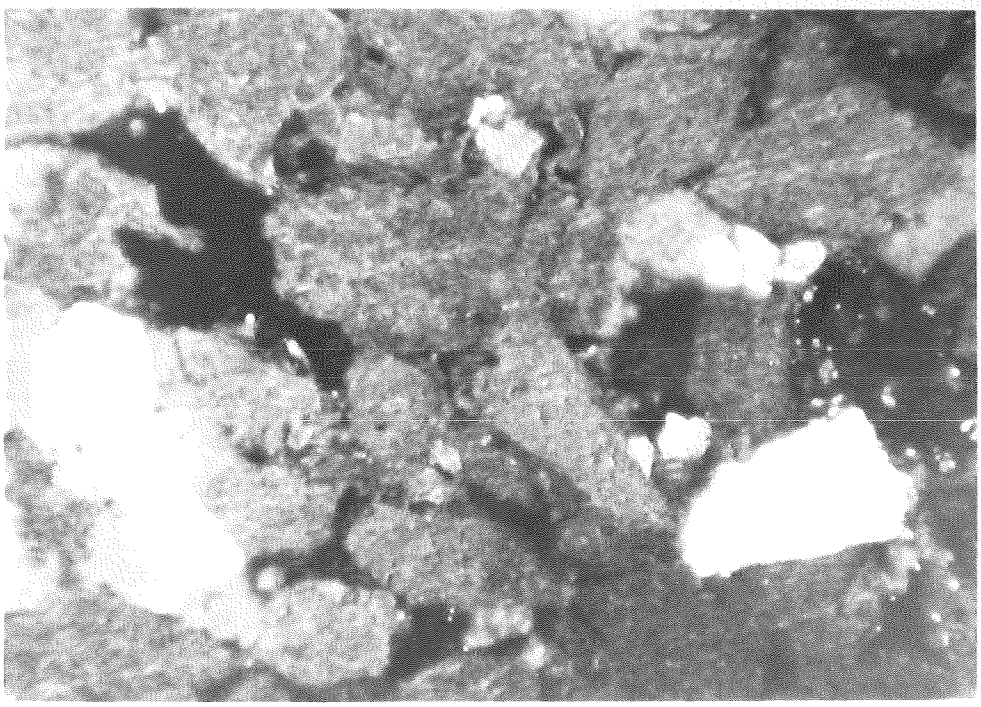

II B

Plate III--(A) Plain light view (125X) of a 177-250u, well sorted, arkose showing large detrital dolomite grain, surrounded by ferroan calcite cement, and replacement of feldspar grain by ferroan calcite along the grain cement boundary. (B) Same field of view under crossed nicols showing abundant long and suture grain contacts and vermiform, authigenic kaolinite partially dissolved from the pore space. Sample #C5-11.

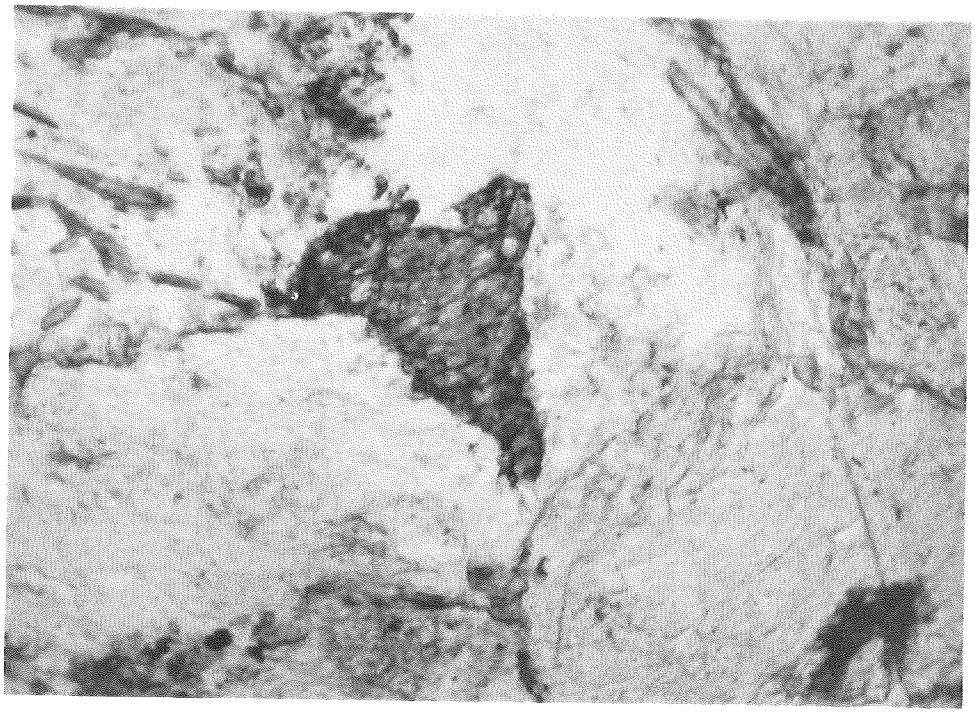

III A

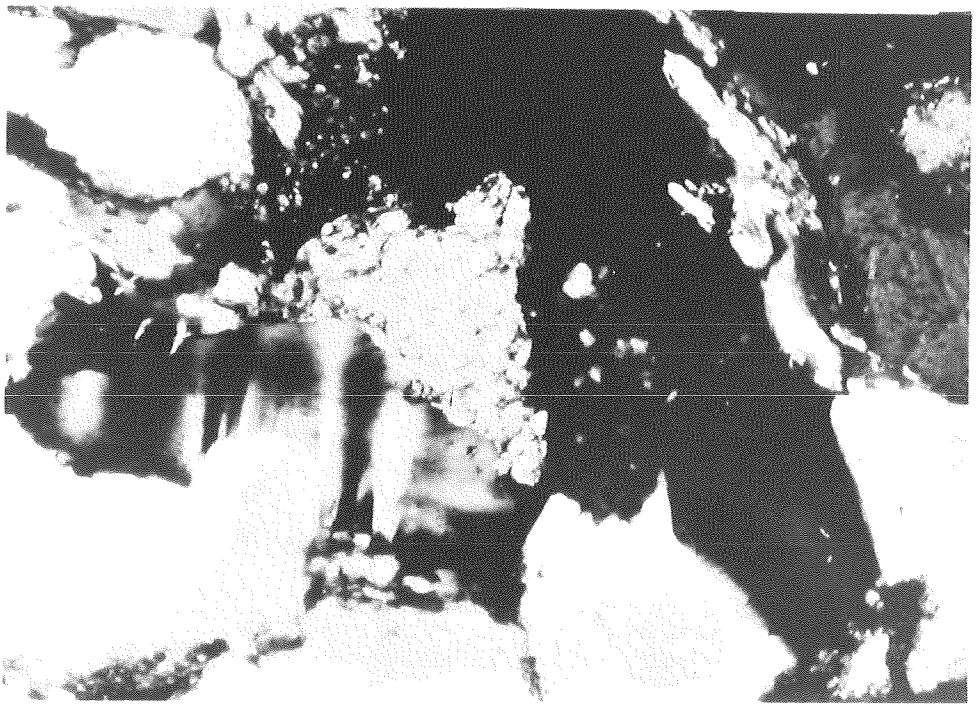

III B

microcline and orthoclase appeared fresher than the perthitic and plagioclase feldspars.

Sedimentary and metamorphic rock fragments were the dominant type of rock fragments occurring in the samples examined with only a trace percentage of igneous rock fragments occurring. Sedimentary rock fragments included siltstone, mudshales, and clayshales in the form of intrabasinal mudrock fragments. Metamorphic rock fragments were dominantly schistose but also included minor amounts of chloritic quartzite. Altogether rock fragments compose 1.0 to 20.5 percent of the rock volume at an average of 11.9 percent. They are uniformly distributed, and elongate grains are parallel or subparallel to bedding. The incompetent rock fragments are commonly squeezed by quartz, feldspar, and competent rock fragments to varying degrees. In some cases, they appear to be more like an interstitial filling than a detrital grain. Sedimentary rock fragments--especially intrabasinal ones--are commonly replaced by siderite.

Mica occurs in a trace amount to 14.5 percent. They are elongate flakes oriented parallel to, and commonly in heavy concentrations along, bedding planes. Accumulations of mica along bedding form planes of weakness where the core or hand samples break easily. Muscovite is by far the most abundant with only trace amounts of biotite or detrital chlorite. Unidentifiable heavy minerals along cleavage planes of muscovite are common. In most samples, the mica flakes are extensively bent or broken and have frayed edges (Plate IV).

In this study, orthochemical constituents include ferroan calcite, kaolinite, siderite, iron oxide, and minor amounts of chlorite. Ferroan

Plate IV -- Plain light view (30X) of an 88-125u, very well sorted, calcareous lithic arkose showing breakage and bending of mica flakes.

IV

calcite occurs as an interstitial cement, overgrowth on detrital dolomite, and rare replacement of quartz and potassium feldspar (Plates V and VI). Kaolinite is an interstitial clay filling and replacement of detrital feldspar with very low birefringence making it hard to recognize in plain light. Scanning electron microscopy indicates that the Kaolinite occurs in euhedral crystal habits filling pore spaces (Fig. 10). Siderite and iron oxide occur in amorphous masses. These masses have a bright orange reflectance in plain reflected light signifying an iron oxide composition (Plate VII).

Siderite and iron oxide are commonly associated in allochemical grains. These are recrystallized, fine grained sedimentary rock fragments very similar to mudrocks found interbedded with the sandstones in this study. Other allochemical grains include dolomite and glauconite (Plates V & VI). Both are rare and occur as random framework size grains. Dolomite grains are commonly surrounded by ferroan calcite rims. In total, the allochems comprised a trace to 1.0 percent of the rock volume.

Opaque grains occurred in a trace amount to 24.0 percent of the rock. They occurred as framework grains, finely disseminated particles, and large accumulations along bedding planes. Opaque grains are comprised of detrital organic material and pyrite. Opaque framework grains are typically subrounded to subangular and are more common in sandstones greater than 125u in grain size. Elongate particles and accumulations along bedding planes are common in most of the sandstones studied. The finely disseminated opaque grains were more abundant in sandstones with a finer (less than 125u) grain size. Pyrite was only recognizable

Plate V--(A) Plain light view (125X) of a 62-88u, very well sorted, lithic subarkose showing dolomite rhombs. (B) Crossed nicols view of same field showing blue stain characteristic of ferroan calcite rimming the dolomite rhomb suggesting that the calcite is an authigenic cement on detrital dolomite. (C) Cathodoluminescent view (30X) of same sample showing rounded shape of dolomite and abundant patchy kaolinite pore filling. Sample #C5-6.

VA

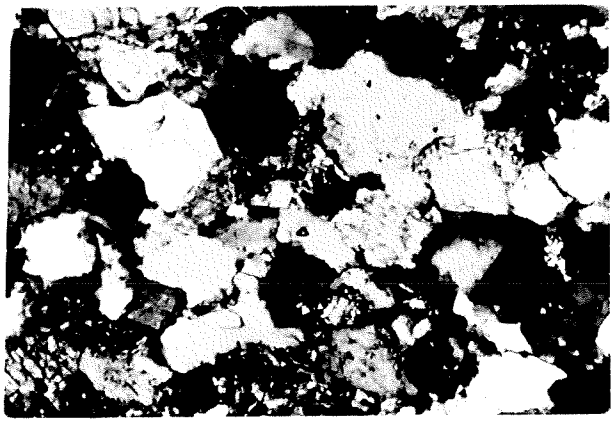

VB

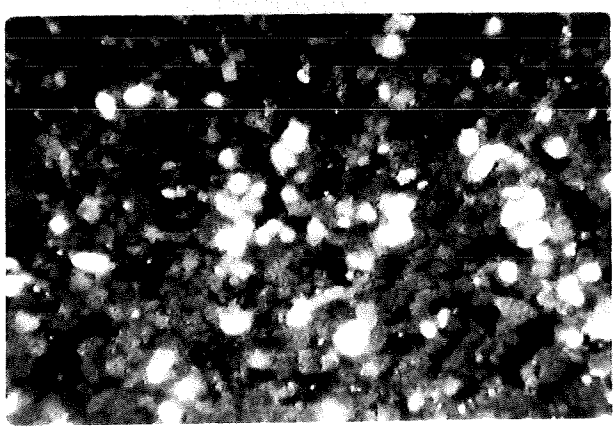

VC

Plate VI -- Crossed nicols view (125X) of a 177-250u, very well sorted, lithic arkose showing an angular, detrital-dolomite allochem with ferroan calcite cement surrounding it and replacing quartz and feldspar grains along grain boundaries. Also, note abundance of long and suture grain contacts. Sample #C5-38.

Plate VII -- (A) Plain light view (125X) of an 88-125u, moderately sorted, lithic arkose showing an amorphous mass of siderite and iron oxide. (B) Same field of view under plain reflected light showing charactistic orange reflectance of iron oxide. Sample #C5-16.

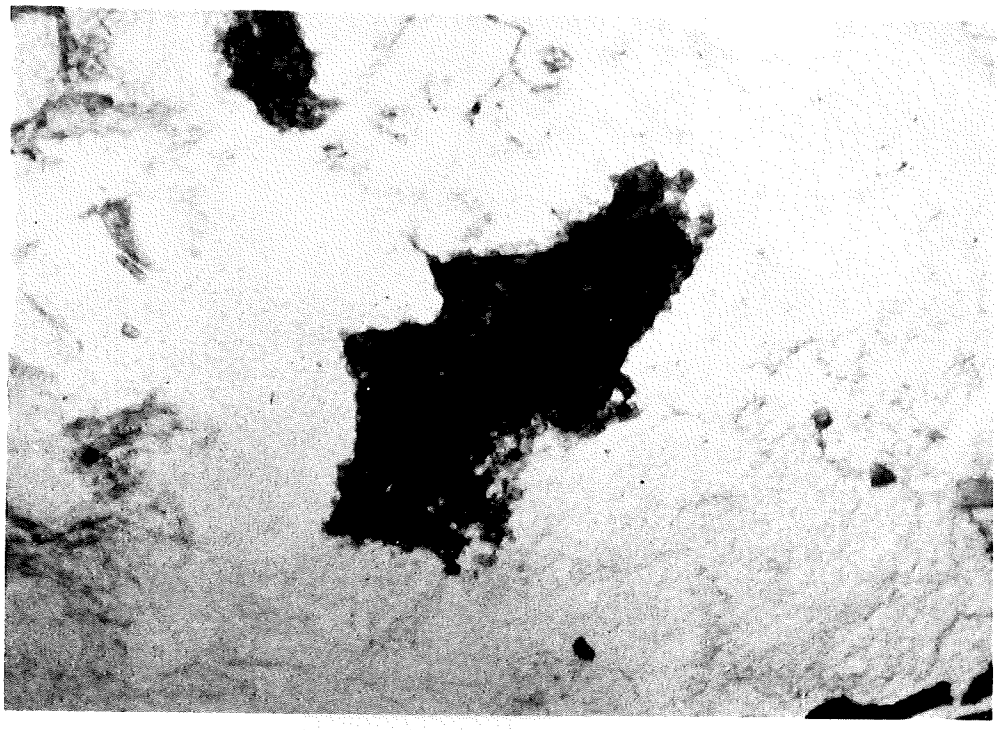

VII A

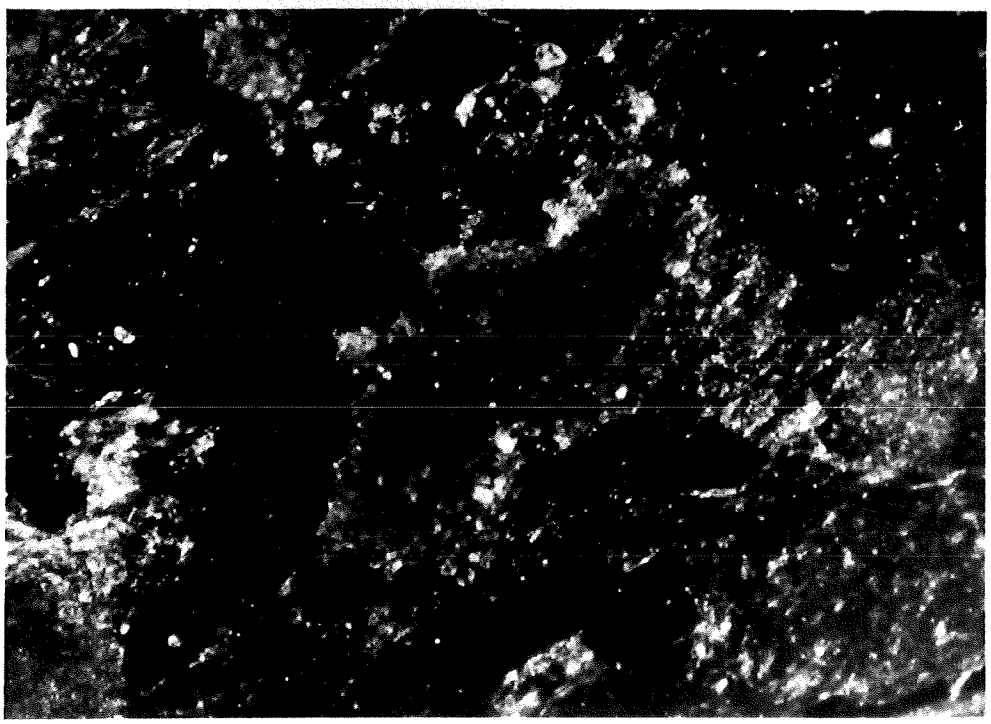

VII B

Figure 10--SEM photomicrograph of pore-filling kaolinite (2000X).

in rare quantities by reflected light.

Heavy minerals were unidentifieable because of their very fine grain size but occurred in a trace amount to 3.0 percent of the rock by volume.

Classification

According to the classification of Pettijohn et al (1973, p. 158, Fig. 5-3) these rocks are lithic arkoses and subarkoses. When subdivided into groups by grain size from medium sand (250-500u) to very fine (62-126u) sand, the samples separate into more or less discrete compositional groups (Fig. 11). The medium grained sandstones are distinct compositionally and are virtually all lithic subarkoses. The fine and very fine grained samples are less distinct compositionally but do show a tendency toward having distinct compositions. The very fine grained samples tend to be arkoses predominantly while the fine grained samples occupy a medial position between the medium and very fine grained samples and consist of equal amounts of arkoses and subarkoses. Stated simply, the percentage of feldspar increases with respect to quartz as grain size decreases.

Texture

Quantitative information on packing proximity was collected. Packing proximity is defined as the number of grain to grain contacts in a traverse divided by the total number of contacts counted in the traverse times 100 ($N_{g-g}/N_t \times 100$; where N_{g-g} = number of grain to grain contacts and N_t = total number of contacts counted). Values for the sandstones in this study range between 64 and 82% for all but three

Figure 11 -- Petrographic classification of samples taken from cores after Pettijohn et al (1973).

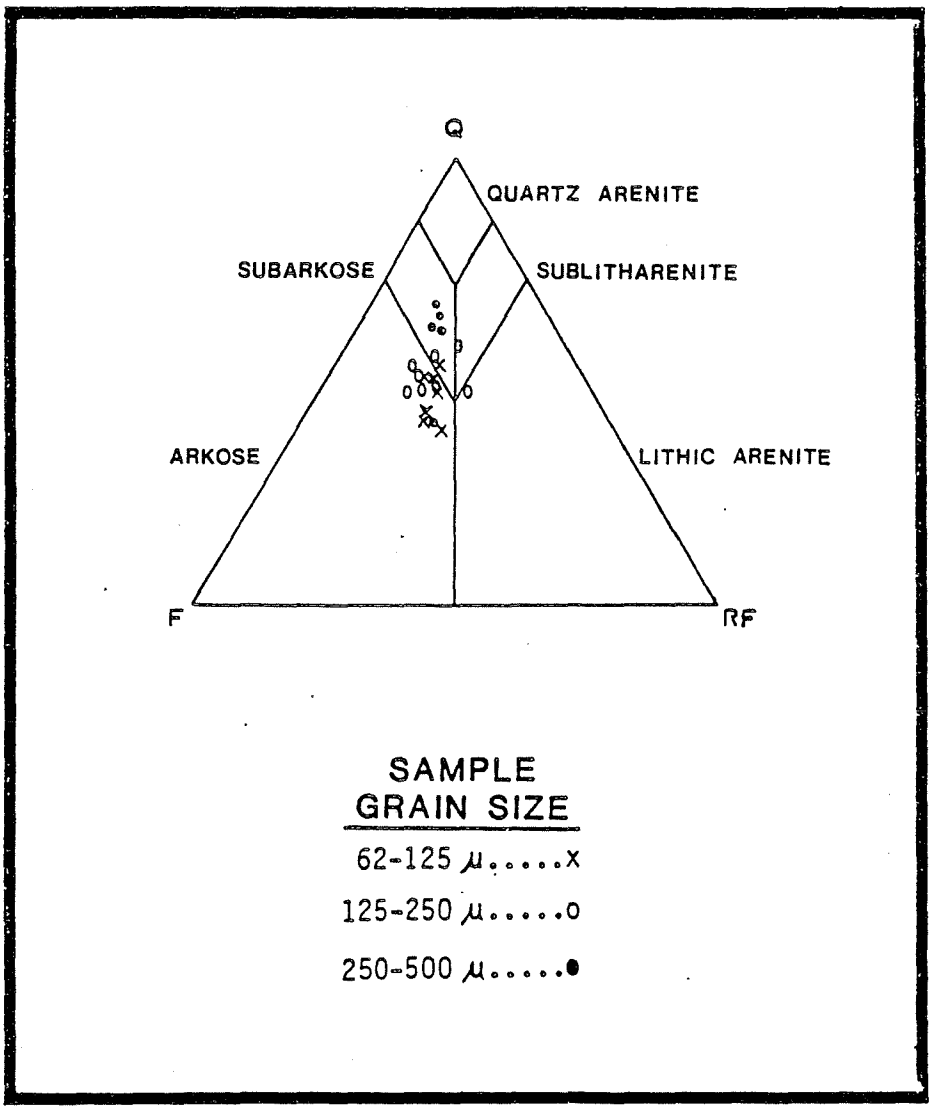

after Pettijohn et al, 1973, fig. 5-3

SANDSTONE CLASSIFICATION

samples. Two of these three had abundant secondary porosity which dramatically increased the number of grain to pore contacts and the third had abundant ferroan calcite cement which increased the number of grain to cement contacts substantially. Kahn (1956) showed, by statistical comparison, that packing-proximity and packing density are proportionally related (where packing density is the sum of grain intercept lengths of a traverse divided by the total length of traverse times 100). I spot checked the packing study sample set for contact strength and weighted contact packing indices as defined by Fuchtbauer (1967) and Hoholick et al (1982), respectively. Contact strength values ranged between 2.0 and 2.4, and weighted contact packing values ranged between 5.5 and 6.4. From comparison with documented values for the St. Peter Sandstone (Hoholick et al, 1982, p. 31) and the Lower Mannville Sandstones (Ho-Shing, 1979, p. 29) these values indicate a depth of burial greater than 5000 feet. Breathitt equivalents in the Southern Appalachian coal field reach thicknesses up to 7000 feet where preserved (Stearns and Mitchum, 1962). This supports the argument for deep burial of the samples in this study.

Other indicators of compaction observed include deformation of phyllosilicate rock fragments and mica flakes. In one or two sandstones, early cementation by ferroan calcite prevented compaction. In other sandstones, the plugging of pores by kaolinite appears to occur after compaction.

The texture of the rocks examined is mature with a few samples ranging into the submature category. Plugging of pores by kaolinite and incompetent rock fragments gives these sandstones a superficially submature appearance, but luminescence analysis shows that this "matrix" is not detrital.

LUMINESCENCE PETROGRAPHY

Cathodoluminescent study of the samples enables description of original texture especially as it differs from diagenetic texture. In other words, cements and non-detrital minerals are easily recognized.

Texture is more easy to see by cathodoluminescence than by standard petrographic analysis because the distinction between framework and non-framework elements is clear. A monomineralic, uniformly distributed matrix of kaolinite exists in most samples (Plate VIII). In medium grained sandstones of the lower to middle part of thick fining upward sequences, there is an absence of pore-filling kaolinite and a concommitant abundance of porosity. For the most part, kaolinite occurs as a pore filling but also occurs as a rim around K-feldspar grains and as isolated patches with an outline resembling a grain boundary (Plate II). It appears to effectively plug most of the pore space in the samples. Framework grains include quartz and feldspar dominantly. There is a noticeable lack of overgrowths on either mineral species. Long, concavo-convex, and suture contacts are abundant, whereas point and floating contacts are relatively rare. With the exception of rare elongate grains, there is no noticeable preferred orientation of these framework grains. The elongate grains do, however, show an orientation subparallel or parallel to bedding. Dolomite grains under luminescent petrography appear to have rounded outlines and a size range comparable to framework grains suggesting a detrital origin. Ferroan calcite, however, has an irregular, patchy outline and a size range inconsistent with normal framework size distributions suggesting an authigenic origin (Plate VIII).

Plate VIII--Four cathodoluminescent views (30X) of samples selected from levee facies (A-Sample #C4-97; C-Sample #C4-82), crevasse splay facies (B-Sample #1A-14), and crevasse channel facies (D-Sample #1A-11). Note patchy distribution of monomineralic kaolinite cement in all samples. Compare dolomite shape (red, rounded, elliptical grains suggesting detrital origin) in A and C to ferroan calcite shape (orange, irregular, patchy outline suggesting authigenic origin) in B and C.

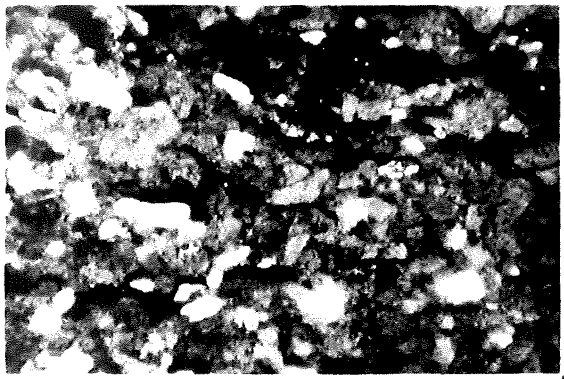

VIII A

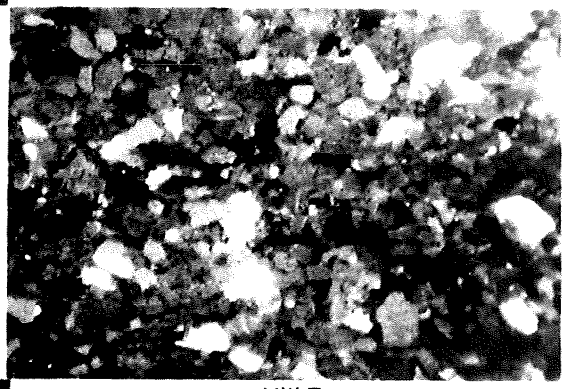

VIII B

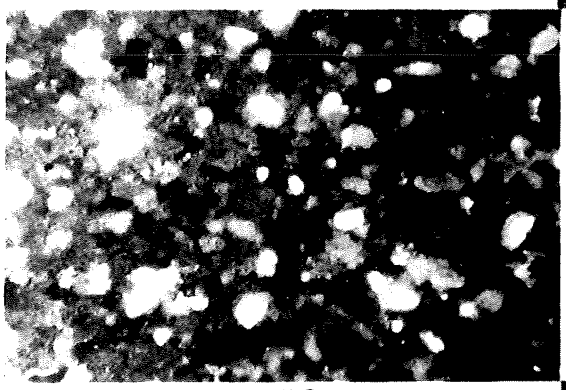

VIII C

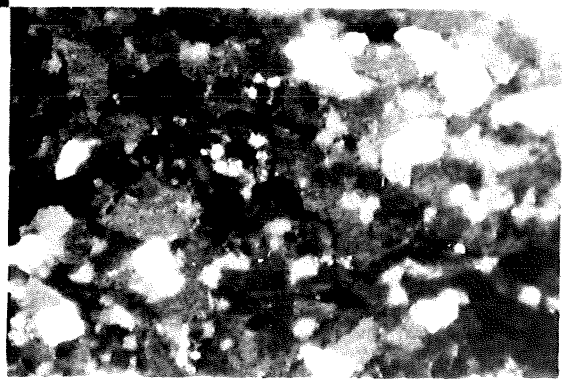

VIII D

DISCUSSION OF RESULTS

SANDSTONE FACIES

Coleman and Prior (1980) and Horne et al (1978) discuss sandstone facies for the Recent Mississippi Delta and the ancient Appalachian Delta, respectively. Table 4 compares terms used, in their studies and in a general review by Elliot (1978), for the different sandstone facies. In this study, the author has adopted the following terms to describe the sandstone facies in core: fluvial-distributary, minor mouth bar/crevasse channel couplet, crevasse splay, bay fill, and levee. The purpose of this section is to discuss facies interpretations of the descriptive vertical sequences examined in this study. These facies interpretations were arrived at by comparing the descriptive vertical sequences with ideal vertical sequences of facies found in the literature.

Fluvial-Distributary

Fluvial-distributary deposits are probably the most impressive sandstone facies in Breathitt Formation outcrops and cores. They form imposing cliffs in road and stream cuts and can be 100 to 120 feet thick in cores. The thick fining upward sequences represent what are termed fluvial-distributary facies in this study. The decrease in grain size upward from a lag deposit over an erosional base, the decrease in flow regime represented by the sequence of sedimentary structures, and the lack of bioturbation all indicate the migration of a point bar in a non-marine fluvial system. This deposit is capped by a rooted levee deposit and coal. Horne et al (1978, Figure 10) illustrate the ideal vertical sequence of the fluvial distributary facies which they derived

Table 4--Comparison table of delta facies terminology.

Table 4--Comparison of Delta Facies Terminology

Coleman and Prior, 1980	Horne et al, 1978	Elliot, 1978
	fluvial-distributary	fluvial distributary
crevasse splays and bay-fills	backswamp/bay-fill/ crevasse splay	crevasse splay and minor mouth bar/ crevasse channel couplets
	levee	levee
distributary mouth bar	distributary mouth bar	disttributary mouth bar

from their work on outcrops in eastern Kentucky and southern West Virginia (Fig. 12). Figures 13 and 14 from Core C4 and C5 show fining upward sequences very similar to the fluvial deposits of Horne et al (1978). The examples from this study are notably thicker 100-120 feet compared with 50-80 feet for Horne et al (1978) and are some what finer grained--medium to very fine grained sand (500-62u) compared with the coarse to medium grained sand of Horne et al (1978). Not all the fluvial distributaries in this study are as thick as the two examples, but the grain size is fairly consistent for all. The thicker accumulation of sand is attributed to local rapid subsidence and/or stacking of channel sequences, and the finer sediment size is attributed to either a more distal position in the delta plain or a time/micro-source area difference.

Minor Mouth Bar/Crevasse Channel Couplet

Whereas the fluvial distributary facies is the most prominent, the crevasse channel and minor mouth bar/crevasse channel couplet (hereafter mmb/ccc) facies are the most abundant facies of the delta system. Coleman and Prior (1980, p.56) put it best: "Given time, eventually another crevasse will form on the bank of the Mississippi, and another period of infilling will ensue, again filling the interdistributary bay with detrital sediments. It is this process of repeated filling, alternating with periods of marsh destruction, subsidence, and reversion to open bay conditions, that forms the bulk of the cyclic deposits in the lower delta plain." Elliot (1978) characterizes this process as a microcosm of the major delta progradation. The above points suggest two important distinguishing features of the crevasse

Figure 13 -- Example of fluvial distributary facies sequence from this study.

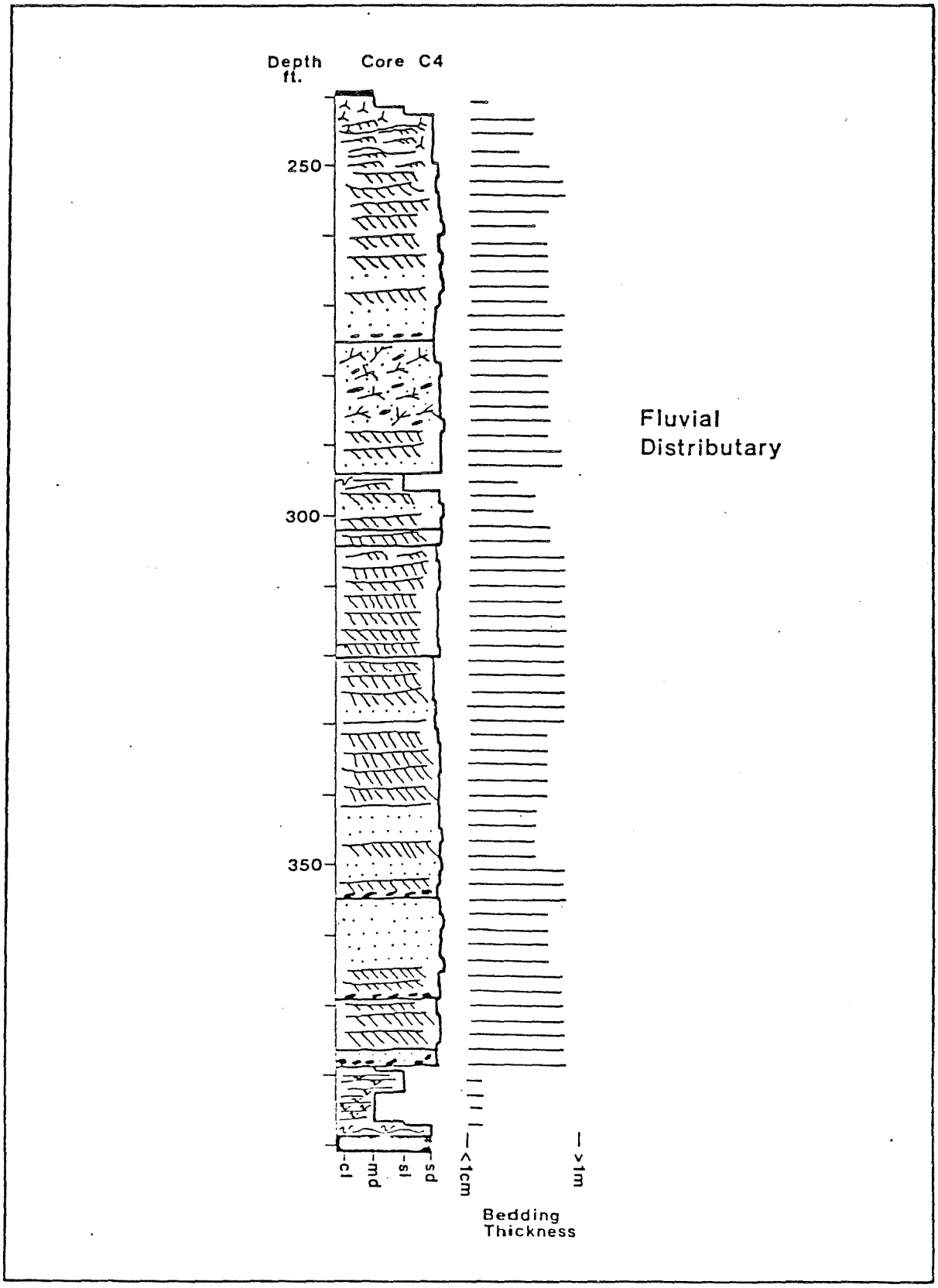
Depth ft.
Core C4
250
300
350
cl
md
sl
sd
<1cm
>1m
Bedding Thickness
Fluvial Distributary

Figure 14 -- Example of fluvial distributary facies sequence from this study.

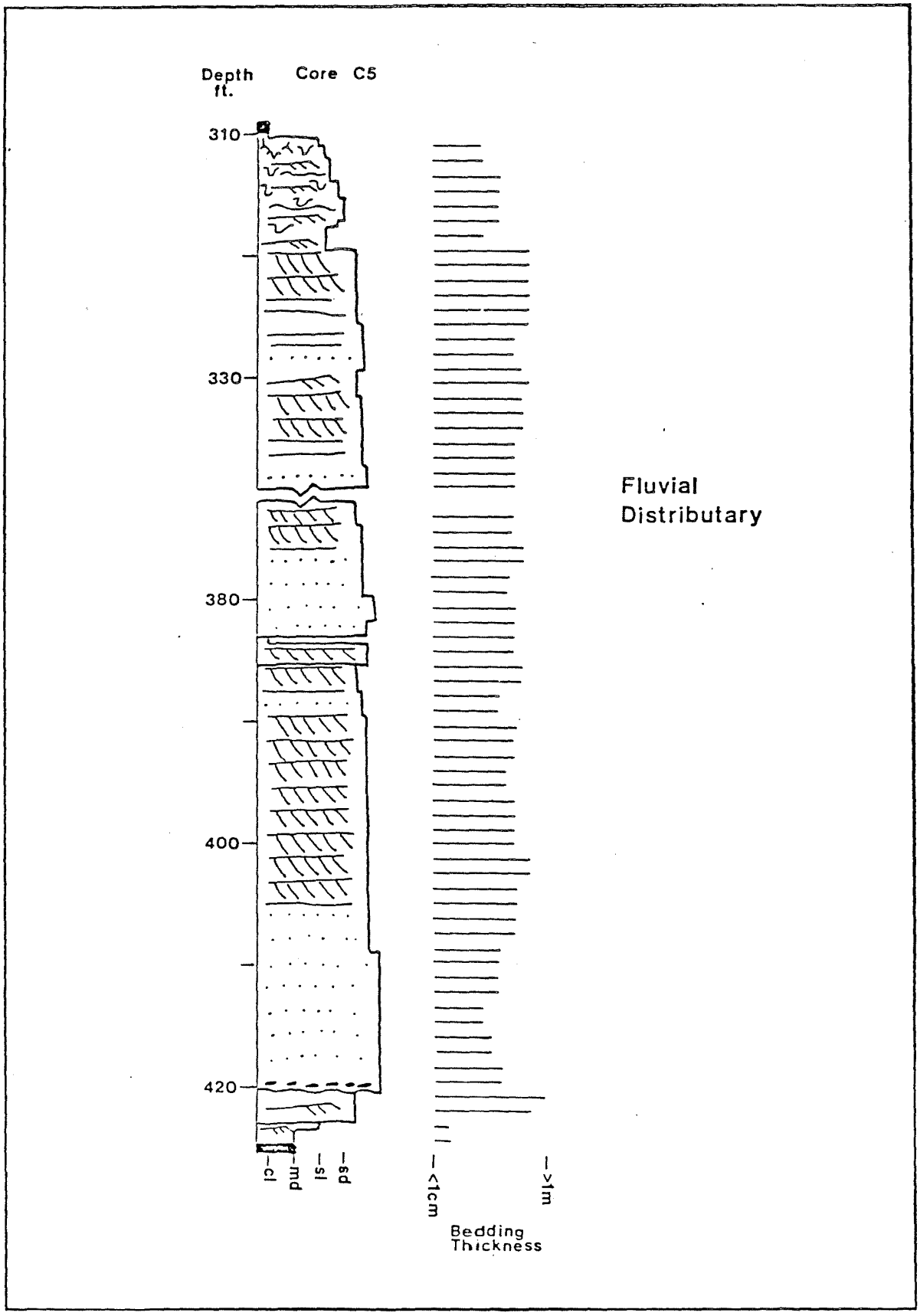
Depth ft.
Core C5
310
330
380
400
420
cl
md
sl
ss
<1cm
>1m
Bedding Thickness
Fluvial Distributary

channel and mmb/ccc facies. One, they are smaller scale deposits than the major distributary deposits and two, they are associated with or have as a significant portion of the sequence, fine grained (mudrock) bay-fill sediments. In most other respects, their nature should closely resemble that of the major distributary type deposits.

A minor mouth bar/crevasse channel couplet (Elliot, 1978) is represented by the coarsening upward/fining upward sequence discussed previously. The coarsening upward component indicates the approach of a crevasse system in the interdistributary bay, and the fining upward component marks the arrival and subsequent migration of the crevasse channel across the bay (Fig. 15). Figures 16 and 17 show examples from this study of the couplet facies. Notice that the channel facies are somewhat thinner (20-40 feet) than their fluvial distributary counterparts and that there is a significant development of the fine grained mudrock bay fill deposit above and below the couplets. In some cases a small scale channel deposit with no minor mouth bar is developed. This may occur because the channel deposit is proximal to the distributary crevasse, or because a more distal channel deposit was deposited more suddenly than a sequence with minor mouth bar development.

Crevasse Splay and Bay-Fill

Crevasse splays represent temporary conditions in deltaic sedimentation when normal interdistributary bay deposition is interrupted by sand deposition. They represent flood stages of the river. Initial deposition is sudden and high energy but wanes rapidly with the falling river stage. Crevasse splay deposition does not continue after normal river

Figure 15 -- Example of minor mouth bar/crevasse channel couplet facies sequence from the Carboniferous of England (Elliot, 1974).

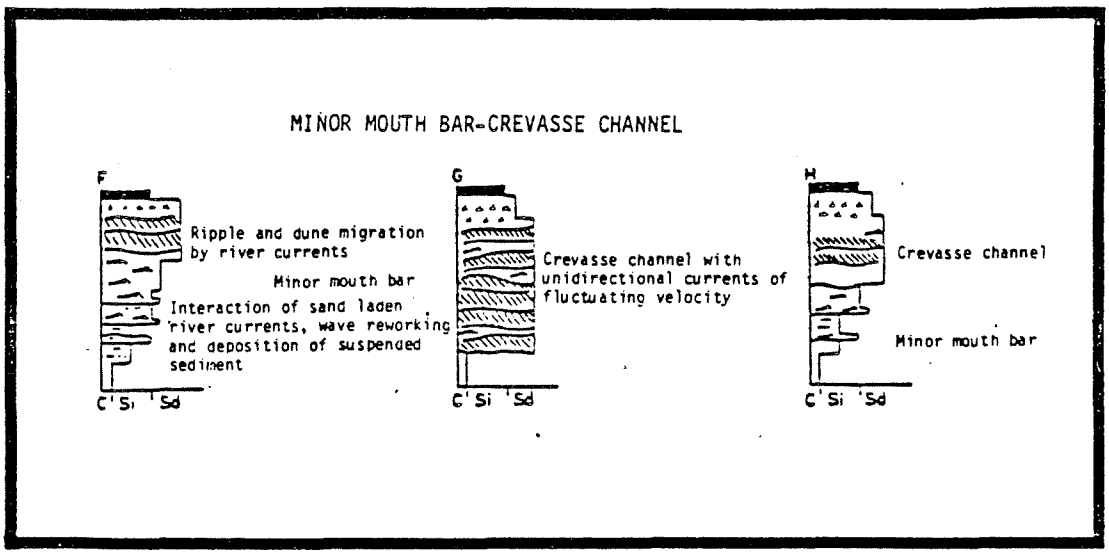
MINOR MOUTH BAR-CREVASSE CHANNEL
F
Ripple and dune migration by river currents
Minor mouth bar
Interaction of sand laden river currents, wave reworking and deposition of suspended sediment
C Si Sd
G
Crevasse channel with unidirectional currents of fluctuating velocity
C Si Sd
H
Crevasse channel
Minor mouth bar
C Si Sd

Figure 16-- Example of minor mouth bar/crevasse channel couplet facies sequence from this study.

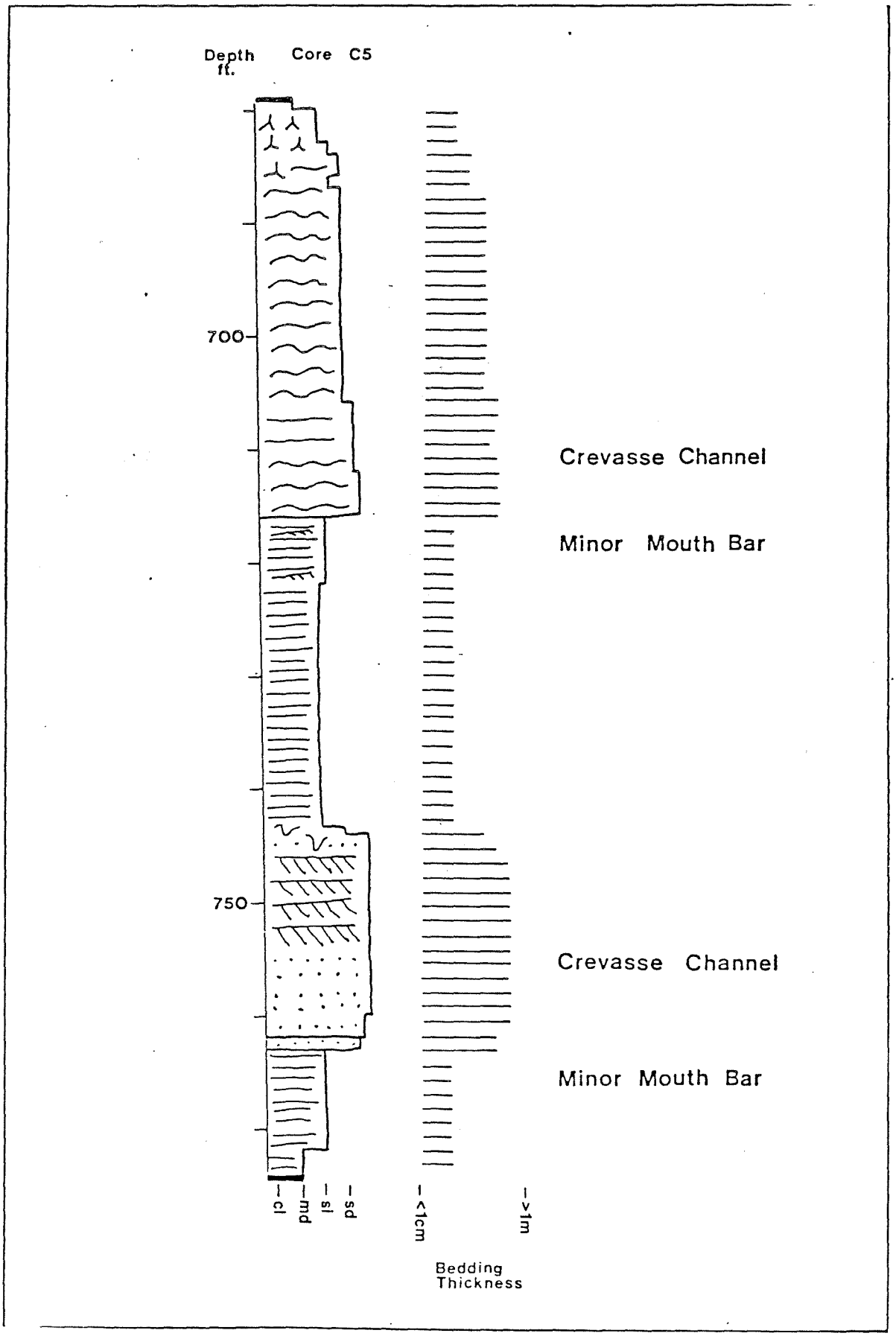
Depth ft.
Core C5
700
750
Crevasse Channel
Minor Mouth Bar
Crevasse Channel
Minor Mouth Bar
cl
md
sl
sd
<1cm
>1m
Bedding Thickness

Figure 17 -- Example of minor mouth bar/crevasse channel couplet facies sequence from this study.

stage is reached. Therefore, they are smaller scale deposits than their crevasse channel counterparts (which do continue after flood stage). All things considered, the splay deposits have a sharp, possibly even erosional, base representing initial high energy conditions, a somewhat abbreviated upward fining grain size and current structure pattern representing waning flow, and a thickness of from 5-20 feet representing their ephemeral existence. Figure 18 shows an example of a crevasse splay examined in this study compared with crevasse splays from Elliot (1974, Fig. 2C).

Bay-fill deposits are represented by the coarsening upward and repeated coarsening upward sequences described above. They are the lateral time equivalent of the fluvial-distributary facies. As the distributary progrades and migrates across the shelf, overbank deposits gradually fill the bay. A single coarsening upward sequence records the uniform progradation of crevasse and overbank deposits associated with a migrating distributary, and a repeated coarsening upward sequence records the nonuniform or interrupted progradation of crevasse and overbank deposits.

Figure 19 illustrates a bay-fill deposit examined in this study compared with a bay-fill deposit from Coleman and Prior (1980, Fig. 20). Coarsening upward sequences in the literature are interpreted either as crevasse and overbank deposits or as distributary mouth bar deposits. In comparison to distributary mouth bar sands, the bay fill sands are much thinner. Horne et al (1978) describe the distributary mouth bar sands in eastern Kentucky as 50-90 feet thick, but the sands of the coarsening upward sequence described here are 12 feet thick at most.

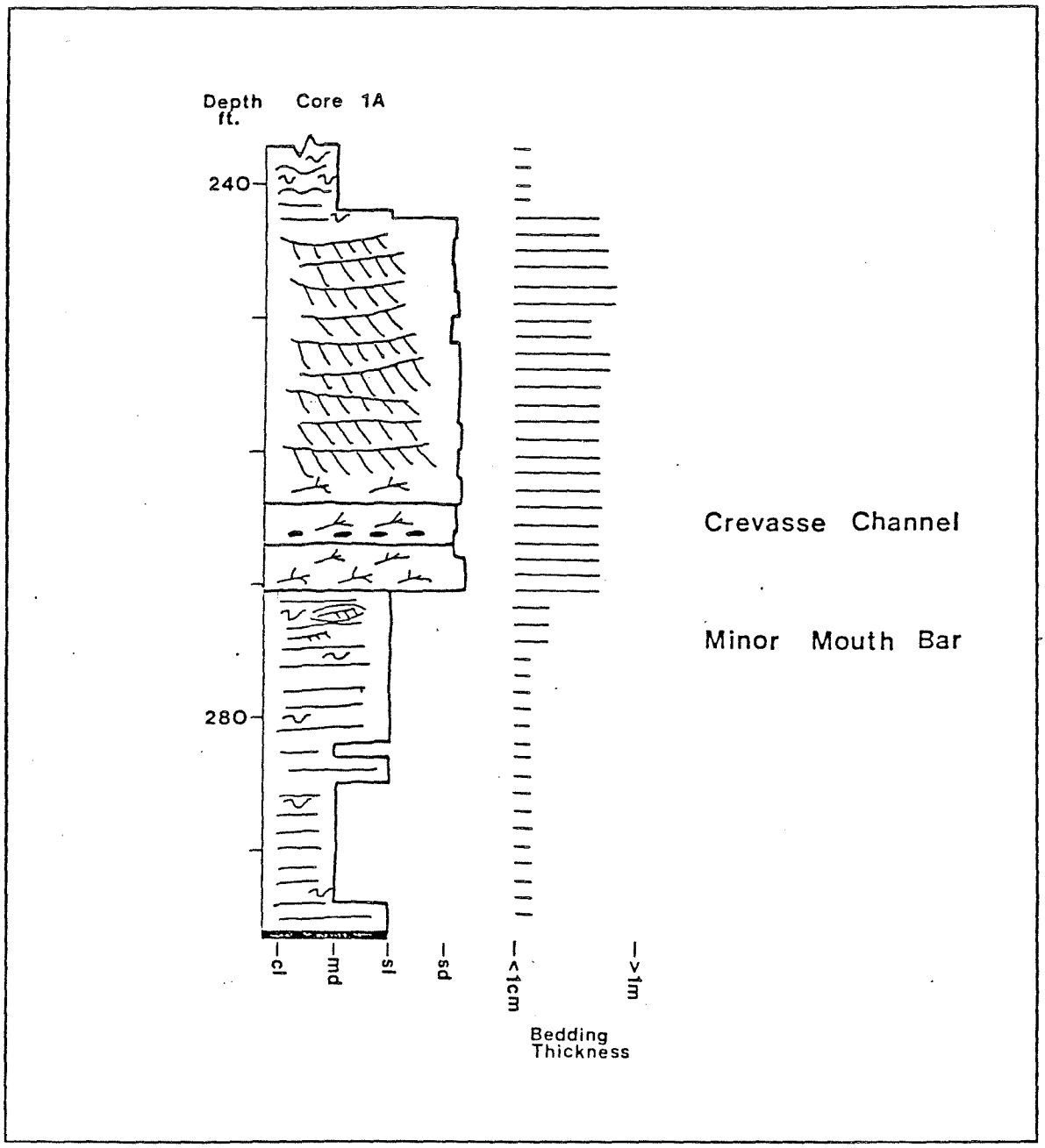
Depth ft.
Core 1A
240
280
cl
md
sl
sd
<1cm
>1m
Bedding Thickness
Crevasse Channel
Minor Mouth Bar

Figure 18 -- Example of crevasse splay facies sequence from this study (bottom) compared with the same facies sequence (top) from the Carboniferous of England (Elliot, 1974).

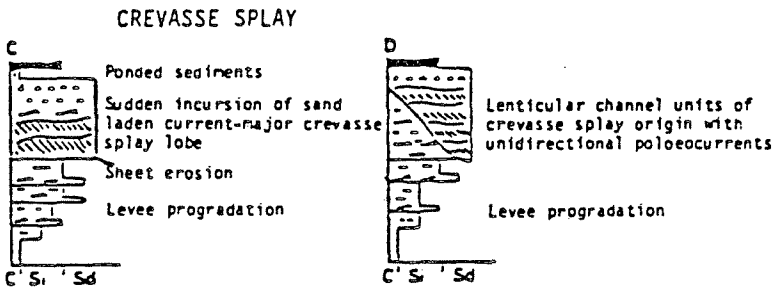

From Elliot [1974, fig. 2C]

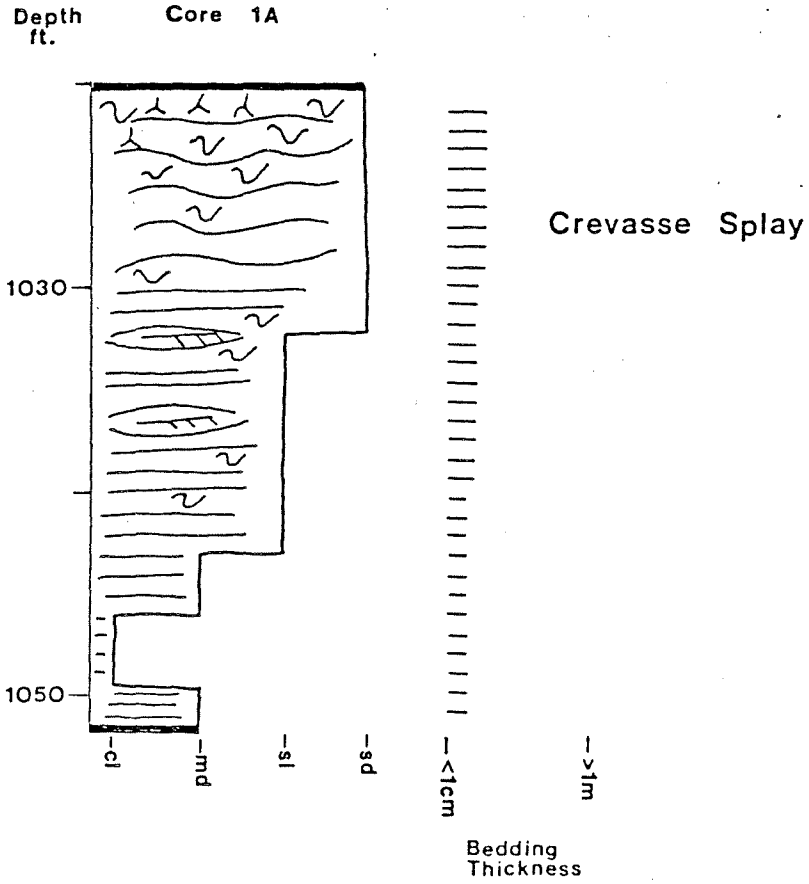

Figure 19 -- Example of bay-fill facies sequence from this study (bottom) compared with the same facies sequence (top) from the Recent Mississippi Delta (Coleman and Prior, 1980, fig. 20).

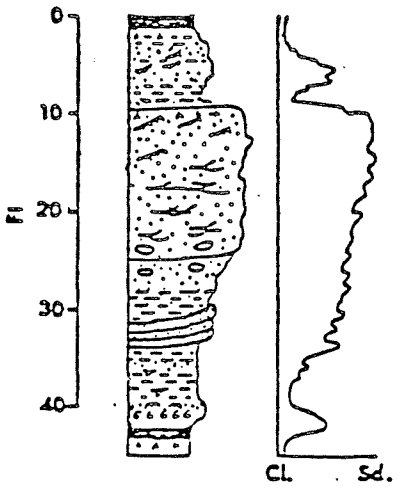

Bay-fill

After Coleman and Prior [1980, fig. 20]

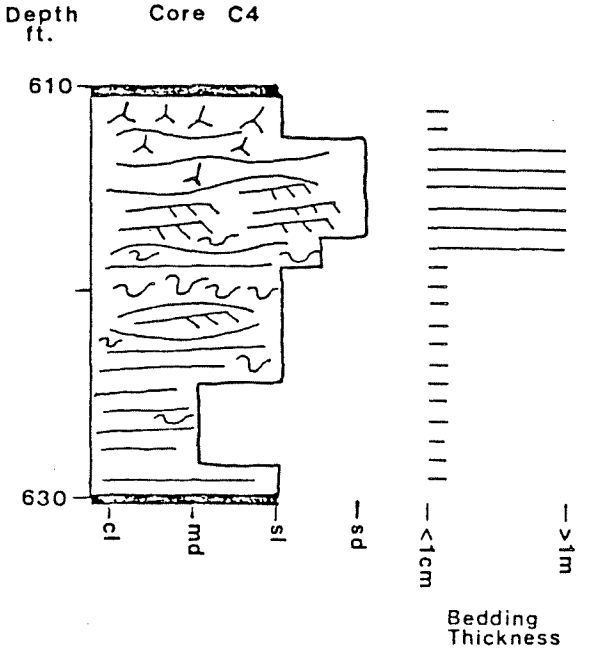

Bay-fill

For this reason, I choose to call these bay-fill sands as opposed to distributary mouth bar sands.

Levee

Figure 20 shows a crevasse splay deposit succeeded by another crevasse splay deposit which is then succeeded by a levee deposit. As explained in the literature, levees are created by overbank flooding characterized by sheet flow and rapid deposition of sand from traction and suspension. They are thin and commonly top the channel deposits.

SUMMARY OF FACIES SEQUENCES

Figure 2 is a summary diagram of the facies sequences in the cores examined in this study. It illustrates three things. First, the cores are unevenly spaced. Core 1A is 32 miles south-southwest of Core C5 and 37 miles south-southwest of Core C4. Cores C5 and C4 are only 5 miles apart. Second, they represent different stratigraphic intervals. Core 1A represents the lower to middle Breathitt Formation whereas Cores C4 and C5 represent the middle to middle-upper Breathitt Formation. Third, they represent different parts of the delta plain environment. Core 1A is about one-third sandstone and two-thirds mudrocks, and its sandstone facies are almost exclusively comprised of crevasse channel and crevasse splay facies suggesting that the core represents sedimentation in a lower delta plain environment. Cores C4 and C5 are about one-half sandstone and one-half mudrocks, and their sandstone facies are comprised dominantly of fluvial distributary and crevasse channel facies suggesting that these cores represent sedimentation in an upper delta plain environment.

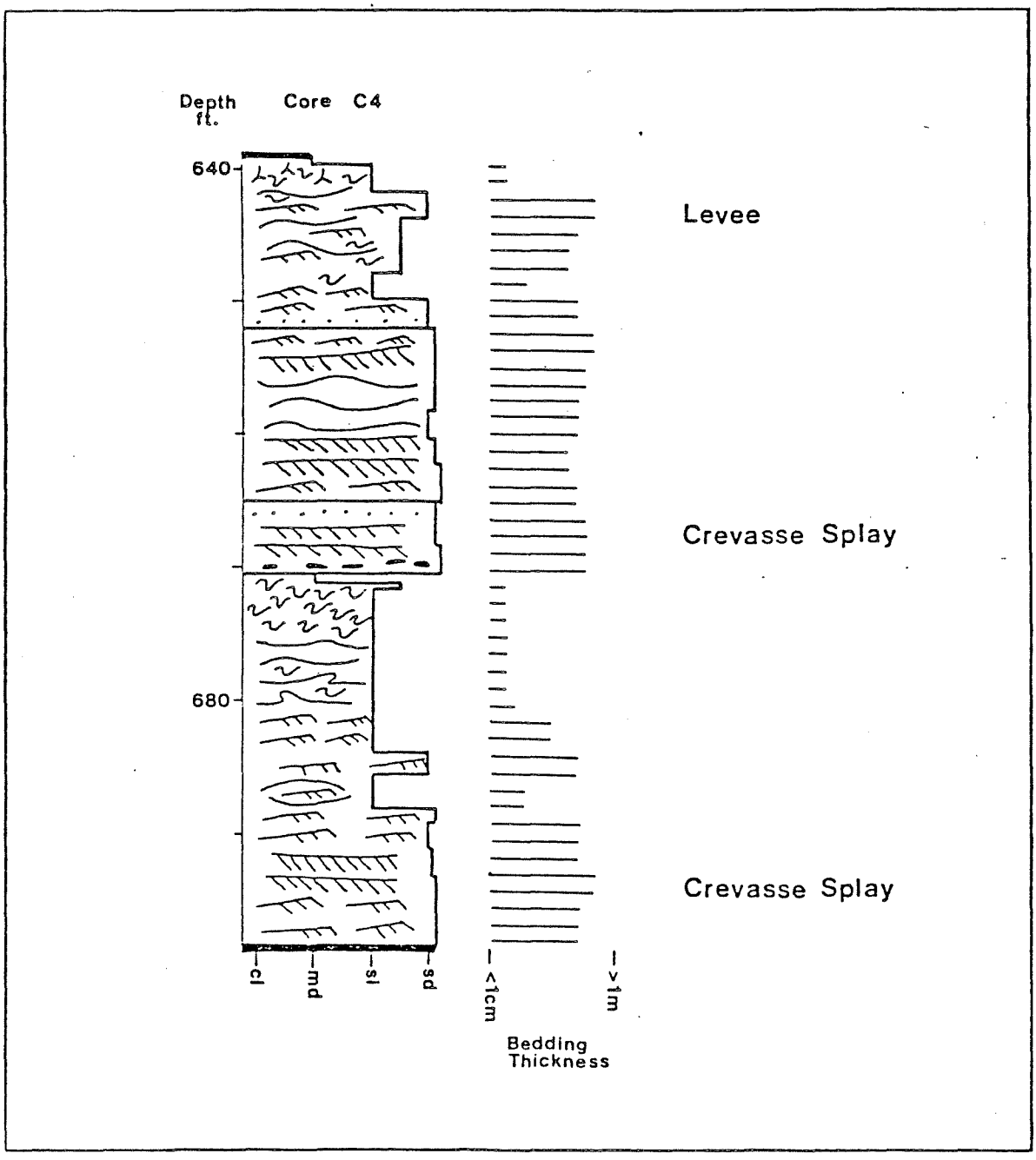
Depth ft.
Core C4
640
680
cl
md
sl
sd
<1cm
>1m
Bedding Thickness
Levee
Crevasse Splay
Crevasse Splay

Figure 20-- Example of crevasse splay-crevasse channel-levee facies sequence from this study.

DIAGENESIS

The concept of diagenesis has been explained from an interpretative point of view by Hayes (1979) and Pettijohn et al (1973, p. 383) among others. In his review, Hayes (1979, p. 127) describes diagenesis in terms of four truths about the holes (porosity) in rocks. They are: 1) Porosity reduction occurs during early stages of burial; 2) Porosity production occurs later, possibly at depth; 3) Chemical changes occur through a kinetic process; and 4) Diagenesis is programmed by contextual influences--provenance, depositional environment, and tectonic setting. These four aspects of diagenesis make a convenient framework for discussing diagenesis in this study.

Porosity Reduction

Porosity reduction is accomplished by compaction, cementation, recrystallization, and replacement. Most previous workers mention the deformation of micas and incompetent rock fragments as evidence for compaction. These indicators were noted in this study as well. Packing proximity values were quite high for all sandstone facies indicating considerable compaction and porosity reduction in these sandstones. In addition, contact strength and weighted contact packing indices indicate that these rocks were buried to a depth of greater than 5000 feet. Thus, overburden pressure was an important factor influencing the physical porosity reduction of the Breathitt Formation sandstones.

Kinetic Process of Chemical Change

The chemical factors influencing porosity reduction include cementation, recrystallization, and replacement. Gardner (1977, p. 192) recognized replacement of feldspar and dolomite by kaolinite and ferroan dolomite as the chemical change most abundant in the Breathitt Formation sandstones. Some dolomite and feldspar replacement was noted in this study, but the dominant chemical change was the kaolinite cementation obvious in luminoscope photos. This pore filling by kaolinite was second only to mechanical compaction as an agent of porosity reduction. Wilson and Pittman (1977, p. 50) give a number of criteria for recognizing authigenic clay in sandstones. Among the criteria applicable to this study are: pure, monomineralic composition; composition markedly different from detrital clay composition; clay particles undeformed by compaction; uneven grain size distribution; and scattered pore filling distribution. The luminescence photo of sample C5-14 (Plate II) illustrates some of these criteria. The bright blue luminescent character of kaolinite is uniform and pure in this sample. The kaolinitic composition is markedly different from the composition of detrital clays found in associated mudrocks. Detrital clays from these mudrocks are dominantly illitic (Kryza, 1982, pers. comm.). Most importantly, if the kaolinite is not authigenic, then the grain size distribution in the sample indicates a hydraulic impossibility--the simultaneous deposition of clay and sand. These are convincing evidence for the secondary nature of the kaolinite.

Wilson and Pittman (1977, p. 49) state that authigenic clays are formed either by direct precipitation from formation water or by

reactions between precursor minerals and formation water. Gardner's model (Gardner, 1977, p. 192) for the diagenesis of these rocks called for both processes. According to his model, a diagenetic profile with three horizons is created by downward movement of water and the concommitant change in water chemistry. Of the three horizons in a sandstone body, the upper horizon is deficient in diagenetic minerals; the middle horizon is rich in authigenic kaolinite; and the lower horizon is rich in dolomite and authigenic ferroan dolomite. Water chemistry changes from silica rich, acidic, fresh water at the top to reducing, low-pH, saline water at the bottom. No such profile was observed in this study. In fact, most samples showed exception to this model. Kaolinite was ubiquitous and occurred with ferroan calcite. Ferroan calcite was found in upper as well as lower horizons of sand bodies.

I believe that the cementation of these Breathitt Formation sandstones is best explained by timing--early and late. Ferroan calcite cementation occurred early where degradation of locally abundant organic matter occurred. In a few rare instances this cement was abundant enough to prevent significant compaction. Kaolinite cement occurred late (evidenced by the undeformed nature of the euhedral crystals in SEM photo; Fig. 10) as a result of feldspar dissolution under deep burial conditions and the change in pore-water chemistry.

Contextual Influences

The position of the fluvio-deltaic complex represented by Breathitt Formation rocks in a foreland basin provided a tectonic setting where loading of thrust sheets to the east caused significant downwarp. In

addition, the source area was less than 200 miles away, which provided quick deposition of many unstable grains that later were dissolved or deformed.

Porosity Production

Previous workers did not recognize any evidence of porosity production in Breathitt Formation rocks. The very-fine and fine grained sandstones with high packing proximities exhibited only minor secondary porosity. The lower part of medium-grained, channel sands, however, are commonly deficient in diagenetic minerals, and have abundant secondary porosity. Plates I and IX show scattered remnants of ferroan calcite and kaolinite cement within large secondary pore spaces. This suggests porosity production by the dissolution of carbonate cements and detrital framework grains. Explaining such porosity as a primary feature is difficult because these clean, medium grained sands were subjected to larger volumes of pore fluid migration than the finer more cemented sands. If anything, these coarser sands would have cemented faster. Heald and Renton (1966, p. 84) in an experimental study concluded that "well sorted coarse sands became cemented faster than fine-grained sands because of the greater influx of cement into the more permeable coarse sand." It would seem, then, that these sands first underwent thorough compaction and cementation and later were subjected to dissolution of cement and detrital grains as porosity production. The same property that made them susceptible to fast cementation provided for their susceptibility to dissolution and porosity enhancement.

Plate IX -- Cathodoluminescent view (30X) of a 250-350u, well sorted, subarkose. Kaolinite cement has been removed from pores (center and right-center). Sample #C5-55.

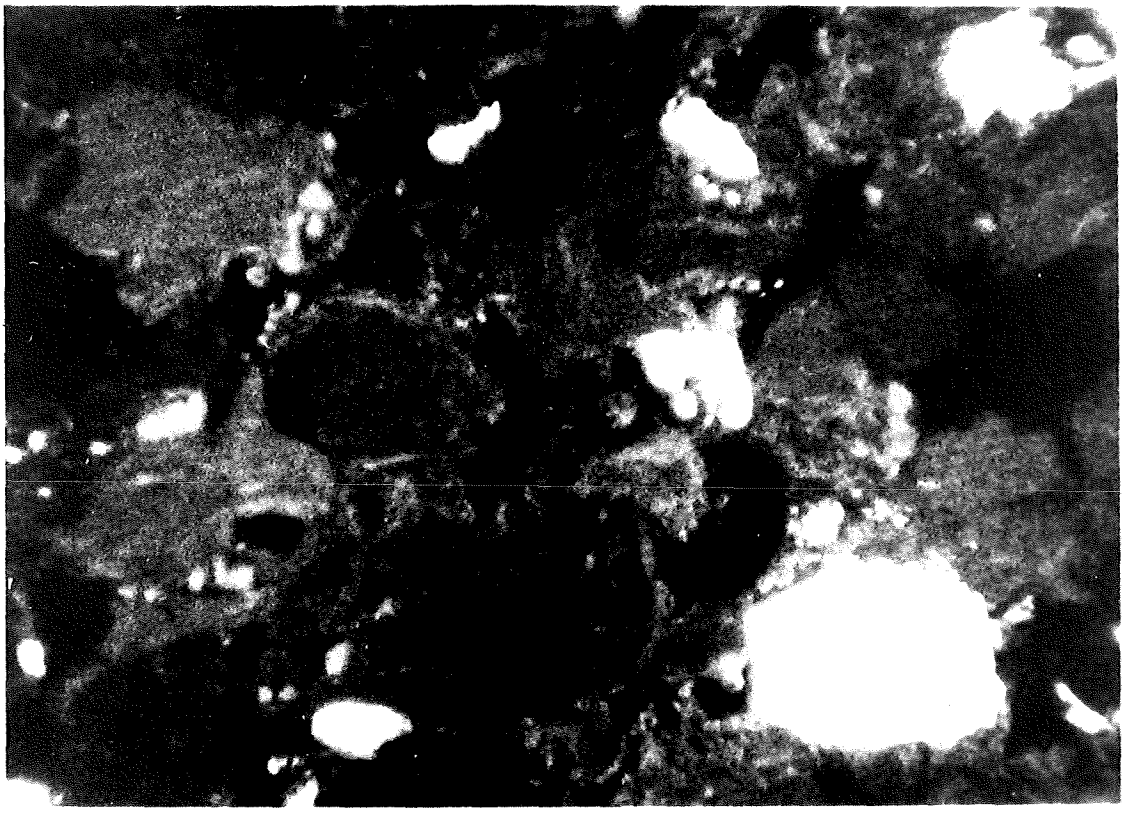

IX

RELATIONSHIP OF DIAGENESIS TO SANDSTONE FACIES

The facies identified by core analysis were fluvial distributary, minor mouth bar/crevasse channel couplets, crevasse splay, bay-fill and levee. Tables 5 and 6 show a graphic representation of the location and thickness of the descriptive and interpretative sequences for each core.

The petrographic analysis showed that the rocks in this study are very-fine to medium-grained, moderately to very-well sorted, lithic arkoses and lithic subarkoses. The cements are ferroan calcite and kaolinite. Quantitative analysis of packing indicates that these were buried 5000 feet or more as does the abundance of suture, long, and concavo-convex grain-to-grain contacts.

Figure 21 is a graph of packing proximity versus sandstone facies that shows all facies were equally affected by compaction. The three exceptionally low values of packing proximity are explained by abundant ferroan-calcite cement which inhibited compaction in one case and by abundant secondary porosity in the other two--both medium grained channel sand deposits--which obscures original packing.

A comparison of facies and packing suggests that facies are not a fundamental factor in diagenesis, but rather that timing and burial depth are the important factors in the diagenesis of the Breathitt Formation sandstones. The comparison suggests that ferroan-calcite cementation occurred early and in rare cases was abundant enough to prevent compaction. In all other cases compaction occurred with the burial of the sediments and was followed by kaolinite cementation from the the dissolution of feldspar at great depth. Medium grained

Table 5--Graphic summary table of the distribution of descriptive vertical sequences in each core.

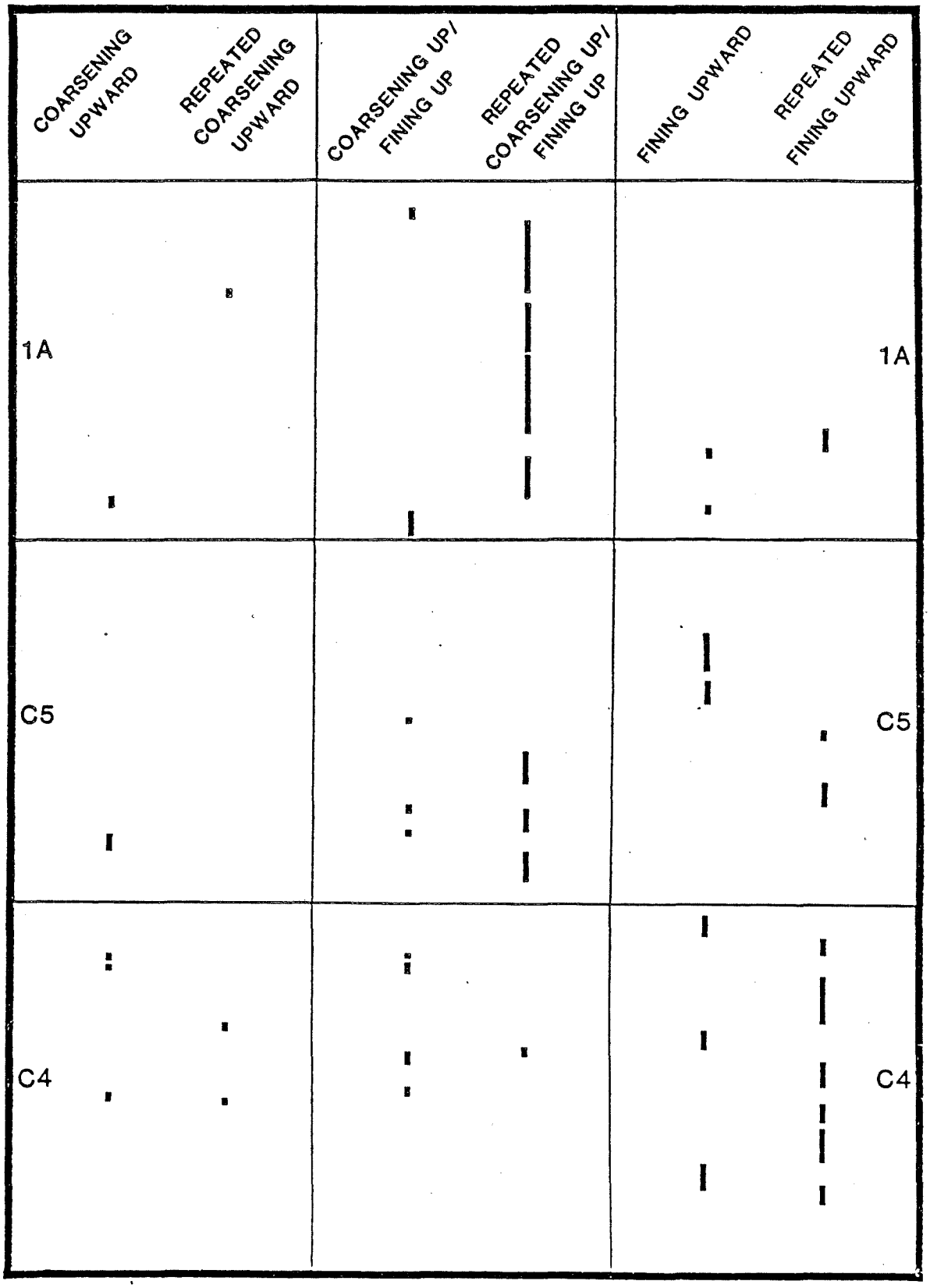
COARSENING UPWARD
REPEATED COARSENING UPWARD
COARSENING UP/ FINING UP
REPEATED COARSENING UP/ FINING UP
FINING UPWARD
REPEATED FINING UPWARD
1A
1A
C5
C5
C4
C4

Table 6--Graphic summary table of the distribution of facies sequences in each core.

CREVASSE SPLAY AND BAY-FILL FACIES	MINOR MOUTH BAR/ CREVASSE CHANNEL COUPLET FACIES	FLUVIAL DISTRIBUTARY CREVASSE CHANNEL FACIES
1A		1A
C5		C5
C4		C4

Figure 21--Graph of packing proximity versus sandstone facies.

Figure 23
GRAPH OF PACKING VS FACIES

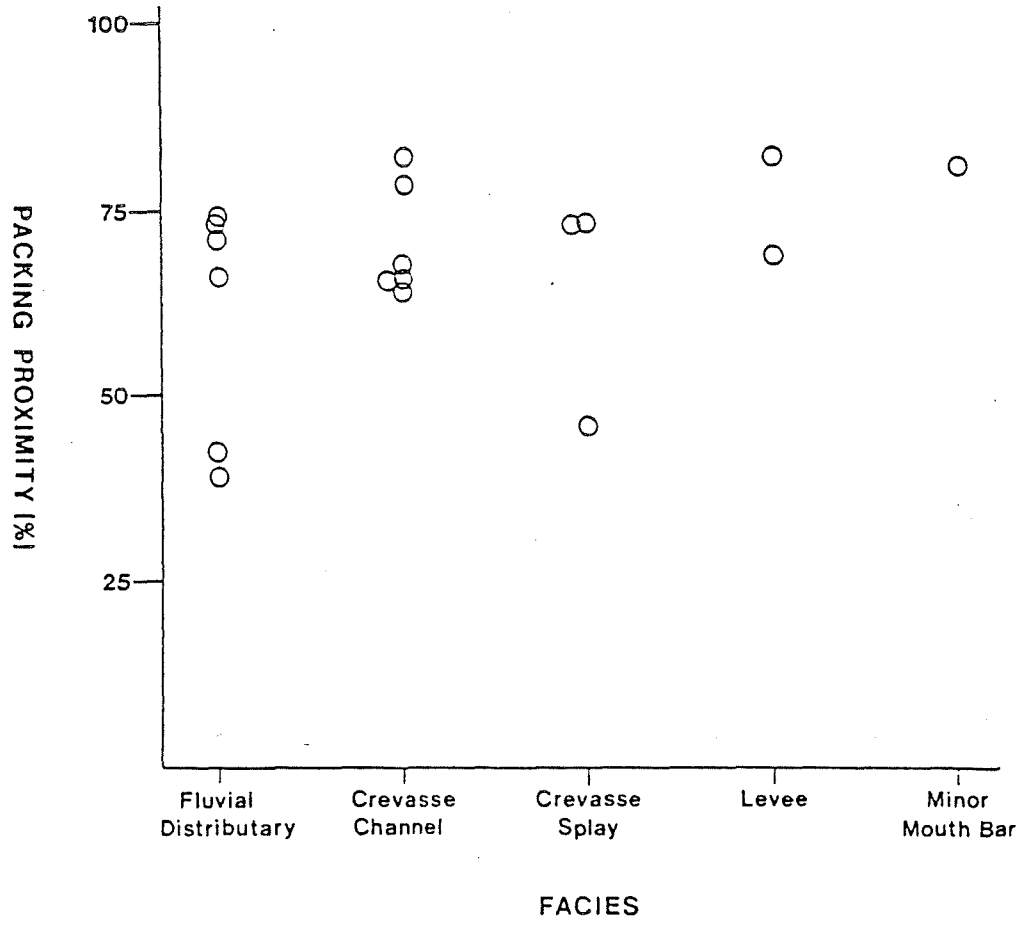

channel sands commonly exhibit abundant secondary porosity as a result of their relative susceptibility to pore fluid migration.

Thus, the diagenetic history of the sandstones in this study can be summed up in terms of porosity reduction followed by porosity production. Porosity was reduced by compaction and later reduced by pore-filling, authigenic kaolinite. Dissolution of cements and detrital grains produced abundant secondary porosity in medium-grained, channel sands.

SUGGESTIONS FOR FURTHER STUDY

Several questions arise after doing this study. Can a relationship between diagenetic properties and sandstone strengths be proven? Such a study could include qualitative study of porosity types (i.e., primary vs. secondary). Sample impregnation by stained epoxy would allow quantitative analysis of porosity in sandstones. Direct comparison of porosity results with engineering results for specific samples would provide the basis for predicting sandstone strengths.

Another study could be made to test the accuracy of facies interpretation based on vertical sequences in core. A field study of outcrop patterns in proximity to cores would provide a comparison of one and two dimensional patterns in the fluvio-deltaic sediments. Extensive fence diagrams and correlations of measured sections in a small area surrounding the core locality would give a three dimensional view and provide better stratigraphic control for facies interpretation of core sequences.

A comparative study of standard petrographic features with luminescent features using photomicrographs of sandstones is another suggestion. This blending of information could lead to a definitive understanding of the complex mineralogy and diagenetic history of these rocks. It would also provide better definition of luminescent properties of the various mineral species.

ACKNOWLEDGEMENTS

The author would like to thank his principal advisor, Dr. W.A. Pryor, and committee advisors, Dr. P.E. Potter and Dr. J.B. Maynard, for their critical advise throughout all stages of this thesis project. A special thanks goes to the Kentucky Geological Survey and Dr. N. Hester, James Cobb, and Patrick Gooding for their generous support of the research. The author is grateful to his colleagues--especially Stephen Waller and Ed Kryza--for the technical discussions and cooperation in field work. Thanks go to Amoco, especially the Word Processing staff, for the logistical support of the thesis preparation. Words cannot express the author's gratitude to his wife and family for the moral support and confidence building essential to the completion of this thesis.

BIBLIOGRAPHY

Acquaviva, D.J., 1978, Stratigraphy and depositional environments of a part of the lower Breathitt formation, Pennsylvanian; near Williamsburg, KY, Master's Thesis, University of Kentucky, 100p.

Almon, W.R., Fullerton, L.V., and Davies, D.K., 1976, Pore space reduction in Cretaceous sandstones through chemical precipitation of clay minerals, Jour. Sed. Pet., v.46, p.89-96.

Arkle, T., 1974, Stratigraphy of the Pennsylvanian and Permian systems of the central Appalachians, in Briggs, G., Carboniferous of the Southeastern United States, GSA Spec. Pap. no.148, p.5-29.

Baganz, B.P., Horne, J.C., and Ferm, J.C., 1975, Carboniferous and Recent Mississippi lower delta plains; a comparison, Gulf Coast Assoc. Geol. Soc. Trans., v.25, p.183-191.

Broussard, M.L. ed., 1975, Deltas, models for exploration, Houston Geol. Soc., Houston, TX, 555p.

Burns, L.K., and Ethridge, F.G., 1979, Petrology and diagenetic effects of lithic sandstones; Paleocene and Eocene Umpqua formation, southwest Oregon, in Scholle, P.A., and Schluger, P.R., Aspects of diagenesis, SEPM Spec. Pub. no.26, p.307-318.

Carrigy, M.A., and Mellon, G.B., 1964, Authigenic clay mineral cements in Cretaceous and Tertiary sandstones of Alberta, Jour. Sed. Pet., v.34, p.461-472.

Coleman, J.M., 1976, Deltas: processes of deposition and models for exploration, Continuing Ed. Pub. Comp., Inc., Champaign, IL, 102p.

Coleman, J.M., Gagliano, S.M., and Webb, J.E., 1964, Minor sedimentary structures in a prograding distributary, Marine Geol., v.1, p.240-258.

Coleman, J.M., and Gagliano, S.M., 1965, Sedimentary structures: Mississippi River deltaic plain, in Primary Sedimentary Structures and their Hydrodynamic Interpretation, SEPM Spec. Pub. no.12, p.133-148.

Coleman, J.M., and Prior, D.B., 1980, Deltaic sand bodies, AAPG Cont. Ed. Course Note Ser., no.15, 171p.

Cook, T.D., and Bally, A.W. eds., 1975, Stratigraphic atlas of North and Central America, Princeton, N.J., Princeton Univ. Press, 272p.

Davies,D.K., and Ethridge, F.G., 1975, Sandstone composition and depositional environment, AAPG Bull., v.59, p.239-264.

Davis, M.W., and Erlich, R., 1974, Late Paleozoic crustal composition and dynamics in southeastern United States, in Briggs, G., Carboniferous of the Southeastern United States, GSA Spec. Paper no.148, p.171-185.

Donaldson, A., 1974, Pennsylvanian sedimentation of central Appalachians, in Briggs, G., Carboniferous of the southeastern United States, GSA Spec. Paper no.148, p.47-79.

Elliot, T., 1974, Interdistributary bay sequences and their genesis, Sedimentology, v.21, p.611-622.

Elliot, T., 1978, Deltas, in Reading, H.G., 1978, Sedimentary environments and facies, New York, Elsevier, p.97-142.

Ferm, J.C., 1962, Petrology of some Pennsylvanian sedimentary rocks, Jour. Sed. Pet., v.32, p.104-123.

Ferm, J.C., 1970, Allegheny deltaic deposits, in Morgan, J.P., Sedimentation modern and ancient, SEPM Spec. Pub. no.15, p.246-256.

Ferm, J.C., 1974, Carboniferous environmental models in eastern United States and their significance, in Briggs, G., Carboniferous of the Southeastern United States, GSA Spec. Paper no.148, p.79-97.

Ferm, J.C., and Cavaroc, V.R., 1968, A nonmarine sedimentary model for the Allegheny rocks of West Virginia, GSA Spec. Paper no.106, p.1-19.

Ferm, J.C., and Melton, R.A., 1977, A guide to cored rocks in the Pocahontas Basin, Carol. Coal Group, Univ. S.C., Columbia, S.C., 90p.

Fisher, W.L., Brown, L.F., Scott, A.J., and McGowen, J.H., 1969, Delta systems in the exploration for oil and gas, Bur. Econ. Geol., Univ. Texas, Austin, 78p.

Flores, P.M., 1978, Petrographic differentiation of depositional environments of sandstones of the Pennsylvanian Breathitt formation, northeastern Kentucky and southwestern West Virginia, Jour. Res. U.S. Geol. Surv., v.6, no.5, p.593-602.

Gardner, T.W., 1977, Paleohydrology, Paleomorphology, and depositional environments of some fluvial sandstones of Pennsylvanian age in eastern Kentucky, Ph.D. Thesis, Univ. of Cincinnati, 216p.

Garrison, R.K., 1977, Paleoenvironmental analysis of the Lost Creek Limestone and associated facies: marine and nonmarine, M.S. Thesis, Univ. of Cincinnati, 338p.

Glaister, R.P., and Nelson, H.W., 1974, Grain size distribution as an aid in facies identification, Bull. Can. Pet. Geol., v.22, p.203-240.

Gooding, Patrick J., 1980, Catalog of well samples, cores, and auger samples on file at Kentucky Geol. Surv., Inf. Circ., Kentucky Geol. Surv., no.3, 408p.

Greensmith, J.T., 1957, Lithology, with particular reference to cementation, of upper Carboniferous sandstones in northern Derbyshire, England, Jour. Sed. Pet., v.5, no.4, p.405-416.

Hawkins, P.J., 1978, Relationship between diagenesis, porosity reduction, and oil emplacement in late Carboniferous sandstone reservoirs, Bothamsall Oilfield, east Midlands, Jour. Geol. Soc. Lond., v.135, p.7-24.

Hayes, J.B., 1979, Sandstone diagenesis-the hole truth, in Scholle, P.A., and Schluger, P.R., Aspects of Diagenesis, SEPM Spec. Pub. no.26, p.127-140.

Heald, M.T., and Renton, J.J., 1966, Experimental study of sandstone cementation, Jour. Sed. Pet., v.36, p.977-991.

Hinrichs, E.N., 1978, Geologic map of the Noble quadrangle, eastern Kentucky, U.S. Geol. Surv., GQ-1476.

Hoholick, J.D., Metarko, T.A., and Potter, P.E., 1982, Weighted contact packing of quartz arenites, Mtn. Geol., v.19, no.3., p.79-82.

Ho-Shing Yu, 1979, Three aspects of sandstone diagenesis: compaction and cementation of quartz arenites and chemical changes in graywackes, Ph.D. Diss., Univ. of Cincinnati, Cinti., OH.

Horne, J.C., 1979, Criteria for the recognition of depositional environments, in Ferm, J.C., Carboniferous depositional environments in the Appalachian region, Univ. S.C. Dep. Geol., Carol. Coal Group, P.295-300.

Horne, J.C., and Ferm, J.C., 1976a, Sandstone models from Appalachian Carboniferous deltas, AAPG abst., v.60, p.680.

Horne, J.C., and Ferm, J.C., 1976b, Carboniferous depositional environments in the Pocahontas Basin, eastern Kentucky and southern West Virginia; a field guide, Univ. of S.C., Columbia, S.C., 129p.

Horne, J.C., and Ferm, J.C., and Caruccio, F.T. et al, 1978, Depositional models in coal exploration and mine planning in the Appalachian region, AAPG Bull., v.62, p.2379-2411.

Huddle, J.W., Lyons, E.J., Smith, H.L., and Ferm, J.C., 1963, Coal. reserves of eastern Kentucky, U.S. Geol. Surv. Bull., no.1120, 247p.

James, C.W., Mack, Greg H., and Suttner, L.J., 1981, Relative alteration of microcline and sodic plagioclase in semi-arid and humid climates, Jour. Sed. Pet., v.51, p.151-164.

Kahn, J.S., 1956, The analysis and distribution of the properties of packing in sand-size sediments, Jour. Geol., vol.64, p.385-395, 578-606.

Keller, W.D., 1981, The sedimentology of flint clay, Jour. Sed. Pet., v.51, p.233-244.

Klovan, J.E., and Billings, G.K., 1967, Classification of geological samples by discriminant-function analysis, Bull. Can. Pet. Geol., v.15, p.313-330.

Kryza, E., (in progress), Composition and slake-durability of Breathitt mudrocks, M.S. Thesis, Univ. of Cincinnati, Cinti., OH.

LeBlanc, R.J., 1975, Significant studies of modern and ancient deltaic sediments, in Broussard, M.L., Delta models for exploration, Houston Geol. Soc., p.13-86.

Lee, K.Y., Danilchik, W., and Rice, C.L., 1977, Geologic map of the Guage quadrangle, Breathitt and Magoffin Counties, Kentucky, U.S. Geol. Surv., GQ-1416.

Meade, R.H., 1966, Factors influencing the early stages of the compaction of clays and sands-review, Jour. Sed. Pet., v.36, p.1085-1101.

Miall, A,D., 1979, Deltas, in Walker, R.G. ed., Facies models, Geoscience Can. Rep. Ser. no.1, p.43-56.

Moore, R.C. et al, 1944, Correlation of Pennsylvanian formations of North America, Geol. Soc. Am. Bull., v.55, p.657-706.

Morgan, J.P., and Shaver, R.H. eds., 1970, Deltaic sedimentation modern and ancient, SEPM Spec. Pub. no.15, 312p.

Pettijohn, F.J., Potter, P.E., and Siever, R., 1973, Sand and sandstone, New York, Springer-Verlag, 618p.

Ping, R.G., 1975, Log of core from a drill hole in southeastern Kentucky, U.S. Geol. Surv. Open-file Rept., no.75-563.

Ping, R.G., 1977, Geologic map of the Cutshin quadrangle, Leslie County, Kentucky, U.S. Geol. Surv., GQ-1424.

Pittman, E.D., 1972, Diagenesis of quartz in sandstones as revealed by scanning electron microscopy, Jour. Sed. Pet., v.42, p.507-519.

Potter, P.E., and Glass, H.D., 1958, Petrology and sedimentation of Pennsylvanian sediments in southern Illinois: a vertical profile, IL Geol. Surv. Dept. of Inv., no.204, 60p.

Pryor, W.A., Fulton, K.J., and Harrison, L.K., 1976, Subsurface stratigraphy and depositional environment of several Holocene Rio Grande deltas, Corpus Christi Geol. Soc., v.28, p.4-11.

Pryor, W.A., and Sable, E.G., 1974, Carboniferous of the eastern Interior Basin, GSA Spec. Pap. no.148, p.281-313.

Reading, H.G. ed., 1978, Sedimentary environments and facies, New York, Elsevier, 447p.

Schmidt, V., and McDonald, D.A., 1979, Texture and recognition of secondary porosity in sandstones, in Scholle, P.A., and Schluger, P.R., Aspects of diagenesis, SEPM Spec. Pub. no.26, p.209-226.

Schmidt, V., and McDonald, D.A., 1976b, The role of secondary porosity in the course of sandstone diagenesis, in Scholle, P.A., and Schluger, P.R., SEPM Spec. Pub. no.26, p.175-208.

Scholle, P.A., 1979, A color illustrated huide to constituents, textures, cements, and porosities of sandstones and associated rocks, AAPG Mem. no.28, 201p.

Shelton, J.W., 1964, Authigenic kaolinite in sandstones, Jour. Sed. Pet., v.34, p.102-111.

Short, M.R., 1979, Early Pennsylvanian Bay-fill environments, Breathitt formation, in Ettensohn, F.R., Carboniferous geology from the Appalachian Basin to the Illinois Basin through eastern Ohio and Kentucky, Univ. of Kentucky, Am. Geol. Inst., p.115-119.

Sippel, R.F., 1968, Sandstone petrology, evidence from luminescence petrography, Jour. Sed. Pet., v.38, p.530-554.

Walker, R.G. ed., 1979, Facies models, Geoscience Can. Repr. Ser., no.1, 211p.

Wanless, H.R., 1939, Pennsylvanian correlations in the eastern Interior and Appalachian coal fields, GSA Spec. Paper no.17, 130p.

Wanless, H.R., 1970, Late Paleozoic deltas in the central and eastern United States, SEPM Spec. Pub. no.15, p.215-246.

Whalley, W.B., 1978, Scanning electron microscopy in the study of sediments, Geo. Abst. Ltd., Norwich, England, 414p.

Wilson, M.D., and Pittman, E.D., 1977, Authigenic clays in sandstones: recognition and influence on reservoir properties and paleo-environmental analysis, Jour. Sed. Pet., v.47, p.3-31.

Zinkernagel, V., 1979, Cathodoluminescence of quartz and its application to sandstone petrology, Contributions to sedimentology, no.8, Stuttgart, Elsevier, 69p.

APPENDIX I

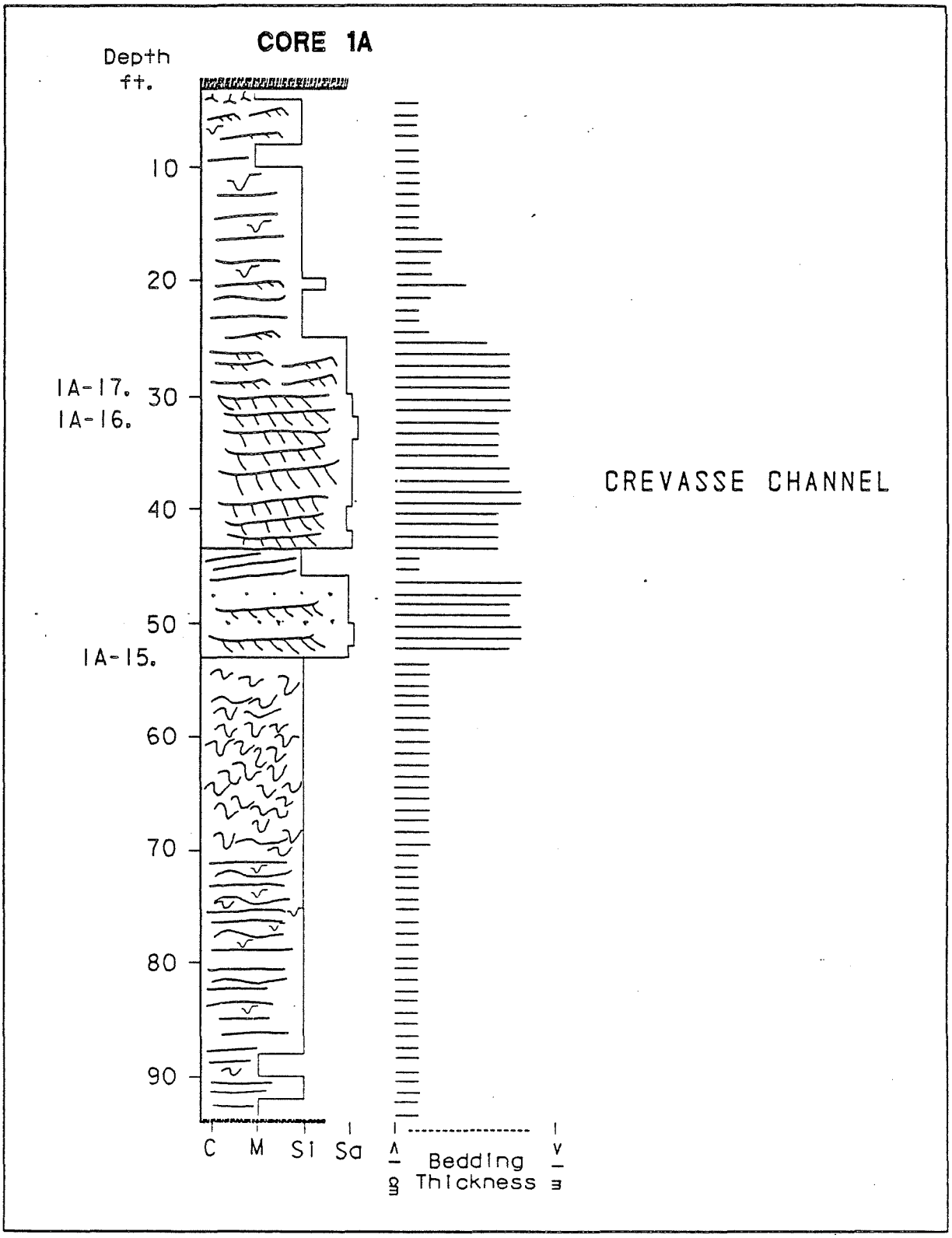
CORE 1A
Depth
ft.
10
20
30
40
50
60
70
80
90
1A-17.
1A-16.
1A-15.
CREVASSE CHANNEL
C
M
Si
Sa
Bedding
Thickness

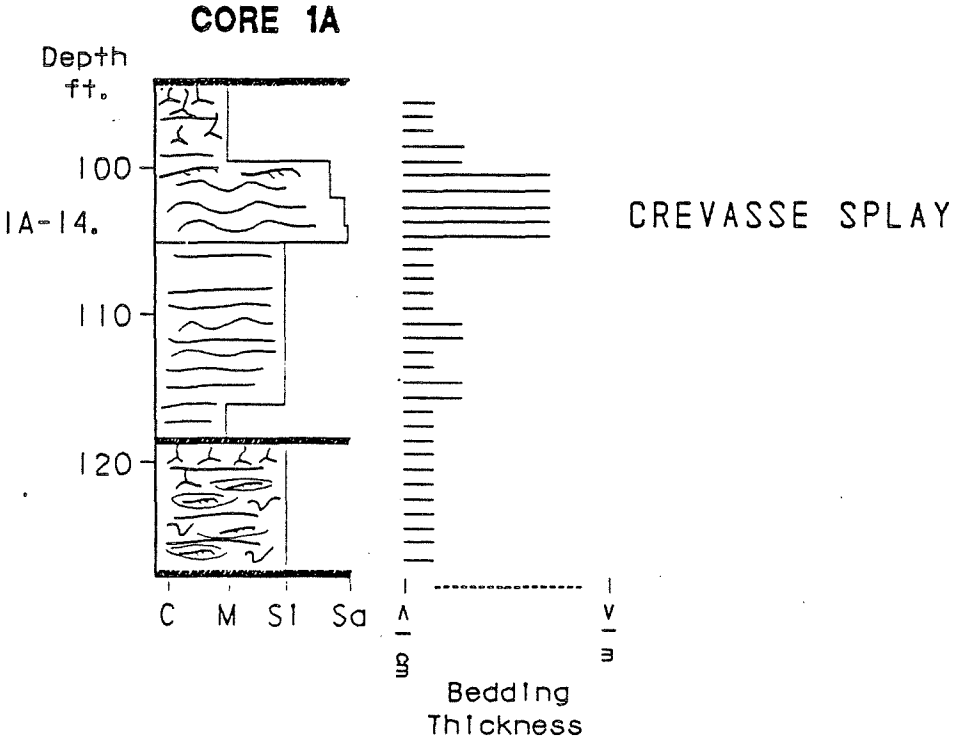
CORE 1A
Depth
ft.
100
110
120
1A-14.
C
M
Sl
Sa
Bedding
Thickness
CREVASSE SPLAY

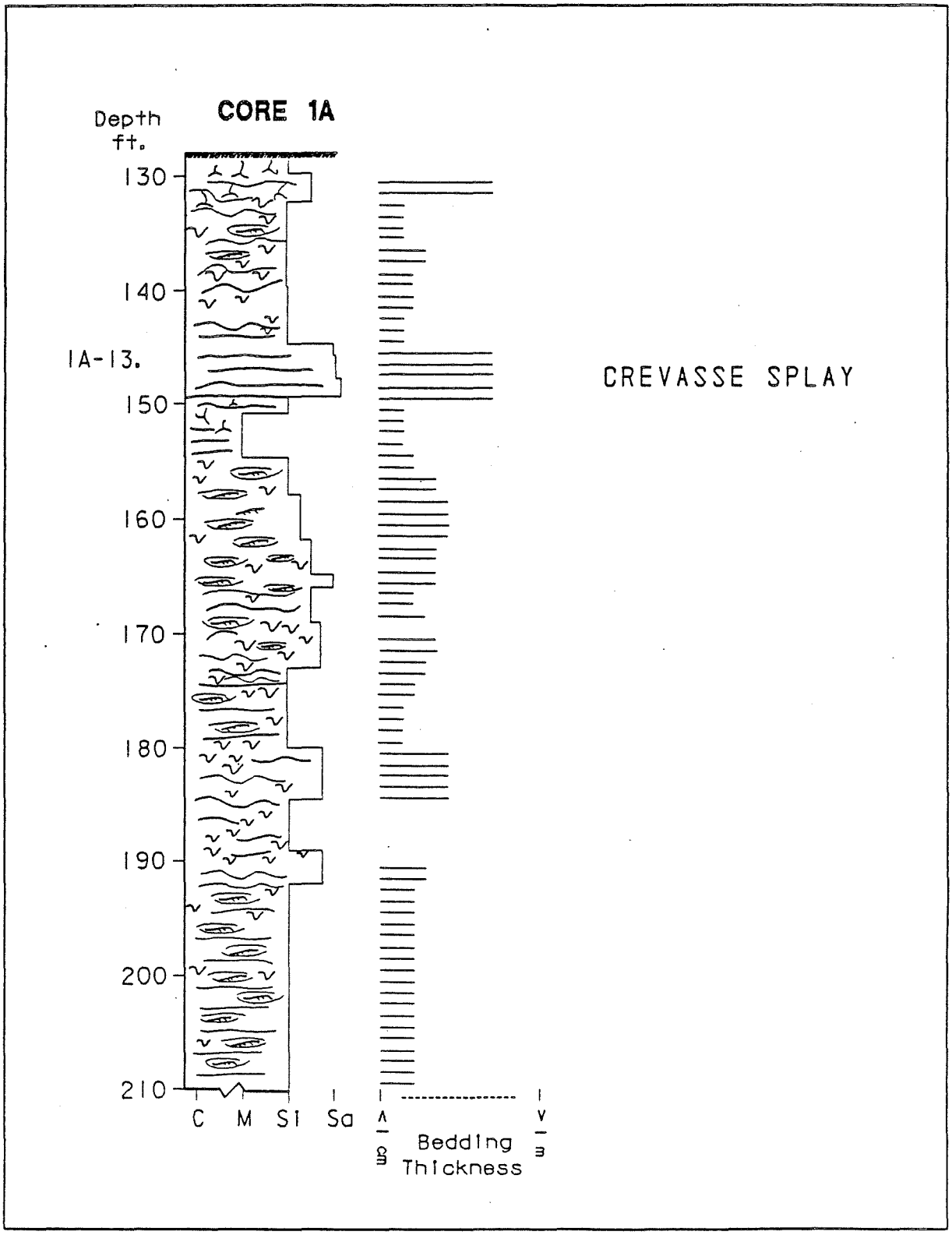
CORE 1A
Depth
ft.
130
140
150
160
170
180
190
200
210
1A-13.
C
M
Sl
Sa
Bedding
Thickness
CREVASSE SPLAY

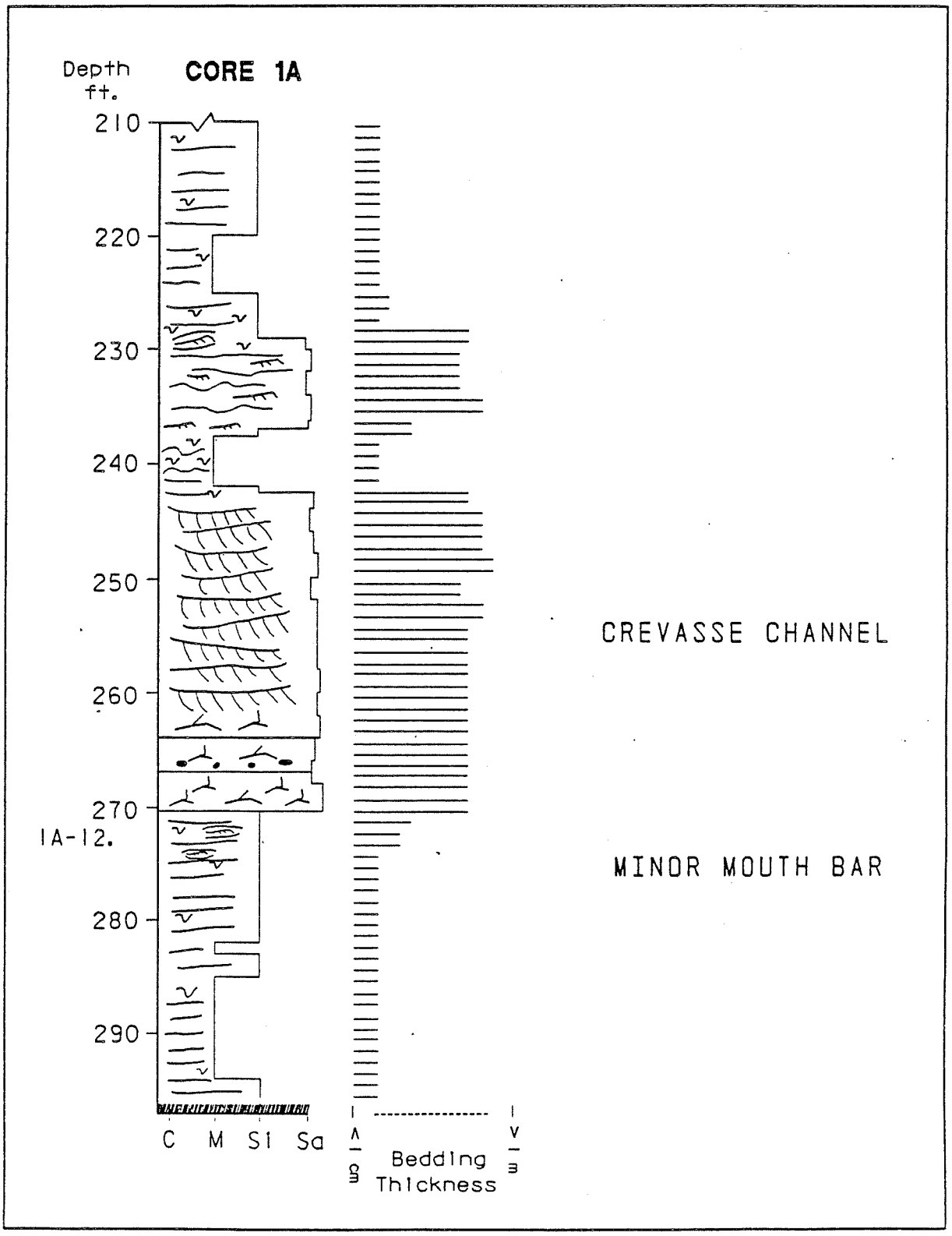
Depth
ft.
CORE 1A
210
220
230
240
250
260
270
280
290
1A-12.
C
M
Si
Sa
Bedding
Thickness
CREVASSE CHANNEL
MINOR MOUTH BAR

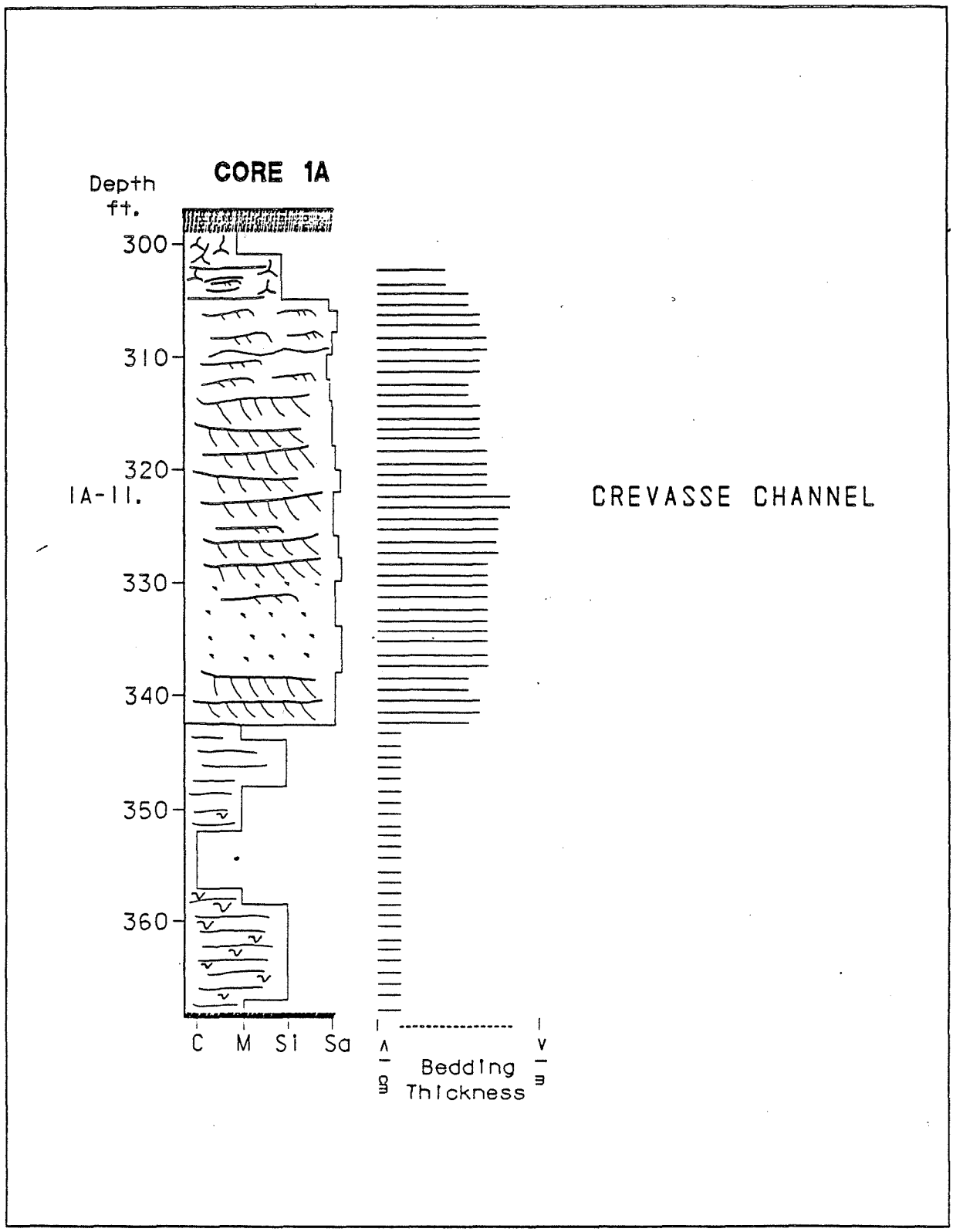
CORE 1A
Depth
ft.
300
310
320
330
340
350
360
1A-11.
C
M
Si
Sa
Bedding
Thickness
CREVASSE CHANNEL

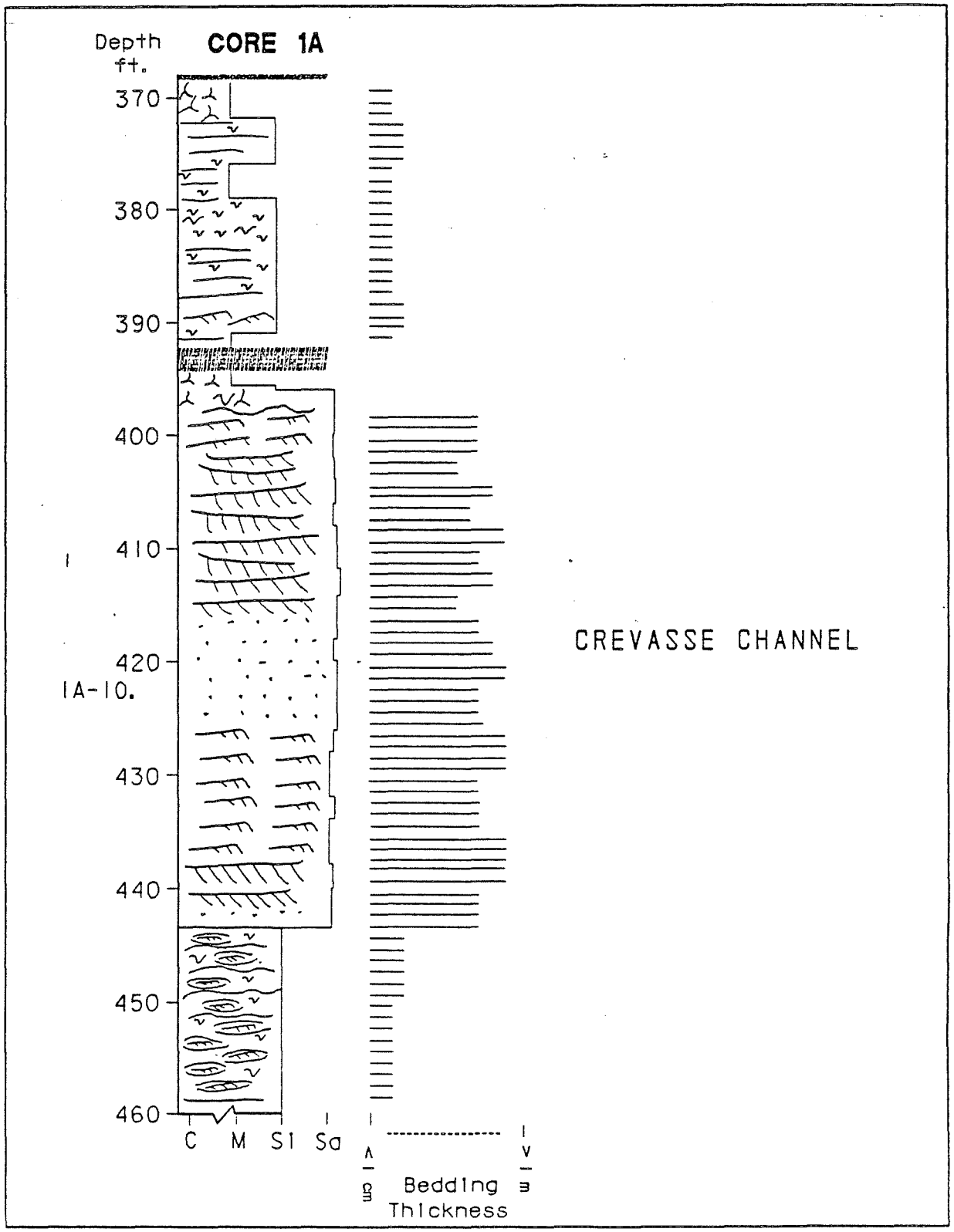
Depth
ft.
CORE 1A
370
380
390
400
410
420
430
440
450
460
C
M
Sl
Sa
Bedding
Thickness
CREVASSE CHANNEL

1A-10.

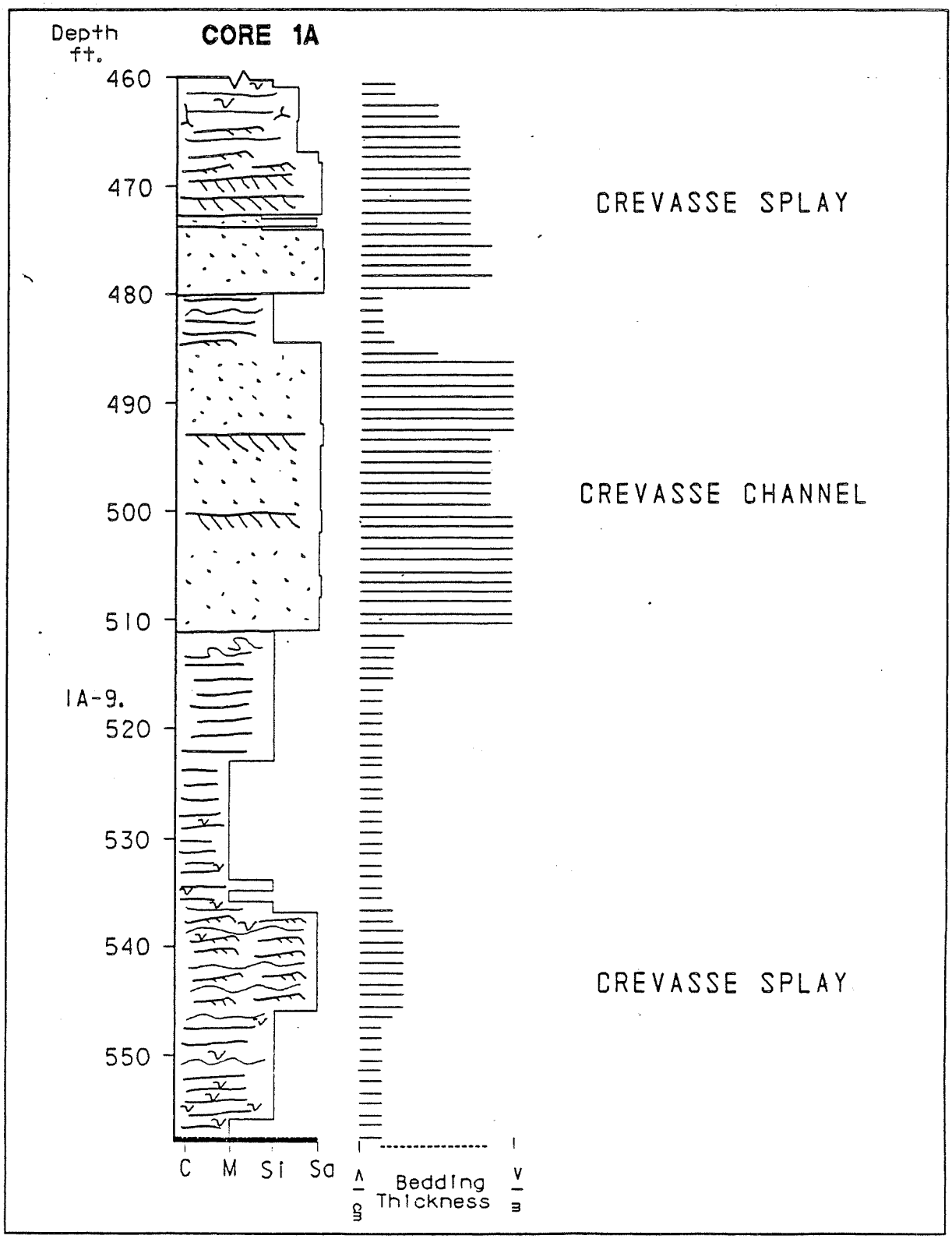
Depth
ft.
CORE 1A
460
470
480
490
500
510
520
530
540
550
CREVASSE SPLAY
CREVASSE CHANNEL
CREVASSE SPLAY
1A-9.
C
M
Si
Sa
Bedding
Thickness

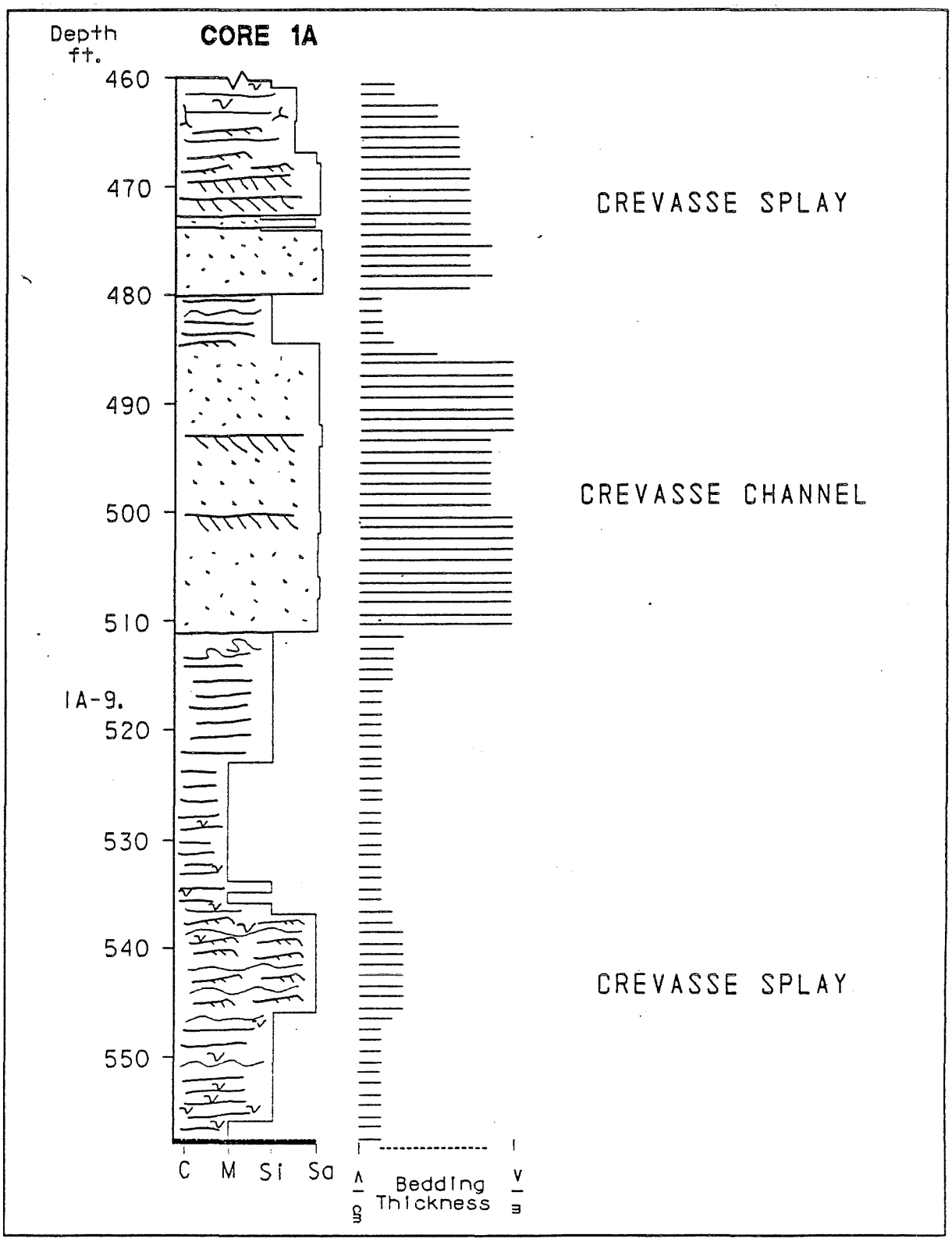
Depth
ft.
CORE 1A
460
470
480
490
500
510
520
530
540
550
1A-9.
CREVASSE SPLAY
CREVASSE CHANNEL
CREVASSE SPLAY
C
M
Si
Sa
Bedding Thickness

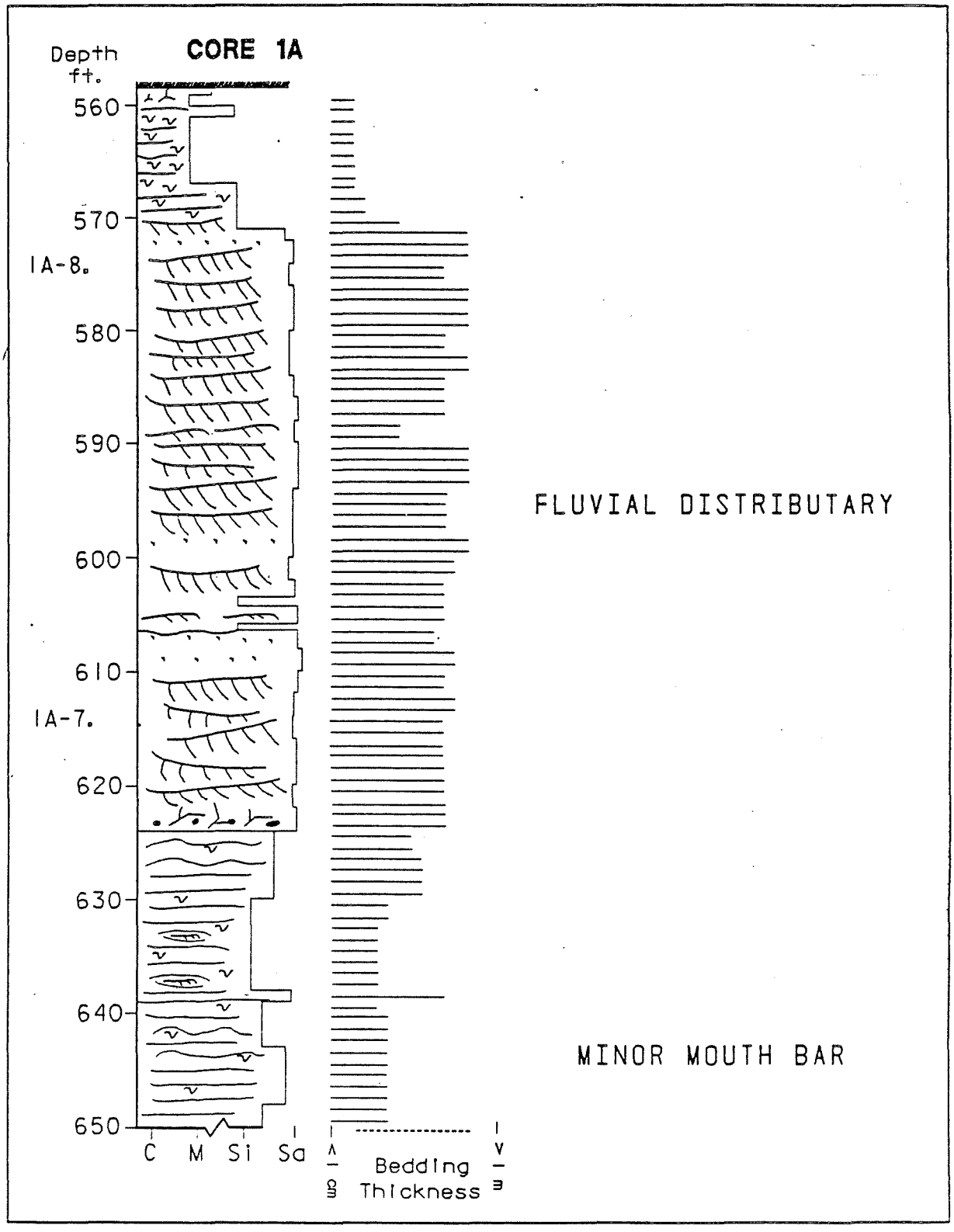
CORE 1A
Depth
ft.
560
570
1A-8.
580
590
600
610
1A-7.
620
630
640
650
C
M
Si
Sa
Bedding
Thickness
FLUVIAL DISTRIBUTARY
MINOR MOUTH BAR

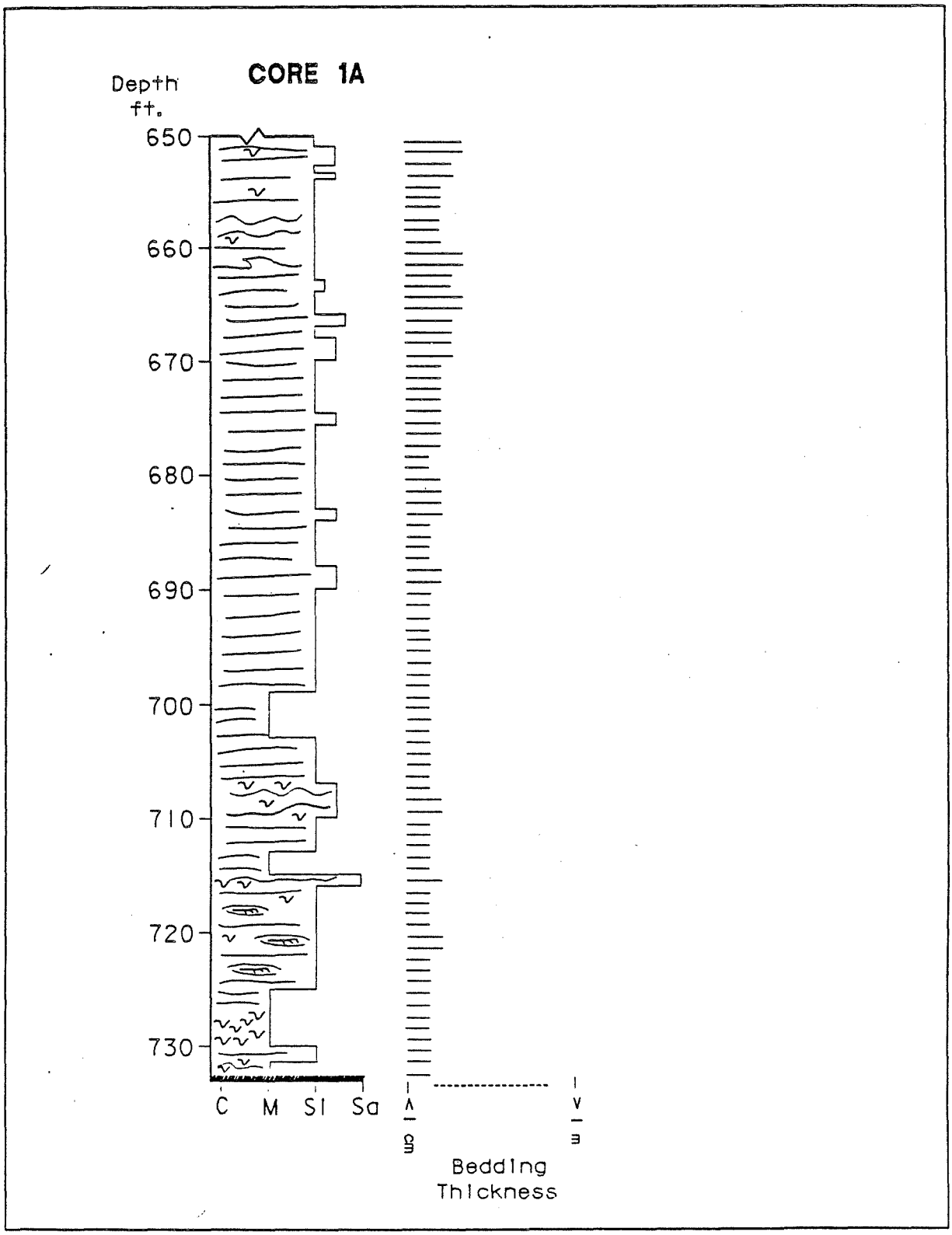
CORE 1A
Depth
ft.
650
660
670
680
690
700
710
720
730
C
M
Sl
Sa
Bedding
Thickness

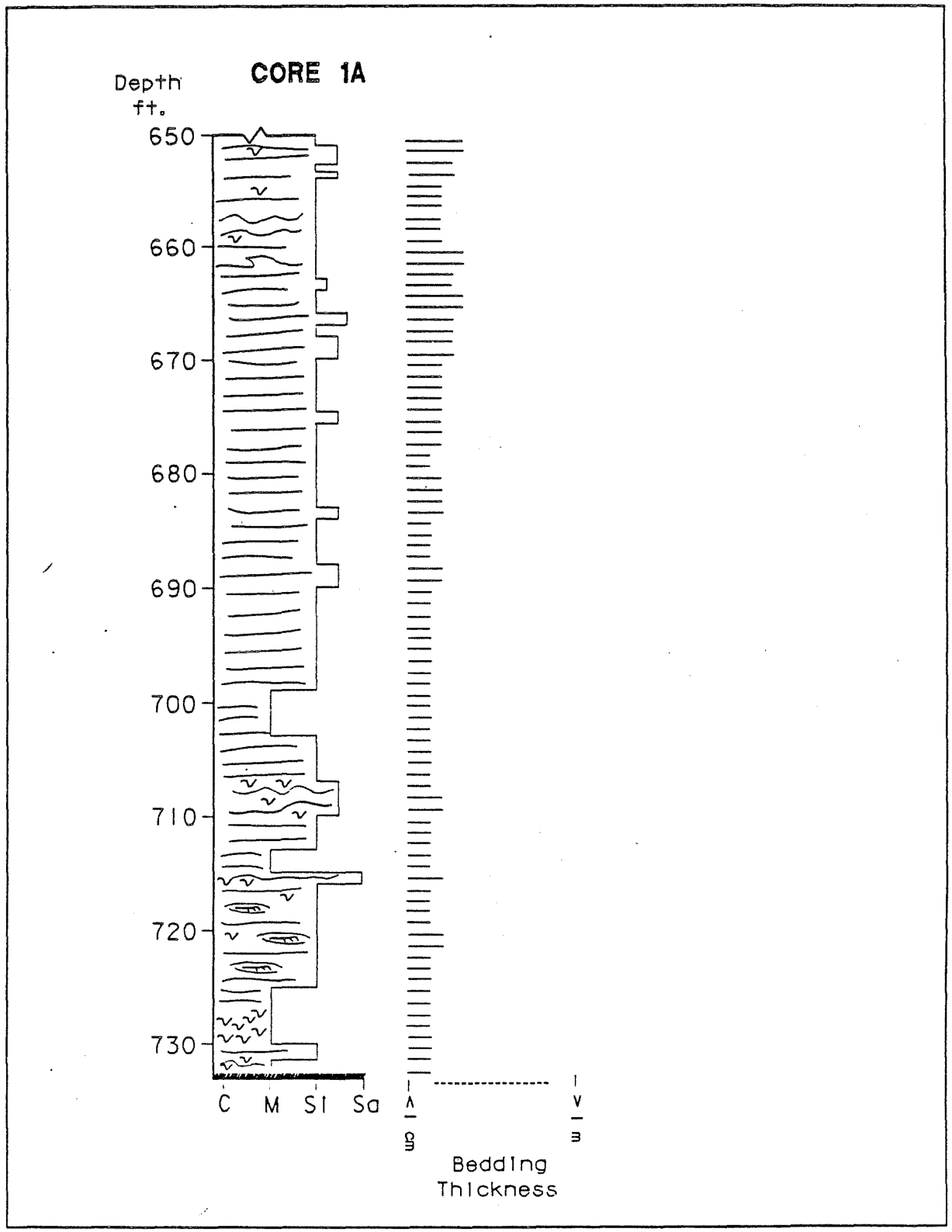
CORE 1A
Depth
ft.
650
660
670
680
690
700
710
720
730
C
M
Sl
Sa
cm
m
Bedding
Thickness

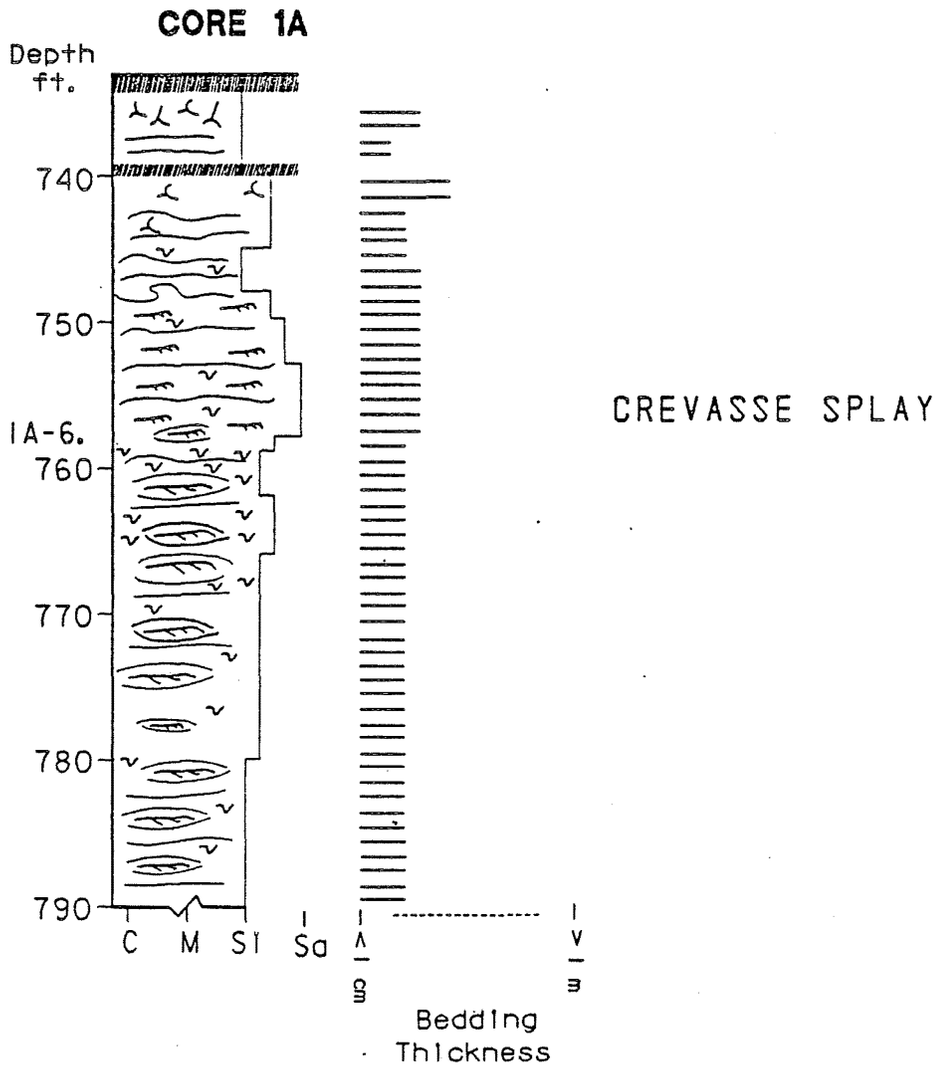
CORE 1A
Depth
ft.
740
750
1A-6.
760
770
780
790
C
M
Sl
Sa
Bedding
Thickness
CREVASSE SPLAY

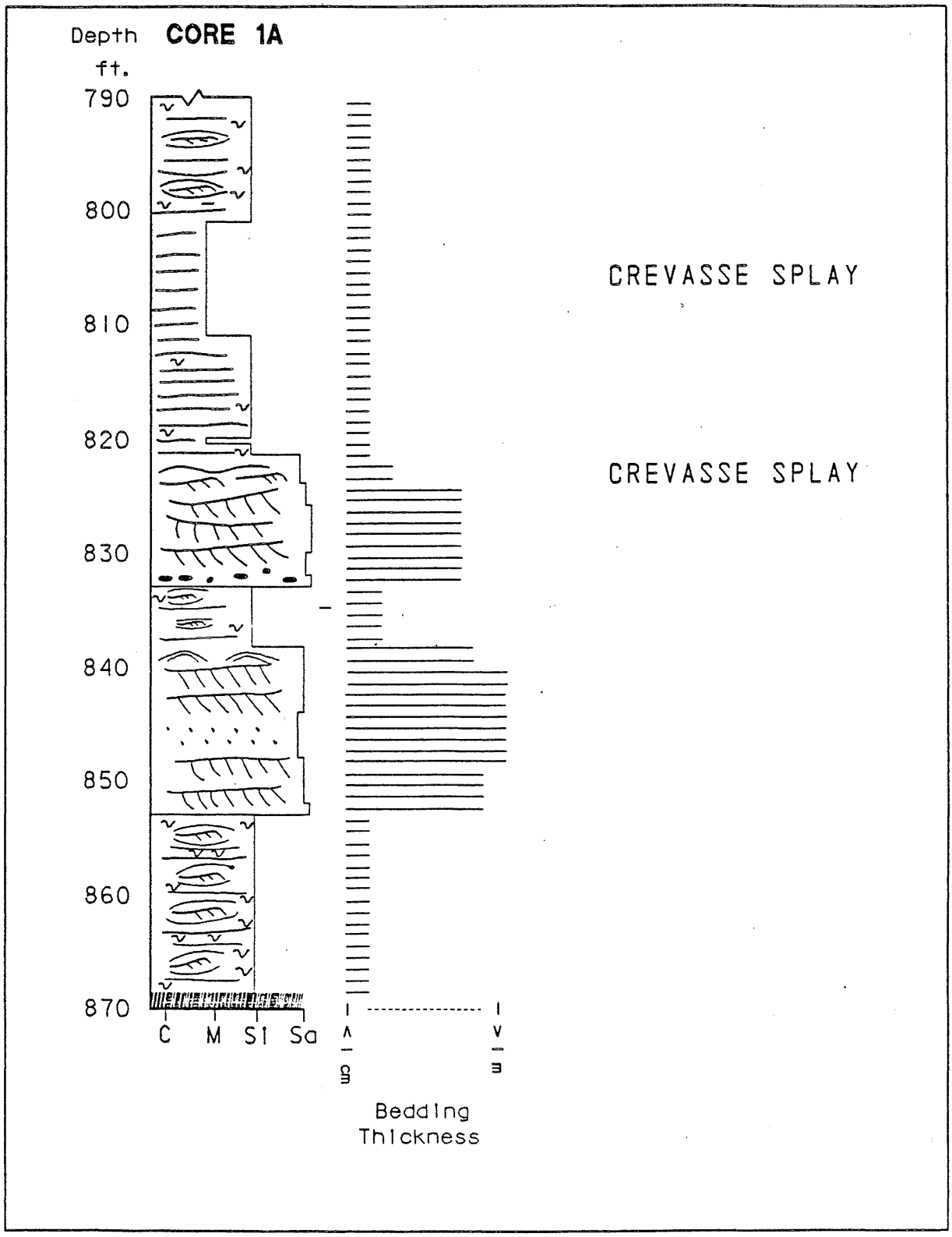
Depth
ft.
CORE 1A
790
800
810
820
830
840
850
860
870
C
M
Sl
Sa
cm
m
Bedding
Thickness
CREVASSE SPLAY
CREVASSE SPLAY

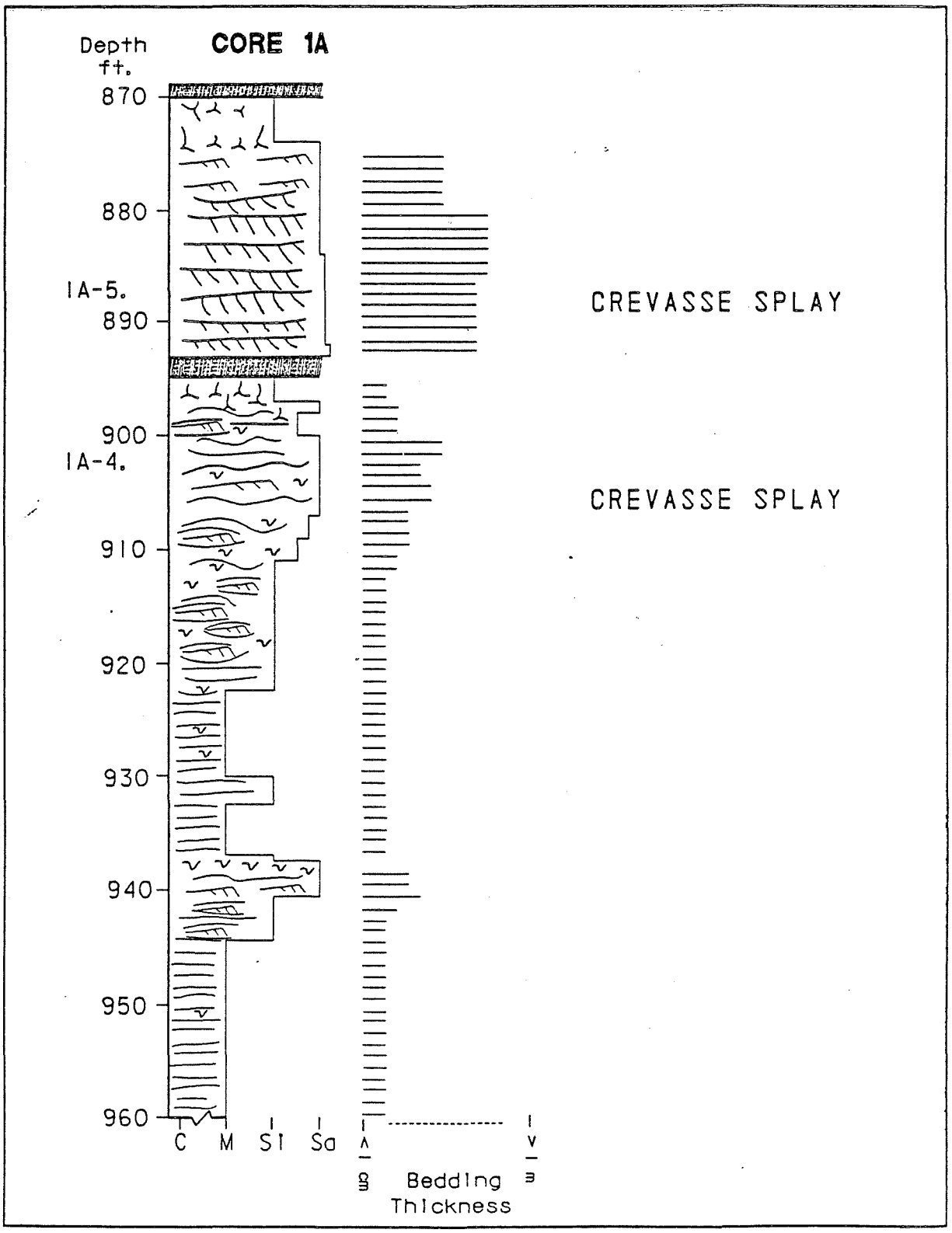
Depth
ft.
CORE 1A
870
880
1A-5.
890
900
1A-4.
910
920
930
940
950
960
CREVASSE SPLAY
CREVASSE SPLAY
C
M
Sl
Sa
Bedding
Thickness

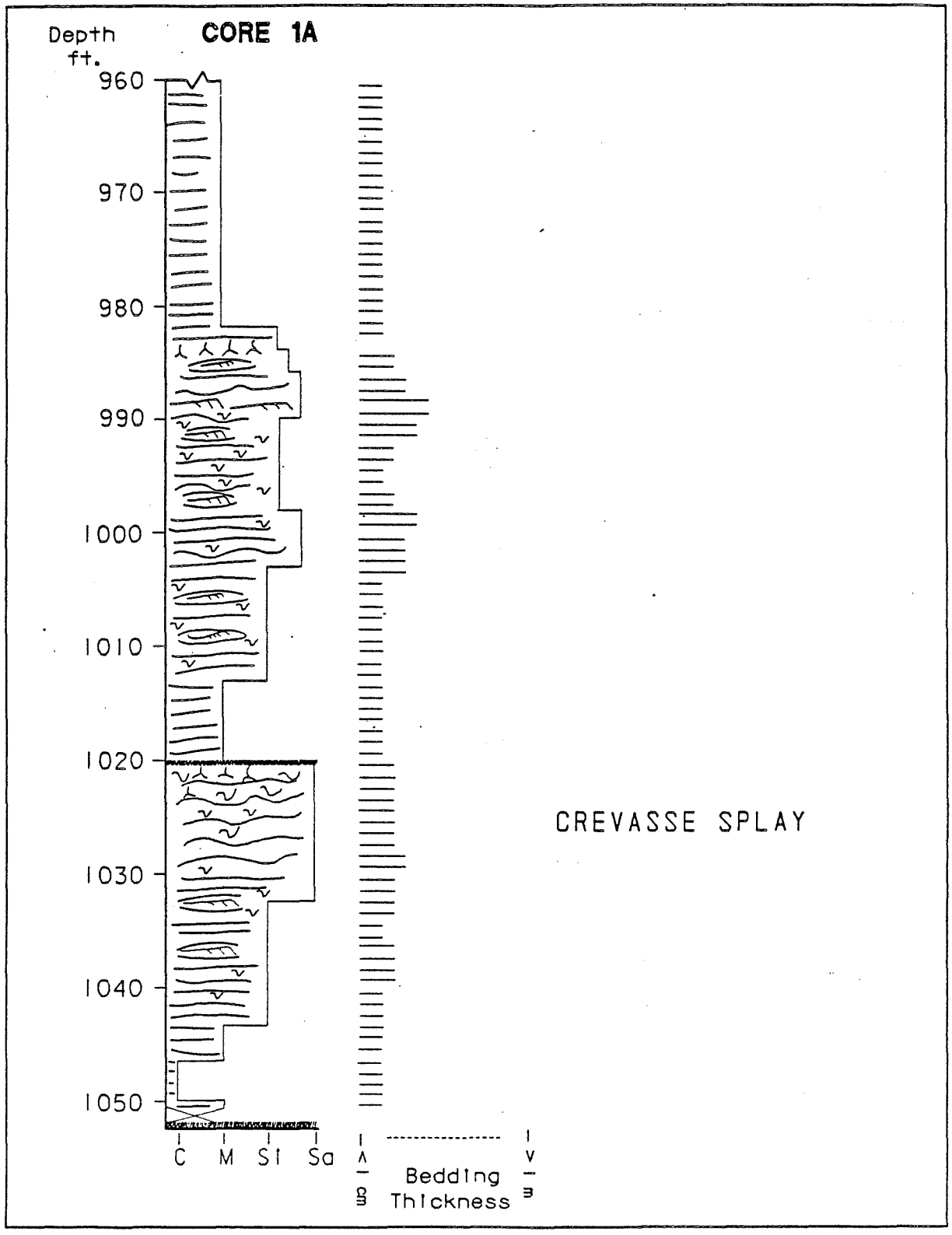
CORE 1A
Depth
ft.
960
970
980
990
1000
1010
1020
1030
1040
1050
C
M
Si
Sa
Bedding
Thickness
CREVASSE SPLAY

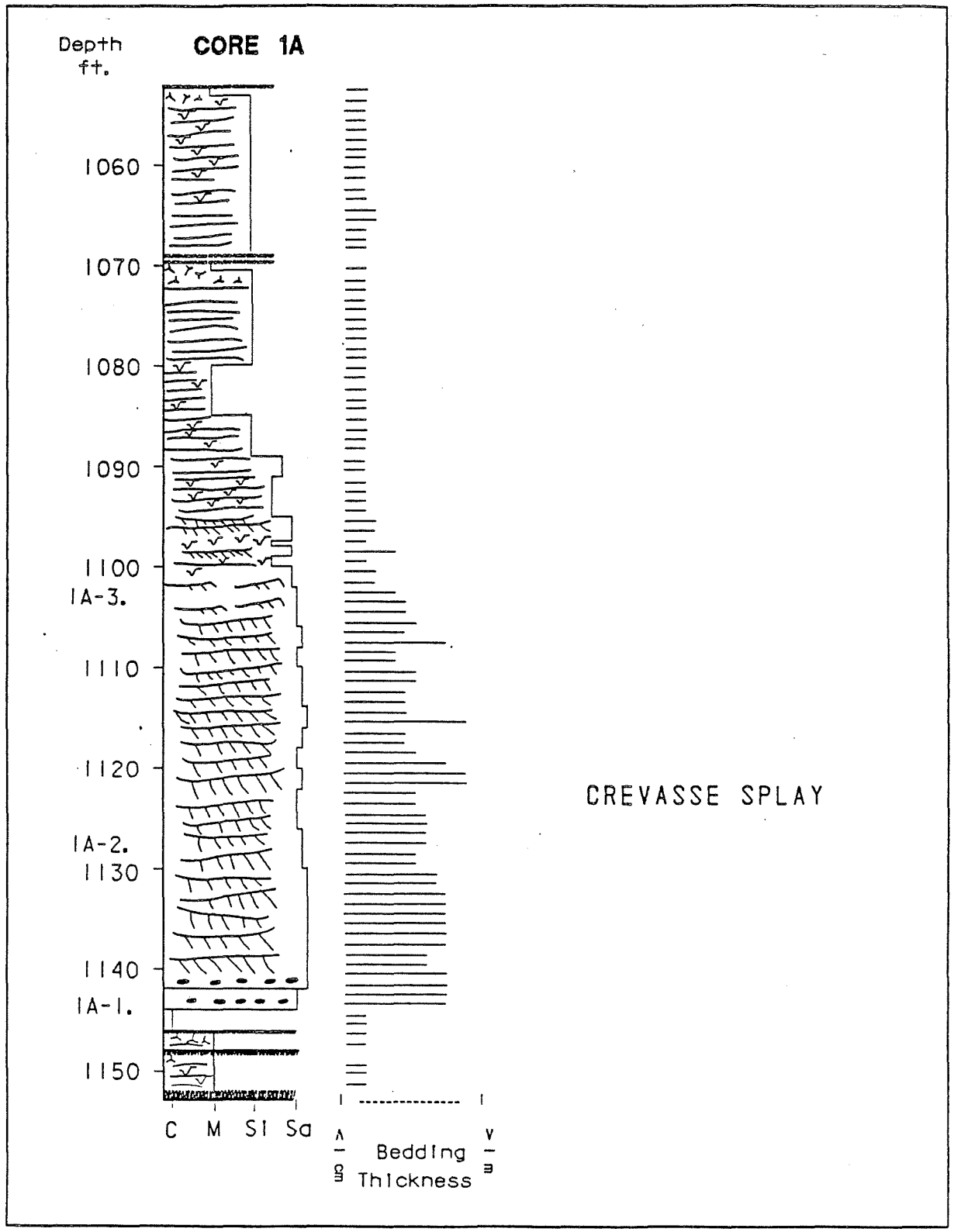
Depth
ft.
CORE 1A
1060
1070
1080
1090
1100
1A-3.
1110
1120
1A-2.
1130
1140
1A-1.
1150
C
M
Sl
Sa
Bedding
Thickness
CREVASSE SPLAY

APPENDIX II

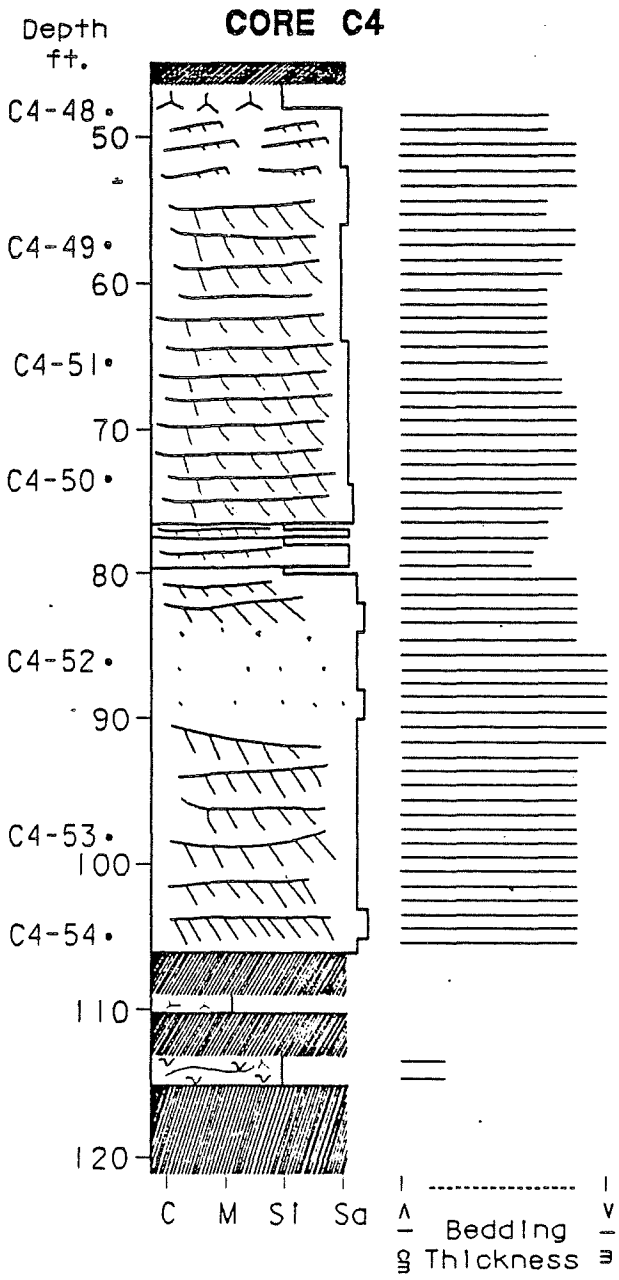

FLUVIAL DISTRIBUTARY

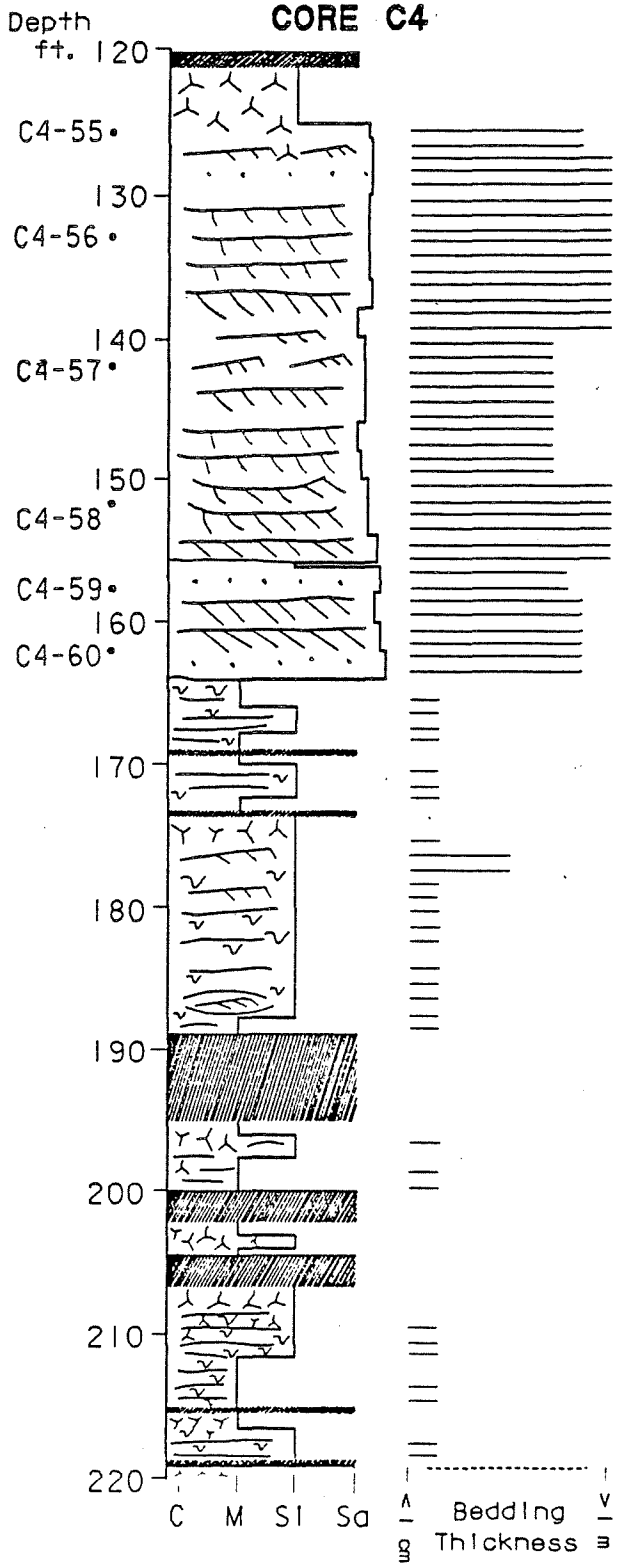
CORE C4
Depth
ft.
120
130
140
150
160
170
180
190
200
210
220
C4-55
C4-56
C4-57
C4-58
C4-59
C4-60
C
M
Sl
Sa
Bedding
Thickness
CREVASSE CHANNEL

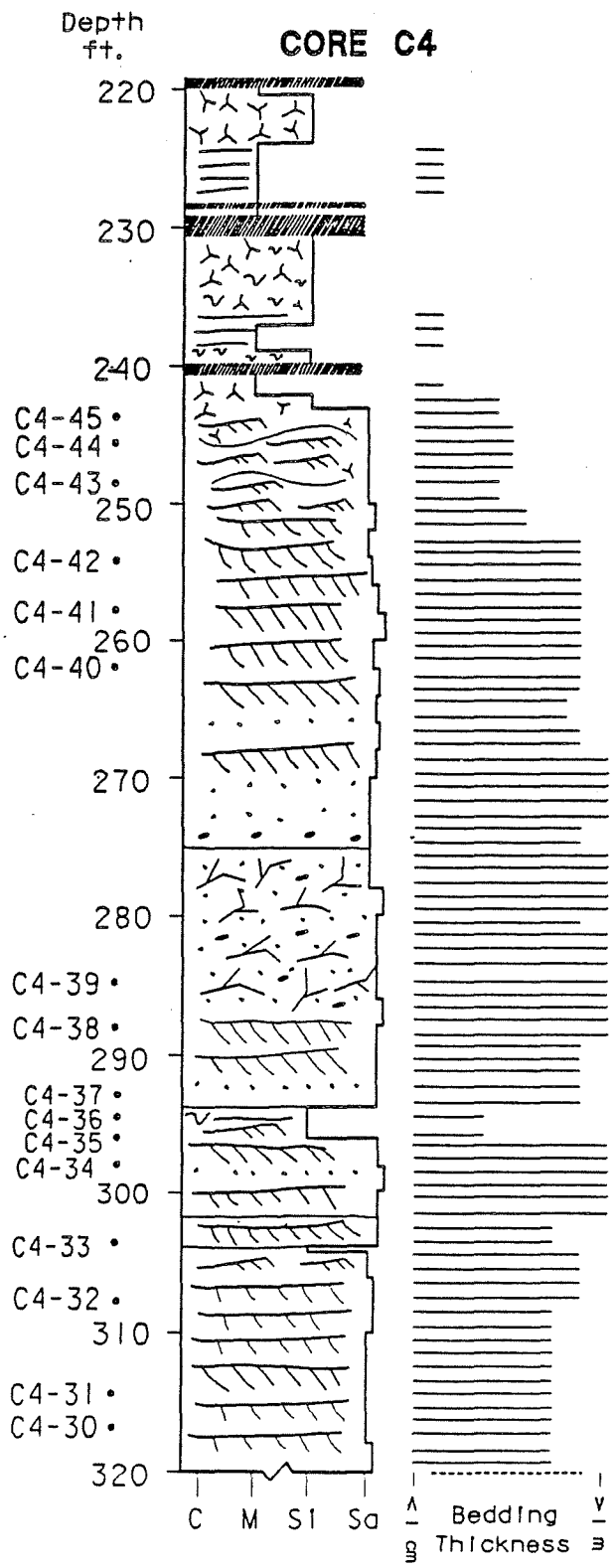

FLUVIAL DISTRIBUTARY

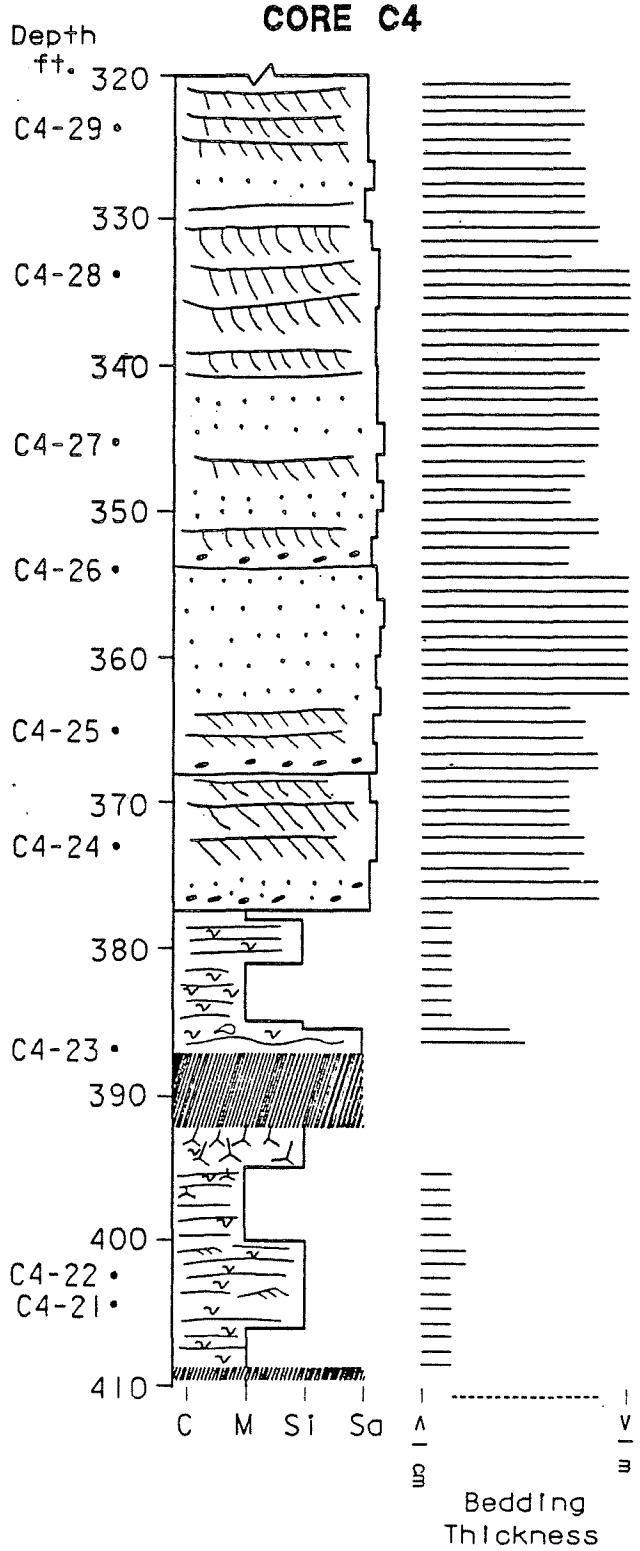

FLUVIAL DISTRIBUTARY

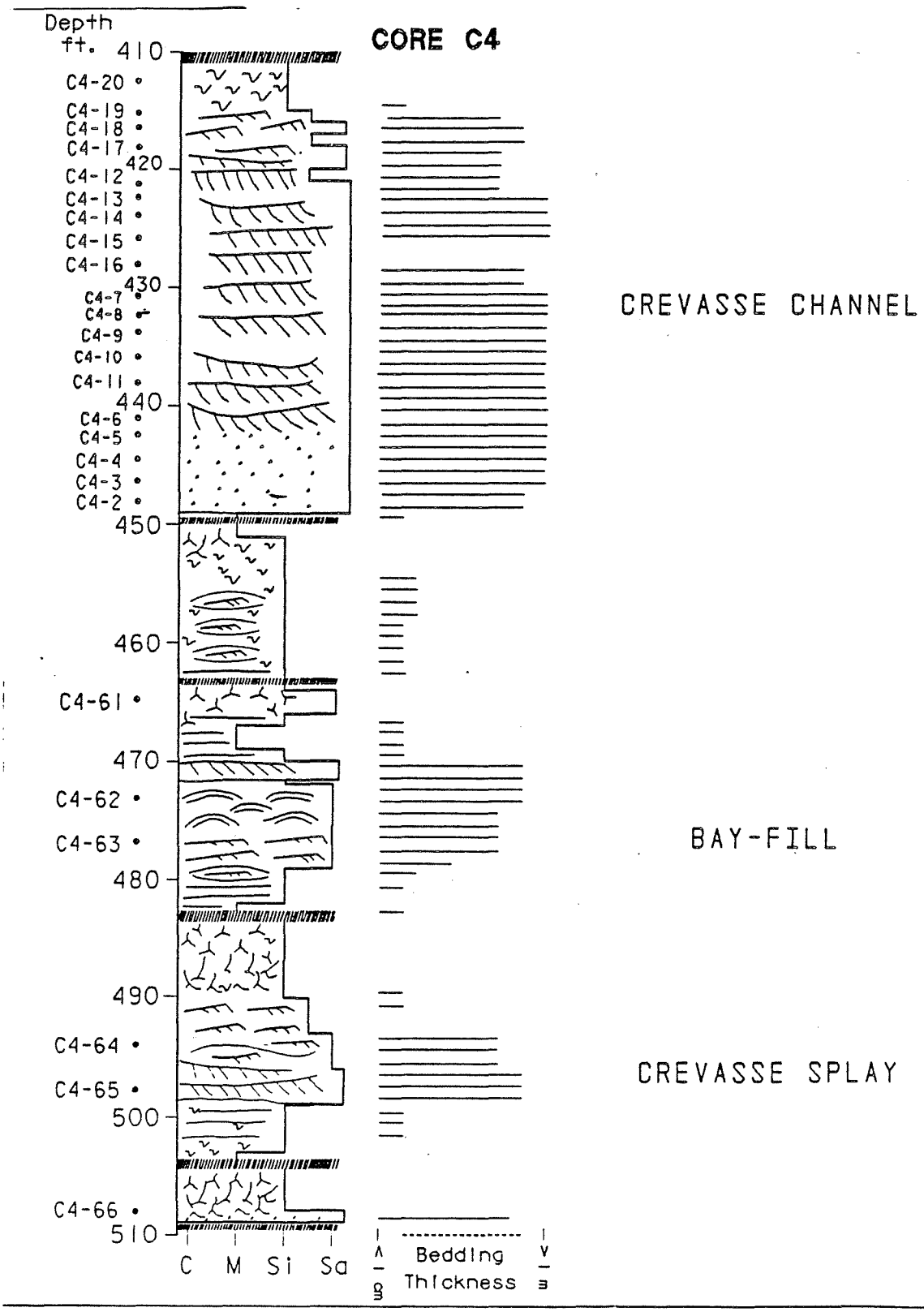
CORE C4
Depth
ft.
410
420
430
440
450
460
470
480
490
500
510
C4-20
C4-19
C4-18
C4-17
C4-12
C4-13
C4-14
C4-15
C4-16
C4-7
C4-8
C4-9
C4-10
C4-11
C4-6
C4-5
C4-4
C4-3
C4-2
C4-61
C4-62
C4-63
C4-64
C4-65
C4-66
C M Si Sa
Bedding Thickness
CREVASSE CHANNEL
BAY-FILL
CREVASSE SPLAY

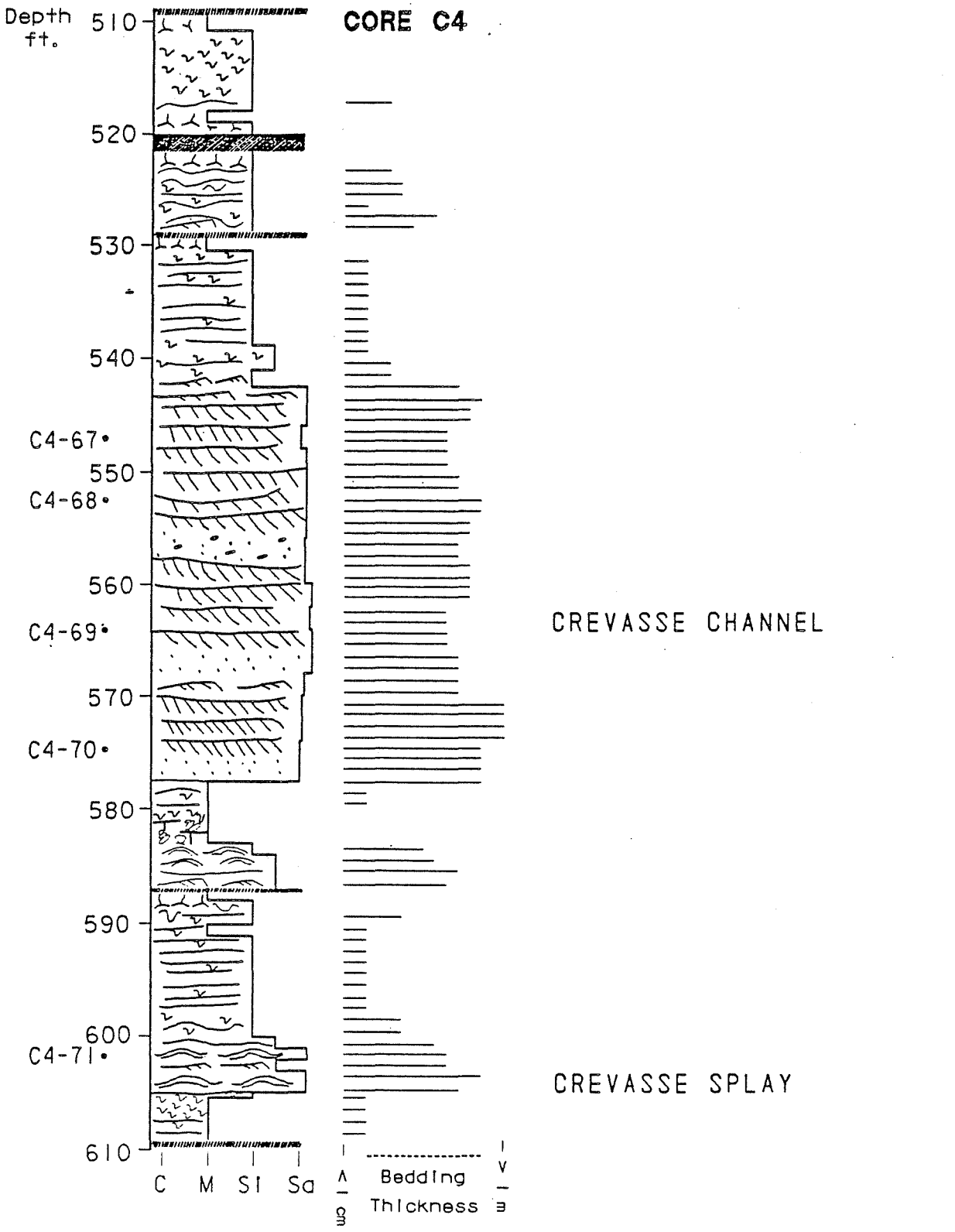
Depth ft.
510
520
530
540
C4-67
550
C4-68
560
C4-69
570
C4-70
580
590
600
C4-71
610
CORE C4
C
M
SI
Sa
Bedding Thickness
cm
m
CREVASSE CHANNEL
CREVASSE SPLAY

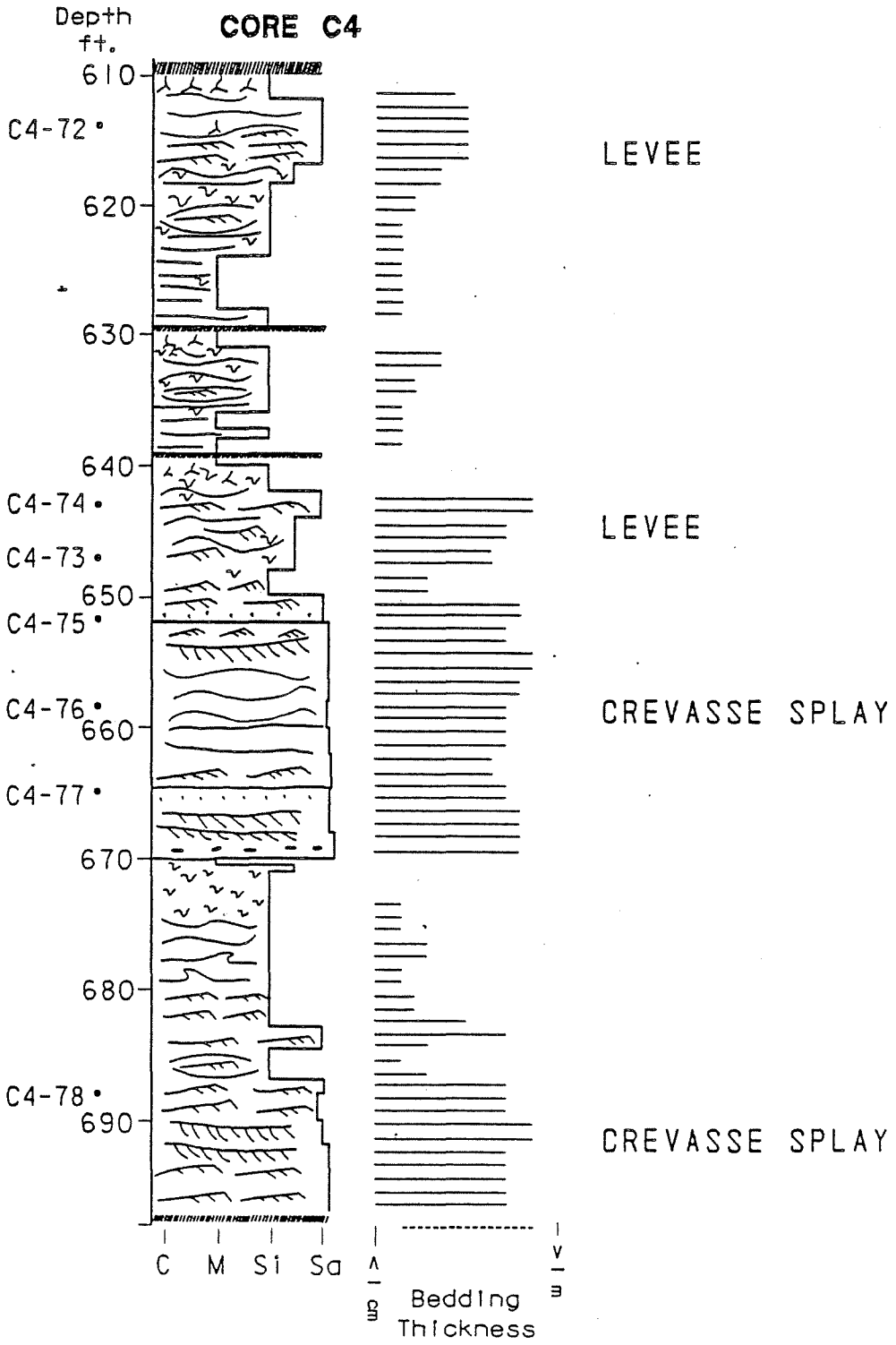
CORE C4
Depth ft.
610
620
630
640
650
660
670
680
690
C4-72
C4-74
C4-73
C4-75
C4-76
C4-77
C4-78
LEVEE
LEVEE
CREVASSE SPLAY
CREVASSE SPLAY
C M Si Sa
Bedding Thickness

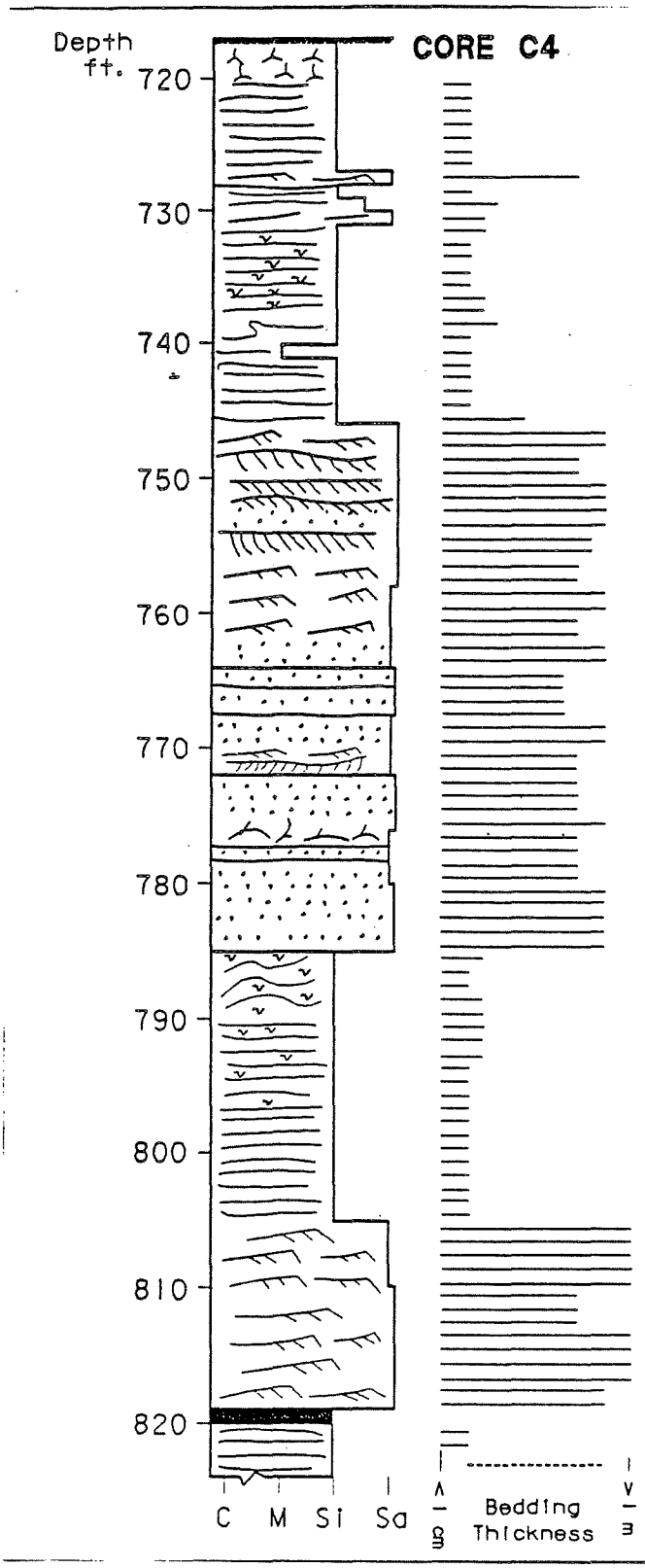
Depth
ft.
CORE C4
720
730
740
750
760
770
780
790
800
810
820
C
M
Si
Sa
Bedding
Thickness
CREVASSE CHANNEL
CREVASSE SPLAY

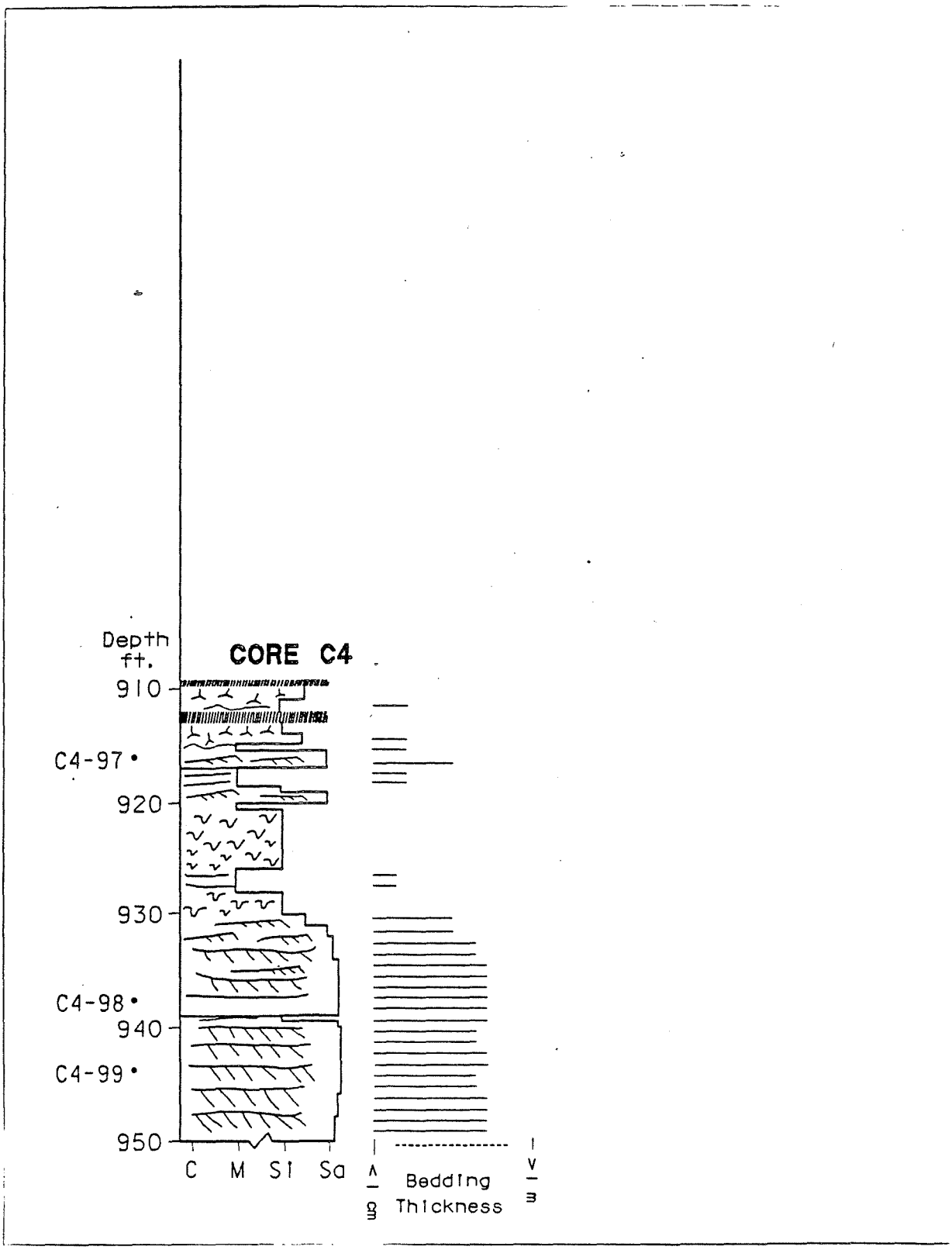
CORE C4
Depth ft.
910
C4-97
920
930
C4-98
940
C4-99
950
C
M
Sl
Sa
Bedding Thickness

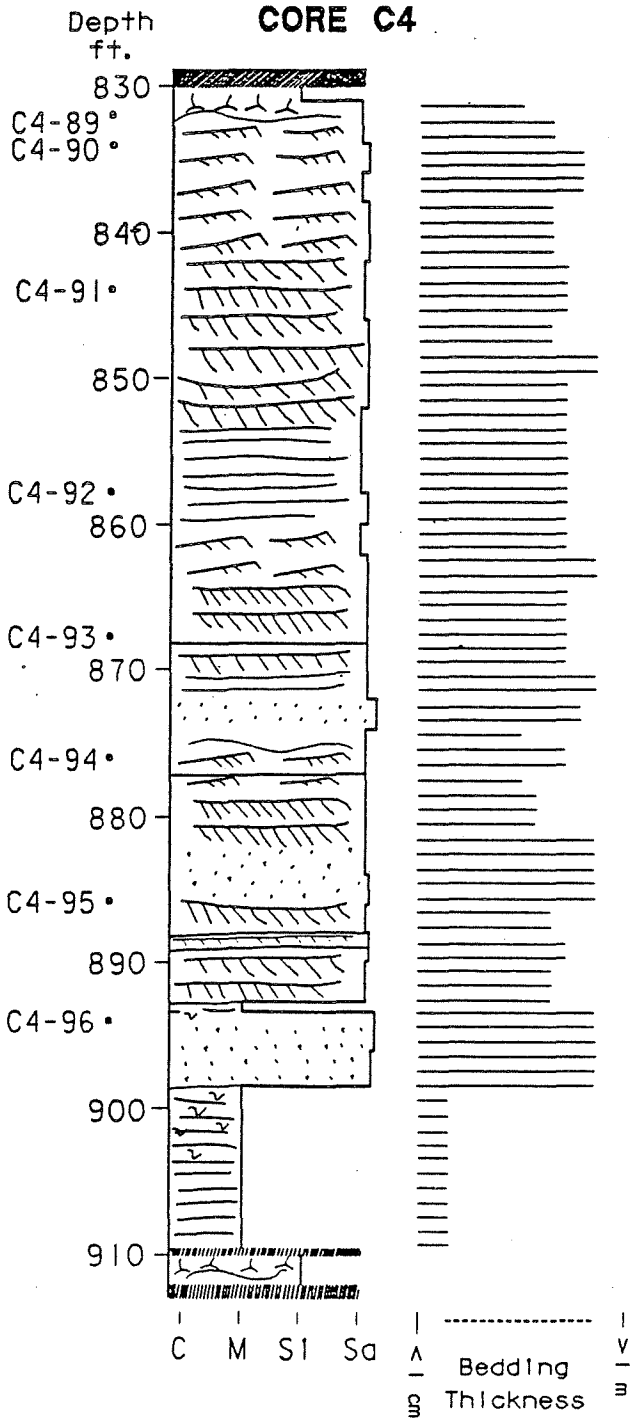

FLUVIAL DISTRIBUTARY

APPENDIX III

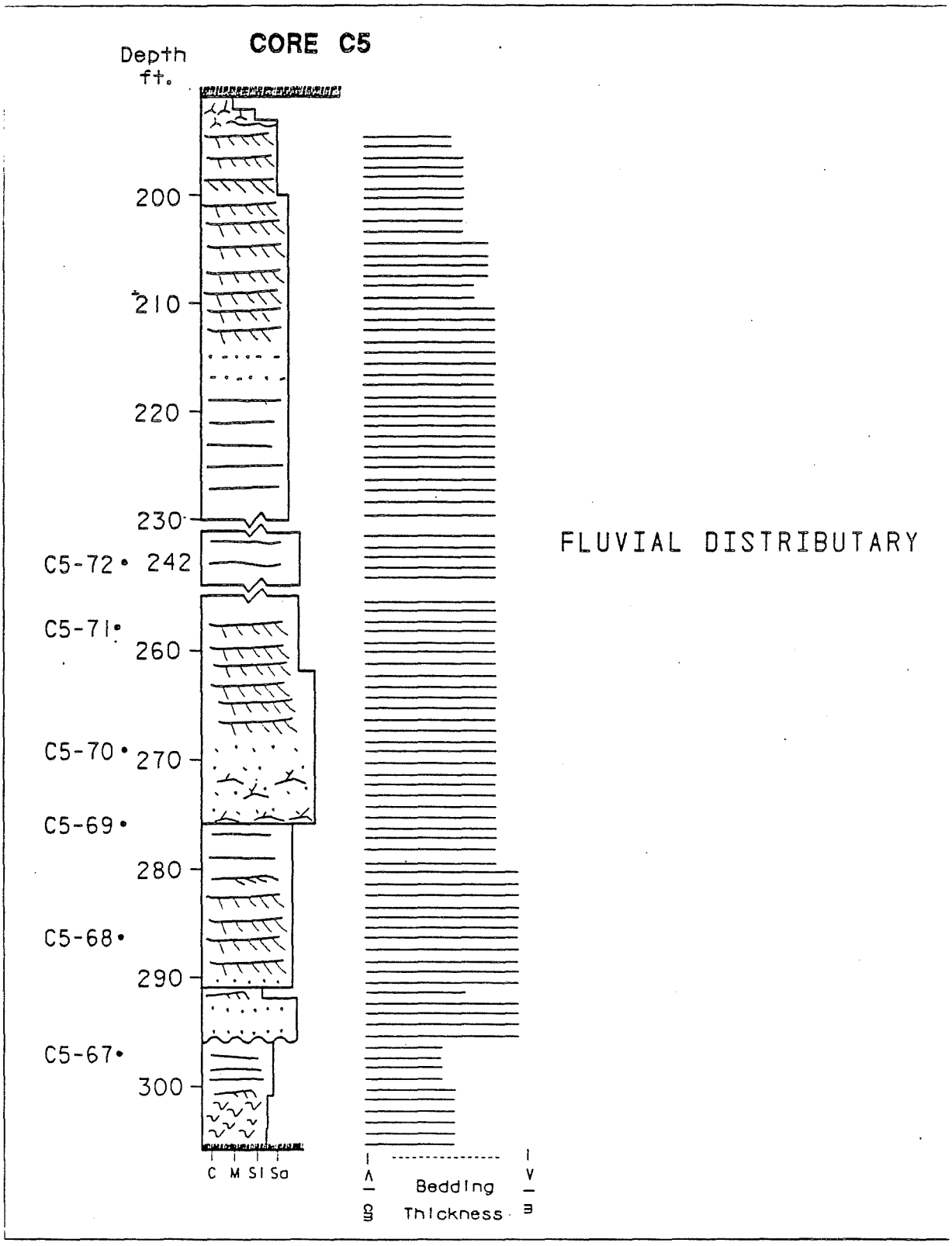
CORE C5
Depth
ft.
200
210
220
230
C5-72 • 242
C5-71 •
260
C5-70 •
270
C5-69 •
280
C5-68 •
290
C5-67 •
300
C M SI Sa
Bedding
Thickness
FLUVIAL DISTRIBUTARY

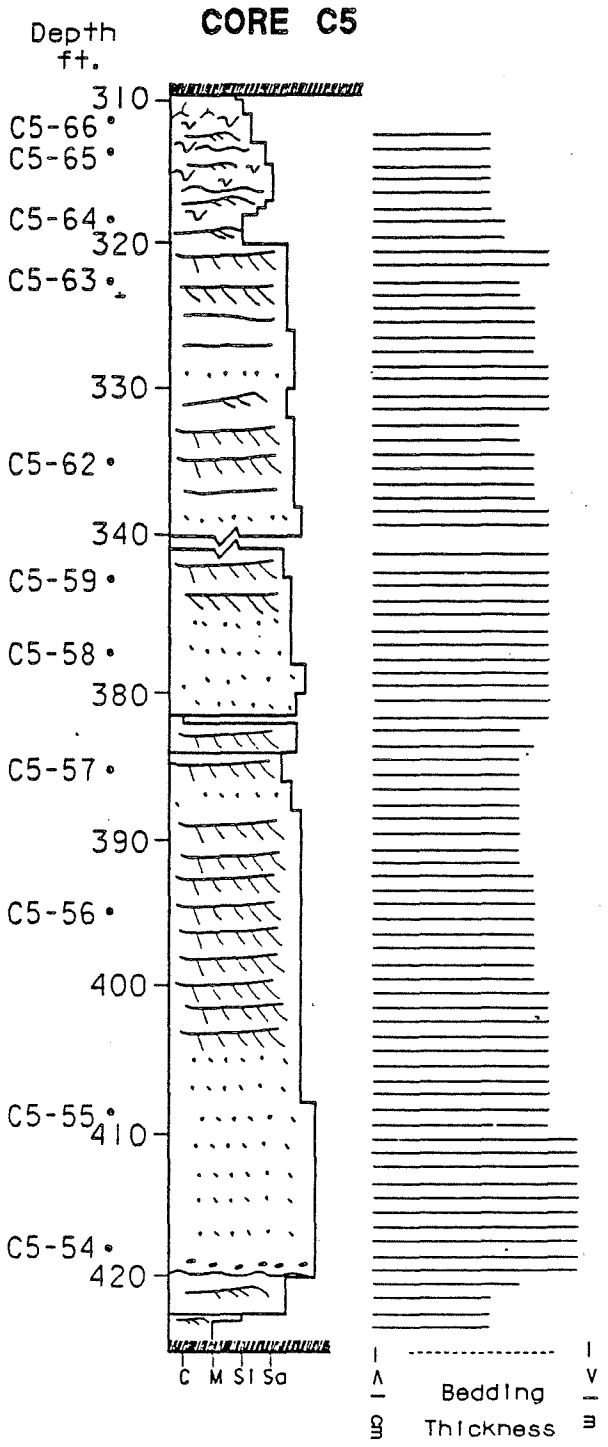
CORE C5
Depth ft.
310
C5-66
C5-65
C5-64
320
C5-63
330
C5-62
340
C5-59
C5-58
380
C5-57
390
C5-56
400
C5-55
410
C5-54
420
C M Sl Sa
Bedding Thickness
FLUVIAL DISTRIBUTARY

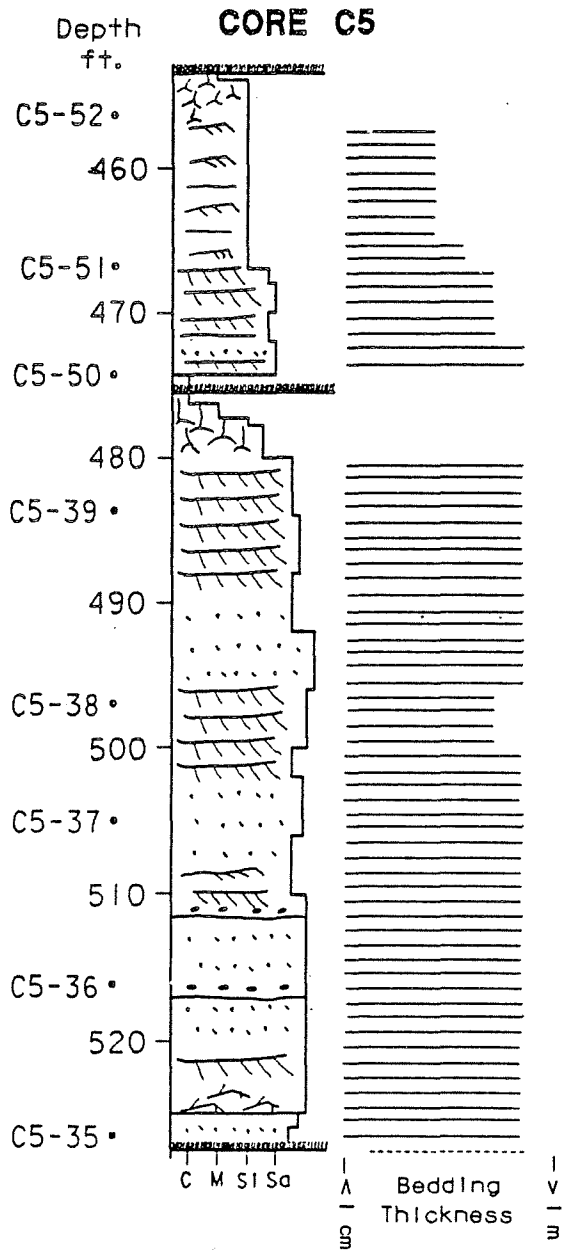
CORE C5
Depth
ft.
C5-52
460
C5-51
470
C5-50
480
C5-39
490
C5-38
500
C5-37
510
C5-36
520
C5-35
C M SI Sa
Bedding
Thickness
CREVASSE SPLAY
FLUVIAL DISTRIBUTARY

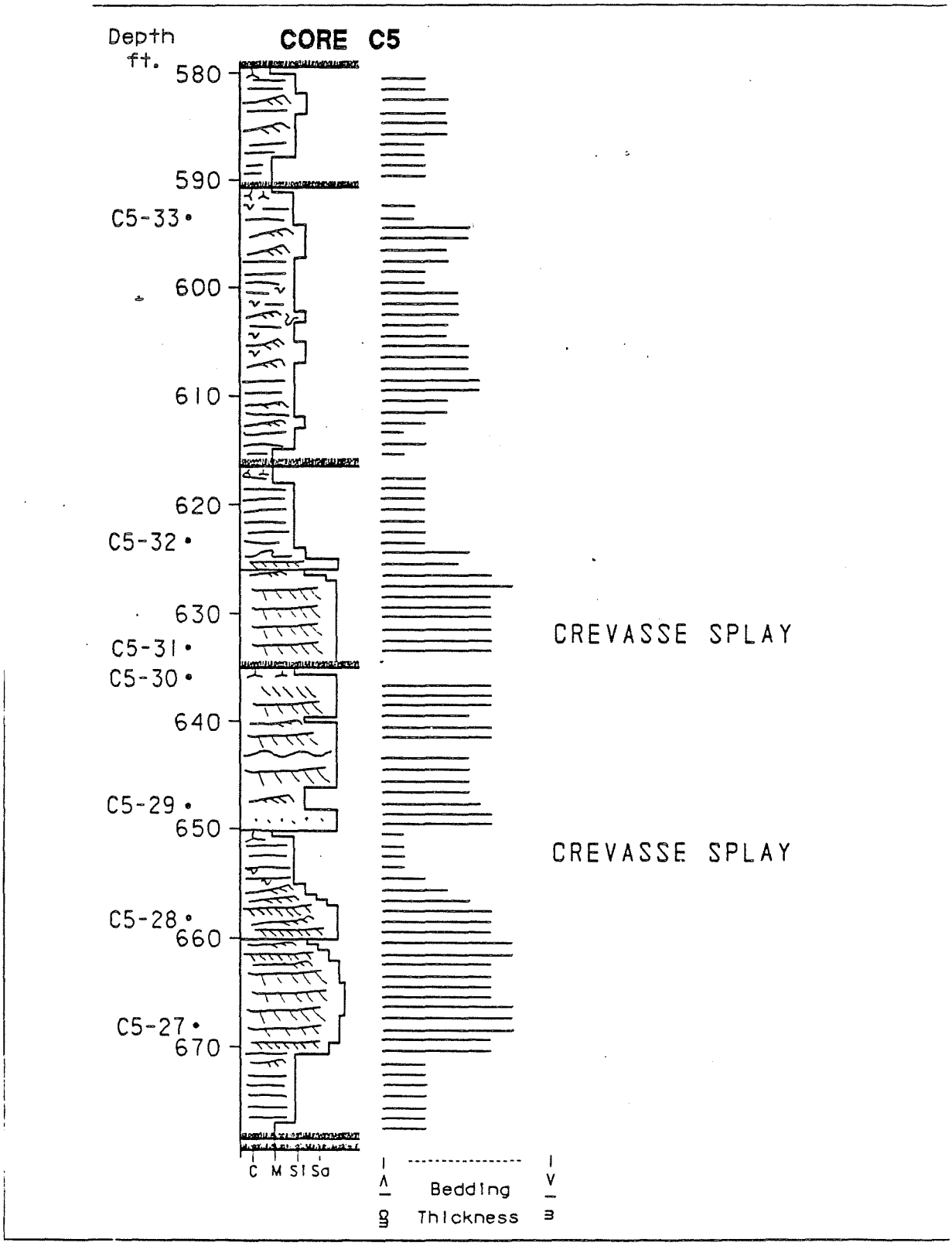
CORE C5
Depth ft.
580
590
C5-33
600
610
620
C5-32
630
C5-31
C5-30
640
C5-29
650
C5-28
660
C5-27
670
CREVASSE SPLAY
CREVASSE SPLAY
C M S1 Sa
Bedding Thickness

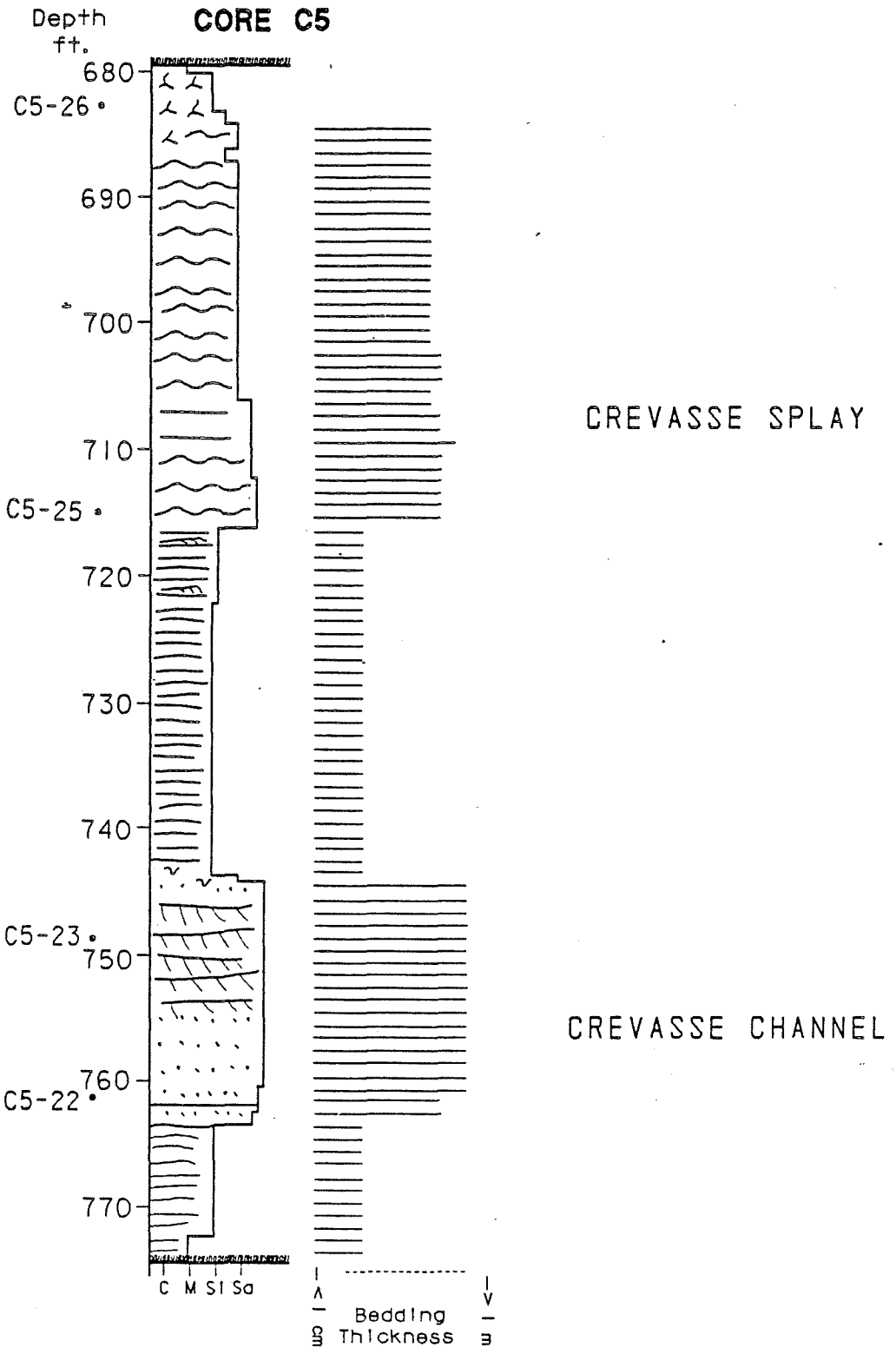
CORE C5
Depth
ft.
680
C5-26
690
700
710
C5-25
720
730
740
C5-23
750
760
C5-22
770
C M SI Sa
Bedding
Thickness
CREVASSE SPLAY
CREVASSE CHANNEL

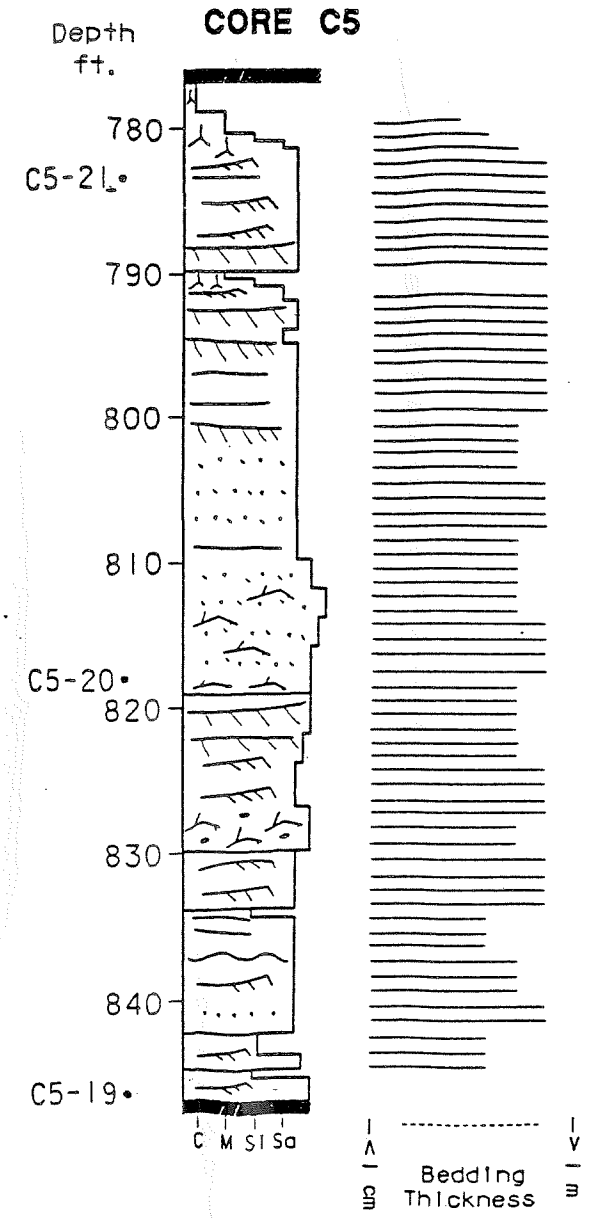

FLUVIAL DISTRIBUTARY

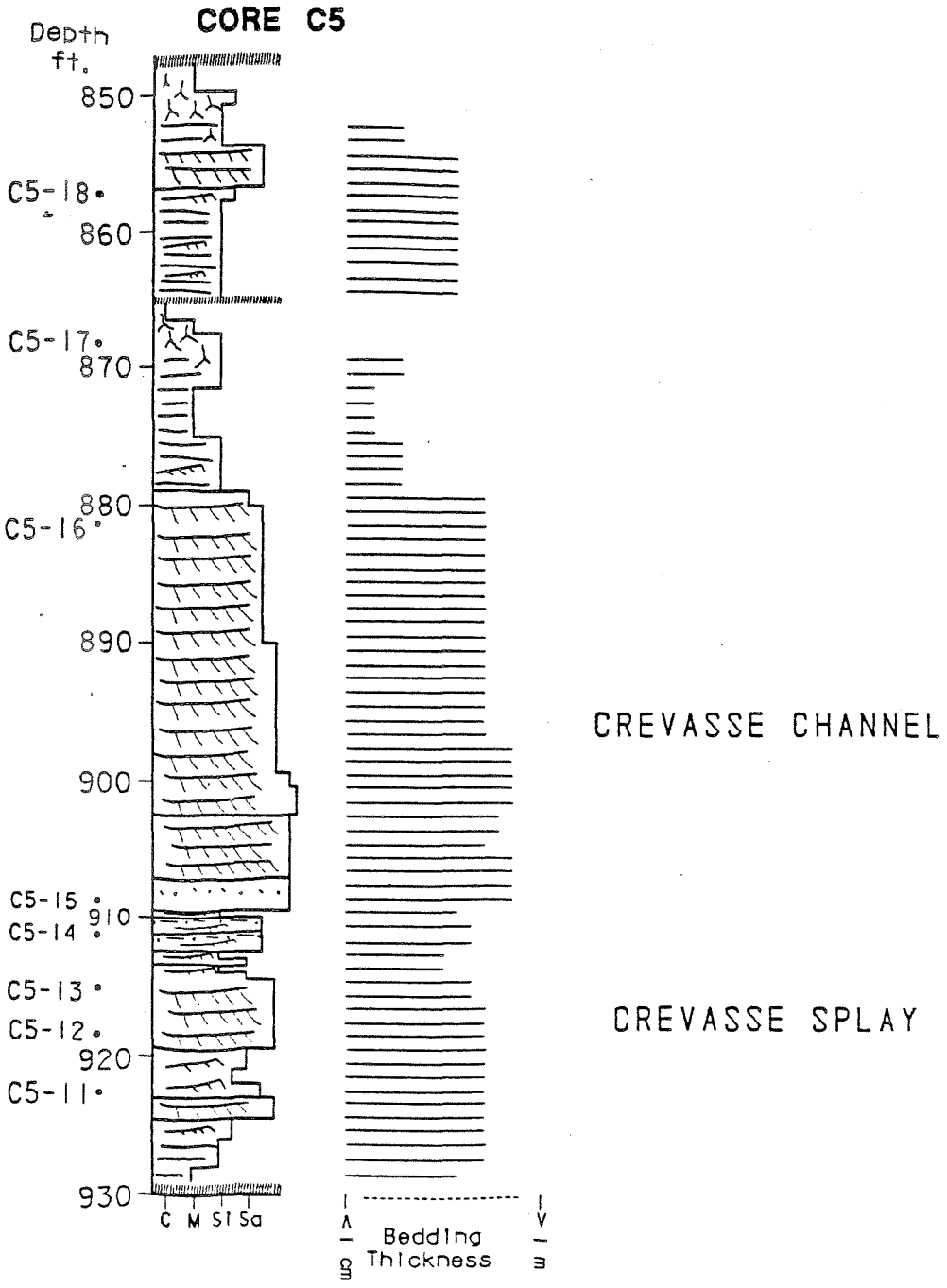
CORE C5
Depth ft.
850
C5-18
860
C5-17
870
880
C5-16
890
900
C5-15
910
C5-14
C5-13
C5-12
920
C5-11
930
C M SI Sa
Avg
Bedding Thickness
V
CREVASSE CHANNEL
CREVASSE SPLAY

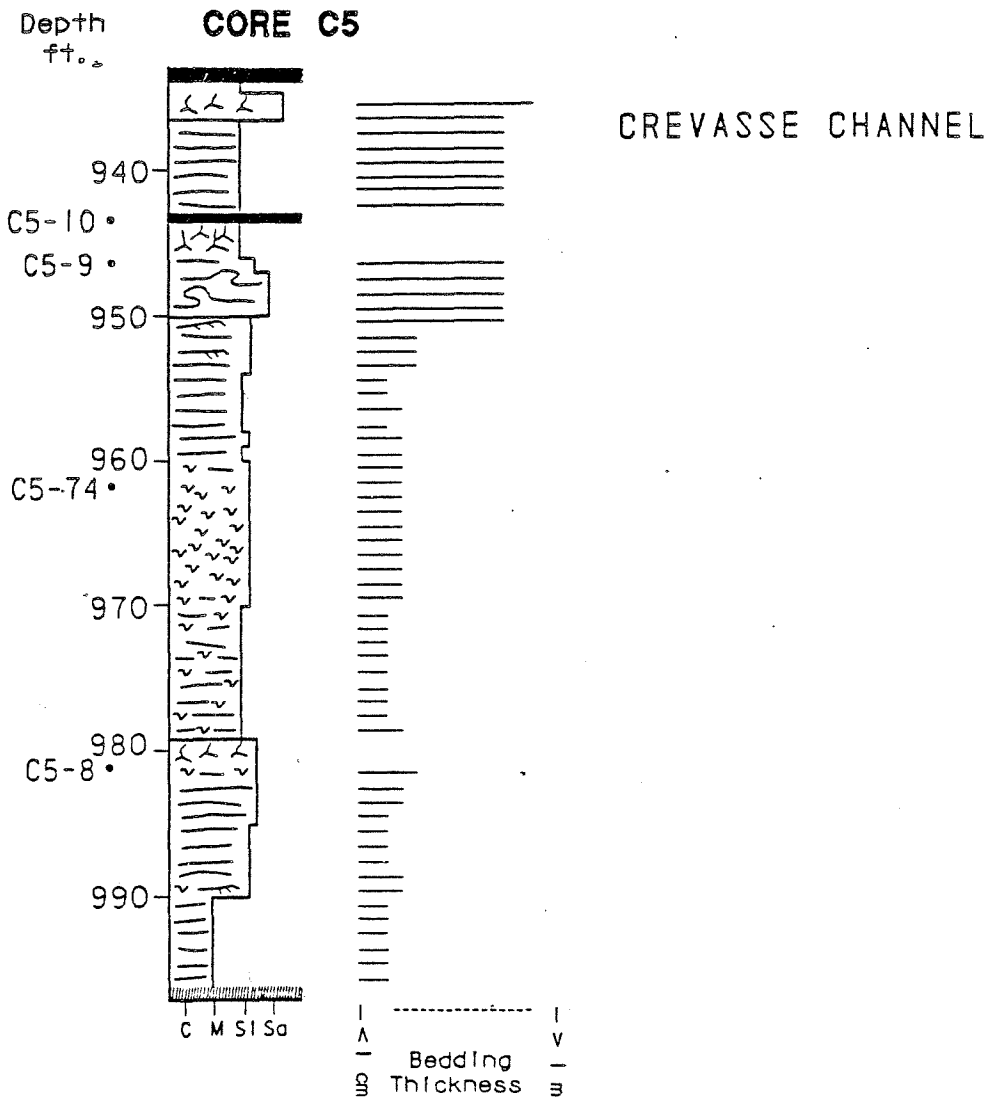
Depth
ft.
CORE C5
940
C5-10
C5-9
950
960
C5-74
970
980
C5-8
990
C M Sl Sa
Bedding
Thickness
CREVASSE CHANNEL

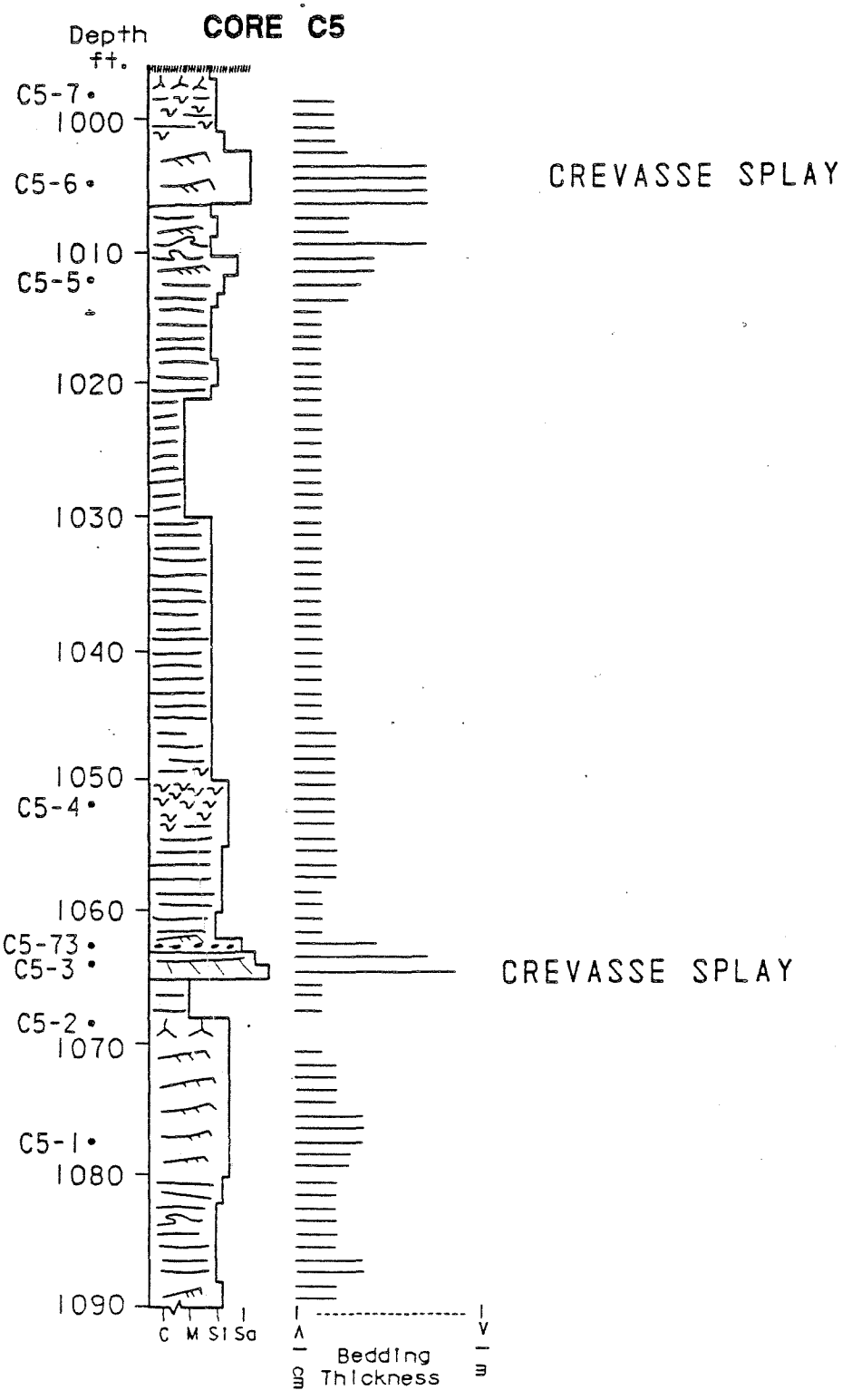
CORE C5
Depth
ft.
C5-7
1000
C5-6
1010
C5-5
1020
1030
1040
1050
C5-4
1060
C5-73
C5-3
C5-2
1070
C5-1
1080
1090
C M SI Sa
A
V
Bedding
Thickness
CREVASSE SPLAY
CREVASSE SPLAY